UNIVERSITÉ CATHOLIQUE DE LOUVAIN

Thesis in Pharmaceutical and Biomedical Sciences

Mechanistic study of PHGDH enzyme inhibition: towards the development of new anticancer drugs

Quentin Spillier

Promoter : Pr. Raphaël Frédérick
UCLouvain

Co-promoter: Pr. Olivier Feron
UCLouvain

Jury members: Pr. Nathalie Delzenne
(President)
UCLouvain

Pr. Marianne Fillet
ULiège

Pr. Didier Lambert
UCLouvain

Pr. Filippo Minutolo
UniPi

Pr. Olivier Riant
UCLouvain

Pr. Johan Wouters
UNamur

JURY COMPOSITION

Promoter

Pr. Raphaël Frédérick

Medicinal Chemistry Research Group (CMFA), Louvain Drug Research Institute (LDRI), Université catholique de Louvain (UCLouvain)

Co-promoter

Pr. Olivier Feron

Pole of Pharmacology and Therapeutics (FATH), Institut de Recherche Expérimentale et Clinique (IREC), Université catholique de Louvain (UCLouvain)

President of the jury

Pr. Nathalie Delzenne

Metabolism & Nutrition (MNut), Louvain Drug Research Institute (LDRI), Université catholique de Louvain (UCLouvain)

Jury Members

Pr. Didier Lambert

Medicinal Chemistry Research Group (CMFA), Louvain Drug Research Institute (LDRI), Université catholique de Louvain (UCLouvain)

Pr. Olivier Riant

Molecular Chemistry, Materials and Catalysis (MOST), Institute of Condensed Matter and Nanosciences (IMCN), Université catholique de Louvain (UCLouvain)

Pr. Johan Wouters

Laboratoire de Chimie Biologique Structurale (CBS), NAmur MEdicine & Drug Innovation Center (NAMEDIC-NARILIS)*, Université de Namur (UNamur)*

Pr. Marianne Fillet

Laboratory for the Analysis of Medicines (LAM), Center for Interdisciplinary Research on Medicines (CIRM), Université de Liège (ULiège)

Pr. Filippo Minutolo

Dipartimento di Farmacia, Università di Pisa (UniPi)

REMERCIEMENTS

Voici venu le moment de clôturer cinq années particulièrement intenses. La réalisation de ce doctorat a nécessité l'encouragement, les conseils et l'aide de nombreuses personnes. Je suis donc très heureux de leur exprimer ici toute ma reconnaissance. Sans eux, ce travail ne serait pas ce qu'il est.

Tout d'abord, je voudrais remercier mon promoteur, le Professeur **Raphaël Frédérick**. Je lui suis particulièrement reconnaissant de m'avoir accordé la chance de réaliser cette thèse au sein de son laboratoire. Merci pour la grande liberté scientifique qu'il m'a octroyée tout au long de ce projet. Merci également de m'avoir impliqué dans de nombreuses collaborations enrichissantes. Cela m'a permis d'améliorer considérablement mon background scientifique tout en gagnant en maturité et en autonomie. Merci encore pour les conseils avisés qu'il m'a prodigués. Plus d'une fois, ceux-ci m'ont permis de me recentrer sur les points capitaux de mon travail. Enfin un tout grand merci pour le soutien, la bonne humeur, la patience et le courage dont il a fait preuve durant les différentes phases d'écriture jalonnant cette aventure.

Mes remerciements vont également à mon co-promoteur, le Professeur **Olivier Feron**. Un grand merci pour les discussions et meetings qui m'ont permis de mieux comprendre le métabolisme tumoral. J'ai ainsi pu appréhender, avec beaucoup plus d'aisance, un domaine d'expertise très éloigné du mien lors de mes débuts. Enfin, merci pour le soutien et les commentaires toujours pertinents. Ces derniers ont permis d'augmenter considérablement la qualité scientifique et la lisibilité de mon manuscrit.

J'exprime aussi ma profonde gratitude au Docteur **Séverine Ravez**. Sans son apport, cette histoire n'aurait pu être aussi enrichissante. Un immense merci à Bibiche pour tout ce qu'elle m'a apporté lors de cette thèse et en dehors. C'est elle qui a façonné, pour une grande partie, le scientifique que je suis devenu. C'est également grâce à elle que ce travail n'est pas si nuuul que ça. Merci pour le soutien, la bonne humeur permanente, la générosité, l'aide et les conseils avisés prodigués sans relâche. Merci pour tous ces moments partagés à Bruxelles, Lille et ailleurs. Merci d'avoir toujours cru en moi, même dans les moments plus difficiles. Et sache que, même si j'ai été à plusieurs reprises Belge, Albanais et Croate, les matchs resteront de grands moments partagés.

Je voudrais ensuite remercier les membres de mon jury pour leurs nombreux conseils ainsi que pour le temps qu'ils m'ont consacré. Ils ont permis à ce travail de voir le jour. Je tiens à remercier le Professeur **Nathalie Delzenne**, présidente du jury, pour son accompagnement depuis le début du projet ainsi que pour sa gentillesse et ses nombreuses remarques scientifiques pertinentes. Merci au Professeur **Didier Lambert** pour ses encouragements et son soutien même lorsque les bases de mon projet n'étaient pas encore suffisamment étayées. Je tiens également à remercier le Professeur **Olivier Riant** pour ses nombreux conseils sur la partie chimique du travail. Ceux-ci ont permis de débloquer plusieurs situations problématiques. Ses commentaires judicieux ont permis l'amélioration de ce manuscrit. Merci au Professeur **Johan Wouters** pour ses conseils et sa contribution à la concrétisation d'une partie conséquente de ce travail. Enfin un merci tout particulier aux Professeurs **Marianne Fillet** et **Filippo Minutolo**, membres externes du jury. Merci de l'honneur qu'ils m'ont fait d'accepter de participer à l'évaluation de ce travail. Merci pour le temps investi et les nombreux commentaires ayant permis son amélioration. Que tous soient remerciés pour les discussions et remarques constructives lors de ma défense privée.

Bénéficiaire d'une bourse Télévie, j'exprime ma profonde gratitude à tous ses donateurs pour leur généreux soutien. Sans cette superbe opportunité, mon projet n'aurait pas vu le jour.

Une thèse ne peut se réaliser sans l'aide et le soutien de toute une équipe. Merci donc à tous mes collègues pour m'avoir soutenu et … supporté durant 5 années riches en rebondissement et en péripéties.

Un grand merci au super grand chef **Bouazza** pour l'aide apportée lors de mes nombreuses manipulations biologiques .Depuis le début, son soutien permanent m'a été précieux. Sa capacité à trouver des solutions aux situations les plus compliquées n'a cessé de m'impressionner. Merci pour sa bonne humeur communicative et pour les nombreux fous rires partagés. Notre séance de natation de midi (légèrement mise de côté ces derniers mois) me manquera. Je tiens également à remercier **Esra** pour l'excellente ambiance qu'elle a su insuffler au labo et ce, malgré les petits moments de tensions traversés par l'équipe. Sa gestion efficace du labo a facilité de nombreux projets. N'oublions pas ses délicieux petits

plats faits maison qui ont contribué à nourrir l'ensemble du labo. Merci à **Charline** pour le courage et la patience dont elle a fait preuve lors de nos expériences cellulaires. Cela nous a permis de surmonter les différents écueils rencontrés. Merci également à **Laurenne Petit** et **Céline Guilbaud** pour leur assistance lors de ces travaux.

Toujours dans le domaine des résultats biologiques, je me dois de remercier particulièrement le Docteur **Cyril Corbet**. Merci Cyril d'avoir aidé un petit chimiste à progresser dans le monde souvent opaque et trouble du métabolisme tumoral. Merci pour toutes les suggestions et commentaires judicieux. Ton expertise de PHGDH et de la biologie cellulaire, en général, m'ont souvent permis de reconsidérer mes résultats sous un angle neuf. Désormais, je pense pouvoir venir travailler sous les hottes de votre labo sans rien contaminer.

Une mention spéciale doit être attribuée à **Alice** et **Julien** qui ont vécu et partagé cette aventure depuis le tout début. Merci à Alice pour son soutien de tous les instants, merci pour les interminables discussions et les inévitables digressions. Nos voyages en voiture accompagnés de ses petits commentaires sur ma façon de conduire m'auront procuré d'immenses fous rires. Son soutien m'a permis de terminer ce mastère sans disjoncter. Enfin, savoir qu'il me suffisait d'un mot judicieusement choisi, d'un signe, pour que la voir se lancer dans un karaoké endiablé dans notre bureau restera à jamais dans ma mémoire. Une chose est sûre, Daphné ne m'avait pas menti. Malheureusement, il lui faudra désormais trouver une autre personne pour les massages. Merci aussi à Juju pour tous les bons moments partagés. Ces congrès où, par le plus grand des hasards, nous étions toujours suivis par une personne qui avait une fâcheuse tendance à ronfler et ainsi nous empêcher de nous reposer. Les moments de détente et de rigolades lors des fins de congrès me manqueront. Merci pour tous les craquages dürüms en semaine. Merci pour toute l'aide apportée lors de la rédaction de cette thèse. Merci à mon photographe officiel. Enfin, même si son esprit français perdure encore quelques fois (champion du monde, quatre-vingt-dix), notre amitié y aura résisté. Bientôt vous aussi clôturerez votre thèse. Nous pourrons alors organiser de super soirées diapos nous remémorant tous ces bons souvenirs.

Merci aussi à **Romain**, a.ka**.** le Poulain. Il reprend officiellement ma place du doctorant le plus cool de tout l'étage. Depuis le mémoire, il fait officiellement partie de la bande PHGDH.

C’est un plaisir de le voir poursuivre sa route au labo (même s’il aurait pu choisir un sujet de thèse plus cool !). Merci Romain pour ton support moral et l’entrainement qui m’ont permis de finir (difficilement) les 20km de Bruxelles. Je n’oublierai pas toutes ces soirées où nous avons pu constater que Bretons et Wallons partageaient les mêmes passions. Désormais, le professeur K nous attend à Vannes pour ouvrir notre labo et enfin travailler sur de la vraie Science (DSF forever).

Merci à toi **Léo** pour ce nombre incalculable de discussions scientifiques et autres que nous avons eues ces 5 années. Merci pour tes conseils, souvent très pertinents et merci pour toutes ces bonnes soirées où nous avons pu contempler la gestion catastrophique de Westeros. Même si je n’arrive pas toujours à suivre le fil de ta pensée, nous avons passé de sacrés bons moments. N’oublie cependant pas qu’il s’agirait de grandir désormais. Merci à **Arina** pour toutes ces intéressantes discussions au cours desquelles nous avons refait le monde. Merci Arina et Léo pour votre accueil, je me suis toujours senti chez vous comme chez moi. Merci également pour tous ces dessins et ces photomontages de qualité qui ont égaillé mon passage au labo. Je n’ai qu’un regret, c’est de ne pas vous avoir fait découvrir les folles kermesses du Namurois. Merci à Archi pour son soutien moral indéfectible tout au long de ces travaux. Enfin comme il m’est impossible de vous dissocier totalement tous les trois, merci à vous pour les émotions lors de ce mariage grandiose (je m’en souviendrai longtemps).

Un grand merci à **Marine** pour m’avoir apporté son soutien. Grâce à elle, les Namurois ont enfin eu voix au chapitre. Merci de m’avoir forcé à aller courir, même si je me suis désisté plus souvent qu’à mon tour. Je la remercie d’avoir supporté mes récriminations pendant ces quelques kilomètres. Merci pour ces grands moments de solitude et d’émotions au cinéma.

Je remercie également **Chiarra** pour l’ambiance extrêmement positive qu’elle a su apporter au labo pendant sa courte période parmi nous. Elle a fait le bon choix en revenant et j’espère qu’elle profitera de cette thèse sans se mettre trop de pression.

Merci aussi aux différents mémorants et stagiaires ayant participé à la progression de ce travail, notamment **Laurent**, **William**, **Alice** et **Gauthier**.

Tout au long de mes recherches, j'ai également eu la chance de rencontrer et de collaborer avec de nombreuses personnes au sein de l'UCL mais aussi à l'étranger. Je voulais profiter de ces pages pour les remercier chaleureusement. Tout d'abord un immense merci au Docteur **Vincent Stroobant** pour l'aide considérable apportée pendant mes recherches. Sa gentillesse ainsi que nos nombreuses discussions m'ont permis d'élargir mon horizon scientifique. Bénéficier d'un regard externe et critique sur ce travail a permis une amélioration significative de sa qualité. Merci pareillement au Docteur **Didier Vertommen** pour sa disponibilité, sa patience et son aide précieuse lors de mes nombreuses expériences de spectrométrie de masse. Son expertise a permis de débloquer mon projet à de nombreuses reprises. Merci au Docteur **Didier Colau** pour sa gentillesse et sa contribution conséquente lors de la production de cette enzyme au comportement si particulier. Merci au Docteur **Judith Unterlass** pour sa disponibilité, ses conseils et son aide dans la réalisation de nombreuses expériences. Un jour nous parviendrons à obtenir une version cristallisée de cette enzyme. Et enfin un grand merci au Docteur **Edouard Mullarky** pour ses conseils et son expertise sur la voie de la sérine. Merci de m'avoir accueilli au sein du laboratoire du Professeur Lewis Cantley. Cela m'a permis de découvrir la recherche aux USA mais aussi cela m'a donné l'envie de poursuivre dans cette voie. Merci aux Namurois pour leur implication dans l'avancement de ce projet.

Je tiens également à remercier les chercheurs du LDRI avec qui j'ai partagé ces quelques années (GNOS, IREC, MNUT, REMA… ils sont nombreux et se reconnaitront).

Un merci tout particulier à **Mireille**, a.k.a. Philippe, pour son soutien et son aide plus que conséquente lors de l'écriture de cette thèse. Cela m'a empêché de baisser les bras plus d'une fois. Merci aussi pour ce déménagement mythique. Merci à **Yasmine** pour l'aura de calme permanent qu'elle répand. Sa gentillesse et son sourire en toutes circonstances me manqueront.

Bien sûr, je n'oublie pas de remercier tout particulièrement ma famille. Merci **Papa** et **Maman** pour votre soutien indéfectible lors des bons comme des mauvais moments (et il y en a eu). Merci d'avoir toujours cru en moi, peut-être même plus que moi. Il est évident de dire que sans vous je ne serais pas là où j'en suis à l'heure actuelle (discours classique de miss France). Vous m'avez permis de me développer et de m'accomplir pleinement, de

réaliser les projets qui me tenaient à cœur. Il n'y a pas de mot assez fort pour vous exprimer toute ma gratitude. Merci d'avoir forgé et, par la suite, accepté mon caractère pendant toutes ces longues années. Je ne le dis pas souvent et je l'écrirai encore moins mais sachez que je vous aime. Merci aussi à **Annie** et **Georges** qui, pendant toutes ces années, ont sans doute constitué ma deuxième famille de cœur. Sachez que votre gentillesse et votre soutien permanents m'ont permis de traverser de nombreuses épreuves et d'en sortir grandi et plus heureux.

Je termine en remerciant les amis qui me soutiennent depuis de très nombreuses années. Merci au groupe des **champions** (**Bram**, **Ju**, **Bastien**, **Carl**, **Nico**, **Eddy**, **JC**, **Mathieu**, **Nat**…) pour tous ces moments épiques vécus ensemble, tous ces restos jusqu'aux petites heures, toutes ces discussions sans aucun sens et toutes ces soirées légèrement foireuses. Grâce à vous, ces années ont passé à une vitesse folle. Merci aussi à **Seb** pour ces parties de kicker endiablées (je finirai un jour par gagner). Merci au groupe des **chimistes de Namur** pour ces belles années partagées. Ensembles, nous en avons vécu de belles histoires tout en découvrant ce monde fascinant. Ce n'est que le début. Un merci tout spécifique à **Skippy**, **Ju**, **Cé**, **Laeti** pour les nombreux moments que nous avons partagés dans la capitale et ailleurs.

Finalement un grand merci au Professeur **Gaston** et à **Chris** pour leur accueil toujours au top. Leur légendaire bonne humeur me donne l'impression perpétuelle de bénéficier d'une seconde maison. Il est désormais grand temps pour vous d'ouvrir une auberge afin d'en faire profiter un maximum de d'amis.

C’est donc tout un chapitre de ma vie qui se clôture avec ces pages. Mais de nombreux autres viennent de s’ouvrir. Au travers de ces remerciements, je me suis efforcé de transmettre ma profonde gratitude pour le soutien qui m’a été apporté. Les mots seront toujours insuffisants pour exprimer à quel point chacun d’entre vous a été important. J’espère également n’avoir oublié personne. Si tel est le cas, sachez que cet oubli est involontaire et que ce n’est que partie remise.

Merci pour tout.

Quentin

« *Le sportif intelligent évite l’effort inutile* »

Professeur M.

Table of content

Table of abbreviations

3-PG	3-phosphoglycerate
3-Ppyr	3-phosphopyruvate
3-Pser	3-phosphoserine
ACT	aspartate kinase-chorismate mutase-tyrA
ALDH	aldehyde dehydrogenase
AML	acute myeloid leukemia
ASB	allosteric substrate binding
ATF4	activating transcription factor 4
CAD	carbamoyl-phosphate synthetase 2, aspartate transcarbamylase, and dihydroorotase
CCT2	T-complex protein 1 subunit beta
CdKn1a;p21	cyclin-dependent kinase inhibitor 1a
CESTA	cellular thermal shift assay
CSLC	cancer stem-like cells
CuET	disulfiram-copper metabolite
D-2HG	d-2-hydroxyglutarate
DNA	deoxyribonucleic acid
DSF	disulfiram
DTT	dithiothreitol
EGFR3	epidermal growth factor receptor 3
eIF4A1	Eukaryotic translation initiation factor 4A1

eIF4E	eukaryotic initiation factor 4E
EMA	european medicines agency
ER	estrogen receptor
ESPR1	epithelial splicing regulatory protein 1
FAAH	fatty acid amide hydrolase
FBLG	fragment-based lead generation
FDA	food and drug administration
FOXM1	forkhead box protein M1
G9A	histone H3 lysine 9 methyltransferase
GCN2	general control nonderepressible 2 kinase
GLS-2	glutaminase-2
GSH	glutathione
H3K9	histone H3 lysine 9
HCV protease	hepatitis C virus protease
HIF	hypoxia inducible factor
HT	hypotaurine
IDH1	isocitrate dehydrogenase 1
JOSD2	josephin-2
LMW	low molecular weight
lncRNA	long non-coding RNA
MAGL	monoacylglycerol lipase

MLL1	myeloid/lymphoid or mixed-lineage leukemia
MLSMR	molecular libraries small molecule repository
MMP-2	matrix metalloproteinase-2
MMP-9	matrix metalloproteinase-9
MOE	molecular operating environment
mRNA	messenger RNA
MST	microscale thermophoresis
NAD^+/NADH	nicotinamide adenine dinucleotide (oxidized/reduced form)
$NADP^+$/NADPH	nicotinamide adenine dinucleotide phosphate (oxidized/reduced form)
NFκB	nuclear factor-kappa B
NMDAR	*N*-methyl-D-aspartate receptors
NRF2	nuclear factor erythroid-2-related factor 2
NSCLC	non-small-cell lung cancer
NSCLC	non-small-cell lung carcinoma
OXPHOS	oxidative phosphorylation
p38 MAPK	p38 mitogen-activated protein kinases
PAL	photo affinity labeling
PDB	protein data bank
PEP	phosphoenolpyruvate
PFAS	phosphoribosylformylglycinamidine synthase
PHGDH	3-phosphoglycerate dehydrogenase

PKCζ	protein kinase Cζ
PKM2	pyruvate kinase isozyme M2
PPP	pentose phosphate pathway
PSA	polar surface area
PSAT-1	phosphoserine aminotransferase-1
PSM	peptide spectrum matche
PSPH	phosphoserine phosphatase
PTC	papillary thyroid carcinomas
RNA	ribonucleic acid
ROS	reactive oxygen species
SAM	s-adenosylmethionine
SAR	structure activity relationship
SCLC	small-cell lung carcinoma
SDS-Page	sodium dodecyl sulfate–polyacrylamide gel electrophoresis
SGOC	serine, glycine, one-carbon
SHMT	serine hydroxymethyltransferase
SR	serine racemase
SSP	serine synthetic pathway
STD	aaturation-transfer difference
TCEP	tris(2-carboxyethyl)phosphine
TGF-*β*	transforming growth factor *β*

THF	tetrahydrofolate
TNBC	triple negative breast cancer
TNBC	triple-negative breast cancer
TNM	tumor/lymph nodes/metastasis
α-KG	*α*-ketoglutarate
β-ME	2-mercaptoethanol

1. Preamble

1. Preamble

In the 1920s, Otto Warburg showed that proliferating tumor cells display increased rates of aerobic glycolysis compared to normal cells, which rely primarily on glucose-fueled mitochondrial oxidative phosphorylation to generate energy. Since the observation, this phenomenon commonly called the "Warburg effect" has become increasingly popular, and elevated glucose consumption by tumors cells is nowadays still considered as a hallmark of cancer cells.[1,2] Indeed, while over the years, other energy substrates including glutamine and fatty acids have been shown to fuel the mitochondrial oxidative metabolism in tumors, glucose has consistently been reported to be converted mainly into lactate in proliferating cancer cells. The ATP yield per glucose molecule is much lower when glycolysis is not coupled to the tricarboxylic acid cycle (TCA) cycle, but the production rate is actually much faster than that when oxidative phosphorylation (OXPHOS) is involved. This fast production of ATP, and thereby the production of biosynthetic intermediates, make the glycolysis process particularly suited to support cancer cell growth.[3]

The glycolytic intermediates are integrated into various metabolic pathways extremely useful for cancer development to generate *de novo* nucleotides, lipids and NADPH (**Figure 1**).

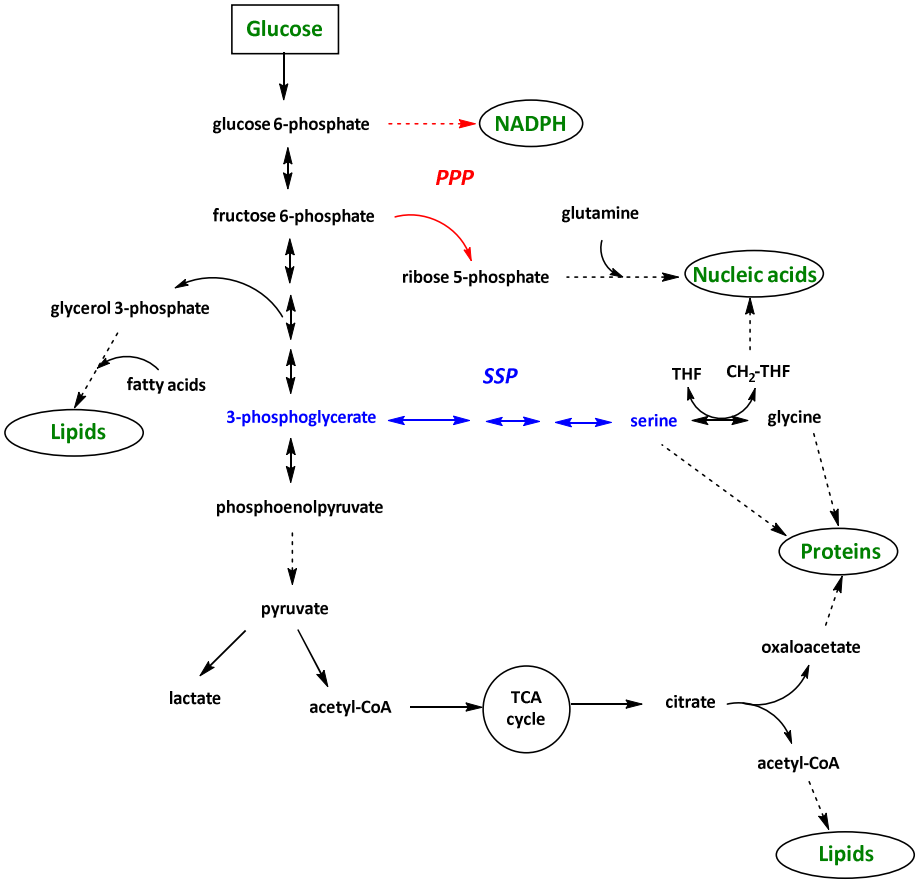

Figure 1: *Glycolysis and associated anabolic pathways. Serine synthetic pathway (SSP) in blue, pentose phosphate pathway (PPP) in red and main components produced through glycolysis in green.*

First, the first cytosolic product of glucose metabolism, glucose-6-phosphate, can be used by the pentose phosphate pathway (PPP) to drive NADPH generation. This product is crucial to maintain cellular redox balance during intense proliferation. Moreover, the PPP allows nucleotides biosynthesis starting from fructose 6-phosphate and the associated carbon flux. Nucleic acids are essential for DNA replication and RNA transcription.

Then, glycolysis can be involved in lipids biosynthesis thanks to the production of glycerol 3-phosphate and its reaction with fatty acids. Other later glycolytic intermediates, such as citrate and acetyl CoA, are used for the same purpose thereby facilitating cellular proliferation.

Finally, proteins are also produced at different branches of glycolysis, as depicted in **Figure 1**. More especially, their synthesis is strongly connected to the serine synthetic pathway (SSP). The latter is activated through 3-phosphoglycerate accumulation and

supplies one carbon metabolism thanks to serine and glycine production. In brief, SSP is involved in diverse cellular processes including methylation reactions, antioxidant defences, lipid head group modifications and nucleotides metabolism.

Due to its crucial importance in cellular development, and more especially cancer, we were particularly interested to investigate this metabolic pathway.

In the Introduction part, we will detail its implication in cancer development and its expression in cancer cells. For multiple reasons, we are especially focused on phosphoglycerate dehydrogenase (PHGDH), the first enzyme of SSP. Indeed, among the reasons that will be detailed during the introcution of this work, PHGDH is amplified in a significant subset of human tumors, and its suppression by RNAi caused a decrease in cancer cell survival and growth.[4,5]

Furthermore, the discovery of drugs that inhibit this enzyme still being in its infancy, all the current chemical inhibitors developed to target the SSP, and particularly PHGDH, will be depicted at the end of this introductive part to strengthen the medicinal chemistry basis of this project.

2. Introduction

This chapter is based on the following publications: Ravez, S., Spillier, Q., Marteau, R., Feron, O., & Frédérick, R. (2017). Journal of Medicinal Chemistry, 60(4), 1227–1237 and Spillier, Q., Feron, O., & Frédérick, R. "Latest insights into PHGDH cellular activity and inhibition", manuscript in preparation.

2. Introduction

2.1. THE SERINE SYNTHETIC PATHWAY (SSP)

2.1.1. Serine: a critical amino acid.

Serine is classified as a nutritionally non-essential amino acid, but metabolically, serine is indispensable and displays a critical role in several cellular processes.[6] Serine can be converted to glycine via the action of the serine hydroxymethyltransferase (SHMT).[7,8] This conversion provides carbon units which drive the synthesis of the 5,10-methylenetetrahydrofolate, a precursor of folates that contribute to purine nucleotide synthesis.[9,10] Additionally, serine can react with palmitoyl-CoA to provide sphingosine. This building block is required for the generation of sphingolipids that constitute the cell membrane. Furthermore, serine is a precursor of several amino acids like glycine and cysteine that are crucial for protein elaboration. Serine can also play a role in the regulation of the redox status due to the fact that serine is involved in the production of NADPH. In summary, serine can provide nucleotide, lipid, amino acid and cofactor building blocks, and thus it can contribute to cell proliferation.[11]

2.1.2. De novo serine synthesis via the SSP

Serine can be imported from the extracellular compartment via an amino acid transporter, but it can also be synthesized by an intracellular pathway. The biosynthesis of serine constitutes a major metabolic pathway that plays a central role in the formation of other amino acids, nucleic acids and phospholipids.[12] The SSP diverts around 10% of the 3-PG from glycolysis to generate serine as well as equimolar amounts of reduced nicotinamide adenine dinucleotide (NADH) and α-ketoglutarate (α-KG). It consists of three successive enzymatic reactions (**Figure 2**). Phosphoglycerate dehydrogenase (PHGDH) catalyzes the first step and produces 3-phosphohydroxypyruvate (3-PPyr) by NAD^+-coupled oxidation of 3-PG. Next, 3-PPyr is converted in phosphoserine by the phosphoserine aminotransferase 1 (PSAT-1) and then into serine by the action of phosphoserine phosphatase (PSPH). Finally, serine can be converted into glycine by SHMT.

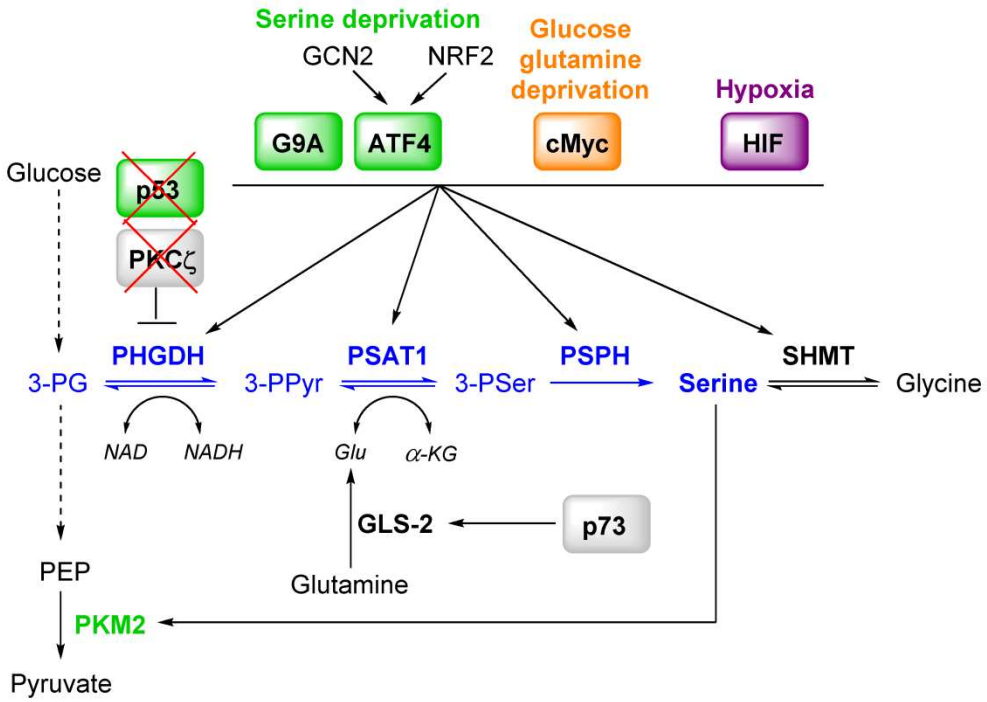

***Figure 2**: Schematic representation of the SSP and its regulator mechanisms. (3-PG: 3-phosphoglycerate; 3-PPyr: 3-phosphopyruvate; 3-PSer: 3-phosphoserine; ATF4: activating transcription factor 4; G9A: histone H3 lysine 9 methyltransferase; GCN2: general control nonderepressible 2 kinase; GLS-2: glutaminase-2; HIF: hypoxia inducible factor; NRF2: nuclear factor erythroid-2-related factor 2; PHGDH: 3-phosphoglycerate dehydrogenase; PEP: phosphoénolpyruvate; PKCζ: protein kinase C zeta; PKM2: pyruvate kinase isozyme M2; PSAT1: phosphoserine aminotransferase-1; PSPH: phosphoserine phosphatase; SHMT : serine hydroxymethyltransferase)*

2.1.3. Upregulation of serine biosynthesis in cancer cells

The SSP was first found increased in homogenates of neoplasic tissues relative to normal tissues by Snell and coworkers in the late 1980s.[13] Since this observation, the elevated rate of serine biosynthesis has been observed in several cancers such as breast cancer and melanoma. Furthermore, it was shown that this increased activity of SSP might be relevant for tumorigenesis.[14]

So far, several mechanisms have been characterized as activators of the pathway in cancer cells. On the one hand, different studies showed that *PHGDH*, the gene encoding the

first enzyme of SSP, is recurrently amplified in melanoma and breast cancer.[4,5,15] On the other hand, recent results validated several factors as activators of the SSP in cancer cells which also determine cancer pathogenesis (**Figure 2**). Firstly, the low level of intracellular serine leads to the activation of the general control nonderepressible 2 kinase (GCN2) and enhances the translation of activating transcription factor 4 (ATF4). The ATF4 induction subsequently increases the transcription of SSP enzyme genes. It was demonstrated that ATF4 can also be induced by the transcription factor nuclear factor erythroid-2-related factor 2 (NRF2) in human non-small cell lung cancer (NSCLC).[16] c-Myc is a well-known regulator of genes involved in metabolism, but its implication in the serine/glycine pathway was highlighted only recently.[17] It was demonstrated that c-Myc activates the SSP by transcriptional upregulation of the expression of SSP enzymes under deprivation of glucose or glutamine. Direct activation of SSP enzymes was also associated to the function of PKM2 to maintain cell proliferation in serine-depleted medium. Indeed, the lower activity of PKM2 in cancer cells promotes the accumulation of upstream glycolytic intermediates like 3-PG which might then be converted to serine through activated SSP enzymes.[18,19] The transcription factor p73 likewise indirectly regulates SSP enzymes through the transcriptional control of glutaminase-2.[20] This enzyme catalyses the conversion of glutamine into glutamate, which in turn drives the SSP. The SSP is also under epigenetic control. Indeed, it was shown that the histone H3 lysine 9 (H3K9) methyltransferase G9A is required for the transcriptional activation of this pathway in response to serine deprivation.[21] Moreover, a recent study demonstrated that hypoxia induces the expression of SSP enzymes, and this phenomenon is mediated by HIF-1 and HIF-2 in a large panel of breast cancer cell lines.[22] Finally, it was reported that tumor suppressors PKC-ζ and p53 repress the expression of PHGDH. Thus, deficiency of PKC-ζ or p53 in cancer cells promotes the activity of PHGDH and drives the SSP.[23–25]

Genomic amplification of SSP enzymes and deregulation of additional mechanisms increase the activation of the serine-glycine biosynthetic pathway in cancer cells. This elevated activation brings about a multitude of metabolic consequences, such as the enhanced synthesis of macromolecules needed for the proliferation of tumoral cells. The knockdown of PHGDH inhibited the growth of cancer cell lines that harbor *PHGDH*

amplification or PHGDH overexpression, but had no effect on lines expressing PHGDH at a normal level. Based on these observations, SSP enzymes appear to be promising drug targets to develop novel anticancer targeted therapies.[26] Currently, the field of drug discovery against SSP enzymes is still in its infancy, and the identification of suitable inhibitor agents could help to understand the emerging biology of these metabolic enzymes. In the second part of this Perspective, we will present an overview of one of the key enzymes of the SSP, PHGDH.

2.2. PHGDH: A PROMISING ANTICANCER DRUG TARGET

PHGDH oxidoreductase has become of increasing interest since 2011 with a rise in related publication activity noted over the past 6 years. As depicted in **Figure 3**, the research has notably highlighted the putative role of PHGDH in cancer development.

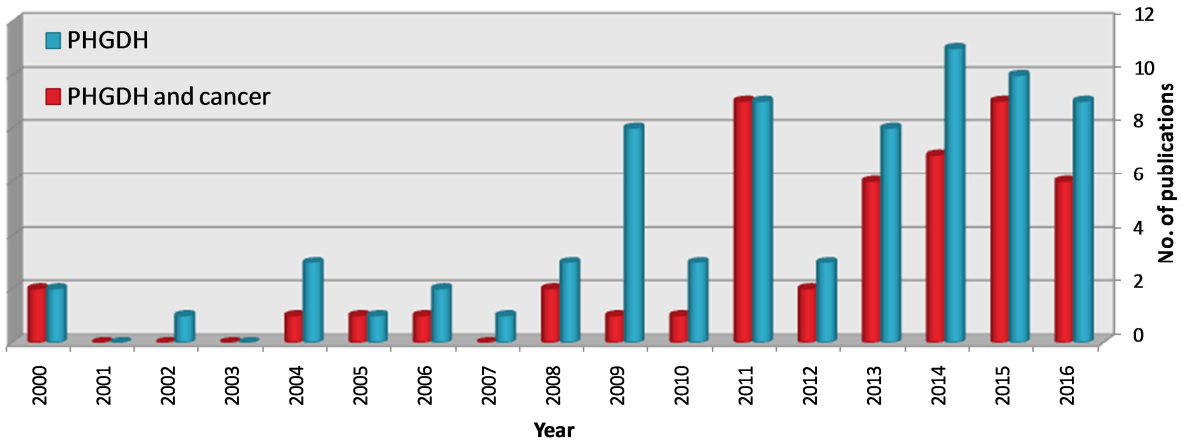

***Figure 3**: PHGDH-related publications since 2000. Data were collected from Scopus.*

2.2.1. Implication of PHGDH in cancer cells

In the 1980s, Snell and coworkers discussed the role of PHGDH in tumorigenic cells.[13] They highlighted the elevation of PHGDH activity in rat hepatomas (1.7 to 10.6 times higher relative to control livers). Despite these encouraging results, studies of human PHGDH only reemerged in 2011 in breast and melanoma cancers and several publications extended the purported role of PHGDH to other cancers.

Breast cancer. A negative-selection RNAi screening using a human breast cancer xenograft model at an orthotopic site in mouse was developed by Possemato *et al*. in 2011 for

identifying novel cancer targets.[4] This method highlighted *PHGDH* as a gene required for *in vivo* tumorigenesis. Moreover, it was determined that this gene is localized in a genomic region of recurrent copy number gain in breast cancer. Subsequently, it was demonstrated that PHGDH protein level is elevated in 70% of ER-negative breast cancers. Zhou and co-workers confirmed this observation in 2013, but suggested that PHGDH is dispensable for the growth and maintenance of tumors *in vivo*.[27] The expression of SSP enzymes was evaluated in six different subtypes of triple negative breast cancer (TNBC) (basal-like, molecular apocrine, claudin-low, immune-related, mixed, and null), and it was shown that the most abundantly expressed SSP enzymes in basal-like TNBC tissues was PHGDH.[28] Furthermore, the study revealed that the expression levels of PHGDH were inversely correlated with clinical prognostic factors. Finally, a recent study highlighted that PHGDH is required for breast cancer progression.[22]

Melanoma. An analysis of human cancers showed that *PHGDH* is recurrently amplified in a genomic region of focal copy number gain most commonly found in melanoma.[5] This type of cancer had the highest frequency of *PHGDH* amplification across a large panel of cancers. Knockdown of PHGDH selectively inhibited the growth of melanoma cells that exhibit PHGDH amplification *versus* those that lack this amplification.[29]

Colon cancer. As shown by Yoon and coworkers in 2015, the expression of PHGDH was significantly higher in colonic tumor tissue than paired normal tissue.[30] The prognostic significance of PHGDH in colorectal cancer was further investigated in 2016 with the work of Jia *et al*. which suggest that evaluation of PHGDH expression could be useful in identifying a high-risk subgroup of colorectal cancer.[31] More precisely, the results demonstrated that high PHGDH protein expression was correlated with advanced TNM stage, larger tumor size and poor outcomes in colorectal cancer patients.

Glioma. In 2013, PHGDH levels were analyzed in tissues from glioma patients and it was shown that PHGDH was highly expressed in astrocytic tumors and increasingly expressed in more aggressive cancer types.[32] Moreover, the suppression of PHGDH in glioma cells

downregulated the expression of multiple factors such as VEGF or MMP-2. Such suppression also reduced glioma cell proliferation, invasion and tumorigenicity *in vitro* and *in vivo*.

Nasopharyngeal carcinoma. Pathological and advanced clinical stages of nasopharyngeal carcinoma (NPC) are often associated with the Epstein-Barr virus. Recently, it was demonstrated that this virus encodes many miRNAs, such as EBV-miR-BART1, that regulate tumour metastasis by regulating PTEN-dependent pathways.[33] The comparison of gene expression profiles between EBV-miR-BART1-expressing NPC cells and the control cells highlighted an upregulation of PHGDH and several other enzymes in EBV-miR-BART1-expressing NPC cells.[34] Thus, these results suggest a novel role of EBV-miR-BART1 in cancer metabolism which remains to be elucidated.

Cervical adenocarcinoma. The expression of PHGDH was evaluated in a subset of cervical adenocarcinoma samples (n = 54) by immunohistochemistry and the results showed an increased PHGDH expression in cervical adenocarcinoma that could be linked with tumor size and prognosis.[35] It was also demonstrated that the *in vitro* suppression of PHGDH expression inhibited the cell proliferation and increased the sensitivity toward cisplatin chemotherapy. Moreover, it was shown that the *in vivo* PHGDH knockdown decreased the tumorigenesis.

Lung cancer. As described above (*Section 2.3.*), the SSP enzymes were upregulated by the expression of p73 in human lung adenocarcinomas.[20] An analysis of a large panel of NSCLC cell lines also revealed that NRF2 controls the expression of the *PHGDH* gene and that the expression of this gene confers poor prognosis in human NSCLC.[16]

Thyroid cancer. A GC-MS analysis was used to investigate metabolomic alterations in papillary thyroid carcinomas (PTC, the most common type of thyroid cancer).[36] Several metabolic enzymes, such as PHGDH and the glucose-6-phosphate dehydrogenase, were found to be significantly increased in PTC. This dysregulated expression of PHGDH was recently confirmed by the work of Sun and coworkers. More precisely, they detailed that the expression of PHGDH was different among thyroid cancer subtypes and that the PHGDH

expression level was higher in poorly differentiated carcinomas or PTC and lowest in medullary carcinomas.[37] Moreover, they showed that a B-Raf V600E mutation was associated with a higher rate of PHGDH expression compared to non-mutant cases in PTC.

Leukemia. A proteomic study revealed that glutamine withdrawal induced the upregulation of PHGDH in leukemia cells contributing to cell survival and relapse post-treatment.[38] In this study, an increase in oxidative stress upon inhibition of glutamine metabolism was identified as the trigger of the upregulation of PHGDH. Interestingly, PHGDH silencing and also the use of a serine-free diet inhibited leukemia cell growth, thereby identifying serine as a key pro-survival actor that needs to be considered to sensitize leukemia cells to glutamine-targeting modalities.

Gastric cancer. In 2016, Xian and colleagues have reported an overexpression of PHGDH (mRNA and enzyme) in cancerous gastric tissues.[39] This expression can be correlated with the histological type, the tumor stage, the preoperative carcinoembryonic antigen and inversely correlated with the 5-year survival rate. PHGDH thus appeared as an independent prognostic factor in gastric cancer.

Lung cancer. Strengthening the link between PHGDH overexpression and the associated weak prognosis in human non-small-cell lung carcinoma (NSCLC), Zhu reported an increase in PHGDH (gene and enzyme) levels in these particular cancer lines.[40] Furthermore, high PHGDH expression could be correlated with a reduced 5-year overall survival and TNM stage making PHGDH an independent prognostic factor in this type of cancer. Interestingly, PHGDH overexpression was also observed in aggressive SCLC and was defined as markers of a lower survival rate.[41]

Glioma. Following previous demonstration of PHGDH overexpression in glioma, Branzoli reported the link between a lower expression and better prognosis in this cancer. Indeed, gliomas showing 1p/19q co-deletion in chromosome arm demonstrated a 40 to 50% lower PHGDH expression and an improve response to treatments.[42] These results suggested that the expression of PHGDH is partly controlled by these chromosomes and that this co-deletion makes the glioma lineages less invasive and more susceptible to treatment.

Pancreatic cancer. Recently, PHGDH overexpression was documented in cancerous pancreatic tissues as compared to healthy ones. This expression is further associated with tumor size, lymph node metastasis, and TNM factors, making PHGDH an independent prognostic marker.[43] Moreover, PHGDH silencing in pancreatic cancer was reported to inhibit cell proliferation, migration and invasion by downregulating the expression of cyclins B1 and D1, matrix metalloproteinase-2 and 9 (MMP-2, MMP-9). Interestingly, Ma also reported that, in pancreatic cells, PHGDH is also able to interact with the translation initiation factors eIF4A1 and eIF4E in order to increase the expression of proteins necessary for tumor growth.[44]

Thalamus tumor. Metabolic enzymes profiling, conducted by Linzey and colleagues on childhood oligodendroglioma, revealed the existence of a fusion protein between epidermal growth factor receptor 3 (EGFR3) and PHGDH. The result suggested that this fusion protein can be used as a prognostic factor for child thalamus tumors.[45]

Table 1. *Overiew of PHGDH expression in cancer cells and some associated parameters*

Cancer	Status	Model	Correlated with
Gastric[39]	Overexpression and genomic amplification	Human	Tumor stage and preoperative carcinoembryonic antigen
Lung adenocarcinoma[40,41]	Overexpression	Human	Poor prognostic
Glioma[32]	Overexpression	Human	Aggressiveness
Pancreatic[43,44]	Overexpression	Human	Tumor size, lymph node metastasis, and TNM factors
Thalamus[45]	Fusion with EGFR3	Human	n.d.
Breast[4,27,28]	Overexpression and genomic amplification	Human	Inversely correlated with clinical prognostic factors
Melanoma[5]	Genomic amplification	Human	n.d.

Thyroid carcinoma[36,37]	Overexpression	Human	n.d.
Leukemia[38]	Overexpression	Human	Cell survival and relapse post-treatment
Nasopharyngeal carcinoma[33,34]	Overexpression	Human	n.d.
Cervical adenocarcinoma[35]	Overexpression	Human	Tumor size and prognosis

All these studies provide the proof-of-concept that PHGDH is a very attractive drug target in a large subset of cancers. Before describing the reported PHGDH inhibitors, we will discuss the expression, the function, and the structure of PHGDH.

2.2.2 Expression of PHGDH

The study conducted by Cho and coworkers in 2000 highlighted two transcripts corresponding to PHGDH mRNA in human normal tissues.[46] The dominant transcript (2.1kb) was expressed in prostate, testis, ovary, brain, liver, kidney, and pancreas, and weakly expressed in thymus, colon, and heart. The same distribution was observed for the minor transcript (710bp), but it was more significant than the dominant transcript in heart and skeletal muscle. As described above, several studies highlighted that the expression of PHGDH at a high level is a hallmark of many cancer cells. A recent study nuances this observation and shows that overexpression of PHGDH is not particularly associated with the malignancy, but rather with the cell lineage.[47] However, it was demonstrated that PHGDH is expressed in two major protein variants (α and β different in 3 kDa in size) and that the ratio of expression between these two variants was associated with malignancy, β variant being associated with cancer invasion. Unfortunately, the nature of the two variants was not determined in this study.

2.2.3. Functions of PHGDH in tumorigenesis

PHGDH catalyzes the reversible conversion of 3-PG to 3-PPyr utilizing NAD^+ as a cofactor. Under standard conditions, the reaction thermodynamically favors the direction from 3-PPyr to 3-PG, while in cells overexpressing the SSP, the reaction is driven toward 3-PPyr due to its consumption by downstream pathway reactions. In addition, it was recently demonstrated

that PHGDH catalyzes NADH-dependent reduction of *α*-ketoglutarate to the oncometabolite D-2-hydroxyglutarate (D-2HG).[48] D-2HG is normally produced in large amounts by isocitrate dehydrogenase mutants in glioma,[49] acute myeloid leukemia (AML)[50] or breast cancer[51] and is sufficient to induce cancer transformation by impacting protein and DNA covalent modifications such as methylation. Thus, *PHGDH* amplification or PHGDH overexpression could potentially influence cell physiology by overproduction of D-2HG. However, it is unlikely that this mechanism directly promotes tumorigenesis, because PHGDH is not a major source of D-2HG.[48] Moreover, a recent study reported that PHGDH is a novel binding partner of the forkhead box protein M1 (FOXM1) in glioma.[32] This protein is commonly overexpressed in many types of human cancer. It is also intimately involved in tumorigenesis because it participates in tumor initiation, growth, and progression, as well as in migration and invasion.[52] By interacting with FOXM1, PHGDH prevents its degradation by the proteasome and therefore reinforces its oncogenic effects.

Interestingly, PHGDH can play a key role in the control of autophagy and apoptosis. A decrease in intracellular serine concentration leads to the production of 1-deoxysphingosine (doxSA), an unusual molecular species of sphingolipid, presumably by serine palmitoyl-CoA transferase (SPT) using l-Ala instead of l-Ser. This abnormal concentration of doxSA is responsible for the activation of p38 mitogen-activated protein kinases (p38 MAPK) which induces the expression of cyclin-dependent kinase inhibitor 1a (CdKn1a; p21).[53] PHGDH, through serine production, plays also a role in the growth and the invasion of glioma, thanks to the racemisation of the l-serine in d-serine by the serine racemase (SR), an enzyme overexpressed in glial cells and neurons. D-serine plays the role of co-agonist at forebrain *N*-methyl-D-aspartate receptors (NMDAR) and promotes aberrant growth through stimulation of these receptors.[54]

In parallel to these effects, the use of serine as a means to fight oxidative stress through the synthesis of conventional antioxidants (GSH, NADPH), is no longer to demonstrate.[10] Among other utilities in cancer development, this oxidative stress response can promote metastatic invasion.[55] Indeed, under hypoxic conditions, HIF will induce the expression of PHGDH to produce more NADPH and fight cell apoptosis. This phenomenon will lead, in breast cancer cells, to an increase in the formation of breast cancer stem cells (BCSCs) responsible for metastases and high mortality.[56] Moreover, the recent work of Shiota on

oxidative balance has highlighted that NADH and GSH are not the only antioxidants produced through PHGDH activation.[57] Hypotaurine (HT) is also produced thanks to this metabolic enzyme. GSH and HT synthesis requires cysteine and is strongly dependent on xCT/CD44 complex that helps this amino acid incorporation from the extracellular space. However, while the synthesis of GSH is strongly impacted by CD44-knockdown conditions, HT cellular concentration is not affected thanks to SSP enzymes upregulation, especially PHGDH, driving glycolysis-dependent activation of serine/glycine-cleavage systems to provide one-methyl group for HT synthesis.

Finally, it was recently reported than PHGDH also allows to limit cancer cell differentiation, leading to a better resistance against classical therapies. Indeed, Sharif's work has demonstrated that a deficiency of PHGDH in embryonic carcinoma stem-like cells (CSLC) leads to a degradation of Oct4 (stemness promoting factors) and an increase in the stability of the differentiation factor B3-tubulin.[58]

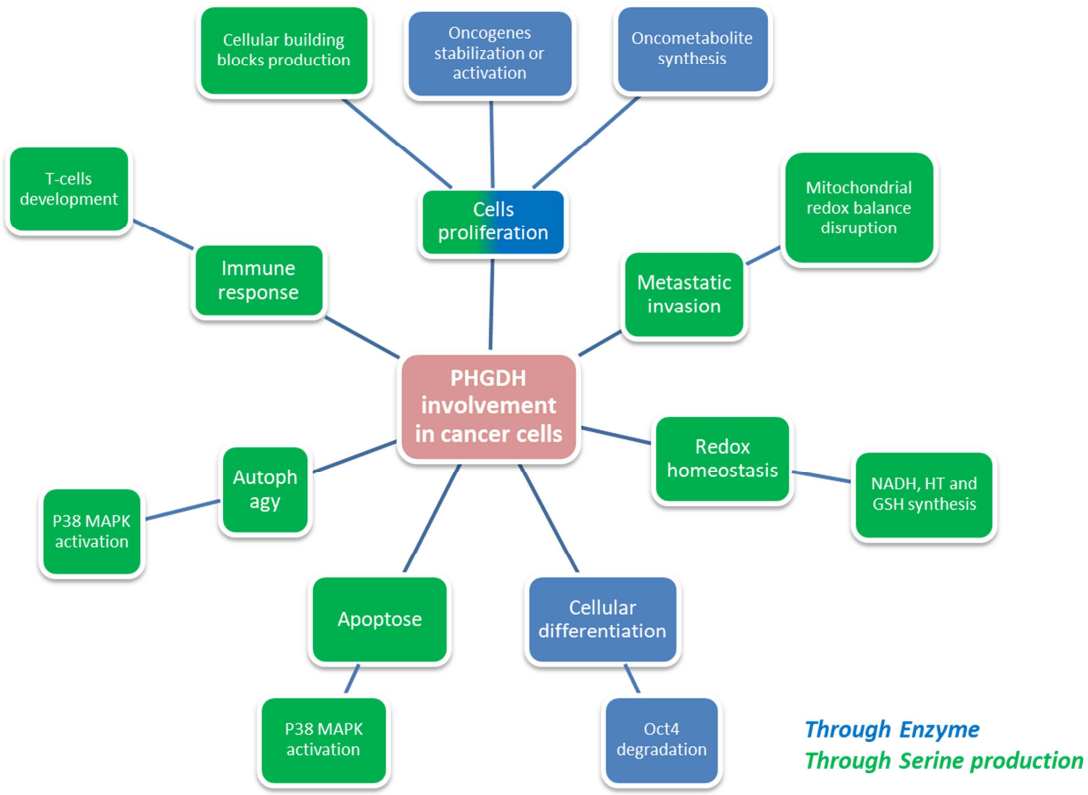

Figure 4: *Overview of PHGDH involvement in cellular processes that could contribute to cancer cells resistance, development and proliferation.*

2.2.4. Structure of PHGDH

The nucleotide sequence of human *PHGDH* gene, encoding the first SSP enzyme, was determined by Cho *et al.* in 2000.[46] The *PHGDH* gene has a predicted 533 amino acid open reading frame, encoding a 56.8 kDa protein. Three types of PHGDH were observed and referred to as types I, II and III. These three types differ in their size and domain composition. Human PHGDH enzymes belong to the type I and present several domains (**Figure 5**). The substrate and the nucleotide binding domains at the amino terminal part play a function in the binding of substrates and catalysis. The regulatory part at the carboxy terminal extremity contains two domains, the ACT (Aspartate kinase-Chorismate mutase-TyrA) domain and the ASB (allosteric substrate binding) domain. The ACT domain is a regulatory domain where l-Serine binds to drive a negative feedback while the ASB domain impairs additional level of allosteric control. Type II enzymes (*E. coli*, *S. cerevisiae* and *Neurospora*) are lacking the ASB domain whereas type III (Entamoebe histalytica) are composed of only the substrate and the nucleotide binding domains.

Human PHGDH belongs to the type I PHGDH enzymes like *M. tuberculosis*, chicken, rat or rabbit PHGDH. Thus, like these enzymes, the human PHGDH is predicted to function as a tetramer. However, the only available human PHGDH structure (PDB 2G76) is crystallized as a dimer, probably because the crystallized truncated protein lacks the C-terminal domains that are involved in inter-subunit interfaces. More detailed structural information would aid in understanding the oligomerization state of PHGDH.

In human PHGDH, the active site is constituted by the substrate binding domain and the nucleotide domain. It is lined by several loop regions of first monomer Arg54–Val59, Ala76-Val83, Asn97-Gly101, Gly152-Leu153, Asp175-Ile178, His206-Leu216, Cys234-Val240, Asp260-Asp269, Cys281-Ser287 and one loop of the second monomer Trp133'-Lys136' (**Figure 5a**).

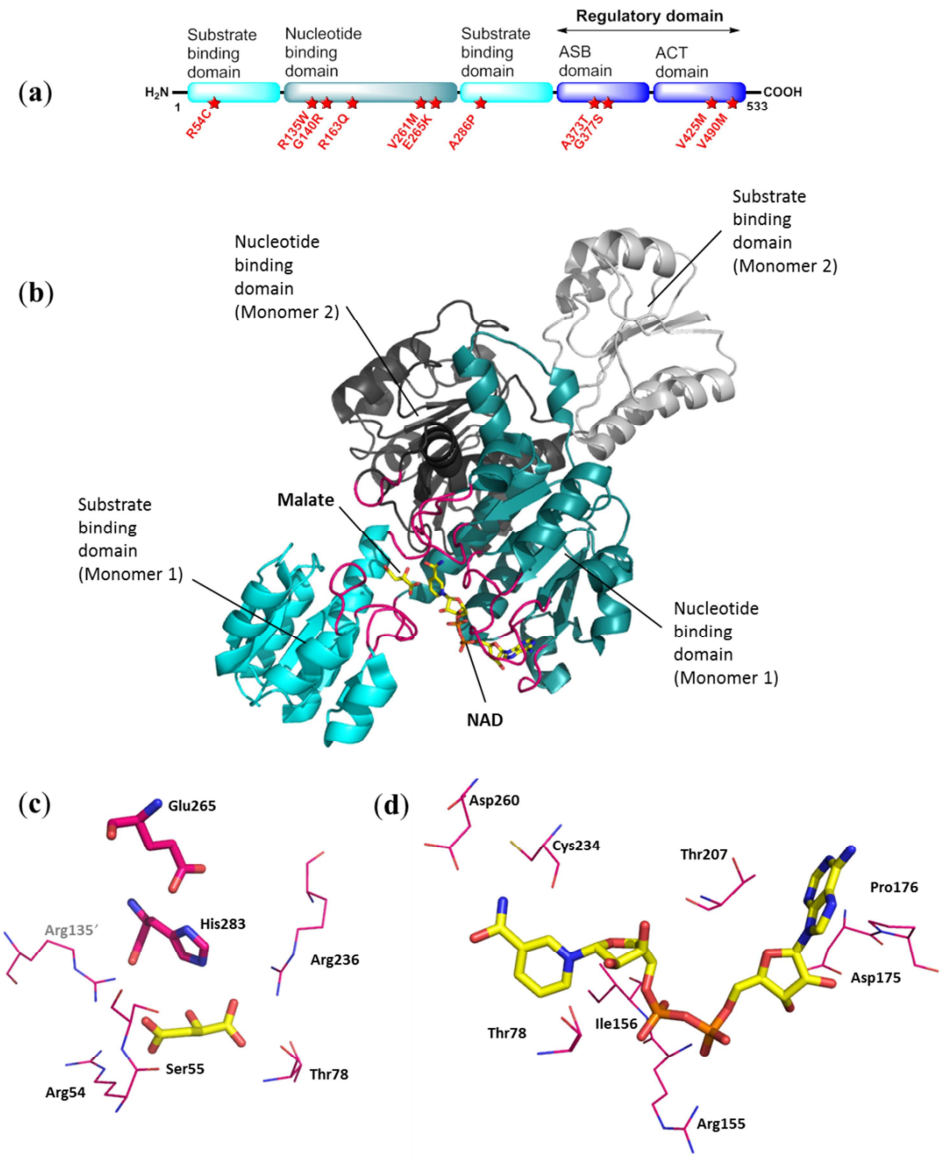

***Figure 5**: (**a**) Linear structure of PHGDH. The positions of PHGDH mutations are indicated in red. (**b**) Human PGDH active site. Malate (substrate analog) and NAD are represented in yellow sticks. The first monomer and the second monomer are represented in cyan and grey, respectively. The nucleotide and substrate binding domains of each monomer are represented in dark and light color, respectively. The figure shows the loops bordering the active site of human PHGDH in pink. (**c**) Interaction of malate with the human PHGDH active site. The figure shows all residues involved in the malate interaction with human PHGDH structure. The key residues His283-Glu265 is represented in sticks. Residues associated with the second monomer are labeled with a "prime" designation. (**d**) Interaction of NAD with the human PHGDH active site. The figure shows only residues involved in the NAD interaction with human PHGDH structure.*

As depicted in **Figure 5c**, the side chains of the basic residues are predominantly oriented toward the active site for binding to the negatively charged substrate. In the 2G76 structure, the carboxylate moiety of substrate analog (malate) forms hydrogens bonds with Arg54 and Ser55 and with Arg135' from the second monomer. The hydroxyl group of malate is pointing toward His283. The second carboxylate group interacts with the crucial residue Arg236 and with Thr78 of the first monomer. Unlike the substrate analog, the NAD interacts only with the first monomer (**Figure 5c**). It interacts more precisely with the Rossmann fold motif commonly found in dehydrogenases that bind NAD^+/NADH as a cofactor.[59] The adenine ring of the cofactor is placed in a hydrophobic pocket made of Pro176 and Thr207. The carboxylate group of the Asp175 in the Rossmann fold forms hydrogen bonds with the hydroxyl groups of the adenosine ribose. Both NAD phosphate groups interact with the main chain amides of Arg155 and Ile156. At last, the ribose sugar forms hydrogen bonds with residues Thr78 and Thr207 while the amide of nicotinamide moiety forms hydrogen bonds with Asp260 as well as the main chain carbonyl of Cys234. The nucleotide binding site is relatively accessible while the substrate binding site is deeper.

2.2.5. Mutations of PHGDH disturb its function

Mutations in SSP enzymes (PHGDH, PSAT or PSPH) cause drastic reduction in the serine concentration in cerebrospinal fluid and serum. This low concentration of serine drives severe neurodevelopmental disorders such as microcephaly, psychomotor retardation and intractable seizures.[60,61] Here, we describe several reported mutations of PHGDH that disturb its function (**Figure 5a**).

The first missense mutations were described at the beginning of the 2000's. Klomp and coworkers suggested that V425M and V490M mutations reduce the enzymatic activity, while Pind and coworkers proposed that a V490M mutation reduces the enzymatic stability.[62,63] It is currently unclear how these mutations in the carboxy-terminal domain affect the PHGDH function. As described above, the Arg135' residue interacts with the tail of malate (**Figure 5b**). Thus, the R135W substitution, reported by Tabatabaie *et al*., would eliminate one of the salt bridges and weaken the overall electrostatic attraction.[64] In the same paper, the authors highlighted four other mutations, one frameshift mutation and three missense mutations (V261M, A373T and G377S). It was demonstrated that the reported missense mutations did

not affect the protein stability or expression but they affect the PHGDH activity. Exome sequencing revealed two other missense mutations (G140R and R163Q) in *PHGDH*.[65] Gly140 and Arg163 residues are localized within the NAD binding domain at the PHGDH dimer interface that is crucial for the optimal function of PHGDH. Substitution of Gly140 by an arginine residue causes steric clash and introduces positive charge at the dimer interface, which would most likely weaken the dimerization by steric hindrance and electrostatic repulsion from two nearby positively charged residues (Lys289 and Arg230). Arg163 participates in a water-coordinated hydrogen-bonding and salt bridge network at the dimerization interface. Therefore, the substitution of arginine by a glutamine residue disturbs the oligomerization state. Three supplementary *PHGDH* missense mutations were recently identified (E265K, R54C and A286P).[66] Through a modeling and 3D-structural analysis, all three residues (Arg54, Glu265, and Ala286) are predicted to be in close proximity to the substrate binding site. Substitution of these residues causes steric clashes with the side chains of neighboring residues and disrupts therefore the substrate binding.[66]

2.2.6. PHGDH inhibitors structural requirements

Due to the physiology of the blood brain barrier, the delivery of L-serine to the central nervous system (CNS) is insufficient. Thus, *de novo* synthesis of serine in the CNS is essential to supply the amino acid required in the brain, and thereby to provide necessary precursors for multiple metabolic pathways such as biosynthesis of neurotransmitters.[60] Based on this observation, a PHGDH inhibitor (or a SSP enzyme inhibitor) must not interfere with serine homeostasis in the CNS, to avoid potential neurological side effects. Thus, designed PHGDH inhibitors must not cross the blood-brain barrier. To compensate the serine deficiency in the peripheral system, exogenous serine supplement might be dosed along with the inhibitor.

To design competitive PHGDH inhibitors that are competitive *versus* other NAD-dependent dehydrogenases, the inhibitor must ideally possess one or several negatively charged groups to interact with the basic side chains of the substrate binding site (Arg54, Arg236 and Arg135') (**Figure 6**). In addition, the molecule should be relatively small to fit in the substrate pocket measuring approximately 10-12Å. The incorporation of a stereogenic center might also be favorable for the design of inhibitors of PHGDH. Indeed, a sequence alignment of active site residues of D-specific dehydrogenases showed that PHGDH shares a

high sequence homology with several members of this family, such as formate dehydrogenase.[67] Thus, like these enzymes, PHGDH is specific for substrates with a D-configuration. Finally, to pick up additional interactions or to enhance physiochemical properties, molecules can be extended into the large NAD pocket (20-22Å).

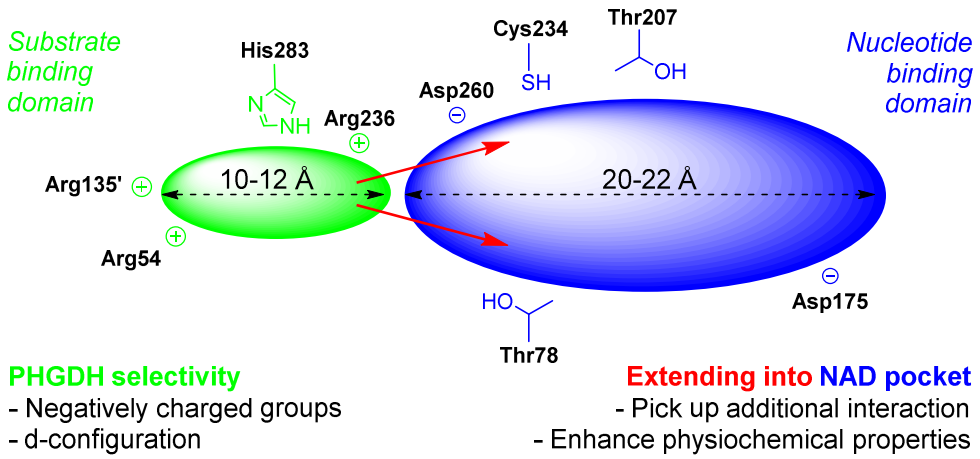

***Figure 6**: PHGDH inhibitors structural requirements. Residues associated with the second monomer are labeled with a "prime" designation.*

2.2.7. Reported PHGDH inhibitors

Several small molecule inhibitors of PHGDH were reported since December 2015. In this section, we will detail the efforts made by three distinct research groups in identifying these inhibitors.

2.2.7.1. NAD competitive inhibitors

*Indole derivative **2.1**.* To discover PHGDH inhibitors, the group of AstraZeneca opted for a Fragment-Based Lead Discovery (FBLD) approach that provided a structurally simple fragment, which was subsequently evolved.[68] A fragment screen, performed by crystallography, provided multiple fragments that bind the adenine region of the NAD binding site. These simple ligands were then grown in multiple vectors to improve their potency and optimized to allow the identification of a potent PHGDH inhibitor (**Figure 7**). This indole derivative **2.1** exhibit a Kd measured by Surface Plasmon Resonance (SPR) of 0.18 µM, a FLINT IC_{50} of 1.4 µM and a good physicochemical profile (Log D < -1; cLogP = 1.1;

solubility = 973 µM).[69] The co-crystal structure of compound **2.1** in the binding pocket of PHGDH highlighted key interactions. For example, the right part of the molecule (indole scaffold) interacts with the NAD binding site while the carboxylate group at the left part interacts with the Arg236 in the 3-PG pocket.

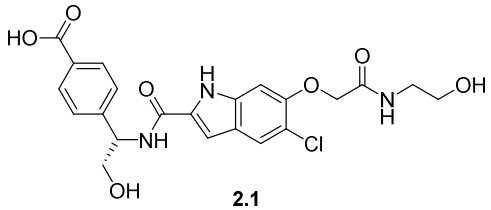

2.1
SPR Kd = 0.18 µM
FLINT IC_{50} = 1.4 µM

Figure 7*: Structure of PHGDH inhibitor* ***2.1*** *developed by AstraZeneca through a FBLD approach.*

Following the pioneering work of Astra Zeneca, other groups were interested in the development of NAD-competitive PHGDH inhibitors. Although the high cellular concentration of NAD (millimolar concentration) remains a challenge in the development of potent NAD-competitive inhibitors, the various compounds that have been reported so far exhibit interesting *in vitro* potencies.

AstraZeneca analogue ***2.4****.* Mullarky *et al.* initially characterized the mode of action of the indole derivative **2.1** reported earlier by Astra Zeneca with the aim to discover more potent compounds.[70] The reversible and competitive profile in this series was confirmed following competition experiments as well as the crystallography. Their analysis particularly revealed the important role of a hydrogen bond between the amide of **2.2** and the carboxylate function of Asp175. The importance of the lipophilicity of the indole skeleton was also highlighted. Mapping of the essential interactions led to the development of a novel indole analogue with improved PHGDH inhibition such as for instance compound **2.3** comprising an oxetane function and characterized by a PHGDH inhibitory potency of 15 nM that is more than 10-fold improvement compared to that of the parent compound. Compound **2.3** also demonstrated a reduction of serine synthesis in cell-based settings. Finally, although **2.3** was shown to act in a NAD-competitive manner, it also exhibits a good selectivity towards PHGDH compared to a small library of other dehydrogenases. A prodrug strategy was applied by the authors in order to further increase the cellular efficiency of compound **2.3**.

This esterified prodrug (**2.4**) showed a micromolar inhibitor potency of *de novo* serine synthesis and slowed the proliferation of PHGDH-dependent tumor lineage (Carney cells). Unfortunately, despite these interesting biological results, the lack of plasma stability of this prodrug did not allowed its use *in vivo*.

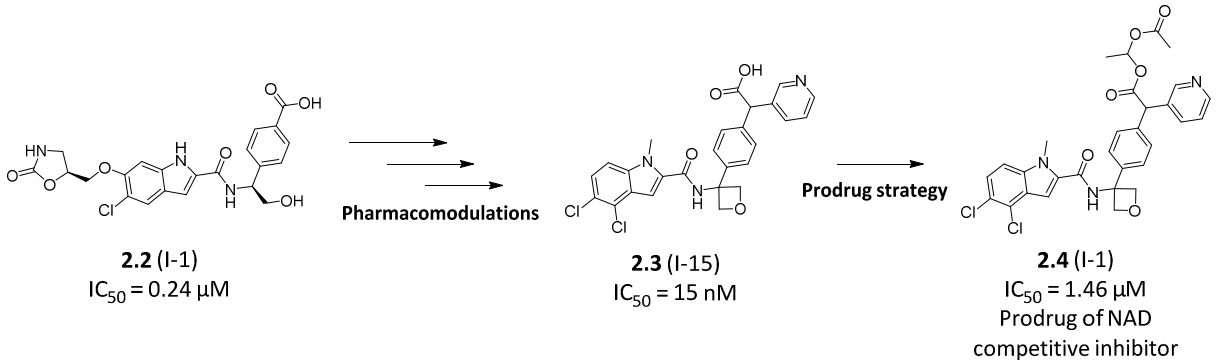

Figure 8: *Strategy followed by Mullarky et al. to obtain NAD competitive inhibitors.*

*Boehringer indole derivative **2.8**.* Using a combined strategy of high throughput screening (HTS) and fragment-based screening (FBS) the team of Weinstabl at Boehringer reported the discovery of very similar indole-based analogues as those initially reported by Astra Zeneca and further optimized by Mullarky.[71] HTS strategy succeeded in identifying the promising hit compound **2.5** whereas FBS, using biophysical methods such as STD, NMR and MST, led to the discovery of the pyrazole hit compound **2.6.** Based on the X-ray crystal structures of each compound with PHGDH, a convergent approach followed by different pharmacomodulations led to compound **2.7**. This compound exhibits a 3nM PHGDH inhibitory potency, was confirmed as a NAD-competitive inhibitor, with a high selectivity for PHGDH compared to other dehydrogenases. In addition, it is characterized by excellent microsomal stability. A prodrug strategy was also preconized to increase cell-permeability leading to the esterified analogue **2.8** which was shown to significantly inhibit *de novo* serine synthesis in several cell models. Unfortunately, as for the compounds developed in Cantley's lab, the weak plasma stability of this compound did not allow its use *in vivo*.

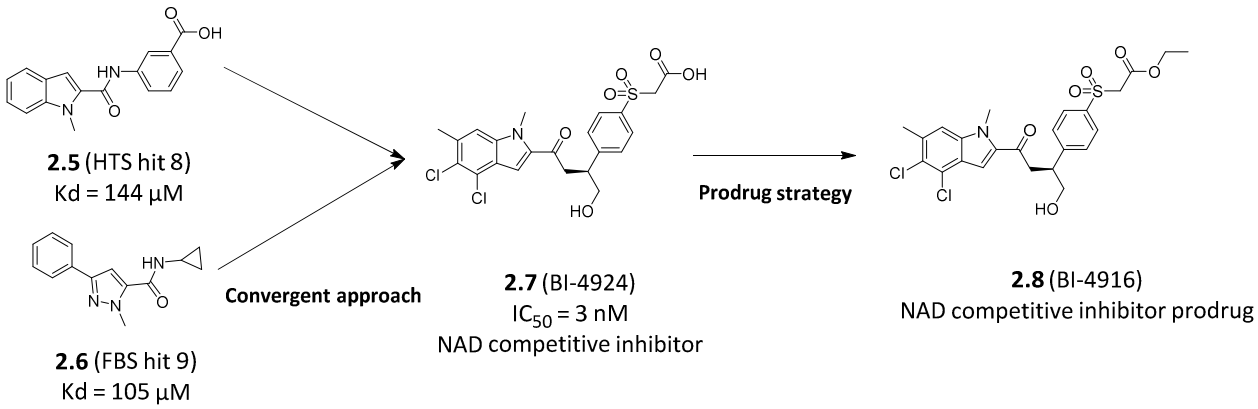

Figure 9: *Strategy followed by Weinstabl et al. to obtain* ***2.8*** *(BI-4916)*

Fragments ***2.9-15.*** Recently, another FBLD approach was reported by the group of N. Curtin.[72] This group screened a library of 600 fragments (CRT Cambridge, UK) against PHGDH using a differential scanning fluorimetry (DSF) assay. Thus, it identified 42 fragments as hits and 15 of them were further investigated in an ITC competition assessment. The ITC assay identified 13 fragments that bind to the NAD^+ binding site and present relatively similar K_d in the milimolar range (a set of the most potent fragments is illustrated in the **Figure 10**). These fragments provide promising starting points for the design of PHGDH inhibitors.

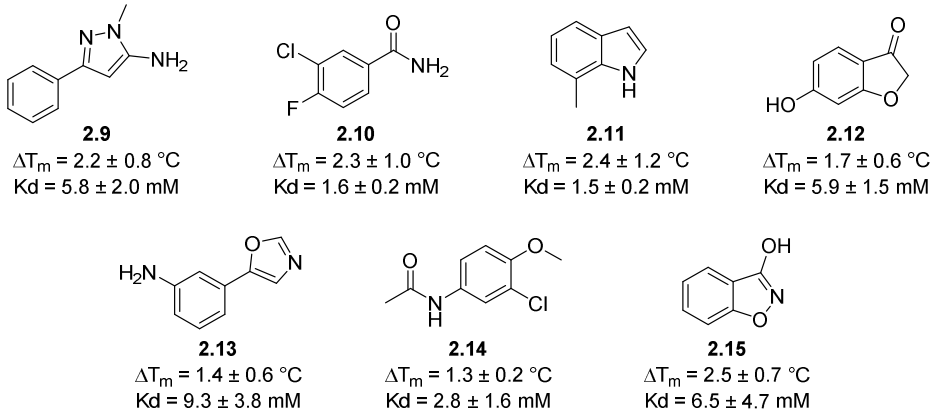

Figure 10*: Structure of the most potent fragments identified by the group of N. Curtin.*

2.2.7.2. Non-competitive inhibitors

Compound ***2.16*** *(CBR-5884)*. Mullarky and coworkers screened a library of 800,000 small molecules using a high-throughput in vitro PHGDH assay.[73] The group identified 408 hits including seven that were selective for PHGDH versus other NAD^+-dependent dehydrogenases (four of them are represented in **Figure 11**). Most of these inhibitors, like

the approved drug disulfiram, target sulfhydryl groups and can react with a PHGDH cysteine residue.

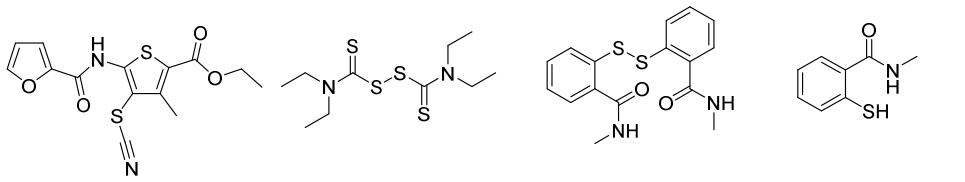

***Figure 11**: Structures of PHGDH inhibitors reported by Mullarky et al.*

The group further investigated the compound **2.16** that shows an IC_{50} value of 33 µM. Via a gas chromatography mass-spectrometry, the authors showed that the molecule **2.16** specifically inhibits de novo serine synthesis by 30%. In addition, they demonstrated that compound **2.16** was able to inhibit cell proliferation in cancer cell lines that overexpress PHGDH and that the compound had no effect on cancer cells that did not overexpress the enzyme. Cellular viability assays revealed that the inhibitor was not cytotoxic at concentrations up to 40 µM. The mechanism by which the molecule **2.16** inhibits PHGDH was then determined. Inhibition constants (K_i) for each substrate (3-PG and NAD) were determined and revealed that compound **2.16** inhibited PHGDH in a noncompetitive mode. Moreover, it was demonstrated that inhibitor **2.16** was progressively more potent with increasing preincubation time (IC_{50} of 7 µM when drug and enzyme were preincubated for 4 h). Based on these results, the authors proposed the following hypothesis: *the noncompetitive binding mode and the time-dependent onset of inhibition suggest that the inhibitor might be interacting with an allosteric site*. To validate this hypothesis, the authors demonstrated that inhibitor **2.16** affects the PHGDH oligomerization state, using a cross-linked analysis. It was reported that the inhibitor shifted the PHGDH equilibrium from the tetrameric to the dimeric state. Despite these encouraging results, the poor stability of the inhibitor **2.16** in mouse plasma limited its *in vivo* evaluation. Thus, medicinal chemistry-based optimization is required before this probe can become an effective therapeutic.

*Compound **2.24** (NCT-503)*. Like the group of Mullarky, Pacold and coworkers opted for a HTS approach to discover PHGDH inhibitors.[74,75] They screened 400,000-compounds of the

NIH molecular libraries small molecule repository (MLSMR) library and identified PHGDH inhibitors containing a piperazine-1-thioamide scaffold. To improve the potency of these inhibitors, a small set of molecules was synthesized (**Table 2**).

***Table 2**. SARs of PHGDH inhibitors reported by Pacold et al.*

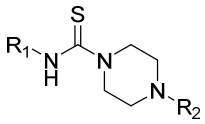

Code	R_1	R_2	PHGDH IC_{50}
2.20	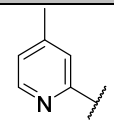	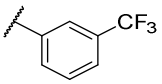	15.3 µM
2.21	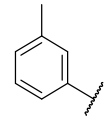	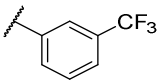	> 57 µM
2.22	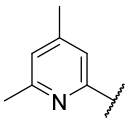	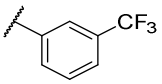	6.5 µM
2.23 (NCT-502)	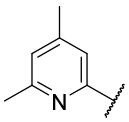	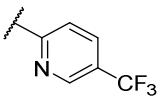	3.7 µM
2.24 (NCT-503)	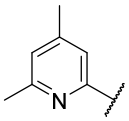	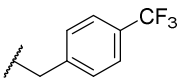	2.5 µM
2.25	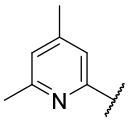	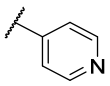	> 57 µM

Replacement of the 4-methyl-pyridine of compound **2.20** by a 3-methylphenyl moiety (**2.21**) resulted in loss of activity, while the addition of a methyl group to C6 (**2.22**) gave an improvement of potency. Then, replacement of the 3-trifluoromethyl group of compound **2.22** by a pyridine (**2.25**) considerably decreases the activity while inhibitor **2.23** (NCT-502)

showed an improvement in potency. Finally, incorporation of an *N*-benzyl group was also well tolerated, as depicted in inhibitor **2.24**. Two potent inhibitors of this study (**2.23** and **2.24**) were inactive against several other dehydrogenases, and showed minimal cross-reactivity in a large panel of GPCRs. Competition and rapid dilution studies revealed a noncompetitive binding mode with respect to the both substrates (3-PG and NAD) and a reversible inhibition for the compound **2.24**. This mechanism of action, similar to that of **2.16**, supports the presence of an allosteric site in PHGDH. Thus, as performed by Mullarky *et al*., it would be interesting to determine whether the molecule **2.24** can affect the PHGDH oligomerization state. Finally, the authors showed that the inhibitor **2.24** was less effective on the C234S PHGDH mutant (Cys234 is localized in the NAD binding site, **Figure 5C**). Subsequently, cell-based assays showed that PHGDH inhibitors exhibit interesting anticancer activity against PHGDH-dependent cell lines but no effect on PHGDH-independent cell lines. In addition, bookkeeping of carbons from ^{13}C-labeled serine and glucose demonstrated surprisingly that PHGDH inhibitors affect serine biosynthesis from glucose as well as the incorporation of carbons from both extracellular and intracellular serine into nucleotides.

*Pyrazole-5-carboxamide derivatives (**2.26-40**)*. A recent patent highlighted small molecule inhibitors of PHGDH.[76] Unfortunately, no information is available on the design of these compounds. The general structure of these inhibitors and one example of the identified hit are highlighted in the **Figure 12**.

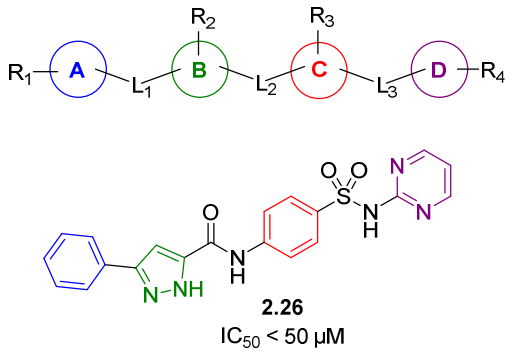

***Figure 12**: General structure of compounds related to the patent WO2016/040449A1 and structure of compound **2.26** (one of the identified inhibitors).*

Several inhibitors disclosed in the patent WO2016/040449A1, and their reported IC_{50} values on full-length PHGDH are described in the **Table 2**. As shown, the *ortho* substitution of the part A (blue) by a hydroxyl (**2.27**), a methoxy (**2.28**) or a fluorine atom (**2.29**) was well tolerated (IC_{50} < 50 µM). However, incorporation of a carboxylic acid (**2.30**) or an amino moiety in *ortho* position of the aromatic A decreased the PHGDH inhibition (IC_{50} > 100 µM). The pyrazolo group of compound **2.26** seems to be very important because the modulation by an isoxazole lowered the affinity for PHGDH as illustrated with compounds **2.33** and **2.34**. Nevertheless, the amino-substitution of pyrazolo group was tolerated by a small moiety (CH_3, **2.35**) but no by a bulkier group (phenyl, **2.36**). As illustrated with inhibitor **2.37**, cyclisation of the amido linker (L_2) and the part C decreased the PHGDH inhibition. Like the pyrazolo group, the sulfamide (L_3) seems to be essential. Indeed, its methylation (**2.38** and **2.39**) reduced the affinity for PHGDH. In addition, its substitution by the terminal aromatic part D was crucial, as shown by the IC_{50} values of inhibitors **2.40** and **2.41**. Finally, modulation of the pyrimidino group (part D) by a pyridine (**2.42** and **2.43**), a furane (**2.44**) or a morpholino moiety (**2.45**) was unfavorable, while the methylation (**2.46**) or di-methylation (**2.47**) of the pyrimidino group was tolerated.

***Table 3**. SARs of PHGDH inhibitors reported in the patent WO2016/040449A1. IC_{50} values: A, < 50 µM; B, 50-100 µM; C, > 100 µM. nd: not determined.*

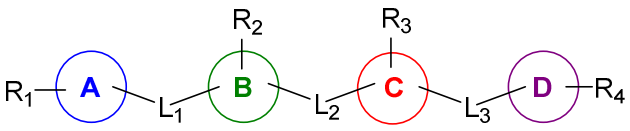

Code	A-L_1-B-	-L_2-C-	-L_3-	-D	PHGDH IC_{50}
2.26	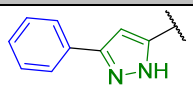	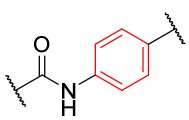	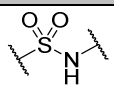	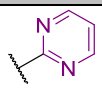	A
2.27 **(I-81)**	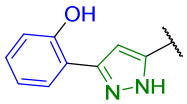		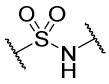		A

2.28 **(I-36)**	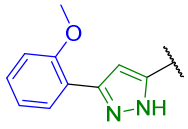	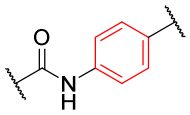	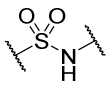		A
2.29 **(I-35)**	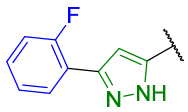	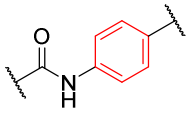	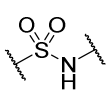		A
2.30 **(I-74)**	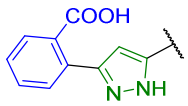	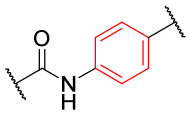	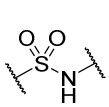	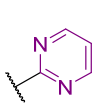	C
2.31 **(I-75)**	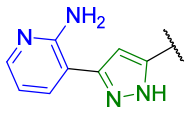	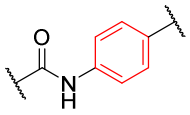	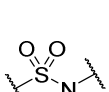		C
2.32 **(I-19)**	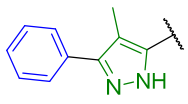	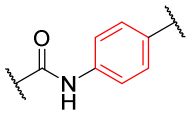	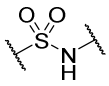		C
2.33 **(I-34)**	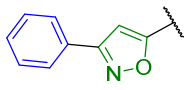	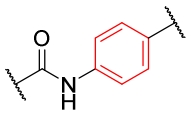	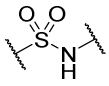		C
2.34 **(I-72)**	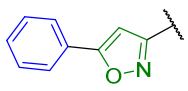	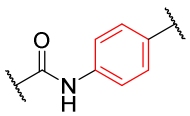	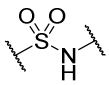		C
2.35 **(I-76)**	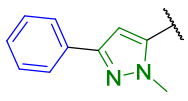	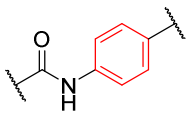	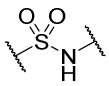		A
2.36 **(I-49)**	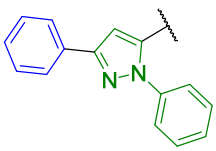	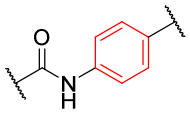	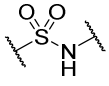		C
2.37 **(I-65)**	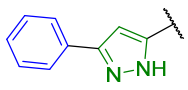	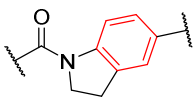	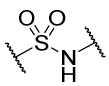		C

2.38 **(I-47)**	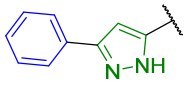	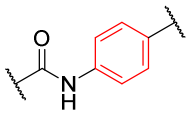	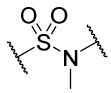		C
2.39 **(I-63)**	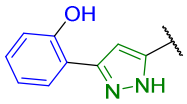	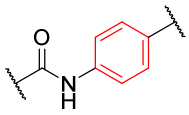	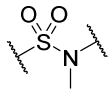		C
2.40 **(I-12)**	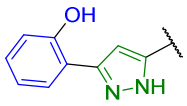	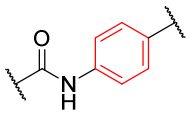	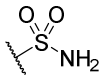	-	C
2.41 **(I-55)**	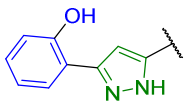	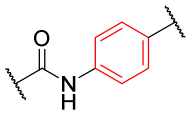	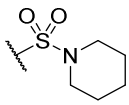	-	C
2.42 **(I-38)**	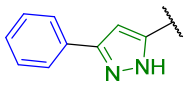	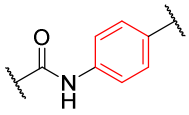	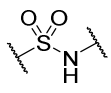		B
2.43 **(I-37)**	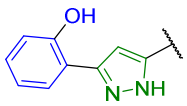	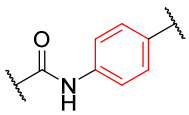	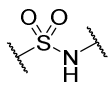		C
2.44 **(I-4)**	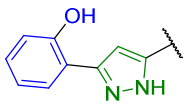	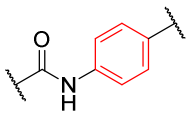	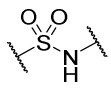	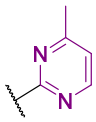	A
2.45 **(I-73)**	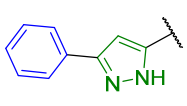	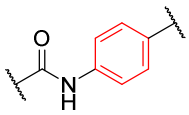	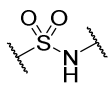	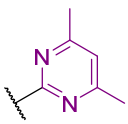	A
2.46 **(I-45)**	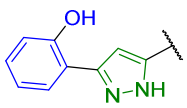	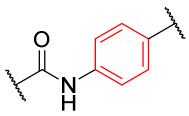	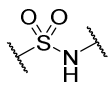	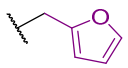	C
2.47 **(I-46)**	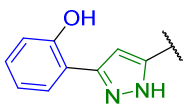	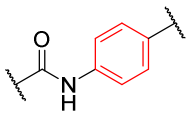	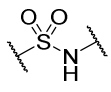	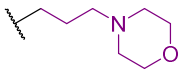	C

*Acyl-hydrazones **2.48** and **2.49**.* In 2016, two allosteric sites on PHGDH were computationally identified by Wang and co-workers using a cavity prediction algorithm.[77] The first (I), sharing at least 5 amino acids with the enzyme active site (Gly 78, Val 79, Asp 80, Asn 81 and Val 82), is located at the interface of the enzyme active site and the Rossman fold, whereas the second (II), smaller, was identified in the substrate binding cavity. Virtual screening experiments at these allosteric sites led to the identification of 98 compounds among which 2 compounds, **2.48** (PKUMDL-WQ-2201) and **2.49** (PKUMDL-WQ-2101) were shown to strongly bind PHGDH by surface plasmon resonance (SPR) experiments. Competition experiments as well as site-directed mutagenesis confirmed the interactions between **2.49** and site I as well as **2.48** with site 2. In addition, cellular assays demonstrated the ability of these two molecules to selectively reduce the proliferation of cancer lines overexpressing PHGDH as well as their potential to significantly reduce intracellular serine and glycine flux. Interestingly, these two inhibitors were also documented to reduce *in vivo* the growth of tumors overexpressing PHGDH.

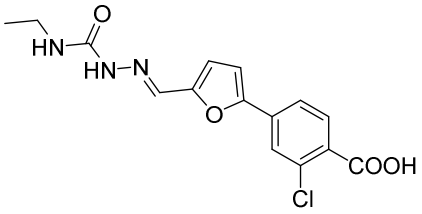

2.48 (PKUMDL-WQ-2201)
IC_{50} = 35.7 μM
Allosteric inhibitor

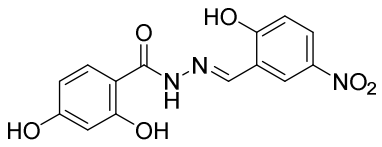

2.49 (PKUMDL-WQ-2101)
IC_{50} = 34.8 μM
Allosteric inhibitor

***Figure 13:** Structures of allosteric inhibitors reported by Wang et al.*

*Compound **2.50** (Azacocone E).* Following the screening of a library of 600 natural compounds using a fluorescent enzymatic assay, Guo and co-workers identified azacocones C and E (**2.50**) as PHGDH inhibitors with inhibitory potency in the micromolar range without affecting other NAD^+-dependent enzymes such as for instance IDH1.[78] Further microscale thermophoresis (MST) and cellular engagement (CETSA) experiments confirmed the binding of these two compounds with PHGDH. The inhibition profile of **2.50** was investigated, and a non-competitive mechanism-of-action regarding the two substrates (3PG and NAD^+) together with time-dependent inhibition was revealed. Interestingly, the compounds were shown to bind at an allosteric site distant from the substrate binding sites notably via two

crucial hydrogen bonds with the arginines 118 and 134. Compound **2.50** demonstrated a promising inhibition of cell proliferation of PHGDH overexpressing lines that was correlated with apoptosis induction. As tumor lines with low PHGDH were not affected, the *in cellulo* selectivity of this compound could also be demonstrated.

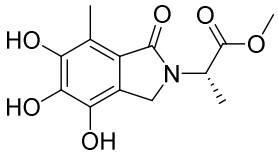

2.50 (Azacoccone E)
IC_{50} = 9.8 µM
Non competitive inhibitor

Figure 14: *Structure of* ***2.50*** *(Azacocone E) inhibitor reported by Guo et al.*

Compound ***2.51*** *(Ixocarpalactone A).* Similarly to the group of Guo, Zheng *et al.* screened a natural compounds library using an isolated enzyme assay to discover new PHGDH inhibitors. This screening identified **2.51**, a withanolide derivative from Physalis ixocarpa as a potent compound. Binding to the target was subsequently confirmed using MST experiments and competition assays demonstrated a non-competitive mode of action with respect to both substrates. Investigation of the mode-of-action of this compound, using a computer-based homology model of the full-length human PHGDH, suggested a new allosteric site located near the active site. It appears that **2.51** would present key steric interactions with the Val301, Pro331 and Ile333 residues and hydrogen bonds with Gln302, Asp305, Thr313 and Pro327 delineating this cavity. Cell-based assays revealed that the compound is not toxic for healthy cells but induce apoptosis of PHGDH-dependent tumor lines. Compound **2.51** was also shown to inhibit tumor proliferation in vivo.

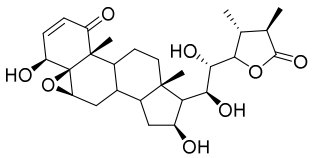

2.51 (Ixocarpalactone A)
IC_{50} = 1.66 µM
Non competitive inhibitor

Figure 15: *Structure of* ***2.51*** *(Ixocarpalactone) as PHGDH inhibitor.*

2.2.8. Overview of identified sites of action on PHGDH

In summary, having a deeper look in the development of more potent PHGDH inhibitors, the most challenging step is the formal identification of new sites of action. However, the highlighting of these areas will allow a rational pharmacomodulation during the investigation of original chemical series.

Due to the lack of full-length human PHGDH structure, a homology model was designed according to the structure of M. tuberculosis PHGDH (1YGY), which was predicted as the closest resembling structure, in order to vizualize the different sites able to regulate PHGDH activity.

Interestingly, this complete vision of PHGDH allows to perceive the great structural diversity of the identified sites but also the diversity of their location on the protein.

In addition to the classical dehydrogenase active site (Rossman fold), no less than 4 new allosteric sites controlling PHGDH activity were discovered in the past three years (**Figure 16**), paving the way for the discovery of potent inhibitors. Indeed, allosteric inhibition could lead to more selective molecules that have not to deal with high intracellular concentration of NAD unlike orthosteric inhibitors. This partly explains why orthosteric inhibitors of PHGDH, although demonstrating greater affinity for the target, have reduced efficacy in more complex biological models, particularly *in vivo*.

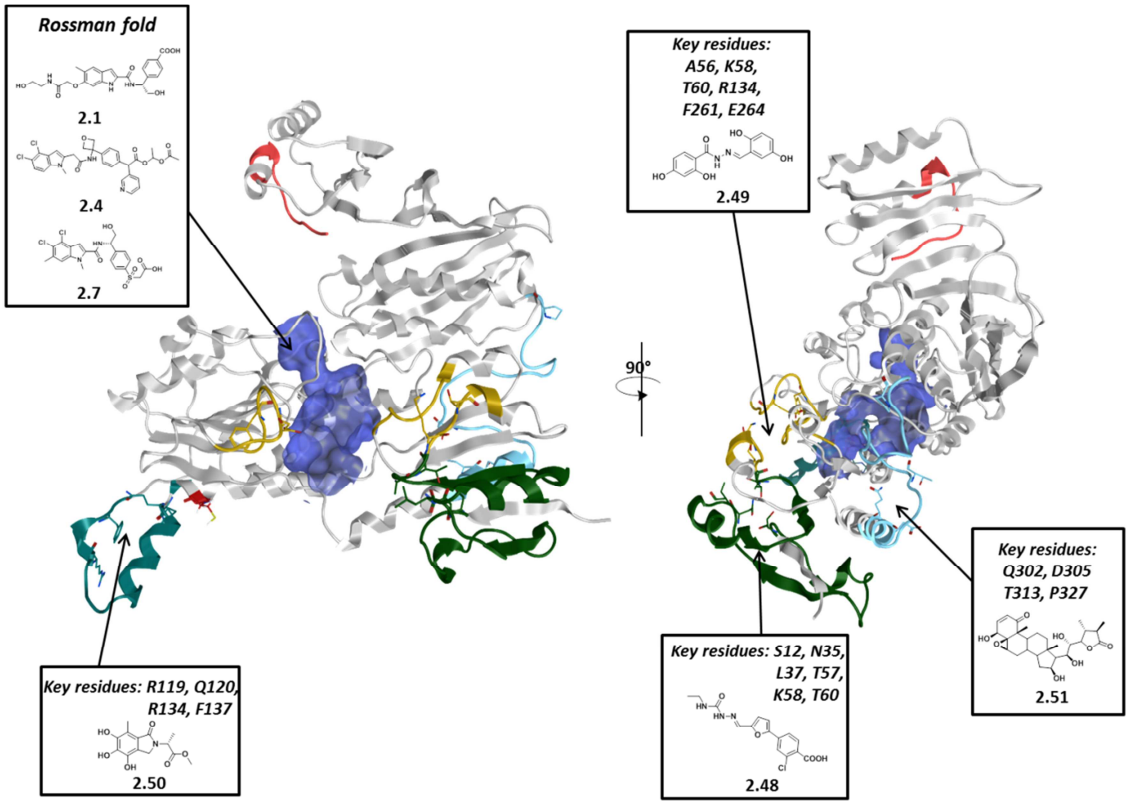

Figure 16: *Homology model of human full length PHGDH (MOE software) with highlight of all inhibitors binding sites and key residues identified so far. Rossman fold and NAD competitive inhibitors (**2.1**, **2.4** and **2.7**) in blue. Allosteric site and related inhibitor **2.48** identified by Wang et al. in green. Allosteric site and related inhibitor **2.49** identified by Wang et al. in yellow. Allosteric site and related inhibitor **2.50** identified by Guo et al. in mint green. Allosteric site and related inhibitor **2.51** identified by Zheng et al. in cyan.*

3. Objectives and strategy

3. Objectives and strategy

3.1. OBJECTIVES

Although the interest in PHGDH is relatively recent, previous studies have demonstrated the crucial importance of this enzyme in many biological phenomena and particularly in cancer. As detailed in the **Introduction**, PHGDH is overexpressed in many cancer cell lines by genomic amplification and/or activation by different transcription factors (ATF4, c-Myc, ...). Interestingly, this overexpression is often linked to a low survival rate and a high aggressiveness. In addition, the proliferative advantages conferred by PHGDH seem to be linked to a multitude of factors such as allowing resistance to oxidative stress and providing the basic components necessary for cell growth. Despite the validation of this enzyme as a target in the development of new anti-cancer therapies targeting tumor metabolism, research on its inhibition by small chemicals has only started very recently. Hence, no inhibitors of PHGDH were reported at the beginning of this work.

As medicinal chemists, we are interested in the identification and optimization of new chemical series able to control the activity of therapeutic targets and, in my case, particularly ones involved in cancer development.

The objective of this thesis is the discovery and the optimization of new PHGDH inhibitors (Figure 1) which could be used as starting point to develop new potent anticancer therapies targeting PHGDH. To reach this goal, PHGDH inhibitors will be identified, chemically optimized and tested in different biological systems. In order to improve their inhibitory properties, their mechanism of action will be detailed thanks to mutagenesis and mass spectrometry experiments. Subsequently, the inhibitors will be used to study the SSP in more complex models to give a better understanding of its role in tumor growth.

3.2. WORK PLAN

The first part of this thesis will consist in the production and purification of PHGDH and the development of a robust enzymatic assay in order to analyze the dehydrogenase activity. This starting point will allow the development of a screening assay using different chemical

libraries. In order to reach efficiently our main objective, these libraries will consist of molecules presenting the greatest structural diversity and the better pharmaceutical properties (solubility, chemical stability…). On one hand, these molecules will come from a commercial library (Prestwick) of low molecular weight molecules (LMW) derived from approved drugs (FDA, EMA and other agencies) and selected by medicinal chemists and pharmacists. On the other hand, we will benefit from the years of expertise of our laboratory by the selection a series of original in-house molecules initially developed for other therapeutic purposes. The results of this screening will be presented in **Chapter 5**.

Thereafter, we will study in detail the different hits identified during the screening. More specifically, we will clearly identify the mode of action of these inhibitors as well as their site of action with the protein. That will help the rational design of more effective molecules on PHGDH. This part of the work will include pharmacomodulation as well as photo-affinity labeling studies. Briefly, a complete investigation on the structure activity relationships (SARs) of the most potent series will be realized in order to highlight the crucial functionalities leading to PHGDH inhibition (**Chapter 6**). In **Chapter 7**, we will be particularly focused on the design of a diazirine probe but also on the development of an MS method able to characterize the inhibitor-protein interaction.

In parallel with these different mechanistic studies, *in cellulo* activities of these compounds will be discussed throughout the manuscript. The development of cellular assays to investigate the selectivity of our compounds towards PHGDH but also their cytotoxicity on normal cell lines will be presented in **Chapters 5, 7 and 8**. We will also explore the biochemical effects of these inhibitors on cell metabolites and try to correlate these effects with cell death. These results will ultimately pave the way for an *in vivo* evaluation of the optimized compounds in order to validate our research strategy.

Finally, the last part of this work will focus on disulfiram, a molecule currently on the market to treat severe forms of alcoholism. As this molecule has demonstrated promising anti-cancer properties, **Chapter 8** will focus on the study of its mode of action on PHGDH as well as its *in cellulo* efficacy in cell lines overexpressing PHGDH. This study should reinforce the interest of this type of compound for anti-cancer therapies targeting cancer metabolism and reinforce repurposing of disulfiram in cancer.

This thesis strategy is depicted schematically in **Figure 17**.

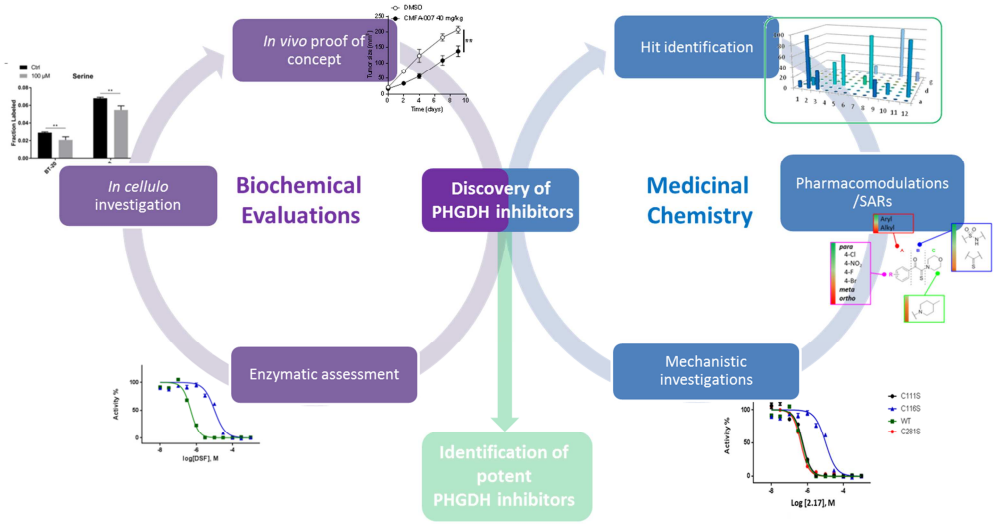

Figure 17: *Key points of the discovery process*

Results

This section is divided in 5 Chapters:

Results

4. Enzymes production

5. α-Ketothioamide derivatives: a promising tool to interrogate phosphoglycerate dehydrogenase (PHGDH)

6. α-ketothioamide SARs based on in vitro PHGDH inhibition

7. Probing the binding site of PHGDH inhibitors using Diazirine photocrosslinking

8. Anti-alcohol abuse drug disulfiram inhibits human PHGDH via disruption of its active tetrameric form through a specific cysteine oxidation

4. Enzymes production

The evaluation and characterization of new PHGDH inhibitors initially required to set up a PHGDH enzymatic assay. During the course of this thesis, diffetent set up were investigated, from the use of PHGDH alone, to the use of the three enzymes of the SSP, PHGDH, PSAT1 and PSPH together with the use of diaphorase. In its final version, and for reasons that will be notably discussed later in the manuscript, the assay that we preconized includes the four enzymes (**Figure 18**).

In summary, this assay allows the direct measurement of the fluorescence produced by the resarufin/resasurine couple upon PHGDH activity. PSAT-1 and PSPH were included in order to mimic the entire serine synthetic pathway and limit the retro-conversion of 3-PPyr to 3-PG by PHGDH (consumption of the product of the reaction 3-PPyr). A complete overview of the development of this assay as well as the various issues encounter will be detailed in **Chapter 9**.

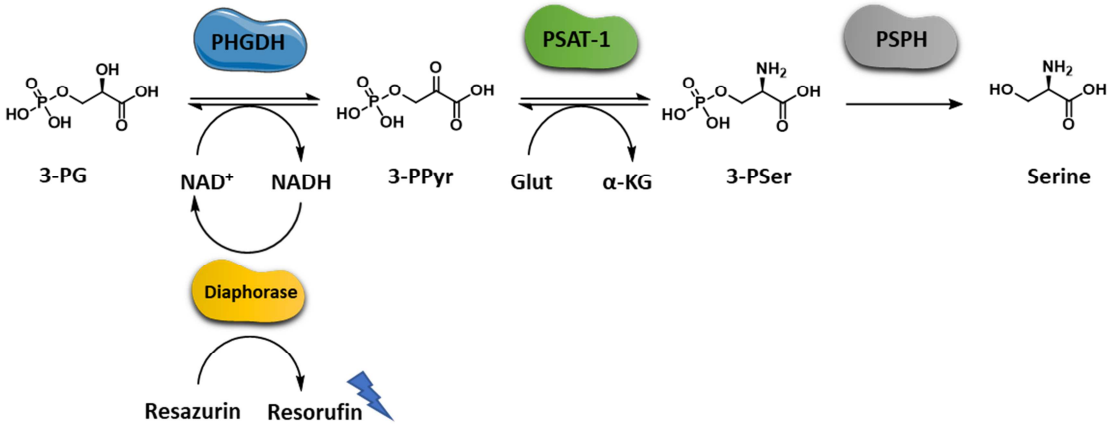

Figure 18: *Overview of the complete enzymatic assay used during this thesis*

This section will focus on the process developed to experimentally produce and purify two enzymes of this assay (PHGDH and PSAT-1) as well as in the characterization of the enzymes obtained. Diaphorase (USBiological) was from commercial source whereas PSPH (UNamur) was kindly supplied by our collaborator on this project.

4.1. WT, MUTATED AND TRUNCATED PHGDH

Intially, at the beginning of this thesis, the PHGDH enzyme was directly purchased from BPS Bioscience. However, because of reproducibility issues with the supplied enzyme from batch to batch, we also developed our own prodruction of PHGDH. The general production protocol, depicted in **Figure 19**, was used for the production of the different forms of PHGDH required throughout our research, that is the wild-type PHGDH, mutated variants (C111S, C116S and C281S, **Chapter 8**) and a truncated version of PHGDH (lacking the 10 final C-terminal amino acids: tr-PHGDH, **Chapter 7**).

Briefly, Rosetta II strain (mutated BL21) were transfected with a plasmid encoding for a N-terminal His-Tagged version of PHGDH and incorporating kanamycin resistance. All the different plasmids presented within this thesis came from a commercial supplier (Addgene for WT PHGDH and Genecust for mutated versions). The transformation of Rosetta II is followed by a selection on agar using two antibiotics (CAM and KAN). The bacteria are then cultivated in large volumes before induction by addition of IPTG. Once the induction is complete, lysis and centrifugation allowed to obtain a solution containing all the soluble proteins extracted from these bacteria. The purification of this lysate is then carried out using HisTrap columns having a strong affinity towards the polyhistidine chain. After complete elution with imidazole, the various fractions are dialyzed, submitted to a purity assessment by SDS-Page and finally stored at -80 ° C.

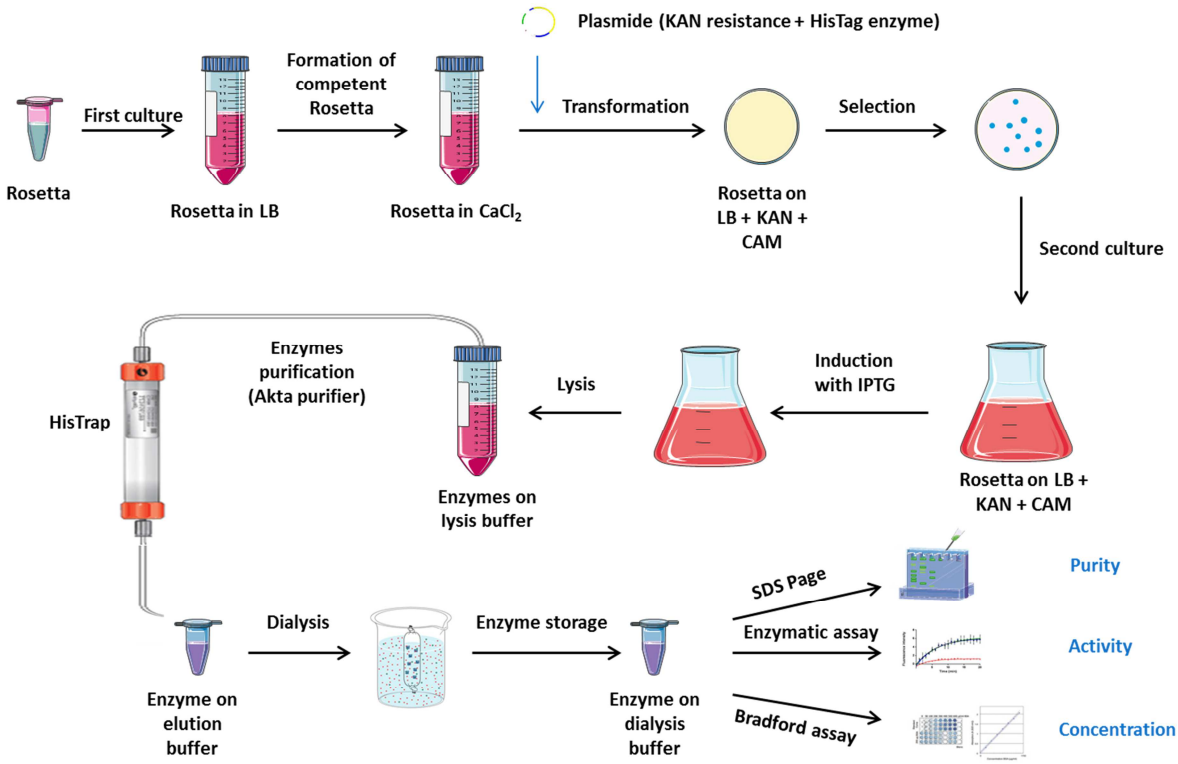

Figure 19: *Overview of the classical production process for PHGDH*

Several parameters were optimized during the production process (**Table 4**). Firstly, the temperature during induction was adapted in order to offer a compromise between the appearance of inclusion bodies at high temperatures and the maximization of production efficiency. Concomitantly, the culture medium was also chosen to maximize the amount of enzyme produced. Indeed, Terrific broth (TB), present the major advantage over the Lysogeny broth (LB) to reduce the medium acidification during bacterial growth. Finally, it appeared that PHGDH was very sensitive to oxidation, showing an enzymatic activity greatly reduced if stored in a solution without reducing agents. Various reducing agents were studied in order to solve this problem. It was found that the use of tris (2-carboxyethyl) phosphine (TCEP) was preferred over other reducing agents like 2-mercaptoethanol (*β*-ME) and dithiothreitol (DTT) because they had reduced stability over time.

Table 4. *Summary of the tested conditions (selected conditions in bold)*

Parameters	Tested conditions
Temperature	16, 18, 20, **24**, 37 (°C)
Culture medium	LB, **TB**
Reducing agent	DTT, *β*-ME, **TCEP**

All these optimizations allowed to significantly modifying the enzyme yield during the productions, ranging from 1.5 mg of PHGDH per liter of culture to more than 120 mg.

In addition to their purity, all the enzymes obtained have subsequently been characterized (**Table 5**).

Table 5. *Summary of K_m values obtained for some representative productions*

Enzymes	3-PG K_m (experimental)	NAD^+ K_m (experimental)	3-PG K_m (reported)[48]	NAD^+ K_m (reported)[48]
WT PHGDH	294.3 ± 12.4 µM	30.4 ± 4.3 µM	260 µM	22 µM
C111S PHGDH	198.5 ± 22.5 µM	25.3 ± 2.8 µM	n.d.	n.d.
C116S PHGDH	232.8 ± 7.8 µM	28.4 ± 5.6 µM	n.d.	n.d.
C281S PHGDH	283.2 ± 16.4 µM	18.4 ± 4.9 µM	n.d.	n.d.
Tr-PHGDH	169.7 ± 11.9 µM	12.8 ± 3.1 µM	n.d.	n.d.

In fact, various issues encountered during the evaluation of our inhibitors raised the question regarding the correct folding of these different enzymes. Unfortunately, the use of a TYCO apparatus (NanoTemper) only allowed very recently to notice a significant modification between the denaturation temperature of productions coming from the same plasmid (55-65°C). Theses changes seem to indicate a relatively high variability in the protein folding, thus making even more difficult the experimental validation of new inhibitors of PHGDH. A detail discussion regarding this issue can be found in **Chapter 9**.

4.2. PSAT-1 PRODUCTION

The protocol used to produce this enzyme is identical to the optimized protocol for PHGDH. It allowed to obtain a large amount of PSAT-1 with K_m values in accordance with data from the literature (**Table 6**).

Table 6. *Summary of Km values obtained for PSAT-1*

Enzymes	**3-PSer K_m (experimental)**	**α-KG K_m (experimental)**	**3-PSer K_m (reported)**[79]	**α-KG K_m (reported)**[80]
WT PSAT-1	25.1 ± 5.3 µM	35 ± 4.2 µM	5 µM	800 µM

5. α-Ketothioamide derivatives: a promising tool to interrogate phosphoglycerate dehydrogenase (PHGDH)

This chapter is based on the following publication: Ravez, S., Corbet, C., Spillier, Q., Dutu, A., Robin, A. D., Mullarky, E., Cantley, L.C, Feron, O., Frédérick, R. (2017). Journal of Medicinal Chemistry, 60(4), 1591–1597.

Q.S. perfomed the enzymatic screening and the chemical syntheses.

Graphical Abstract

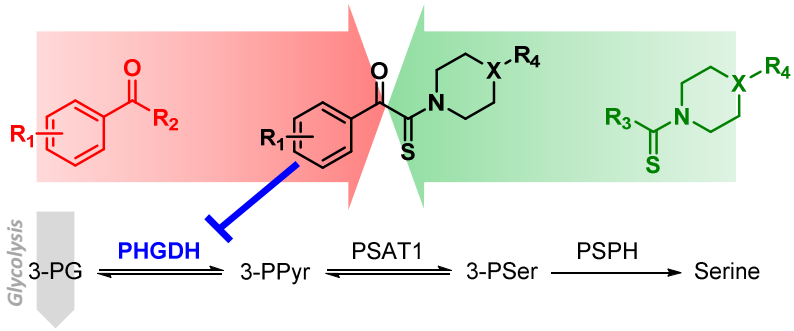

5.1. INTRODUCTION

In this chapter, we will first detail the development and validation of a straightforward enzymatic assay suitable for high-throughput screening. This assay will be used to investigate different libraries of small molecules. Then, the mode of action of a specific inhibitor, identified through a convergent pharmacophore approach, and its pharmacomodulation will be detailed. Finally, we will study the ability of these compounds to inhibit the activity of the enzyme in cell-based models.

5.2. RESULTS AND DISCUSSION

5.2.1. Enzymatic assay development.

Prior to screening the compound library, we initially optimize a robust quantitative enzymatic assay that is based on PHGDH activity. More precisely, PHGDH oxidizes 3-PG to 3-PPyr with NAD^+ as the electron acceptor to yield NADH. The formation of 3-PPyr is therefore directly correlated with the NADH formation and the enzymatic activity of PHGDH can be monitored by following the fluorescence intensity (excitation wavelength 340 nm; emission wavelength 460 nm). After optimization of the assay (**Fig. S1)**, we have undertaken the process of hit identification.

5.2.2. Primary screening.

As described in **Fig. 20**, the primary screening was carried out on a compound library of 336 molecules from a fragment library and an in-house compound collection at high concentration (100 µM). Commercial fragments (**5.1-4)** were purchased from Prestwik Chemical™, and most of them are derived from actual drugs following smart fragmentation. The in-house collection was composed by original molecules (**5.5-15**) showing a large structural diversity.

Of the 336 samples initially screened, 29 compounds (8.6%) exhibited an inhibitory effect and among them, 15 molecules (4.5%) decreased PHGDH activity by greater than 50%. Among them, two molecules were quinone derivatives (**5.1** and **5.15**). It was well known that quinones represent a class of toxicological compounds which can promote a variety of side effects *in vivo*, including acute cytotoxicity, immunotoxicity, and carcinogenesis.[81] For this

reason, these three molecules were not selected for the optimization process. The screening also highlighted promising fragments like **5.6** that will be the subject of further optimization studies.

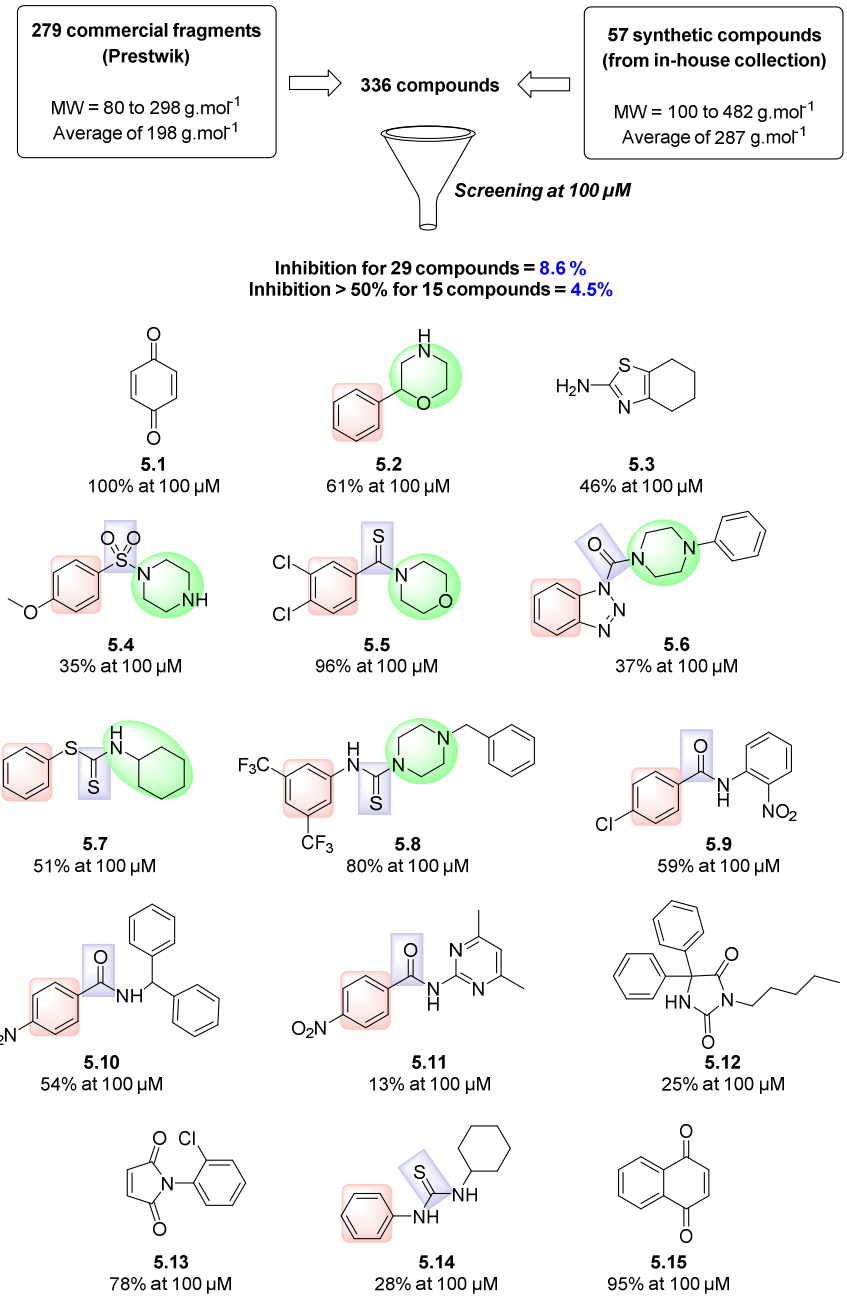

Figure 20: *Process of hit identification. Fisrt general scaffold of PHGDH inhibitor with aromatic ring in red, linker in blue and cyclic amine in green. PHGDH inhibition percentage at 100 µM is represented under each identified hit.*

As highlighted in **Fig. 20**, the screening also highlighted several inhibitors that present common structural groups. For example, several compounds contain a nitrogen moiety such as morpholine, piperazine or cyclohexamine that is often attached to a thiocarbonyl (**5.5-8,5.14**). This observation is consistent with the recent results of Pacold *et al*. that highlighted PHGDH inhibitors containing a piperazine-1-carbothioamide scaffold (See compound **2.24**).[74] Four other compounds (**5.9**-**12**) showed an acetophenone part attached to a bulky group such as aniline, biphenylmethylamine or aminopyrimidine.

5.2.3. PHGDH inhibitors design.

Based on the primary screening, we have merged the arylketo moiety of compounds **5.9-11** and the highlighted thioamide template to design *α*-ketothioamides (**Fig. 21**). This operation of design which was undertaken is sometimes referred to as convergent pharmacophore synthesis.

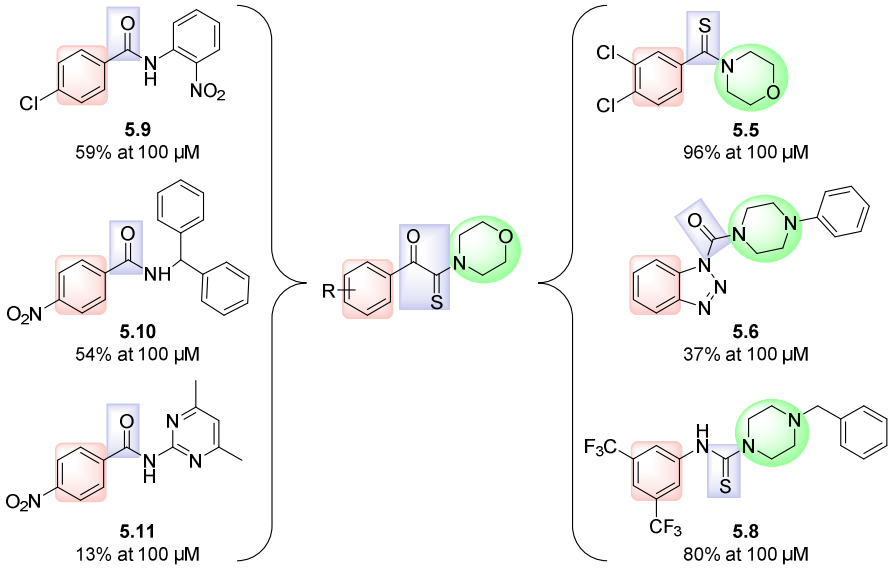

Figure 21: *Process of convergent pharmacophore operation to design α-ketothioamides. General scaffold of PHGDH inhibitor with aromatic ring in red, linker in blue and cyclic amine in green.*

5.2.4. Chemistry.

To warrant a proof of concept, a limited set of *α*-ketothioamides was synthesized (**Scheme 1**). Firstly, the bromination of appropriate acetophenone (1 eq) was carried out in the presence of dibromine (1.2 eq) and TBAB in chloroform. The resulting product was

engaged in the Willgerodt-Kindler reaction without any further purification according to a reported procedure.[82] DMF, octasulfur (1.5 eq), and morpholine (3 eq) were introduced into the reaction mixture and the reaction proceeded to completion at room temperature.

Scheme 1. *Synthetic pathway of α-ketothioamide derivatives.*[a]

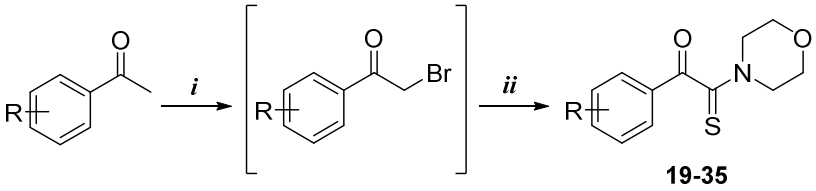

19-35

5.16: R = H **5.17**: R = 2-F **5.20**: R = 2-Cl **5.23**: R = 2-Br **5.26**: R = 2-I **5.29**: R = 2-NO_2 **5.32**: R = 4-Ph
5.18: R = 3-F **5.21**: R = 3-Cl **5.24**: R = 3-Br **5.27**: R = 3-I **5.30**: R = 3-NO_2
5.19: R = 4-F **5.22**: R = 4-Cl **5.25**: R = 4-Br **5.28**: R = 4-I **5.31**: R = 4-NO_2

[a]Reagents and conditions: (***i***) Br_2, $CHCl_3$, TBAB, rt for 2h; (***ii***) S_8, morpholine, DMF, rt.

5.2.5. Enzymatic evaluation.

All the synthesized compounds (**5.16-32**) were evaluated on PHGDH thanks to a coupled-enzyme assay (**Table 7**). The compound **5.22** is the strict fusion between hit compounds **5.9** and **5.5** identified during the primary screening. Given the IC_{50} values of these three compounds on PHGDH (8.7, 75.2 and 16.0 µM, respectively), we can validate the design based on the convergent pharmacophore synthesis. In addition, within this concise series of *α*-ketothioamides, it appears that the *para*-substitution in the aryl moiety is more favorable than the substitution in the *ortho* or *meta*-position as illustrated by the fluoro (**5.19**: 68.9 µM), chloro (**5.22**: 8.7 µM), and nitro (**5.31**: 35.1 µM) derivatives. However, only the 4-chloro derivative **5.22** exhibits a better inhibition than the non-substituted *α*-ketothioamide **5.16**.

5.2.6. Cellular assays.

To determine if the preliminary SARs can be translated to cellular activities, the non-substituted compound (**5.16**), the 4-substituted derivatives (**5.19**, **5.22**, **5.25**, **5.29** and **5.32**) as well as the 2- and 3-chloro α-ketothioamides (**5.20** and **5.21**) were evaluated in several cell-based assays (**Table 7**).

First of all, the proliferation ability of the three selected cancer cell lines (MDA-MB-231, human breast adenocarcinoma cells (PHGDH-); SiHa, human cervix carcinoma cells (PHGDH+); HL-60: human promyelocytic leukemia cells (PHGDH+); see immunoblots in **Fig.**

22A, 22C) was evaluated in serine replete or deplete medium. As depicted in **Fig. 22B, 22D**, extracellular depletion of serine had low effect on proliferation of high PHGDH-expressing lines (SiHa and HL-60-shScr) while the lack of serine considerably decreased the proliferation of the cell line lacking PHGDH (MDA-MB-231 and HL-60-shPHGDH). Given that the ability to proliferate in the absence of extracellular serine is indicative of a high dependence for serine synthesis, SiHa and HL-60-shScr cell lines should be sensitive to *α*-ketothioamides. Conversely, the identified inhibitors should have no effect on MDA-MB-231 and HL-60-shPHGDH cell lines.

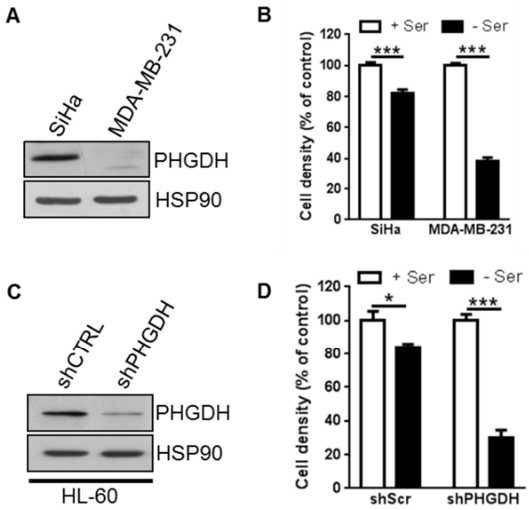

Figure 22: *Ability of the selected cancer cell lines to proliferate in serine replete or deplete medium. (***A** and **C***) Representative immunobolot for PHGDH. (***B** and **D***) Cell growth extent (for 5 days) in either serine-replete (+Ser) or serine-deplete (-Ser) medium. Data are shown as mean ± SEM (*n ≥ 3*).*

Subsequently, the selected molecules were evaluated on the following systems: (*i*) in MDA-MB-231 lacking PHGDH, (ii) in SiHa and HL-60 expressing PHGDH in serine-replete or serine-deplete medium and (*iii*) in HL-60 with PHGDH knockdown (shPHGDH) (**Table 7**). Assays in deplete-serine medium were expected to enhance the *de novo* serine synthesis and increase the cell sensitivity toward the inhibitors.

As expected, all tested molecules had no effect on the MDA-MB-231 and HL-60-shPHGDH cell lines sensitive to serine removal. In contrast, the inhibitors (except compound **5.19**)

exhibit interesting inhibition of SiHa and HL-60 cell proliferation in serine-replete (+Ser) medium. For example, compound **5.22** shows IC_{50} values of 21.0 and 50.5 µM on SiHa and HL-60, respectively. According to plan, the amino acid depletion (-Ser) enhanced the efficacy of the inhibitors by a factor of 3 for SiHa line and a factor 1.5 to 5.5 for the HL-60 line. In these conditions, compound **5.22** had an IC_{50} of 6.6 and 15.5 µM on SiHa and HL-60, respectively. Finally, the preliminary SARs established were confirmed in the cellular assay. Indeed, *ortho*- and *meta*-chloro compounds (**5.20** and **5.21**) that show no inhibition in the *in vitro* assay, also show no cell proliferation inhibition on all systems (IC_{50} > 100 µM).

N°	R	PHGDH (IC_{50}, µM)	MDA-MB-231	SiHa		HL-60 shCTRL		HL-60 shPHGDH
				+ Ser	- Ser	+ Ser	- Ser	
5.9		75.2	> 100	> 100	57.5	> 100	83	> 100
5.5		16.0	> 100	19.1	5.6	24.3	7.0	> 100
5.16	H	30.9	> 100	71.7	7.9	> 100	18.3	> 100
5.17	2-F	> 200	*nd*	*nd*	*nd*	*nd*	*nd*	*nd*
5.18	3-F	> 200	*nd*	*nd*	*nd*	*nd*	*nd*	*nd*
5.19	4-F	68.9	> 100	> 100	43.3	> 100	64.4	> 100
5.20	2-Cl	> 200	> 100	> 100	> 100	> 100	> 100	> 100
5.21	3-Cl	> 200	> 100	> 100	> 100	> 100	> 100	> 100
5.22	4-Cl	8.7	> 100	21.0	6.6	50.5	15.5	> 100
5.23	2-Br	160.7	*nd*	*nd*	*nd*	*nd*	*nd*	*nd*
5.24	3-Br	> 200	*nd*	*nd*	*nd*	*nd*	*nd*	*nd*
5.25	4-Br	130.7	> 100	20.4	7.9	37.2	16.9	> 100
5.26	2-I	> 200	*nd*	*nd*	*nd*	*nd*	*nd*	*nd*
5.27	3-I	> 200	*nd*	*nd*	*nd*	*nd*	*nd*	*nd*
5.28	4-I	177.7	> 100	25.7	9.3	19.6	7.1	> 100
5.29	2-NO_2	> 200	*nd*	*nd*	*nd*	*nd*	*nd*	*nd*
5.30	3-NO_2	88.1	*nd*	*nd*	*nd*	*nd*	*nd*	*nd*

5.31	4-NO_2	35.1	> 100	22.8	7.6	17.6	6.0	> 100
5.32	4-Ph	> 200	*nd*	*nd*	*nd*	*nd*	*nd*	*nd*

***Table 7**. PHGDH inhibition and cell proliferation inhibition results of compounds **5.5**, **5.9** and **5.16-32**.*

[a]All experiments to determine IC_{50} values were performed with at least triplicates at each compound dilution, and all IC_{50} values were averaged when determined in two or more independent experiments. *nd* = not determined.

5.2.7. Mechanism of action of compound 5.16.

To characterize the mechanism by which *α*-ketothioamides inhibit PHGDH, we have undertaken competition and rapid dilution assays with the leader of the series (**5.16**). Inhibition constants (K_i) for compound **5.16** with respect to 3-PG and NAD^+ were determined (**Fig.23**).

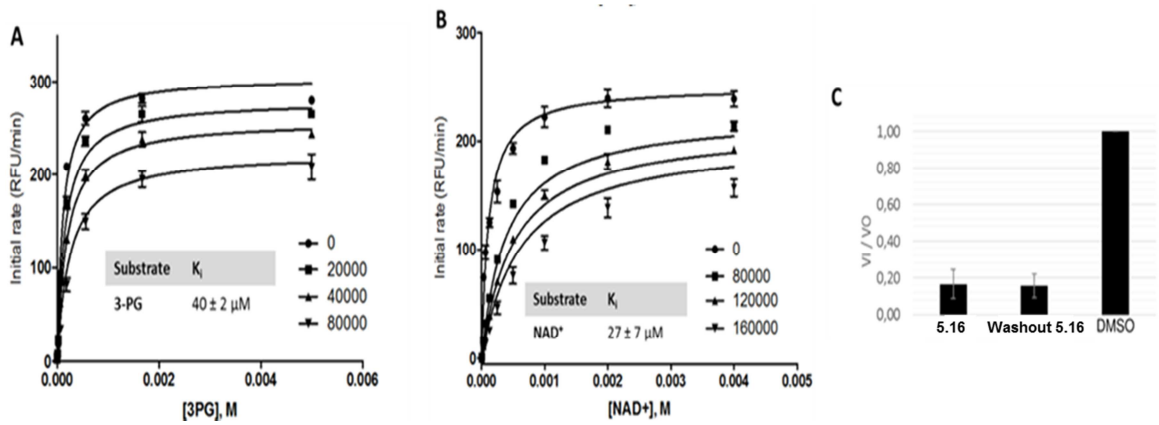

***Figure 23:** Mechanism of action of compound **5.16**. Inhibition constants (K_i) were determined by titrating (**A**) 3-PG and (**B**) NAD^+ at four concentrations of **5.16** (in nanomolar). (**C**) Washout experiment of compound **5.16**.*

As highlighted in **Fig. 23A, 23B**, the *α*-ketothioamide **5.16** inhibits PHGDH in a noncompetitive mode of action with respect to both substrates. The determined K_i values are 40 ± 2 µM and 27 ± 7 µM for 3-PG and NAD^+, respectively. Moreover, the rapid dilution experiment in **Fig. 23C** suggests that compound **5.16** may be a covalent inhibitor since enzymatic activity is not recovered after dilution.

5.3. PRELIMINAR CONCLUSION

Recent studies implicate PHGDH as an attractive drug target in tumors that overexpress PHGDH or amplify the *PHGDH* gene. In the present work, we explored whether this enzyme was druggable with small molecules using a screening approach. Initially, we established a straightforward fluorescence-based enzymatic assay that allowed us to screen around 350 molecules. Structure analyses of these hits highlighted common structural elements such as a thioamide or acetophenone part. On these observations, a convergent pharmacophore approach led to the synthesis of *α*-ketothioamides that appear as promising *in vitro* PHGDH inhibitors. Moreover, cellular assays confirmed that the identified inhibitors selectively abrogated the proliferation of cancer cell with elevated PHGDH expression. These encouraging results open the way to the development of a novel series of PHGDH inhibitors around the *α*-ketothioamide scaffold.

5.4. HIT IDENTIFICATION (UNPUBLISHED DATA)

Besides the *α*-ketothioamides reported, several other chemical series that could be used as starting points for the development of PHGDH inhibitors were also highlighted. These small-molecules, their origin and their efficacy on the PHGDH isolated enzyme assay are reported in **Table 8**. For clarity, only compounds showing more than 30% inhibition at 100 µM are depicted in this Table and IC_{50} are determined only for inhibition percentage higher than 50%.

Table 8. Main hits and their PHGDH inhibition (IC_{50}, µM or inhibition percentage).

Compounds	Structure	Origin	Inhibition % at 100 µM	IC_{50} (µM)
5.33	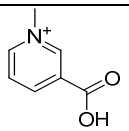	Prestwik	30 %	n.d.
5.34	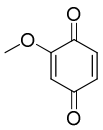	Prestwik	100 %	1.3 [0.73-1.84]

5.35	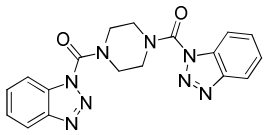	CMFA	46 %	n.d.
5.36	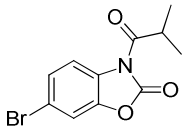	CMFA	43 %	n.d.
5.37	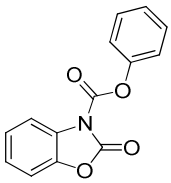	CMFA	33 %	n.d.
5.38	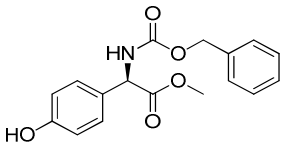	CMFA	47 %	n.d.
5.39	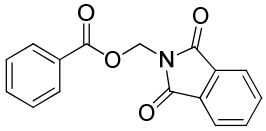	CMFA	41 %	n.d.
5.40	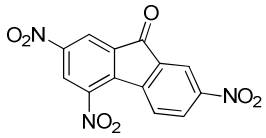	CMFA	30 %	n.d.
5.41	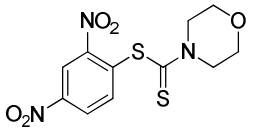	CMFA	82 %	21.3 [15.6-27.4]
5.42	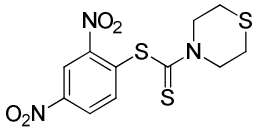	CMFA	100 %	4.7 [3.22-5.98]
5.43	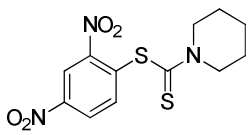	CMFA	95 %	7.8 [3.24-12.5]
2.17	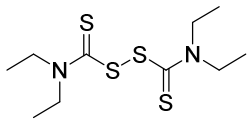	CMFA	100 %	0.59 [0.37-0.95]

[a]All experiments to determine IC_{50} values were performed in triplicates at each compound dilution. In brackets: 95 % confidence interval.

As a result of this screening, other compounds inhibiting PHGDH were also identified. Despite a high PHGDH inhibition the quinones (**5.34, 5.39**) were rejected due to various *in vivo* side effects and known high cytotoxicity.[81] Some benzoxazole (**5.36**, **5.37**) and benzotriazole (**5.35**) derivatives were also identified. These compounds were previously synthesized in our laboratory to target the human fatty acid amide hydrolase (FAAH) and monoacylglycerol lipase (MAGL) enzymes.[83,84]

Interestingly, some analogues of the α-ketothioamides were also identified (**5.41**-**43**). These molecules led us to envisage the pharmacomodulation of the ketothioamide central linker to design new PHGDH inhibitors. This part will be detailed in **Chapter 6**.

Finally, disulfiram (**2.17**), a well-known inhibitor of aldehyde dehydrogenase (ALDH) was also identified as one of the most potent PHGDH inhibitor in our hands. This drug is currently on the market to treat alcoholism and was also used by Lambert and his group to design new potent MAGL inhibitors.[85] A detailed study of Disulfiram and analogues as PHGDH inhibitors will be detailed in **Chapter 8**.

5.5. EXPERIMENTAL SECTION

5.5.1. General chemistry.

All reagents were purchased from chemical suppliers and used without purification. Thin-layer chromatography (TLC) was performed using silica gel 60 F254 plates, with observation under UV when necessary. Melting points were recorded on an Electrothermal IA9000 melting point system. ^{1}H NMR spectra were recorded an AVANCE II 400 MHz Bruker spectrometer with $CDCl_3$ or DMSO-d_6 as the solvent. ^{13}C NMR spectra were recorded at 100 MHz. All coupling constants are measured in hertz (Hz), and the chemical shifts (δ_H and δ_C) are quoted in parts per million (ppm) relative to TMS (δ_0), which was used as the internal standard. Data are reported as follows: chemical shift, multiplicity (s = singlet, d = doublet, t = triplet, q = quartet, br = broad, m = multiplet), integration, and coupling constant (Hz). High-resolution mass spectroscopy (HRMS) analyses were carried out on a LTQ-Orbitrap XL hybrid mass spectrometer (Thermo Fisher Scientific, Bremen, Germany). Data were acquired in positive ion mode using full-scan MS with a mass range of 100-1000 m/z. The orbitrap operated at 30000 resolutions (FWHM definition). All experimental data were acquired using daily external calibration prior to data acquisition. Appropriate tuning of the electrospray ion source was done. The following electrospray inlet conditions were applied: flow rate, 100 µL min^{-1}; spray voltage, 5 kV; sheath gas (N_2) flow rate, 20 a.u.; auxiliary gas (N_2) flow rate, 10 a.u.; capillary temperature, 275 °C; capillary voltage, 45 V; tube lens, 80V. High-performance liquid chromatography (HPLC) analyses were performed on a LC system using YMC-Triart C-18 (250 mm x 4.6 mm, 5µm) column as the stationary phase. Mobile phase contained water/CH_3CN (30:70, v/v) and maintained isocratically at the flow rate of 1 mL/min. The column temperature was maintained at room temperature. The peaks were monitored at the wavelength of 215 nm. The purity of all compounds tested was greater than 95%, as determined by HPLC and ^{1}H NMR.

5.5.2. General procedure for the synthesis of α-ketothioamide analogs (5.16-5.32).

To a stirred solution of ethanone derivative (1 eq) in chloroform was added dropwise a solution of dibromine (1.2 eq) in chloroform. After 2 hours, the solvent was evaporated *in vacuo* to give a crude oil consisting mainly of 2-bromo-1-(substituted)-ethanone compound along with trace amounts of 2,2-dibromo-1-(substituted)-ethanone compound. The mixture

was used without purification in the next step. To the synthesized or commercial 2-bromo-1-(substituted)-ethanone derivative were added in sequence DMF, cyclooctasulfur (1.5 eq) and morpholine (3 eq). The mixture was then stirred at room temperature. After completion, the reaction mixture was quenched with distilled water to give a precipitate which was further washed with distilled water. The residue was recrystallized or purified by silica gel chromatography if necessary.

5.5.3. 1-Phenyl-2-morpholino-2-thioxoethanone (5.16).

Brown solid (73%). This compound was synthesized according to the general procedure described above. Acetophenone (2.00 g, 16.60 mmol) and dibromine (1.01 mL, 19.90 mmol) were mixed in chloroform (15 mL) to obtain the 2-bromo-1-phenyl-ethanone and this intermediate was reacted in a second time with morpholine (4.34 mL, 49.80 mmol) and sulfur (0.79 g, 24.90 mmol) in DMF (10 mL). Methanol was used for recrystallization to afford the title compound. R_f 0.2 (cyclohexane/EtOAc 8:2). Mp: 110-112°C. ^{1}H NMR (400 MHz, $CDCl_3$): δ_H (ppm) 3.59-3.62 (t, 2H, *J* = 4.8 Hz), 3.69-3.71 (t, 2H, *J* = 4.8 Hz), 3.90-3.92 (t, 2H, *J* = 4.8 Hz), 4.33-4.35 (t, 2H, *J* = 4.8 Hz), 7.48-7.52 (m, 2 ArH), 7.59-7.65 (m, 1 ArH), 7.99-8.01 (d, 2 ArH, *J* = 8.2 Hz). ^{13}C NMR (100 MHz, $CDCl_3$): δ_C (ppm) 47.13, 51.95, 66.40, 66.52, 128.99 (2C), 129.86 (2C), 133.26, 134.48, 187.90 (C=O), 195.70 (C=S). HRMS (ESI^+): *m/z* calcd for $C_{12}H_{13}NO_2S$ $(M + H)^+$ 236.0739, found 236.0737.

The synthetic procedures of compounds 5.17-5.32 are detailed in annexes (Chapter 11).

5.5.4. Primary PHGDH Screen.

PHGDH inhibition assay was performed in black polypropylene 96-well plates (Sigma-Aldrich) using NAD (Sigma-Aldrich) as cofactor and 3-phosphoglycerate (Sigma-Aldrich) as substrate. Tested compounds were dissolved in DMSO. The final concentration of DMSO in assay solutions was 10 %, which was shown to have no effect on PHGDH activity. The reaction volume per well was 50 µL. Each assay was carried out in triplicate. Briefly, a solution buffer (100 mM Tris HCl buffer (pH 8.8), 400 mM NaCl, 0.2 mM DTT, 1 mM NAD and 0.5 mM 3-PG) was added at various concentrations of tested compounds. Then, an amount of 100 ng of PHGDH (human recombinant protein, BPS Bioscience) is added to start the reaction. Finally,

the product formation, correlated with NADH formation, is instantly monitored for 7 min at 25°C using a SpectraMax spectrophotometer at an excitation wavelength of 360 nm and emission wavelength of 460 nm.

5.5.5. PHGDH assay.

PHGDH activity was measured in 96-well plates (96 µL per well) at 37 °C by monitoring resorufin fluorescence (Ex 550 nM/Em 580 nM) over time with a FLUOstar Omega (BMG Labtech). PSAT1 was included to prevent product inhibition of PHGDH. Assays were performed in PHGDH assay buffer (50 mM Tris, pH 8.5, and 1 mM EDTA). Substrates and enzyme concentrations were as follows: 3-PG, 240 µM; NAD^+, 120 µM; glutamate, 30 mM; resazurin, 0.1 mM; PHGDH, 12 ng/µL; PSAT1, 20 ng/µL, diaphorase 0.18 µg/µL except for K_i measurements where one of the PHGDH substrates was held constant at 3 mM whereas the other substrate was titrated. For K_i measurements, drug and enzyme were preincubated for 30 min. Initial rate plots were fit using Prism 6. Chemicals were purchased from Sigma.

5.5.6. Cell models and cytotoxicity assay.

All cell lines were acquired in the last 3 years from ATCC where they are regularly authenticated by short tandem profiling. Cells were stored according to the supplier's instructions and used within 6 months after resuscitation of frozen aliquots. SiHa cervix carcinoma cells and MDA-MB-231 breast cancer cells were routinely cultured in DMEM supplemented with 10% FBS and antibiotics. For the cytotoxicity assay, cells were seeded at low density I 96-well plates in serine containing media. Media were then aspirated and cells were incubated in fresh serine-replete or-deplete media containing drugs or vehicle (DMSO). Cells were grown for 5 days at 37°C with drug and media changed daily before assaying cell viability using a Presto Blue assay (Life Technologies) according to manufacturer's instructions.

5.5.7. Immunoblots.

Protein extraction and western blot analysis were carried out as reported elsewhere (Polet *et al.* 2016 Oncotarget).[38]

5.5.8. Dilution experiment.

Compound **5.16** (160 µM) or DMSO control was incubated with the enzyme mix for 45min at 37^{o}C. At the end of the incubation the enzyme drug mix was diluted 10-fold using assay buffer and concentrated back to the original volume by centrifuging through a 10kD molecular weight cut-off filter. Subsequently enzyme activity was measured via the PHGDH assay. An undiluted compound (160 µM) condition was included as a positive control for inhibition.

5.6. SUPPORTING INFORMATION

5.6.1. Enzymatic assay optimization

PHGDH oxidizes 3-PG to 3-PPyr with NAD^+ as the electron acceptor to yield NADH. The formation of 3-PPyr is directly correlated with the NADH formation (Ex 340 nm / Em 460 nm). Thus, the enzymatic activity of PHGDH can be monitored by following the fluorescence intensity at an excitation wavelength of 340 nm and emission wavelength of 460 nm. Prior to developing a robust quantitative assay, we initially set out to optimize the activity of the PHGDH. Oxidoreductase activity was screened at varying enzyme, cofactor and substrate concentrations by monitoring the oxidation of NADH spectrophotometrically. The tolerance of the enzymatic assay to DMSO was studied at a DMSO concentration ranging from 5% to 20% (**Fig. S1**). For this present study, the concentrations of Tris HCl pH 8.8, NaCl and DTT were set at 100 mM, 400 mM and 0.2 mM, respectively, and the temperature was kept at 25°C.

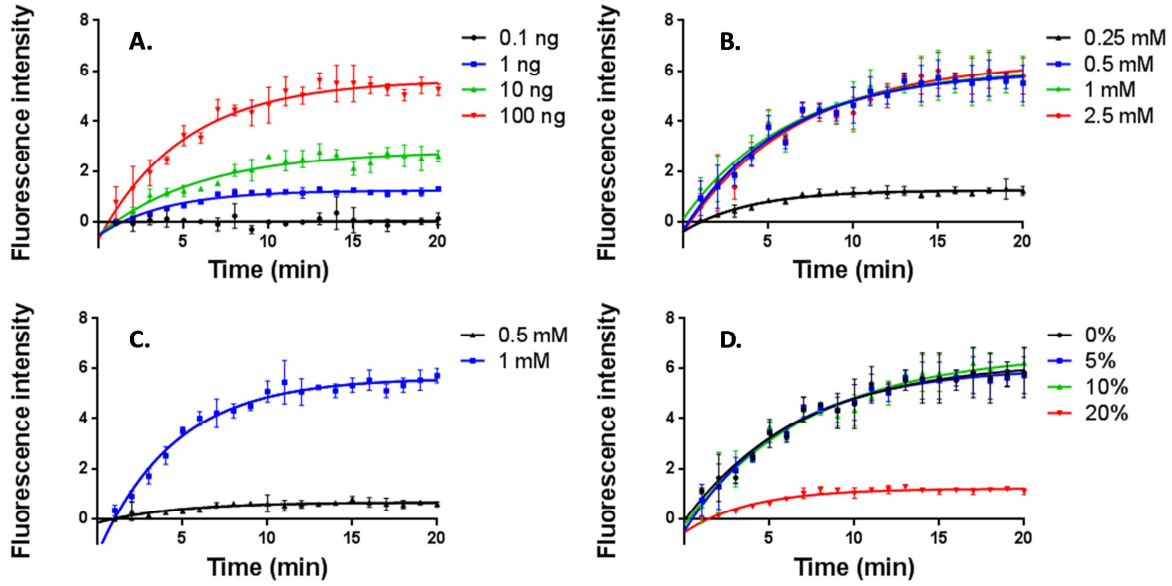

***Figure S1**: Optimization of the enzymatic assay for drug screening. (A) Variation of PHGDH concentration (2.5 mM 3-PG, 1 mM NAD). (B) Variation of 3-PG concentration (100 ng PHGDH, 1 mM NAD). (C) Variation of NAD concentration (100 ng PHGDH, 2.5 mM 3-PG). (D) Influence of DMSO (100 ng PHGDH, 2.5 mM 3-PG, 1 mM NAD). Data were analyzed using GraphPad software.*

Minimizing the amount of enzyme was an important consideration for controlling the cost of assays. Thus, we sought to determine enzyme concentrations that would generate a sufficient fluorescent signal. Representative curves obtained with PHGDH quantity ranging from 1 ng to 100 ng, are shown in Fig. S1A. As depicted, a quantity of 100 ng of PHGDH was sufficient to achieve a robust assay window. The concentration of 3-PG and NAD^+ in an assay is also an important consideration. Concentration of 3- PG was varied between 0.25 and 2.5 mM and two concentrations of NAD^+ were evaluated (Fig. S1B and Fig. S1C). Optimal concentrations of 3-PG and NAD were 0.5 mM and 1 mM respectively to detect a correct fluorescent signal. Compounds from the database were stored at 10 mM in DMSO and the final concentration of DMSO in assay solutions was 10%. As depicted in Fig. S1D, this percentage of DMSO was tolerated by PHGDH. Thus, the optimized conditions consisted of PHGDH (100 ng), 3-PG (0.5 mM), and NAD (1 mM). In these conditions, the rate of substrate conversion was found to be linear during the five first minutes. The K_m value of 3-PG was then determined by fitting the data to the Michaelis–Menten equation. The calculated K_m value (0.19 ± 0.03 mM) is consistent with the reported K_m value of 0.26 ± 0.03 mM.

Notes

S.R., R.F. and O.F. designed the experiments, analyzed the data and wrote the manuscript. C.C. designed the cellular experiments. Q.S. and S.R. perfomed the enzymatic screening and the chemical syntheses. E.M, A.R and L.C.C. have contributed to the enzymatic evaluation.

6. α-ketothioamide SARs based on in vitro PHGDH inhibition

This chapter is the result of the work of Spillier, Q., Ravez, S., Verdickt, L. and Lefranc, W.

Following the identification of the α-ketothioamides as promising PHGDH inhibitors, our aim was to improve the efficacy of this series by chemical optimization. Then, we evaluated the newly synthesized analogues using an isolated enzyme assay. **Regarding the previous published data, it is important to note that the IC_{50} values are slightly shifted due to a new PHGDH production. A discussion regarding the enzyme activity and the different assays that were used can be found in Chapter 4.**

6.1. RESULTS AND DISCUSSIONS

Compound **5.16** is characterized by an aryl group (part A) and a morpholine moiety (part C) that are connected by an α-ketothioamide linker (part B) (**Figure 24**). The structure-activity relationships in this series were investigated by modulation of the aromatic moiety or by insertion of alkyl groups on part A, introduction of different amino moieties on part C and variation of the nature of the linker (part B). As a result, a library of 42 compounds (**Table 9**) was assembled (see Supporting Information for chemical synthesis and characterization of each derivative).

Table 9. *Results of PHGDH inhibition (IC_{50}, µM)*

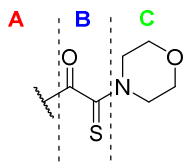

5.16, 5.21, 5.22 and 6.1-8

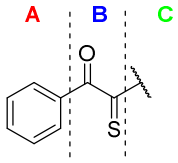

6.9-18

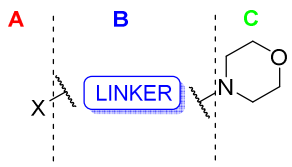

6.19-39

	Part A	PHGDH IC_{50} (µM)		Part C	PHGDH IC_{50} (µM)
5.16	Phenyl	111.1 [87.3-131.2]	**6.9**	Pyrrolidine	> 150
5.22	4-Chlorophenyl	20.3 [15.6-26.4]	**6.10**	4,4-Difluoropiperidine	> 150
5.21	3-Chlorophenyl	> 150	**6.11**	4-Methylpiperidine	85.1 [37.8-191.2]
6.1	2,4-Dichlorophenyl	77 [65.3-98.6]	**6.12**	Piperidine	> 150
6.2	Cyclohexyl	> 150	**6.13**	Diethylamine	> 150
6.3	4-Pyridine	> 150	**6.14**	Thiomorpholine	> 150
6.4	3,4-Dichlorophenyl	> 150	**6.15**	*N*-methylpiperazine	> 150
6.5	2-Naphtyl	> 150	**6.16**	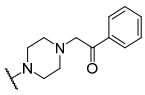	> 150
6.6	Ethyl	> 150	**6.17**	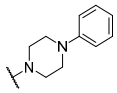	> 150
6.7	Adamantine	> 150	**6.18**	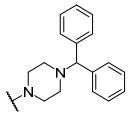	> 150
6.8	*t*-Butyl	> 150			

	X	Part B	PHGDH IC_{50} (µM)		X	Part B	PHGDH IC_{50} (µM)
6.19	Phenyl		> 150	**6.30**	Phenyl		> 150
6.20	Phenyl		106 [63.2-178.8]	**6.31**	Phenyl		> 150
6.21	Phenyl		> 150	**6.32**	Phenyl		> 150
6.22	Phenyl		> 150	**6.33**	Phenyl		> 150
6.23	Phenyl		> 150	**6.34**	Phenyl		92.1 [58.4-145.2]
6.24	Phenyl		> 150	**6.35**	4-Chlorophenyl		10.4 [8.01-13.6]
6.25	Phenyl		> 150	**6.36**	4-Chlorophenyl		21.6 [15.9-29.4]
6.26	Phenyl		> 150	**6.37**	Cyclohexyl		19.4 [11.7-32.1]
6.27	Phenyl		> 150	**6.38**	4-Pyridine		28.2 [20.2-39.2]
6.28	Phenyl		> 150	**6.39**	Ethyl		45.8 [39.1-53.5]
6.29	Phenyl		> 150				

[a]All experiments to determine IC_{50} values were performed in triplicates at each compound dilution. In brackets: 95 % confidence interval.

All compounds were evaluated *in vitro* using a PHGDH isolated enzyme assay at a single compound concentration of 150 µM in triplicate. IC_{50} values were determined for the most potent derivatives (**Table 9**, **Figure 24**). To our surprise, most of the pharmacomodulations did not afford more potent PHGDH inhibitors. At the left side (part A) of the molecule, only aryl groups led to potent PHGDH inhibitors whereas introduction of alkyl groups in this position resulted in inactive derivatives. Moreover, substitutions on the aryl moiety are only tolerated in the *para*-position with the chlorinated derivative **5.22** being the most potent. Then, except for the 4-methylpiperidine analogue, it was very clear that modulating part C (right-side amino moiety) of the molecule decreased or abolished the inhibitory potency. Regarding the influence of the linker, only replacement of the *α*-ketothioamide (part B) with a thioamide (**6.20**), or a sulfonohydrazide (**6.34**) led to equally potent PHGDH inhibitors whereas all other modulations led to inactive derivatives (IC_{50} > 150 µM). Interestingly, with the thioamide and sulfonohydrazide linkers, the introduction of a chlorine in the *para*-position, again, improved the inhibitory potency compared to the non-substituted analogue (**6.35** and **6.36**) (**Figure 24B**).

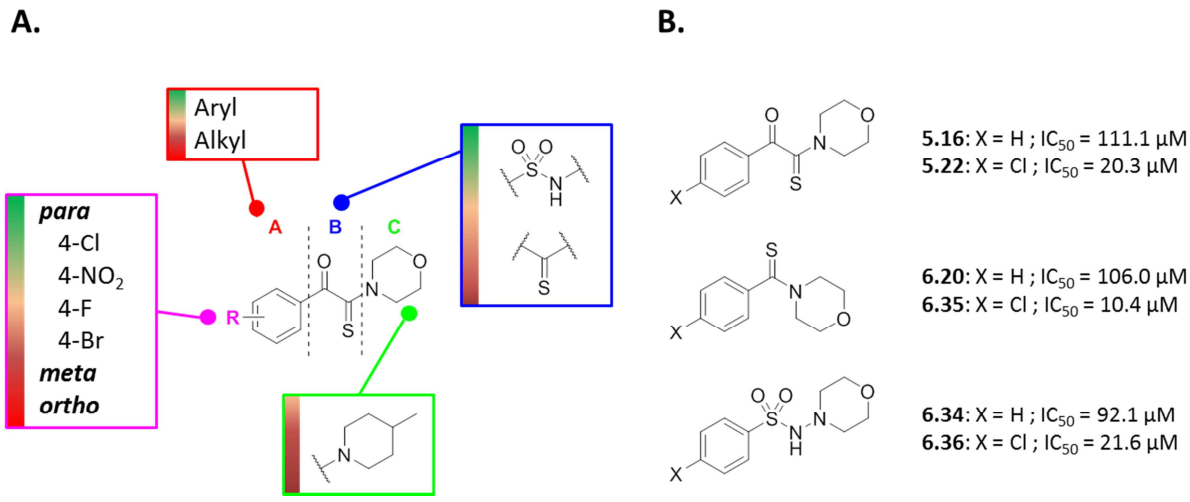

Figure 24: *Overview of the structure–activity relationships. Color code: green > yellow > red, for decreasing PHGDH inhibition (A). Influence of the p-chloro substitution on the potency of PHGDH inhibition (**B**).*

Among all the investigated compounds, the para-chlorinated derivatives **5.22**, **6.35** and **6.36** result in the highest PHGDH inhibition.

Even if these pharmacomodulations appeared relatively flat, some SAR can be highlighted. Firstly, the aromatic part of the molecule seems to be crucial since its replacement by alkyl functionalities or other substituted or not, aromatic rings leads to compounds that are not PHGDH inhibitors. Indeed, *ortho* and especially *meta* substitutions lead to a significant lost in activity. Fortunately, *para*-substituted analogues, particularly with halogens demonstrated a high affinity towards PHGDH. For example, chlorine substitution leads to a 5-fold improvement on IC_{50} values compared to compound **5.16**. Regarding the linker modifications, two other scaffolds were successfully identified. Interestingly, the thioamide and sulfonohydrazide derivatives revealed a good potency and relatively similar SARs with para-substitution with chlorine atom being the best substitution.

In summary, all previous information combined with the issue to further optimize this scaffold led us to investigate in more details the mechanism-of-action in this series. This will be the subject of the next chapter.

It should be noted that the investigation of the thioamide and sulfonohydrazide family is being currently pursued in the lab.

6.2. SUPPORTING INFORMATION

6.2.1. General Chemistry.

All reagents were purchased from chemical suppliers and used without purification. Thin-layer chromatography (TLC) was performed using silica gel 60 F254 plates, with observation under UV when necessary. Melting points were recorded on an Electrothermal IA9000 melting point system. ^{1}H NMR spectra were recorded on an AVANCE II 400 MHz Bruker spectrometer with $CDCl_3$ or DMSO-d_6 as the solvent. ^{13}C NMR spectra were recorded at 100MHz. All coupling constants are measured in hertz (Hz), and the chemical shifts (δH and δC) are quoted in parts per million (ppm) relative to TMS (δ0), which was used as the internal standard. Data are reported as follows: chemical shift, multiplicity (s = singlet, d =doublet, t = triplet, q = quartet, br = broad, m = multiplet), integration, and coupling constant (Hz). High-resolution mass spectroscopy (HRMS) analyses were carried out on a LTQ-Orbitrap XL hybrid mass spectrometer (Thermo Fisher Scientific, Bremen, Germany). Data were acquired in positive ion mode using full-scan MS with a mass range of 100−1000m/z. The orbitrap operated at 30000 resolutions (fwhm definition). All experimental data were acquired using daily external calibration prior to data acquisition. Appropriate tuning of the electrospray ion source was done. The following electrospray inlet conditions were applied: flow rate, 100µL/min; spray voltage, 5 kV; sheath gas (N_2) flow rate, 20 au; auxiliary gas (N_2) flow rate, 10 au; capillary temperature, 275°C; capillary voltage, 45 V; tube lens, 80 V. High-performance liquid chromatography (HPLC) analyses were performed on a LC system using a YMC-Triart C-18 (250 mm×4.6 mm, 5µm) column as the stationary phase. Mobile phase contained water/CH_3CN (30:70, v/v) and was maintained isocratically at the flow rate of 1 mL/min. The column temperature was maintained at room temperature. The peaks were monitored at the wavelength of 215 nm. The purity of all compounds tested was greater than 95%, as determined by HPLC and ^{1}H NMR.

The synthetic procedures of compounds 5.16, 5.21, 5.22 and 6.1-39 are detailed in annexes (Chapter 11).

6.2.2. PHGDH Assay.

The enzymatic assay was adapted from a previously described procedure.[86] In brief, the reactions were performed in PHGDH assay buffer (50 mM Tris, pH 8.5, and 1 mM EDTA)

following resorufin fluorescence emission (Ex 550 nm/Em 580 nm) over time. Substrate and enzyme concentrations were as follows: 240 µM 3-PG; 120 µM NAD^+; 30 mM glutamate; 0.1 mM resazurin; 12 ng/µL human PHGDH; 20 ng/µL human PSAT1; 0.18 µg/µL diaphorase. The final concentration of DMSO in the assay mixture was set to 5%.

7. Probing the binding site of PHGDH inhibitors using Diazirine photocrosslinking

This chapter is based on the following publication: Spillier, Q., Ravez, S., Corbet, C., Dochain, S., Vertommen, D., Mullarky, E., Unterlass, J., Thabault, L., Prévost, J.R.C., Degavre, C., Es Saadi, B., Cantley, L.C., Feron, O., Frédérick, R. ACS Chemical Biology. Under revision.

Graphical Abstract

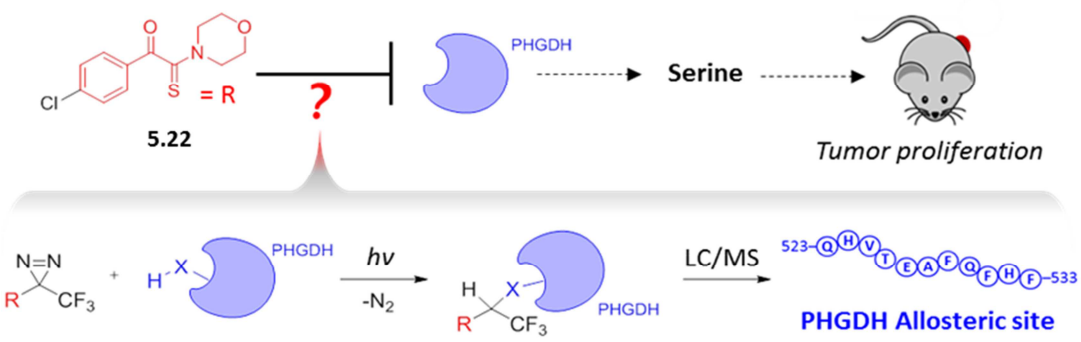

7.1. PREAMBLE: IDENTIFICATION OF THE SITE OF ACTION OF THE *α*-KETOTHIOAMIDE COMPOUNDS

Intrigued by the relatively flat SARs obtained for the *α*-ketothioamides series (**Chapter 6**), we set out to investigate the site of action of this family of compounds on PHGDH. Several techniques are reported in the literature to identify an enzymatic site of action. These methods will be briefly introduced hereunder.

7.1.1. Competition studies

Competition studies deal with the study of the ability of a molecule to compete with the enzyme co-factor(s) and/or substrate(s). By titrating these substrates with different concentrations of inhibitors, the enzyme activity can be studied and hence the target binding site identified. In our case, such studies showed that *α*-ketothioamides act as uncompetitive inhibitors with respect to both PHGDH substrates (NAD^+ and 3PG). Therefore, we concluded that this series would bind at an allosteric site of the enzyme.

7.1.2. Crystallography

Crystallographic experiments are one of the most accurate methods to reveal the interactions between a molecule and an enzyme. Usually, this can be done by growing a protein crystal in the presence of the investigated molecule (co-crystallization) or by soaking a crystal of this enzyme with a solution containing the compound.[70] X-ray diffraction analysis then allows to map the different interactions. Nowadays, a large number of therapeutic agents on the market were developed and optimized using these techniques.[87–89] Currently, there is no crystal structure of the full-length human PHGDH. Few years ago, the closest version reported was a truncated version of human PHGDH (PDB code: 2G76) with much of the C-terminal part missing (**Figure 25A**). More recently, the Helleday group reported an even smaller version of the protein, essentially constituted of its active site but still showing enzymatic activity (**Figure 25B**).[90]

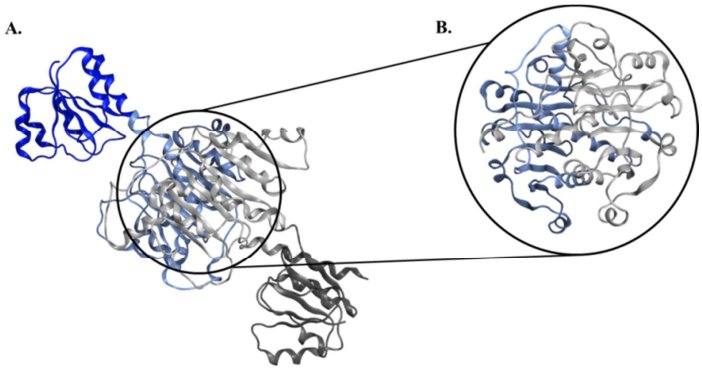

Figure 25: A. *Crystallographic structure of PHGDH* ***2G76*** *with zoom on the short truncated version.* ***B.*** *Crystallographic structure of truncated PHGDH* ***5NZO****. In blue monomer A and monomer B in grey.*

Tentative crystallographic experiments with our *α*-ketothioamide series were carried out in collaboration with the group of Prof. Johan Wouters (UNamur) and Dr. Judith Unterlass (Helleday lab) on these two versions of the protein. Unfortunately, and despite soaking and co-crystallisation tests carried out on these truncated versions of PHGDH, these experiments did not allow us to obtain crystals with a sufficient resolution. In **Chapter 9**, a discussion can be found regarding the issue encountered notably regarding X-ray experiments.

7.1.3. Docking

Docking studies is another method reported in the literature either to virtually screen chemical libraries on a target or to predict a potential site of action.[91–94] It consist in the simulation of the binding position of a small-molecule in a target binding site by mean of docking software. Avalaible softwares in the lab are MOE (ChemComp) of GOLD (CCDC). However, the allosteric mode of action reported for the *α*-ketothioamide series together with the absence of a full-length PHGDH crystal structure prevent the use of a computational approach in our case.

7.1.4. NMR

Recently novel NMR experiments, either protein-observed or ligand-observed were reported to detail the binding mode of small-molecules to enzymes. Protein-observed methodologies usually require ^{15}N-enriched protein which we did not consider in the present work. Ligand-observed experiments such as Saturation-Transfer Difference (STD)[95] or

Waterlogsy[96] experiments could be envisaged in the lab thanks to the recent acquisition of a 600MHz NMR apparatus. However, because these methods rely on a transfer of saturation from the ligand to the enzyme, the use of irreversible inhibitors is not appropriate.

7.1.5. Chemical labeling

Chemical labeling relies on the formation of a covalent bond between a molecule of interest and its biological target.[97,98] This method is commonly used to determine the *in cellulo* mode of action of a compound. In some cases, the molecule studied already possesses a reactive function able to directly bind to the protein (such as for instance a thiol function, carboxylic acid, or free amine). In other cases, when these reactive functions are not initially present on the molecule, a function that can react with particular amino-acid residues must be chemically added to the molecule. The photoactivatable diazirine is one of these preferred functions. Briefly, once in contact with the target, the diazirin-based photoactivatable ligand (PALs) will form a highly reactive chemical carbene species upon UV irradiation and react with the protein (**Figure 26**).[99] Then, different methods such as fluorescence quenching, recognition by a specific antibody, mass spectrometry, electrophoresis… can be used to detect modified amino-acid and, hence, infer the potential site-of-action of the compound.

In our work, on one side, we studied the formation of a direct covalent bond between an reactive function-bearing inhibitor (disulfiram, DSF) and PHGDH, and on the other side, we used a photoactivatable diazirine-bazed probe to study the binding of the *α*-ketothioamides.[100] The results obtained are detailed in the following **Chapter 7** and **8**.

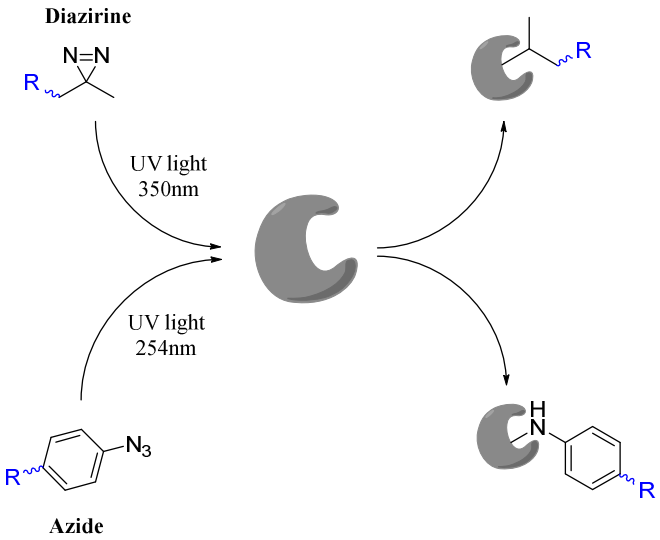

Figure 26: *Two classical classes of PALs and their reactivity.*

7.1.6. Mutagenesis

To confirm the site-of-action suggested by the chemical-labelling study, site-directed mutagenesis experiments are usually performed. This approach consists in the mutation of the amino acids labeled using the photoactivatable probe or the reactive inhibitor.[101,102] The analysis of the inhibitory potency of the studied inhibitor on the mutated enzyme allow to confirm or not the site of action.

7.2. INTRODUCTION

As depicted in **Fig. 27**, besides indole derivative **2.1** developed by Astra Zeneca as NADH competitive inhibitors, all reported molecules were shown to act as non-competitive inhibitors and are characterized with PHGDH inhibitory potency in the micromolar range. Indeed, the high physiological concentration of NADH (0.3 mM) hampers the design of competitive inhibitors. On the other hand, the development of non-competitive, allosteric PHGDH inhibitors is a promising approach notably to overcome the problem of specificity against other NAD-dependent enzymes.

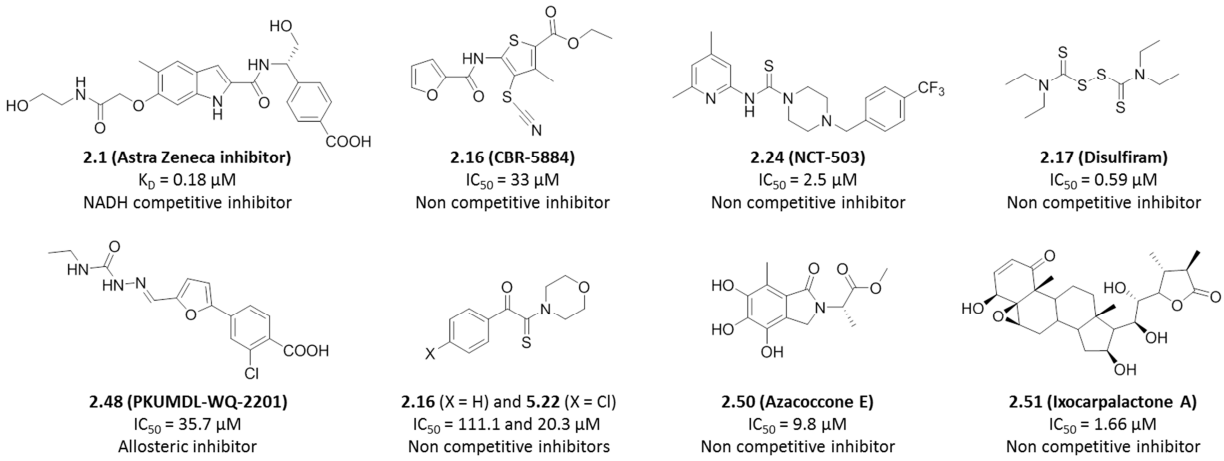

Figure 27: *Overview of some reported PHGDH inhibitors.*

Yet, until very recently, only two different allosteric sites were identified for PHGDH, the ASB (Allosteric Substrate Binding) and the ACT (Aspartate kinase-Chorismate mutase-TyrA) domains. These two domains, located at the C-terminal part of the protein, have, up to date, never been targeted to develop PHGDH inhibitors. In fact, the role of these allosteric domains in the control of PHGDH activity remains poorly understood. In 2016, Wang and coworkers suggested two other allosteric sites of PHGDH, the first located at the interface of the enzyme active site and the NAD binding domain, and the second, smaller, in the substrate binding cavity.[77] More recently, Zheng and coworkers suggested another potential allosteric site located at the back-side of the active site and which could be the site of action of the PHGDH inhibitor **2.50**.[103]

These examples demonstrate the importance of detailing the mechanism-of-action of newly developed PHGDH inhibitors in order to better understand the mechanisms involved in PHGDH regulation and foster the development of new inhibitors. In the present chapter, the mechanism-of-action and *in vivo* activity of compound **5.22** was investigated with a view to establish the proof-of-concept that *α*-ketothioamides can exert anticancer activity through PHGDH inhibition, and possibly identify novel PHGDH regulation mechanisms.

7.3. RESULTS AND DISCUSSION

7.3.1. Preliminary SARs based on in vitro PHGDH inhibition

Previous studies in our laboratory highlighted compound **5.16** and the *para*-substituted analogue **5.22** as promising PHGDH inhibitors. Early investigations of the structure-activity relationships (SARs) revealed the importance of this *para*-substitution pattern (**Figure 28**, compare the *para*-chlorinated derivative **5.22** and the *meta*-chlorinated analogue **5.21**, for instance[86]).

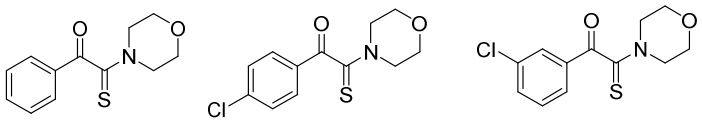

5.16
IC_{50} = 111.1 µM
[87.3-131.2]

5.22
IC_{50} = 20.3 µM
[15.6-26.4]

5.21
IC_{50} > 150 µM

***Figure 28**: α-ketothioamide inhibitors and preliminary SAR investigations*

In this work, **5.22** was also shown (i) to be selectively toxic to PHGDH-dependent tumor cell lines (SiHa and HL-60) compared to PHGDH-independent tumor cell lines (MDA-MB-231 and HL-60 shPHGDH)[86], (ii) to be as potent as the used reference PHGDH inhibitor, **2.24** (NCT-503) (**Table 10**) in these cellular models[74] and (iii) to be non-toxic on healthy fibroblast cells (BJ-5ta). Taken together, these data highlighted the *α*-ketothioamide **5.22** as an interesting pharmacological tool to further detail the biology of PHGDH.

Table 10. *Cell proliferation inhibition data*

	PHGDH-dependent tumor cell lines				PHGDH-independent tumor cell lines		Non-tumor cell line
	HL-60		**SiHa**		**HL-60 shPHGDH**	**MDA-MB-231**	**BJ-5ta**
Compound	**+Ser medium**	**-Ser medium**	**+Ser medium**	**-Ser medium**	**±Ser medium**	**±Ser medium**	**+Ser medium**
5.16*	>100*	83.1*	71.7*	7.9*	>100*	>100*	>100
5.22*	24.3*	7.0*	21.6*	6.6*	>100*	>100*	>100
2.24 (NCT-503)	47.5	10.1	22.7	6.5	>100	>100	>100

All experiments to determine IC_{50} values were performed with at least triplicates at each compound dilution, and all IC_{50} values were averaged when determined in two or more independent experiments. *Values previously published in Ravez *et al*.[86]

7.3.2. In-vivo evaluations

Based on the results in the cell-based assays, the anticancer potential of compound **5.22** was thus further evaluated *in vivo*. To this end, nude mice bearing SiHa tumor xenografts were treated with vehicle (DMSO) or compound **5.22** (40 mg/kg, I.P.) for 9 days (**Figure 29**).

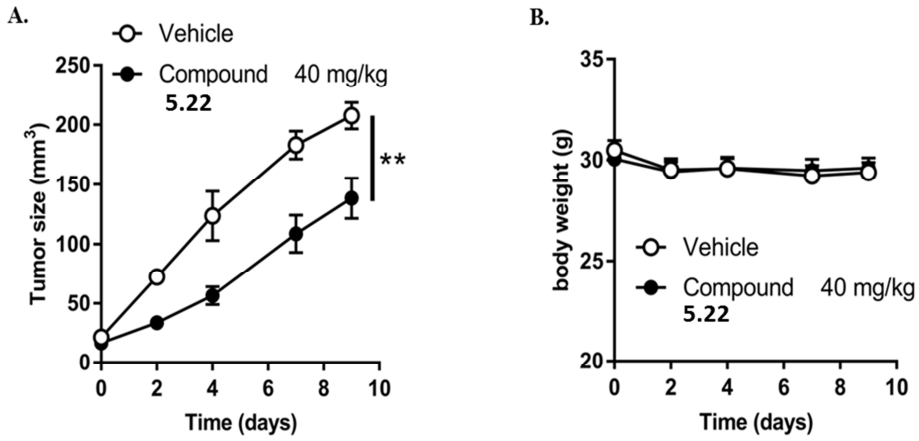

***Figure 29**: In vivo efficacy of compound **5.22**. SiHa tumor xenografts volume evolution (A) and mice body weight evolution (B) during the 9-day treatment with **5.22**. Data points are the mean of 5 animals, and error bars represent standard error of the mean. **, p < 0.01.*

Remarkably, at 40mg/kg, the *α*-ketothioamide **5.22** significantly reduces the volume of PHGDH-dependent SiHa tumor xenografts while not causing any weight-loss during the 9-days of treatment. These promising *in vivo* data for compound **5.22** prompted us to further detail the mechanism-of-action in this series to help the design of more potent compounds.

7.3.3. Effect of compound 5.22 on the de novo synthesis of serine

We first set out to demonstrate that **5.22** reduces cell proliferation by decreasing the global serine flux. To this end, serine synthesis was assessed by stable isotope tracing with labelled glucose ([U-^{13}C] glucose) to measure glucose incorporation into glycolytic intermediates (pyruvate and 3-PG) and hence serine (**Figure 30A**). The experiment was performed in the presence or absence of compound **5.22** at 100 µM, which is the approximate IC_{50} concentration on breast cancer cell lines (BT-20 and MDA-MB-468), two tumor cell lines known to overexpress PHGDH and being dependent on the SSP (**Figure 30**).

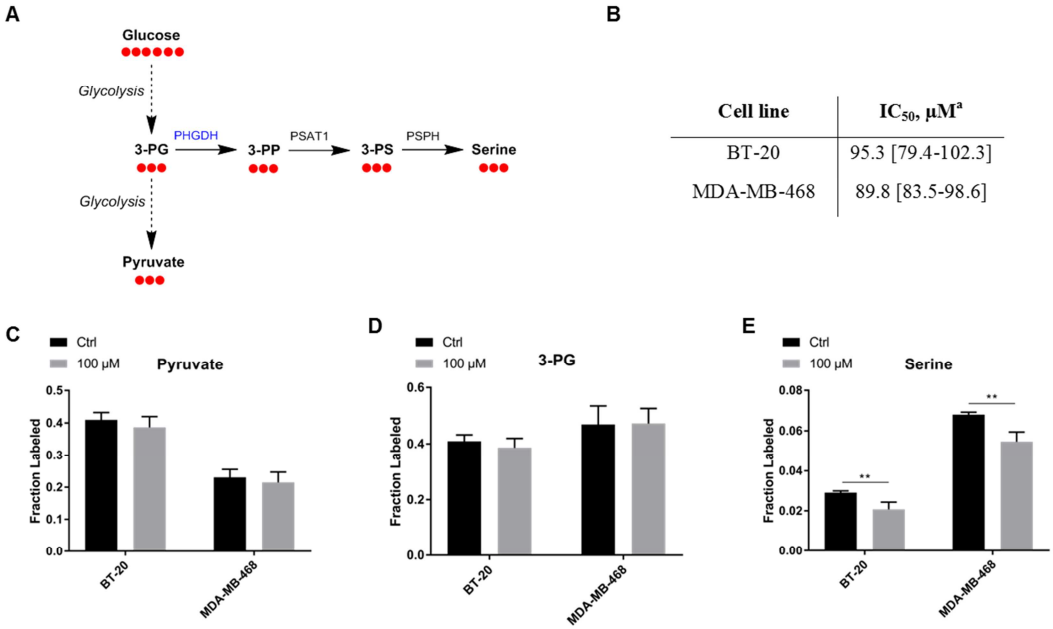

***Figure 30**: Effect of inhibitor **5.22** on the incorporation of [U-^{13}C] glucose carbons into glycolytic metabolites in BT-20 and MDA-MB-468 cell lines. Schematic overview of the serine biosynthesis pathway with the number of carbons highlighted by red dots (**A**). BT-20 and MDA-MB-468 cells proliferation inhibition (IC_{50}) by compound **5.22** (n = 6 for each condition, IC_{50} values were averaged on two or more independent experiments, square brackets indicate 95 % confidence interval) (**B**). Experiment monitoring pyruvate (**C**), 3-PG (**D**) and serine (**E**). The y axis indicates the labelled fraction of the analysed metabolite derived from glucose (M+3) metabolite level relative to total metabolite level. All experiments to determine M+3 metabolite values were performed in quintuplicate for each inhibitor concentration. **, p < 0.01.*

Coherently, **5.22** does not affect the concentration of the glycolytic intermediates 3-PG and pyruvate (**Figure 30C** and **30D**). However, it significantly reduces the production of serine from [U-^{13}C]glucose (**Figure 30E**). This experiment thus confirms that **5.22** selectively decreases *de novo* serine synthesis by inhibiting the SSP pathway.

7.3.4. MST evaluation

Microscale thermophoresis (MST) was then used to appraise the binding of **5.22** to PHGDH. Experiments confirmed that **5.22** effectively binds to PHGDH with a Kd value (35.02 µM) in the same range as the determined IC_{50} concentration. In contrast, the *meta-*

substituted analogue **5.21**, used as a negative control in this experiment, showed no appreciable binding in the experimental conditions (**Figure 31**).

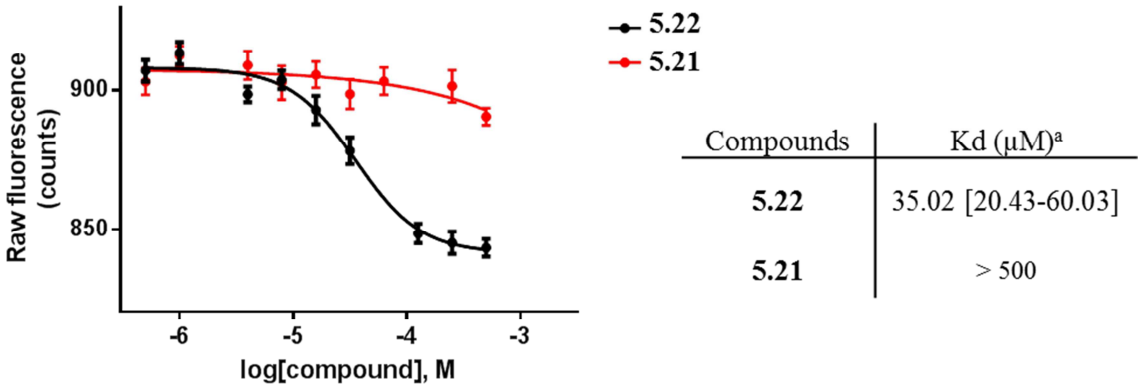

Compounds	Kd (µM)[a]
5.22	35.02 [20.43-60.03]
5.21	> 500

Figure 31*: Measurement of binding affinity between* ***5.21****,* ***5.22*** *and PHGDH by MST. Dose-response curves of compounds* ***5.21*** *and* ***5.22*** *on isolated PHGDH protein. Binding affinities (Kd) of* ***5.21*** *and* ***5.22*** *(Kd values were determined from two independent experiments performed in triplicates at each compound dilution, in brackets: 95 % confidence interval).*

Altogether, these results demonstrate that compound **5.22** can inhibit the SSP in cells through its interaction with PHGDH, suggesting that the *in vivo* anticancer activity is, at least in part, due to PHGDH inhibition. However, at this stage, apart from a previously reported non-competitive mode of inhibition with respect to both substrates and an apparent irreversible profile, the precise binding mode of **5.22** to PHGDH remained mostly unclear.[14] Because our tentative to crystallize PHGDH with **5.22** proved, in our hands, to be unsuccessful, a photo-reactive crosslinking strategy was preconized.

7.3.5. Design and synthesis of the photoactivatable probe 7.8

The reactive photoactivatable probe **7.8** was designed based on our initial SAR study indicating that the *para*-position on the aryl moiety is preferred. We therefore envisaged to incorporate the well-known photoactivatable trifluoromethyl diazirine moiety in this particular *para*-position using a reported chemical strategy.[100]

The chemical synthesis of the target molecule **7.8** started with the protection of the commercially available ketone **7.1** to its dioxolane **7.2** (**Scheme 2**). A two-step procedure consisting of a lithium/halogen exchange followed by addition of ethyl trifluoroacetate

afforded the ketone **7.3**. Then, condensation of **7.3** with hydroxylamine and subsequent tosylation led to the intermediate **7.5**. Afterwards, diaziridine formation with ammonia followed by oxidation to the desired diazirine **7.6** proceeded smoothly. Finally, deprotection of the ketone and its further *α*-bromination led to the dibromoketone **7.7** that was treated in the Willgerodt-Kindler conditions to deliver the photoactivable probe **7.8**.

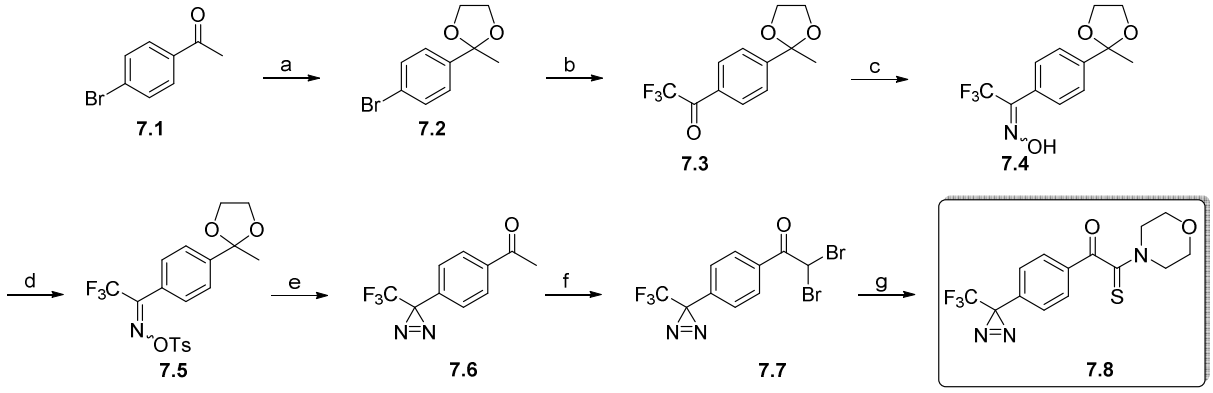

Scheme 2. *Synthetic pathway of diazirine **7.8**. (a) ethylene glycol and PTSA.3H_2O, toluene, 110°C, 24h, quant. (b) (i) n-BuLi, THF, -78°C, 2h (ii) ethyl trifluoroacetate, THF, -78°C, 3h, 31%. (c) $NH_2OH.HCl$, NaOH, EtOH, 78°C, 18h, 96%. (d) pTsCl, Et_3N, DMAP, CH_2Cl_2, rt, 18h, quant. (e) (i) NH_3/MeOH, THF, rt, 18h. (ii) I_2, Et_3N, MeOH, rt, 1h. (iii) PTSA, H_2O/acetone, rt, 18h, 50%. (f) Br_2, TBAB, $CHCl_3$, rt, 18h, 89%. (g) S_8, morpholine, DMF, rt, 48h, 82%.*

7.3.6. Evaluation of the photoactivable probe 7.8

Before investigating a possible adduct between the photoactivatable probe **7.8** and PHGDH, its PHGDH inhibition potency was evaluated and an IC_{50} value of 571 µM was obtained. This low inhibitory potency compared to the parent *α*-ketothioamide **5.22** is relatively consistent with the previously identified SARs highlighting the limited possible pharmacomodulations in this position. Still, we hypothesized that although lower potency than **5.22,** this tool compound could help us to reveal the binding mode in this series.

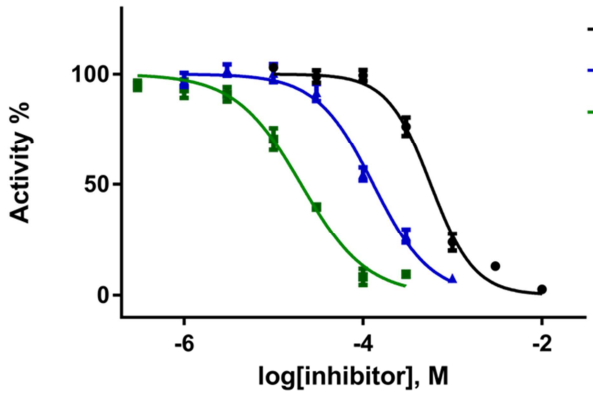

Compounds	PHGDH IC_{50}, µM
5.16	111.1 [87.3-131.1]
5.22	20.3 [15.6-26.4]
7.8	570.7 [451.6-721.2]

Figure 32: *Dose-response curves of compounds **5.16**, **5.22** and **7.8** on isolated PHGDH. IC_{50} values were determined from two independent experiments performed in triplicates at each compound dilution, in brackets: 95 % confidence interval.*

7.3.7. Photoactivation and mass spectrometry analysis

Photoactivation experiments were performed with the diazirine **7.8** in the presence or absence of compound **5.22** at various concentrations in order to analyse the potential competition for the same binding site of these two compounds.

Briefly, PHGDH was incubated with or without inhibitor **5.22** for one hour and then the diazirine derivative **7.8** (1 mM) was added for 30 minutes. The labelling with the photoactivatable diazirine was performed by irradiation at 350 nm for 10 minutes. Finally, the enzyme-inhibitor complex underwent a trypsin digestion and the resulting peptides were analysed by nanoUPLC/MS. As a result, several peptides were identified, some of them being covalently modified by the diazirine **7.8** (see **Table S1** in Supporting Information). Interestingly, among the detected peptides, only the ^{523}QHVTEAFQFHF^{533} C-terminal peptide, that is part of the ACT (aspartate kinase-chorismate mutase-TyrA) domain[104] of PHGDH (**Figure 33A**), could be titrated out by addition with the competing compound **5.22**. Indeed, only the percentage of labelling of this particular peptide was reduced (from 43 % to 6 %) upon addition of **5.22**, thus suggesting that this particular peptide is most probably part of an allosteric binding site for the *α*-ketothioamide **5.22** (**Table S2** in Supporting Information).

To the best of our knowledge, this ACT domain in PHGDH has never been reported before as a potential target binding site. Interestingly, in lower organisms like *E. coli* this domain is a regulatory domain where l-serine binds to induce a negative feedback inhibition of the

enzyme (**Figure 33B**). However, in human PHGDH (Type I enzyme), this serine inhibition no longer occurs due to mutations of key binding residues.[105] The allosteric inhibition by our α-ketothioamides, even if they act on the ACT domain, should therefore be linked to a different and novel mechanism.

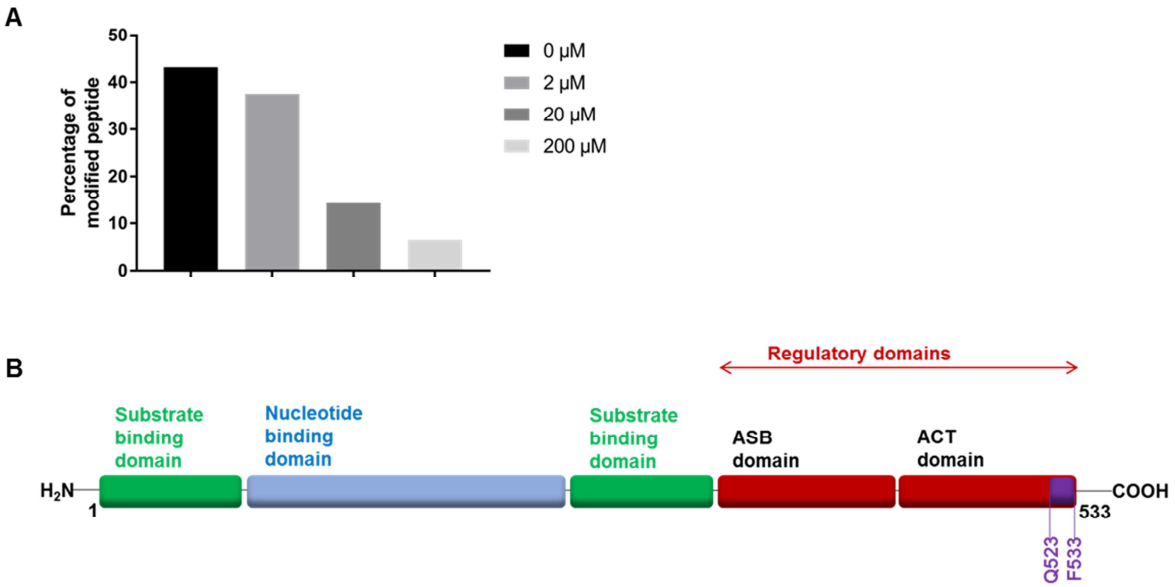

Figure 33: *Result of the photoactivation experiment. Percentage of the modified QHVTEAFQFHF peptide after incubation with compound* ***5.22*** *at different concentrations (**A**). Determined from the peptide spectrum matches (PSMs) of their precursors after trypsinization and analysis by nanoUHPLC/MS. Compound* ***5.22*** *was incubated with PHGDH in 50 mM Tris and 1 mM EDTA at pH 8.5 during 1 hour before adding 1 mM of* ***7.8****. In x axis, compound* ***5.22*** *concentration. Schematic structure of full-length human PHGDH with substrate binding domain in green, nucleotide binding domain in blue, regulatory domains in red and diazirine modified peptide in purple (**B**).*

7.3.8. Mutagenesis experiments

Finally, to demonstrate our hypothesis that **5.22** binds to the allosteric site on PHGDH delineated by the ^{523}QHVTEAFQFHF^{533} C-terminal peptide, that is part of the ACT domain, mutagenesis experiments were conducted. To this end, a PHGDH mutant lacking the ^{523}QHVTEAFQFHF^{533} C-terminal site (PHGDH-tr) was produced. Interestingly, this mutant

retained its enzyme activity in the same range to that of the native PHGDH. However, the inhibitory potency of **5.22** on the mutant was found to be completely abolished (**Figure 34**), hence demonstrating that the ^{523}QHVTEAFQFHF^{533} C-terminal site is indeed the target of **5.22.** As a comparison, **2.17** (disulfiram/DSF), a well-known PHGDH inhibitor acting at an allosteric site distant from the site identified herein[15], displayed the same PHGDH inhibitory potency both for the native and truncated enzymes.

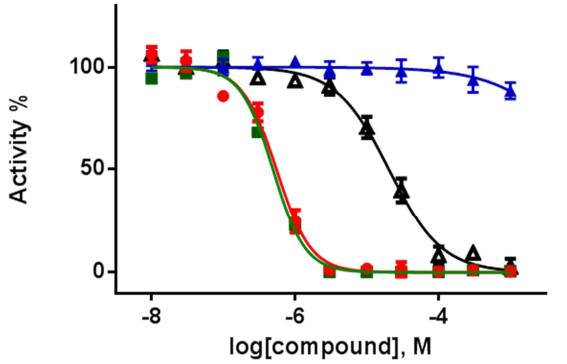

Compounds	PHGDH (WT) inhibition (IC50, µM)	PHGDH (tr) inhibition (IC50, µM)
5.22	20.3 [15.6-26.4]	> 300 µM
2.17	0.59 [0.37-0.95]	0.78 [0.43-1.08]

Figure 34: *Dose-response curves of compounds **5.22** and **2.17** on isolated PHGDH (WT and tr). IC_{50} values were determined from two independent experiments performed in triplicates at each compound dilution, in brackets: 95 % confidence interval.*

7.4. CONCLUSIONS

In this study, we were initially interested in evaluating the *in vivo* anticancer potential of a series of *α*-ketothioamide PHGDH inhibitors. Interestingly, using an orthotopic xenograft tumor mouse model we demonstrated that one representative *α*-ketothioamide compound (**5.16**) effectively exerts a promising anticancer activity, without affecting body weight or resulting in any signs of toxicity in the mouse model.

With the aim to fuel the development of new anticancer drugs, we next set out to detail the mechanism-of-action of **5.22** on PHGDH. To this end, the global serine flux was analysed using stable isotope tracing with ^{13}C labelled glucose and demonstrated that **5.22** significantly reduces the serine flux. Then, the use of microscale thermophoresis experiments allowed us to support the binding of **5.22** with PHGDH. With the aim to decipher the exact binding of **5.22** on PHGDH a crosslinking strategy using a photoactivatable diazirine probe was used and led to the identification of a previously

unknown allosteric site on PHGDH delineated by the ^{523}QHVTEAFQFHF^{533} C-terminal peptide, that is part of the PHGDH ACT domain, as the target binding site. Mutagenesis experiments further corroborated our hypothesis.

Although the structure of the allosteric site identified here is not known as it was not resolved in the various X-ray data available on human PHGDH, our data pave the way to the development of novel anticancer agents acting along a particularly original mechanism-of-action.

7.5. EXPERIMENTAL SECTION

7.5.1. General Chemistry.

All reagents were purchased from chemical suppliers and used without purification. Thin-layer chromatography (TLC) was performed using silica gel 60 F254 plates, with observation under UV when necessary. Melting points were recorded on an Electrothermal IA9000 melting point system. ^{1}H NMR spectra were recorded an AVANCE II 400 MHz Bruker spectrometer with $CDCl_3$ or DMSO-d_6 as the solvent. ^{13}C NMR spectra were recorded at 100MHz. All coupling constants are measured in hertz (Hz), and the chemical shifts (δH and δC) are quoted in parts per million (ppm) relative to TMS (δ0), which was used as the internal standard. Data are reported as follows: chemical shift, multiplicity (s = singlet, d =doublet, t = triplet, q = quartet, br = broad, m = multiplet), integration, and coupling constant (Hz). High-resolution mass spectroscopy (HRMS) analyses were carried out on a LTQ-Orbitrap XL hybrid mass spectrometer (Thermo Fisher Scientific, Bremen, Germany). Data were acquired in positive ion mode using full-scan MS with a mass range of 100−1000m/z. The orbitrap operated at 30000 resolutions (fwhm definition). All experimental data were acquired using daily external calibration prior to data acquisition. Appropriate tuning of the electrospray ion source was done. The following electrospray inlet conditions were applied:flow rate, 100µL min−1;spray voltage, 5 kV; sheath gas (N2)flow rate, 20 au; auxiliary gas (N2)flow rate, 10 au; capillary temperature, 275°C; capillary voltage, 45 V; tube lens, 80 V. High-performance liquid chromatography (HPLC)analyses were performed on a LC system using a YMC-Triart C-18(250 mm×4.6 mm, 5µm) column as the stationary phase. Mobile phase contained water/CH_3CN (30:70, v/v) and was maintained isocratically at the flow rate of 1 mL/min. The column temperature was maintained at room temperature. The peaks were monitored at the wavelength of 215 nm. The purity of all compounds tested was greater than 95%, as determined by HPLC and ^{1}H NMR.

The synthetic procedures of compounds **5.16**, **5.21**, **5.22** and the diazirine probe **7.8** are detailed in annexes (Chapter 11).

7.5.2. PHGDH Assay.

Enzymatic assay was adapted from a previously described procedure.[86] In brief, the reactions were performed in PHGDH assay buffer (50 mM Tris, pH 8.5, and 1 mM EDTA) following resorufin fluorescence emission (Ex 550 nm/Em 580 nm) over time. Substrates and enzyme concentrations were as follows: 240 µM 3-PG; 120 µM NAD^+; 30 mM glutamate; 0.1 mM resazurin; 12 ng/µL human PHGDH; 20 ng/µL human PSAT1; 0.18 µg/µL diaphorase. The final concentration of DMSO in the assay mixture was set to 5%.

7.5.3. PHGDH-tr Purification.

pET28a human PHGDH-tr (Genecust) were transformed into BL21 *Escherichia coli*, the protein was produced and tested following a reported procedure.[15] Protein purity was assessed via SDS/PAGE and Coomassie staining.

7.5.4. MST assay.

MST measurements were performed on a Nanotemper Monolith NT.115 instrument (Nano-Temper Technologies) using Red-dye-NHS fluorescent labeling. PHGDH was labeled with the Monolith RED-NHS 2nd generation labeling dye according to manufacturer's instructions (Nanotemper Technologies). Measurements were performed in 50 mM Tris buffer pH 8.5, 250 mM NaCl, 10 mM $MgCl_2$ and 100 µM DTT containing 0.05 % P-20 in premium-treated capillaries (NanoTemper Technologies). Experiments were performed in triplicates using 40 % LED power, medium MST power, LaserOn time was 20 sec, Laser Off time 3 sec.

7.5.5. Diazirine irradiation.

Human PHGDH (5µg) was incubated 30' at room temperature with compound **7.8** in classical assay buffer (50 mM Tris, pH 8.5, and 1 mM EDTA). The mixture was then irradiated on ice using Stratalinker UV Crosslinker 1800 at 350 nm for 10'.

7.5.6. Mass spectrometry experiments, Orbitrap Lumos.

Mass spectrometry experiments were carried out on an Orbitrap Lumos, following a previously reported procedure, with some modifications.[106] A local protein database containing the human PHGDH sequence (accession Uniprot O43175) was used to process the

obtained MS/MS data. Mass error was set to 10 ppm for precursor ions and 0.6 Da for fragment ions. Oxidation on Met; diazirine (+315.068) and carbamidomethyl (+57.021 Da) were considered as variable modifications on Cys, His, Phe, Thr and Met.

7.5.7. Cell models and cytotoxicity assay.

SiHa cervix cancer cells, HL-60 leukemia cells (shCtrl and shPHGDH), BT-20 and MDA-MB-468 breast cancer cells were purchased from ATCC and cultured in DMEM medium supplemented with 10% heat-inactivated Fetal Bovine Serum (FBS) and 1% penicillin/streptomycin. For the cytotoxicity assay, cells were seeded at low density in 96-well plates in serine containing media following a previously reported procedure.[86] Media was then aspirated, and cells were incubated in fresh serine-replete or -deplete media containing compounds at indicated concentrations or vehicle (DMSO). Cells were grown for 5 days at 37°C with drug and media changed daily before assaying cell viability using a Presto Blue assay (Life Technologies) according to manufacturer's instructions.

7.5.8. BT-20 and MDA-MB-468 Serine Labeling Time Course and Acute Drug Treatments with ^{13}C6-Glucose Tracing.

BT-20 or MDA-MB-468 cells were acclimated to growth in MEM supplemented with 10% dialyzed FBS, 1 % penicillin-streptomycin by culturing for 1 week (approximately three passages). Cells were plated at 9 × 105 cells per 6-cm dish 1 day prior to the experiment. For acute drug inhibition assays, media was replaced with fresh media containing compound **5.22** (10 μM, 30 μM, 100 μM) or vehicle control (DMSO/0.5 %) for 1 h. Then media was aspirated, cells were washed with PBS, and fresh glucose-free MEM supplemented with [^{13}C]6-glucose (3g/L; Sigma) and 10% dialyzed FBS containing drug or DMSO was added. After 2 h, cells were quickly washed with cold PBS on ice and flash frozen. Polar metabolites were then extracted and analyzed as described in the LCMS methods.[73]

7.5.9. LCMS Metabolite Analysis.

Polar metabolites were extracted with 2 mL of MeOH/H_2O (4:1) for 30 min on dry ice, scraped, transferred to 2-mL tubes, centrifuged (30 min, 21,000 × g), and the supernatants were dried under vacuum. Targeted LCMS analysis was performed on a Q Exactive Orbitrap

mass spectrometer (Thermo Scientific) coupled to a Vanquish UPLC system (Thermo Scientific). The Q Exactive operated in polarity-switching mode. A Sequant ZIC-HILIC column (2.1 mm i.d. × 150 mm, Merck) was used for separation of metabolites. Flow rate was 150 µL/min. Buffers consisted of 100% acetonitrile for A, and 0.1% NH_4OH/20 mM CH_3COONH_4 in water for B. Gradient ran from 85 to 30% A in 20 min followed by a wash with 30% A and reequilibration at 85% A. Metabolites were identified on the basis of exact mass within 5 ppm and standard retention times. Metabolites and their [^{13}C]-isotopologues were identified on the basis of standard retention times and exact mass within 5 ppm. Relative quantitation was performed based on metabolite peak area. All data analysis was done using in-house written scripts.

7.5.10. Xenograft models.

All experiments involving mice received the approval of the ethic committee from the Université Catholique de Louvain (approval ID 2016/UCL/MD/018) and were carried out according to national animal care regulations. Seven-week old female NMRI nude mice were purchased from Elevage Janvier and approximately $2x10^6$ SiHa tumor cells were injected subcutaneously in the left flank of the animals. When tumors reached a mean diameter of 5 mm, compound **5.22** (40 mg/kg; resuspended in DMSO) was daily injected intraperitoneally. Tumor size was tracked every 2-3 days with an electronic caliper and determined using the formula: (length x width² x p)/6.

7.6. SUPPORTING INFORMATIONS

7.6.1. Peptides tables

Table S1. PHGDH peptides (after trypsination) showing a diazirine modification after treatment at 1 mM of **7.8**.

Peptide sequence[a]	m/z observed MH+ (Da)	m/z calculated MH+ (Da)	Δ (ppm)	Chemical modification
^{59}VTADVINAAEK^{69}	1130.60723	1130.60518	1.81	/
^{59}VTADVINAAEK^{69}	1445.66509	1445.67318	-5.6	Diazirine
^{76}AGTGVDNVDLEAATR^{90}	1488.73076	1488.72888	1.27	/
^{76}AGTGVDNVDLEAATR^{90}	1803.79106	1803.79688	-3.22	Diazirine
^{120}QIPQATASMK^{129}	1074.56621	1074.56121	4.66	/
^{120}QIPQATASMK^{129}	1389.62029	1389.62921	-6.42	Diazirine
^{352}GTIQVITQGTSLK^{364}	1345.77104	1345.76856	1.85	/
^{352}GTIQVITQGTSLK^{364}	1660.84599	1660.83656	5.68	Diazirine
^{470}TQTSDPAMLPTMIGLLAEAGVR^{491}	2272.06311	2272.16756	3.17	/
^{470}TQTSDPAMLPTMIGLLAEAGVR^{491}	2587.23172	2587.23556	-1.48	Diazirine
^{523}QHVTEAFQFHF^{533}	1390.65752	1390.65386	2.63	/
^{523}QHVTEAFQFHF^{533}	1705.71256	1705.72186	-5.45	Diazirine

[a]Superscripted numbers indicate the amino acid numbering of human PHGDH.

Table S2. PHGDH peptides (after trypsination) showing a diazirine modification after treatment at 1 mM of **7.8** and **A.** 0 µM **B.** 2 µM and **C.** 20 µM **D.** 200 µM of **5.22**. Percentage of modified peptides was obtained based on the PSMs ratio between modified and unmodified peptides. [a]Superscripted numbers indicate the amino acid numbering of human PHGDH.

Peptide sequence[a]	**m/z observed MH+ (Da)**	**m/z calculated MH+ (Da)**	**^ (ppm)**	**Percentage of modified peptides**
^{523}QHVTEAFQFHF^{533}	1705.71256	1705.72186	-5.45	43.2 %

A. Compound **5.22** concentration 0 µM

Peptide sequence[a]	**m/z observed MH+ (Da)**	**m/z calculated MH+ (Da)**	**^ (ppm)**	**Percentage of modified peptides**
^{523}QHVTEAFQFHF^{533}	1705.71292	1705.72186	-5.24	37.5 %

B. Compound **5.22** concentration 2 µM

Peptide sequence[a]	**m/z observed MH+ (Da)**	**m/z calculated MH+ (Da)**	**^ (ppm)**	**Percentage of modified peptides**
^{523}QHVTEAFQFHF^{533}	1705.71282	1705.72186	-5.30	14.3 %

C. Compound **5.22** concentration 20 µM

Peptide sequence[a]	m/z observed MH+ (Da)	m/z calculated MH+ (Da)	Δ (ppm)	Percentage of modified peptides
^{523}QHVTEAFQFHF^{533}	1705.71274	1705.72186	-5.35	6.53 %

D. Compound **5.22** concentration 200 µM

8. Anti-alcohol abuse drug disulfiram inhibits human PHGDH via disruption of its active tetrameric form through a specific cysteine oxidation

This chapter is based on the following publication: Spillier, Q. Anti-alcohol abuse drug disulfiram inhibits human PHGDH via disruption of its active tetrameric form through a specific cysteine oxidation. Sci. Rep. 9, 4737 (2019).

Graphical Abstract

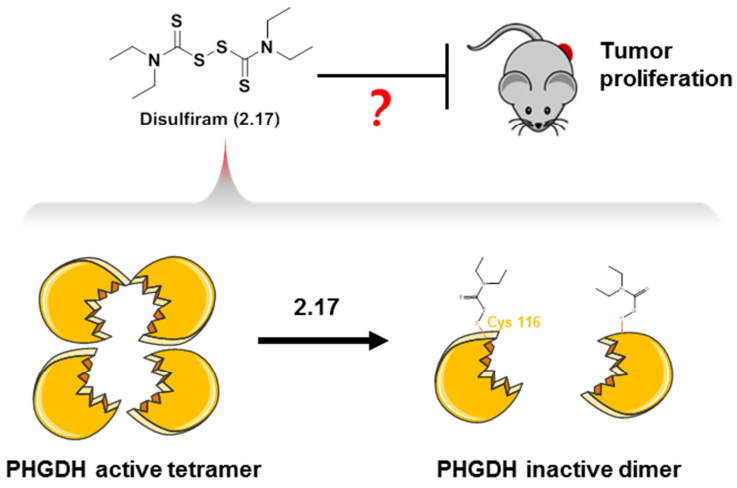

8.1. PREAMBLE: BRIEF HISTORY OF 2.17 (DISULFIRAM), FROM THE RUBBER INDUSTRY TOWARDS NOVEL ANTICANCER AGENT

Among the other series of PHGDH inhibitors that we identified during the screening, disulfiram (**Figure 35**) appeared promising for several reasons. But before going further, it seemed important to have a deeper look into Dilfiram's history.

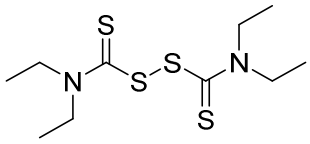

***Figure 35**: **2.17** (Disulfiram) structure*

The first chemical synthesis of **2.17** was reported in 1881 by Grodzki, although this molecule did not seem to be of interest to the scientific community.[107] However, it appeared 20 years later that tetraethylthiuram disulfide could play a role in the rubber industry due to its ability to accelerate the vulcanization process.[108] It was only years later that a potential anti-alcohol application started to emerge. The massive use of **2.17** as a vulcanization agent had confronted a large population of workers to its potential side effect. In 1937, Williams reported for the first time that the exposed workers appeared far less tolerant to alcohol ingestion, thus suggesting the potential use of this molecule against alcoholism.[109] However, at this point the suggestion was not followed.

Despite this, the possible use of **2.17** as a therapeutic agent was not abandoned. In the early 1940s, research highlighted the potential of this molecule to act as a promising drug against scabies[110] and intestinal worms. Intrigued by this therapeutic effect, Jacobsen and Hald established a link with cell oxidation by the formation of a chelate with copper. Because of this chelation, the absorption of copper is decreased and the oxygen transport chain of the parasites is disrupted.[111] However, before commercializing the drug as a vermicide, Jacobsen decided to test the drug on himself in order to study the side effects. Having experienced strong side effects (such as accelerated heart rate, shortness of breath, nausea and visual disturbance) when **2.17** was used in combination with alcohol, they concluded that this drug could be useful to treat alcoholism. However, due to the lack of interest in treating alcoholism during this period, it was only two years later that research was

resumed.[112] Further studies on ethanol metabolism led by Jacobsen, Raby and Widmark demonstrated that disulfiram acts as an inhibitor of aldehyde dehydrogenase (ALDH) leading to the accumulation of acetaldehyde, the main ethanol metabolite in the body.[113–115] Compound **2.17** was then commercialized, under a stabilized copper complex form, in 1949 under the name of "Antabuse" in Denmark and approved by the Federal Drug Administration in 1951 in the USA.[116] Although the hopes in this miracle cure were not fully answered, Antabuse became the main anti-alcohol abuse treatment in our countries.

Nowadays, this molecule is less and less used for this indication. Indeed, at the recommended dose, numerous side effects were reported. Compound **2.17** can cause neurotoxicity, leading to extrapyramidal symptoms, but can also induce liver toxicity.[117,118] However, over the years, disulfiram was also studied in order to treat other diseases. In 1952, Pindborg reported than **2.17** could be used to treat certain dental diseases caused by lack of vitamin E.[119] In 1966, Schirmer was the first to demonstrate an anti-cancer effect from **2.17**.[120] As a result, the 80s saw an intensification of research on this particular property (**Figure 36**).

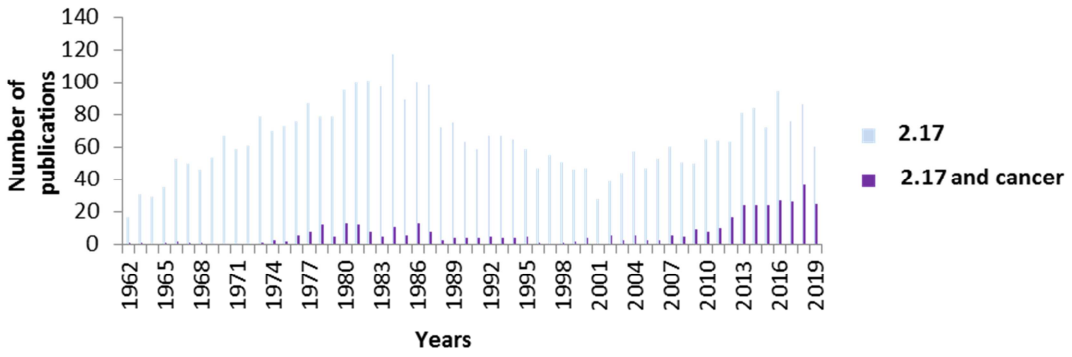

***Figure 36**: Disulfiram and cancer-related publications. Data were collected from Pubmed*

Numerous studies have thus demonstrated the effect of this molecule to reduce carcinoma formation in rats. Subsequently, these results could be extended in rat models to leukemias, breast and liver cancers.[121–124] For example, in 1981, the Hozumi group reported the antioxidant capacity of disulfiram in the inhibition of differentiation of mouse myeloid

leukemia cells.[125] Other studies are interested in the use of **2.17** co-treatment to reinforce the anti-cancer effect and limiting major side effects. Thus, Hacker was able to demonstrate that the administration of disulfiram, during treatment with cyclophosphamides, allowed to increase its effectiveness while limiting the bladder damages often associated with this type of treatment.[126] This synergic effect was also reported by Hrushesky during the use of cisplatin in animals and humans models.[127] Despite these promising data in **2.17** repurposing, unsatisfactory clinical results, mainly related to excessive cytotoxicity, led in the 1990s to a decrease in the study of this molecule. Nevertheless, the main discovery of this period has brought a first mechanistic understanding of this anticancer effect. In 1998, Lin's group demonstrated that the chemopreventive ability of disulfiram may be related to an interaction with NFkappaB, c-fos/c-jun, and p53.[128] Extensive research on **2.17** metabolites led them to the conclusion that coordinative modulation of these different proteins can induce apoptosis by stopping the G1/S cycle. Unexpectedly, a renewed interest in **2.17** repurposing was observed in the early 2000s.

Indeed, its ability to slow the progression of prostate cancer, glioblastomas and melanomas in humans was highlighted in different major researches.[129–131] A new mechanistic understanding was updated by the Chang group during their investigation in the **2.17** inhibition of matrix metalloproteinases (MMPs).[132] They demonstrated its ability to suppress the invasion of osteosarcoma cells via the inhibition of MMP-2 and MMP-9. Currently, studies conducted on disulfiram or one of these active metabolites, CuET complex (**Figure 37**), demonstrate that it can be responsible for the inhibition of numerous cancer types proliferation.

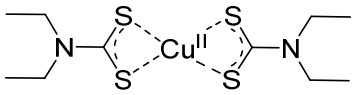

***Figure 37**: CuET major DSF metabolite*

However it is only very recently that a clear anticancer mechanism for **2.17** was detailed when Skrott *et al.* demonstrated that an *in vivo* metabolite of **2.17** could act as an inhibitor of NPL4, an adaptor of segregase p97 (also called VCP), essential for the recycling of proteins involved in multiple regulatory and stress-response intracellular pathways.[133] IThe group of Bartek actually demonstrated that a DTC–copper complex named

bis(diethyldithiocarbamate)–copper (CuET) forms *in vivo*, thereby providing the anti-cancer metabolite of **2.17**.[133]

During the same period, effects of DSF in other diseases were also investigated. The team of Ambudkar reported in 2005 that disulfiram can also be used as a potential treatment of fungal infections.[134] More recently, its role as a potential treatment against Lyme disease through the inhibition of *Borrelia burgdorferi* proliferation was published.[135] In 2016, it also appeared that this molecule can be used in order to treat HIV *via* the reactivation of latent HIV infection. In this optic, **2.17** is currently under investigation in combination with Vorinostat (a histone acetylase inhibitor).[136]

8.2. INTRODUCTION

In our opinion, following the identification of **2.17** as a potent PHGDH inhibitor it seemed very interesting to dig deeper into this question. It is important to keep in mind that disulfiram is an approved drug that it is currently under investigation in numerous clinical studies in the field of cancer.[137] Its repurposing in the therapy of cancer is foreseen. This would provide a new effective drug, avoiding expensive development phases before its commercialization,[138,139] **2.17** having a well-known ADME profile[140] and a fairly broad efficiency on various tumor lines in pre-clinical models.[141] Besides the potential repurposing of **2.17** in cancer, the understanding of the mechanism-of action of **2.17** on PHGDH could lead to the development of novel anticancer agent acting a particularly original mechanism of action.

In this chapter, we set out to examine structure–activity relationships (SAR) in a series of disulfiram analogs and to elucidate its mechanism-of-action.

8.3. RESULTS AND DISCUSSION

8.3.1 Analogues screening

As a first step to detail our understanding of the binding of **2.17** on PHGDH, some preliminary SAR were investigated around the bis(dithiocarbamate) central core. To this end, a library of 20 disulfiram analogues developed earlier[85] by our team was screened on purified PHGDH using an isolated enzymes inhibition assay.[86] Compared to the parent compound (**2.17**), apart from compound **8.1**, all the attempts to replace the diethylamino side chain in **2.17** (**8.2-15**) afforded similarly active compounds (**Table 11**). On the contrary, replacing the central symmetric bis(dithiocarbamate) motif by either an acetamido carbamodithioate (**8.16**), a thioacetamido carbamodithioate (**8.17**), or a methylene dicarbamidodithioate (**8.18-19**) led to compounds that inhibit PHGDH only weakly or inactive compounds. These relatively flat SAR for **2.17** analogues possessing the symmetrical bis(dithiocarbamate) central core (**2.17,8.2-15**) led us to suspect either (i) unspecific binding, (ii) binding at a site distant from the PHGDH active site (allosteric binding) or possibly (iii) covalent inhibition. Puzzled by this question we set out to detail the mechanism-of-action of **2.17** on PHGDH.

***Table 11**. PHGDH inhibition (IC_{50}) of **2.17** analogues*

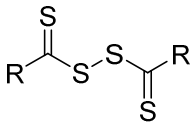

2.17
and 8.1-15

Cmpd	R	PHGDH inhibition (IC_{50}, µM)[a]	Cmpd	R	PHGDH inhibition (IC_{50}, µM)[a]
2.17 (DSF)	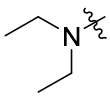	0.59 [0.37-0.95]	**8.10**	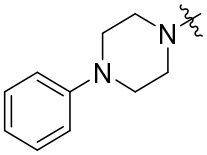	0.41 [0.27-0.60]
8.1	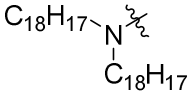	> 1 mM	**8.11**	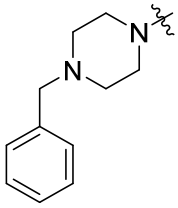	22.5 [14.0-39.9]
8.2	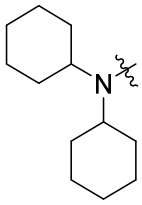	1.39 [1.03-1.89]	**8.12**	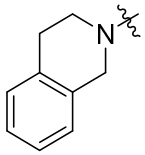	0.38 [0.29-0.50]
8.3	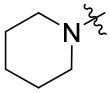	0.51 [0.45-0.77]	**8.13**	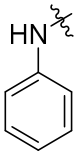	0.36 [0.20-0.62]
8.4	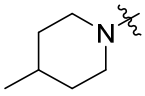	0.58 [0.44-0.77]	**8.14**	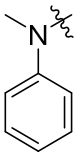	0.42 [0.33-0.54]
8.5	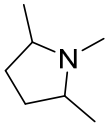	0.42 [0.36-0.48]	**8.15**	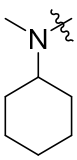	1.01 [0.67-3.52]

8.6	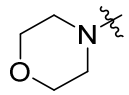	0.21 [0.18-0.25]	**8.16**	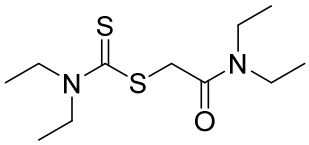	> 1 mM
8.7	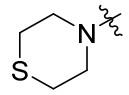	0.34 [0.23-0.51]	**8.17**	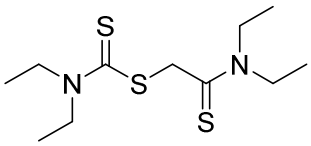	36.38 [19.99-66.19]
8.8	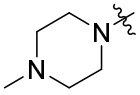	0.17 [0.14-0.21]	**8.18**	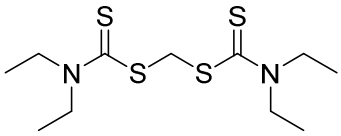	45.86 [29.15-72.16]
8.9	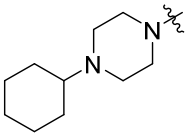	0.57 [0.46-0.69]	**8.19**	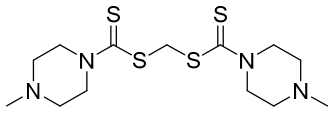	67.32 [29.42-154.18]

[a]All experiments to determine IC_{50} values were performed in triplicates at each compound dilution. Under bracket: 95 % confidence interval.

Unspecific binding was ruled out by adding, in the inhibition assay buffer, Triton-X, a detergent well-known to abrogate inhibition data *via* product aggregation, and measuring a similar IC_{50} (See **Supporting Information Figure S2**).

8.3.2. Mechanism of action

Then, both a rapid dilution and an incubation assays were performed to investigate the possible formation of a covalent adduct between PHGDH and **2.17** as already suggested on other targets.[142]

As reported on **Figure 38A**, PHGDH inhibition increases, along incubation time, from no inhibition (100% residual activity) in the absence of **2.17**, to 100% inhibition after 45 min incubation with **2.17**. These results suggest that **2.17** acts as a time-dependent inhibitor on PHGDH. Moreover, after a rapid dilution of the enzyme/inhibitor complex, the PHGDH activity was not restored indicating that **2.17** shows most probably an irreversible inhibition mechanism (**Figure 38B**).

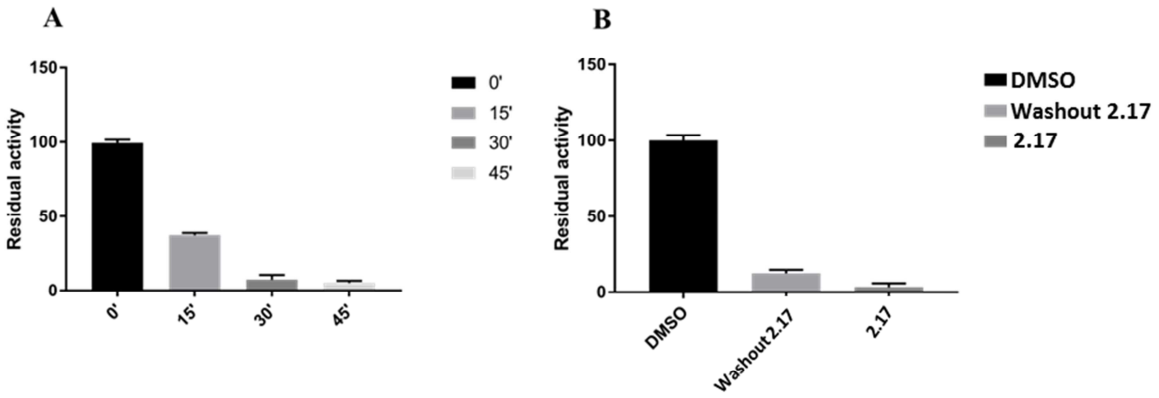

***Figure 38**: Characterization of PHGDH inhibition by **2.17.** Residual activity percentage of PHGDH **A.** upon incubation with **2.17** (50 µM) for the indicated times and **B.** after the rapid dilution assay experiment with **2.17** (50 µM). After the dilution (washout **2.17**), the activity of the protein was not recovered (100% = DMSO ctrl) but remain similar to normal treatment with **2.17**, demonstrating an irreversible mode of action. All experiments values were performed in triplicates at each compound dilution and error bars show the standard deviation. Data were collected at 37°C with a PHGDH concentration of 12 ng/µL in 50 mM Tris and 1 mM EDTA at pH 8.5.*

8.3.3. CuET complex

Because previous studies showed that **2.17** anti-cancer activity is copper-dependent, and Skrott *et al.* found that the disulfiram metabolite diethyldithiocarbamate containing copper ions (CuET) is responsible for the anti-cancer activity through inhibiting the p97 segregase adaptor NPL4, we verified whether PHGDH inhibition could result from the formation of this copper complex. To this end, we synthesized the diethyldithiocarbamate (DTC)-copper complex CuEt and analyzed wtPHGDH inhibition. As a result, an IC_{50} in the 10µM range, that is about 16-fold weaker compared to **2.17** itself, was obtained (**Figure 39**). These data demonstrate that although CuEt is known to be responsible, at least in part, for the anticancer activity of **2.17**, PHGDH inhibition is not driven by the formation of this disulfiram metabolite copper complex.

A.

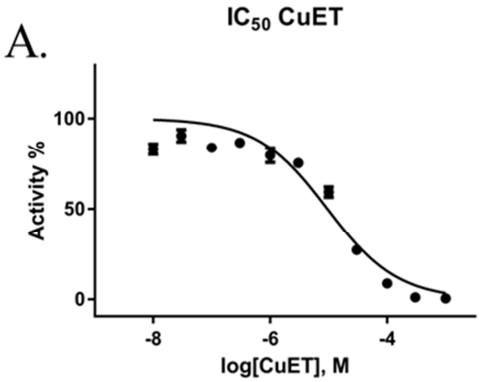

B.

PHGDH	PHGDH inhibition (IC_{50}, µM)[a]
Wild type	9.49 [4.93-18.2]

***Figure 39**: **A.** Dose-response curve of CuET on WT PHGDH **B.** PHGDH inhibition (IC_{50}) of CuET[a]. All experiments to determine IC_{50} values were performed in triplicates at each compound dilution.Under bracket: 95 % confidence interval. Data were collected at 37°C with a PHGDH concentration of 12 ng/µL in 50 mM Tris and 1 mM EDTA at pH 8.5*

8.3.4. Investigation on cysteine(s)

Next, because **2.17** is known to oxidize cysteine residues through the formation of a disulfide bridge such as depicted in **Figure 41A**, we incubated PHGDH with 100 µM of disulfiram for 2h and performed a western blotting of PHGDH alone and after incubation with **2.17**. As a control we also used a reference thiol-modification assay, the 4-acetamido-4'-maleimidylstilbene-2,2'-disulfonic acid (AMS).[143] This thiol-modifying agent is known to bind to free sulfhydryl group of cysteine, providing a 462 Da size shift in protein mass for each cysteine oxidized thus resulting in a change in migration (**Figure 40**), a phenomenon similar to what we expect with **2.17** although with a mass shift of 147 Da by cysteine potentially oxidized. As observed from **Figure 41**, when comparing PHGDH alone (line A) and PHGDH after incubation with **2.17** (line C) no clear shift in mass between the two lines is observed, probably reflecting a very small shift in mass. On the contrary, a clear and large shift in mass can be seen when comparing PHGDH alone (line A) with PHGDH after incubation with AMS (line B), indicating the oxidation of several cysteine residues by AMS. Finally, when PHGDH is first incubated with **2.17** and then with AMS a broader mass profile is observed, suggesting, in part, a competition between AMS and **2.17** leading to several distinct masses (line D). Altogether these results support the hypothesis that PHGDH is oxidized by **2.17** through cysteine(s) modification.

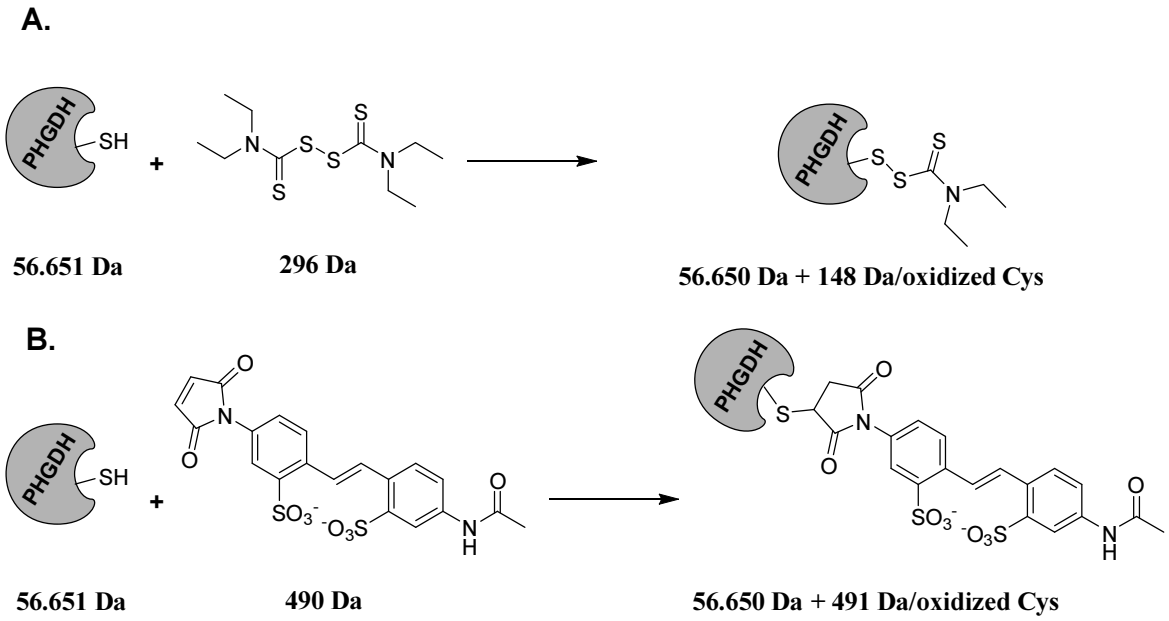

***Figure 40**: Proposed Mechanism of Interaction between PHGDH and **A. 2.17 B.** 4-acetamido-4'-maleimidylstilbene-2,2'-disulfonic acid (**2.17** and **AMS** reacts with sulfhydryl groups of free (reduced) cysteine residues forming a mixed disulfide). Masses after coupling are given for only one reactive cysteine.*

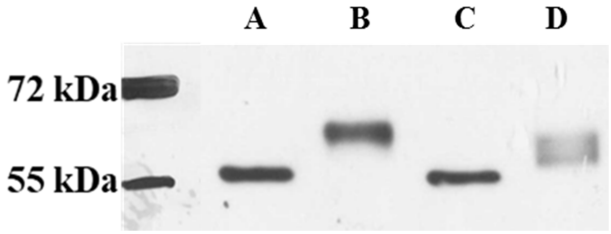

***Figure 41**: Western-blot of the different conditions. All samples were incubated with DSF and/or AMS during 1h at room temperature before running on a 12% SDS-Tris-Glycine Page gel. **A**. PHGDH. **B**. PHGDH with 2 mM AMS. **C**. PHGDH with 100µM **2.17**. **D.** PHGDH with 100 µM **2.17** and 2mM AMS. Original uncropped Western-blot is available in the Supplementary Information File Figure S3.*

8.3.5. Mass spectrometry

To unambiguously confirm this hypothesis and possibly identify the cysteine residues involved in this interaction, mass spectrometry experiments were undertaken. Briefly, PHGDH was incubated for 30min with various concentrations of disulfiram (0.1x IC_{50}, 1x IC_{50}

and 10x IC_{50}). At the end of the incubation, chloroacetamide was added and incubated 15' in large excess in order to block the remaining free cysteines residues for the following analysis. The protein was separated from the medium (removal of the remaining chloroacetamide and **2.17** by liquid/liquid extraction with $CHCl_3/H_2O$) followed by trypsinization and analysis of the peptides by nanoUHPLC/MS.

The results indicated that peptides including 12 out of the 13 Cys residues of the full length PHGDH could be identified and tracked, to allow a semiquantitative determination of their relative abundances before and after **2.17** treatment based on the total number of identified peptides sequences. From these 12 cysteine residues, 9 are not oxidized upon disulfiram treatment and 3 are subject to oxidation (Cys111, 116, 281), although at very different levels (See **Supporting Information Table S3**). Among these 3 cysteine residues, only two, Cys116 and to a lesser extent Cys111, are found to be oxidized by **2.17** at the IC_{50} concentration that is 0.5 µM (**Figure 42**). Interestingly, these data are in agreement with recent results from the team of Marletta[144] which demonstrated that PHGDH could also be inhibited by the specific *s*-nitrosation of the same Cys116 residue. This particular cysteine thus seems to play a crucial role in PHGDH activity and moreover could constitute a novel interaction site for PHGDH inhibition.

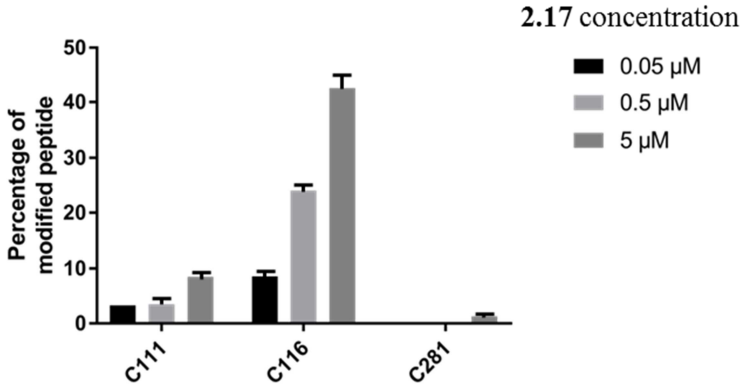

***Figure 42**: Percentage of the three oxidized cysteine residues (C111, C116 and C281) at tested concentrations. Determined from the peptide spectrum matches (PSMs) of their precursors after trypsinization and analysis by nanoUHPLC/MS. **2.17** at various concentrations was incubated with PHGDH in 50 mM Tris and 1 mM EDTA at pH 8.5. All experiments values were performed in duplicates at each compound dilution and error bars show the standard deviation.*

8.3.6. Mutagenesis on PHGDH

Altogether, these data strongly suggest a mechanism of action for **2.17** on PHGDH involving oxidation of the Cys116 residue. To validate this hypothesis, we set out to investigate the inhibitory potency of **2.17** on a mutant form of PHGDH where the Cys116 was mutated to a serine residue (PHGDH C116S). Interestingly, this mutant is known to retain a catalytic activity comparable to the wild type enzyme.[144] We actually showed that the human PHGDH C116S mutant is only weakly inhibited by **2.17**, with a 20-fold decrease in the inhibitory potency, in comparison to the wild type enzyme (**Table 12**). Although this observation is a clear indication that C116 oxidation is critical for PHGDH inhibition, it also suggests that oxidation of other cysteines such as C111 and C281 might be involved in PHGDH inhibition albeit to a lesser extent as demonstrated recently in the works of Marletta.[144]

Table 12**: WT and C116S PHGDH inhibition (IC_{50}) of **2.17

PHGDH	**PHGDH inhibition (IC_{50}, µM)[a]**
Wild Type	0.59 [0.37-0.95]
C116S mutant	10.23 [6.68-15.65]

[a]All experiments to determine IC_{50} values were performed in triplicates at each compound dilution, and all IC_{50} values were averaged when determined in two or more independent experiments. Under bracket: 95 % confidence interval.

8.4.7. Involvement of Cysteines 111 and 281 in PHGDH inhibition (unpublished data)

In order to conclude the investigation on the site of action of **2.17**, we also produced the C111S and C281S mutated proteins. Once more, the enzymatic activity of these dehydrogenases was preserved. As depicted in **Figure 43**, disulfiram inhibition of these mutants remained similar to the one observed with the wild type enzyme. This result strengthens the fact that Cys116 plays a crucial role in PHGDH inhibition through the formation of a disulfide bridge while the importance of others cysteines remains minor.

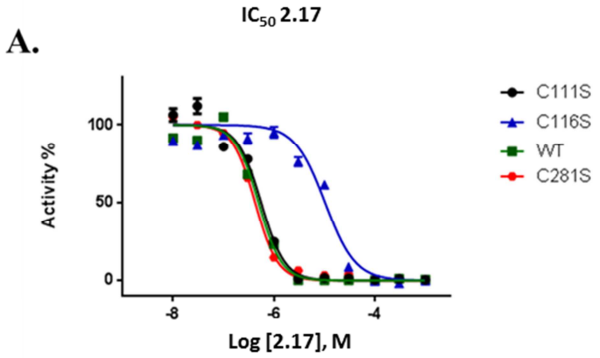

B.

PHGDH	PHGDH inhibition (IC50, µM)[a]
Wild Type	0.59 [0.42-0.72]
C111S mutant	0.52 [6.68-15.65]
C116S mutant	10.23 [6.68-15.65]
C281S mutant	0.42 [0.37-0.48]

***Figure 43**: **A.** Dose-response curve of **2.17** on WT, C111S, C116S and C281S PHGDH **B.** PHGDH inhibition (IC_{50}) of **2.17**. [a]All experiments to determine IC_{50} values were performed in triplicates at each compound dilution. In brackets: 95 % confidence interval. Data were collected at 37°C with a PHGDH concentration of 12 ng/µL in 50 mM Tris and 1 mM EDTA at pH 8.5*

8.4.8. Computationnal validation

With a view to understand the interaction of **2.17** with PHGDH on Cys116 at the molecular level, we focused our interest on an already described X-ray crystal structure of a truncated form of PHGDH (**Figure 44**). This truncated version shows 11 of the 13 cysteine residues and allowed to visualize the interaction site in more details.

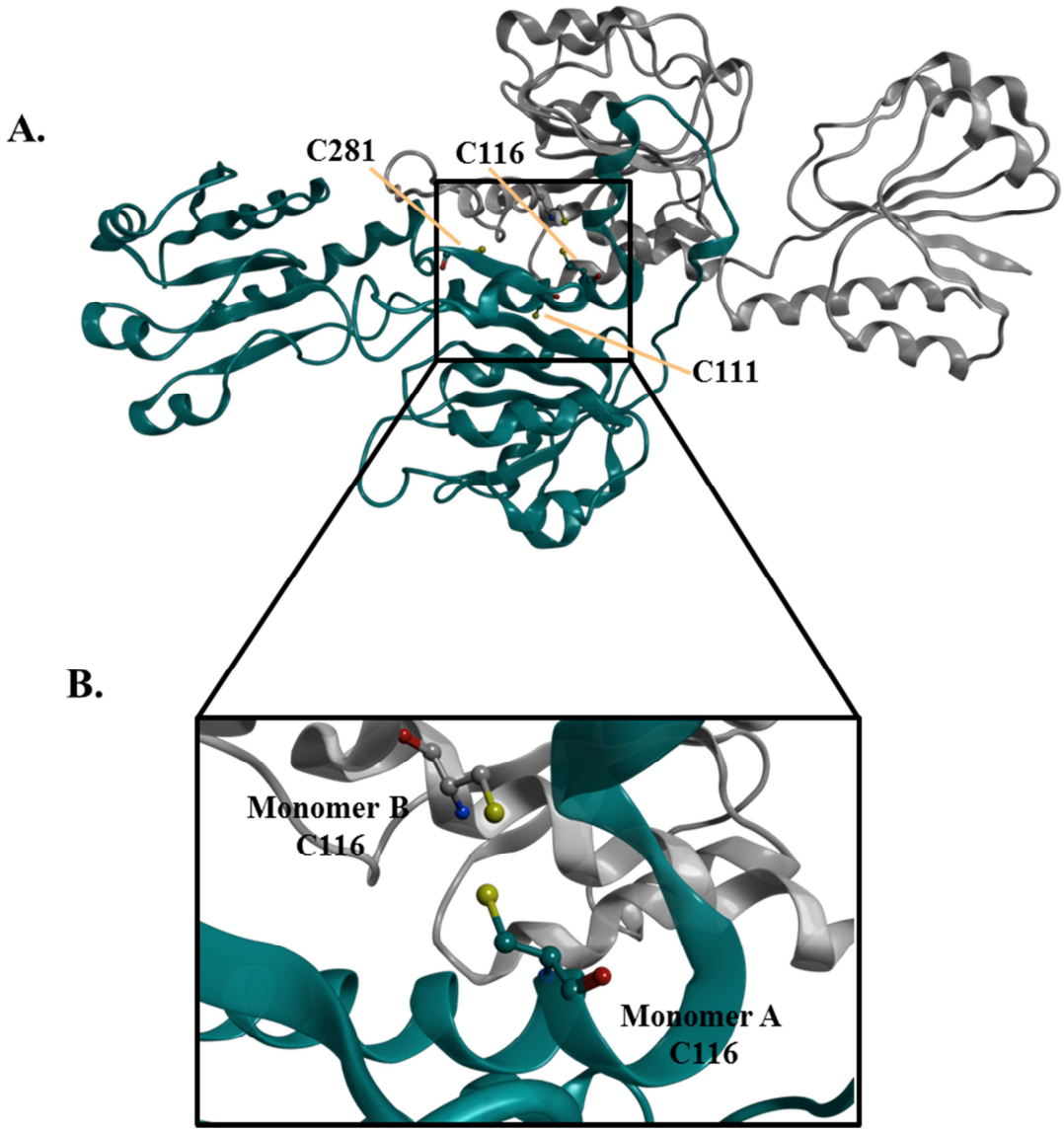

***Figure 44**: **A**. Overview of the PHGDH cysteine residues (111, 116 and 281) (PDB code 2G76). **B**. Zoomed-in region highlighting the targeted Cys116 on the two monomers.*

As it can be observed from **Figure 10**, the Cys116 residue is located at a key position, at the interface of two PHGDH monomers. According to the results of Marletta,[144] suggesting that S-nitrosation of Cys116 can lead to the formation of a disulfide bridge with the adjacent monomer and then to the formation of an inactive protein, we hypothesized that oxidation of the Cys116 residue by **2.17** would similarly lead to PHGDH inhibition *via* modification of its oligomeric state.

8.4.9. Cross linking experiment

To confirm this hypothesis, a cross-linking experiment, using bis-sulfosuccinimidyl suberate (BS3) as cross-linker, was finally undertaken with PHGDH alone or PHGDH after treatment with increasing concentrations of **2.17**. As clearly observed from **Figure 45**, although PHGDH alone is in a tetrameric form as previously reported,[145] PHGDH inhibition by **2.17** leads to a concentration-dependent shift from the tetrameric to the dimeric, and to a lesser extent to the monomeric, form of PHGDH, thus corroborating our hypothesis. Since **2.17** is known to induce the formation of disulfide bridges through the formation of a diethyl(dithiocarbamate) intermediate as exemplified on **Figure 44A**,[146] the results obtained here suggest that disulfiram would inhibit PHGDH by disruption of the active tetramer either into an inactive dimer resulting from the formation of a disulfide bridge between two Cys116 residue on two adjacent monomers, or to a lesser extent to an inactive diethyl(dithiocarbamate) intermediate monomer.

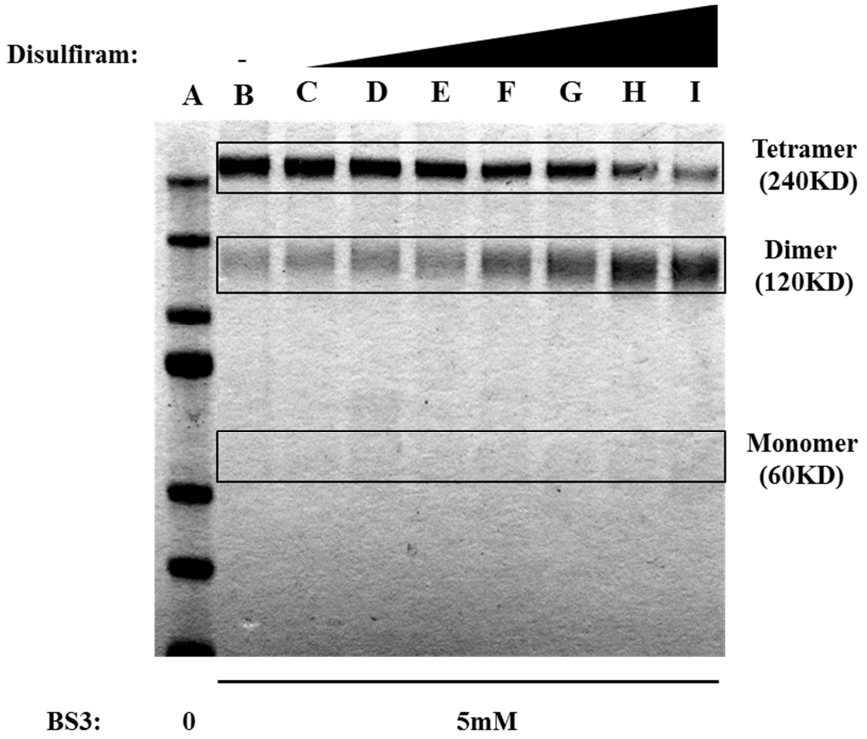

Figure 45*: Cross-linking experiment of PHGDH with BS3 at various* ***2.17*** *concentrations (****A****. MW marker.* ***B****. 0 µM.* ***C****. 1 µM.* ***D****. 5 µM.* ***E****. 10 µM.* ***F****. 50 µM.* ***G****. 100 µM.* ***H****. 250 µM.* ***I****. 500 µM.). PHGDH was incubated with* ***2.17*** *during 30' before cross-linking. Lane B was used as control without* ***2.17****. Lane A (MW marker) was used to deduce the oligomerization state of PHGDH.*

8.4.10. Cellular evaluation

Finally to detail the relationship between the ability of **2.17** to disrupt PHGDH tetramer and its anti-cancer activity, we set out additional experiments aiming to assess the effect of **2.17** on two cancerous cell lines : UM-UC-3 human transitional cell carcinoma that constitutively express PHGDH (UM-UC-3-PHGDH+) and a variant of these cells that do not express PHGDH (UM-UC-3-PHGDH-) (**Figure 46**)

When cells that do not express PHGDH (UM-UC-3-PHGDH-) are treated with **2.17**, a tumor cell proliferation inhibition (IC_{50}) of 3,64 µM is obtained, whereas cells expressing PHGDH (UM-UC-3-PHGDH+) appear to be more susceptible to disulfiram treatment with an IC_{50} of 0,77 µM. Although the difference remains weak (~5-fold), probably because other anti-proliferative mechanisms are involved upon disulfiram treatment, tumor cell proliferation inhibition is higher for cells expressing PHGDH.

Our results thus corroborate, at least in cell-based settings, our initial hypothesis that PHGDH inhibition by **2.17** contributes to its overall anticancer activity.

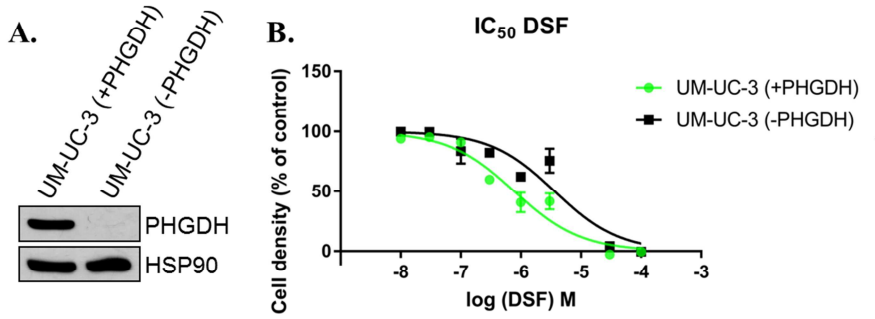

C.

UM-UC-3	Cell proliferation inhibition (IC_{50}, µM) by DSF
+PHGDH	0.775 [0.614-0.984]
-PHGDH	3.64 [2.50-5.29]

Figure 46: *A. Representative immunoblot for PHGDH on UM-UC-3 cancer cells ; B. Dose-response curves of* ***2.17****. C. UM-UC-3-PHGDH- and UM-UC-3-PHGDH+ cell proliferation inhibition by* ***2.17****. All experiments to determine IC_{50} values were performed in n=6 at each compound dilution, and all IC_{50} values were averaged on two or more independent experiments. Under bracket: 95 % confidence interval.*

8.5. CONCLUSION AND PERSPECTIVES

In conclusion, in this chapter, we have shown that **2.17**, a FDA-approved aldehyde dehydrogenase inhibitor used as a treatment for chronic alcoholism, and some structural analogues are PHGDH inhibitors. Through biochemical and mass spectrometric experiments, we detailed the mechanism-of-inhibition of PHGDH by **2.17** and demonstrated that it involves the disruption of the active PHGDH tetramer into either an inactive dimer covalently linked by a disulfide bridge involving Cys116 on adjacent monomers or, to a lesser extent, an inactive monomer intermediate. Using cell-based settings, we also demonstrated our initial hypothesis that PHGDH inhibition by **2.17** contributes to its overall anticancer activity.

Because it is known that **2.17** is metabolized *in vivo* (elimination half-life for DSF was reported to be 7.3h after a single-dose administration of 250mg of disulfiram[147]) into notably the diethyldithiocarbamate (DTC) metabolite which undergoes copper complexation, and hence provides anticancer activity for **2.17**, our results suggest that the non-metabolized circulating **2.17** could also provide anticancer activity but through a completely different mechanism of action involving PHGDH inhibition. Also, the maximum plasma concentration

of **2.17** (Cmax) being reported to be 1.28 µM, that is around 2-fold higher than the IC_{50} of **2.17** on PHGDH in the cell-based assay (0.77µM), one can hypothesized that exposure to **2.17** *in vivo* could be sufficient to provide anticancer activity *via* PHGDH inhibition.

8.6. METHODS

8.6.1. PHGDH Assay.

Enzymatic assay was adapted from a previously described procedure.[86] NADH fluorescence emission (Ex 340 nm/Em 460 nm) was followed over time. Assays were performed in PHGDH assay buffer (50 mM Tris, pH 8.5, and 1 mM EDTA). Substrates and enzyme concentrations were as follows: 3-PG, 240 μM; NAD^+, 120 μM; glutamate, 30 mM; PHGDH, 12 ng/μL; PSAT1, 20 ng/μL. The final concentration of DMSO in assay mixture was set to 5%.

8.6.2. Dilution Experiment.

Dilution experiment was conducted following a reported procedure.[86] **2.17** (5 μM) or DMSO control was incubated with PHGDH for 45 min at 37 °C. Undiluted **2.17** (5 μM) was included as a positive control for inhibition.

8.6.3. WT and C116S PHGDH Purification.

pET28a human PHGDH and pET28a human C116S PHGDH were transformed into BL21 *Escherichia coli*. A single colony was grown to an OD_{600} 0.6 in 1 L of Luria broth. Protein expression was induced with 1 mM isopropyl thiogalactopyranoside (IPTG). The culture was chilled on ice for 30 min, cultured for 18h at room temperature and pelleted (6,000 g, 20 min). Pellets were resuspended in 60 mL of lysis buffer (50 mM Tris, pH 8.5, 10 mM $MgCl_2$, 300 mM NaCl, 10% glycerol, 5 mM imidazole) and sonicated, and cell debris were pelleted by centrifugation (20,000 × *g*, 30 min). The supernatant was collected and purified using Akta purifier on HisTrap™ FF column (GE Healthcare). After column equilibration with wash buffer (50 mM Tris, pH 8.5, 10 mM $MgCl_2$, 300 mM NaCl, 10% glycerol and 30 mM imidazole), bound proteins were eluted with elution buffer (50 mM Tris, pH 8.5, 10 mM $MgCl_2$, 250 mM NaCl, 10% glycerol, 250 mM imidazole) and collected (1-mL fractions). Fraction protein content was measured via a Bradford assay. The most concentrated fractions were pooled and dialyzed overnight into 4 L of dialysis buffer (50 mM Tris, pH 8.5, 10 mM $MgCl_2$, 250 mM NaCl, 20% glycerol, 0.15% 2-mercaptoethanol). Protein purity was assessed via SDS/PAGE and Coomassie staining.

8.6.4. Mass spectrometry experiments.

Mass spectrometry experiments were carried out on an Orbitrap Lumos, following a previously reported procedure, with some modifications.[148] A local protein database

containing the human PHGDH sequence (accession Uniprot O43175) was used to process the obtained MS/MS data. Mass error was set to 15 ppm for precursor ions and 0.6 Da for fragment ions. Oxidation on Met; disulfiram, (+147.025 Da) and carbamidomethyl (+57.021 Da) were considered as variable modifications on Cys.

8.6.5. Cross-linking experiments.

PHGDH (3 μg) was incubated with **2.17** (1 μM, 5 μM, 10 μM, 50 μM, 100 μM, 250 μM, 500 μM) or vehicle control (DMSO) in 25 mM HEPES, pH 7.3, and 1 mM NAD^+ in 18 μL total volume for 30 min on ice. BS3 (S5799; Sigma) cross-linker dissolved in PBS was added to a final concentration of 5 mM and incubated for 30 min under shaking at room temperature. The reaction was then quenched for 15 min by adding 1 M Tris, pH 7.5, to a final concentration of 28 mM. Cross-linked proteins were mixed with sample buffer, boiled for 5 min, and run on SDS/PAGE. Gels were stained with Gelcode blue stain reagent (24592; Thermo) overnight and destained according to the manufacturer's instructions.

8.6.7. Cell models and cytotoxicity assay.

UM-UC-3 (PHGDH+ and PHGDH-) bladder cancer cells were purchased from the ATCC and cultured in DMEM medium supplemented with 10% heat-inactivated Fetal Bovine Serum (FBS) and 1% penicillin/streptomycin. Cells were seeded at 2500 cells/well in 96-well plates in serine depleted media (MEM). DSF or vehicle (DSMO) was added and cells were grown for 48 hours. Viability was assessed using Presto Blue reagent (Life Technologies) according to manufacturer's instructions.

8.6.8. Chemicals.

All reagents were purchased from chemical suppliers and used without purification. Copper/DSF complex was obtained according a previously described procedure.[149]

8.6.9. Immunoblots.

Western blot and immunoblot analysis were performed according a reported procedure. [150]

8.7. SUPPORTING INFORMATION.

8.7.1. Triton X effect on 2.17 IC_{50}.

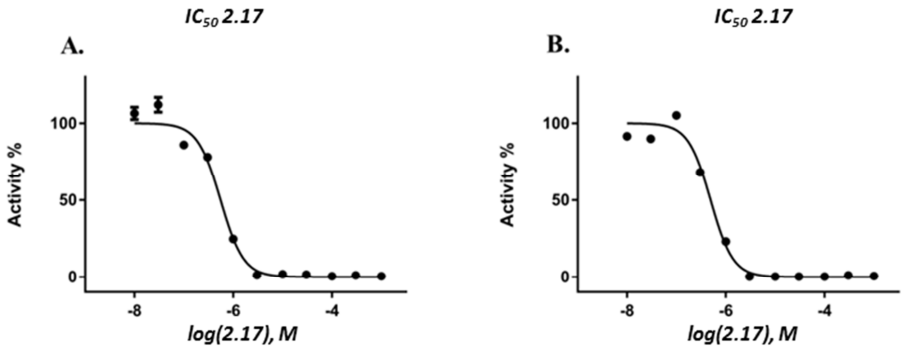

Figure S2: *IC_{50} curves of **2.17** on PHGDH WT A. without Triton X (0.53 µM) B. with Triton X 0.01% (0.49 µM). All experiments values were performed in triplicates at each compound dilution and error bars show the standard deviation. Data were collected at 37°C with a PHGDH concentration of 12 ng/µL in 50 mM Tris and 1 mM EDTA at pH 8.5.*

8.7.2. 2.17 inhibition on WT and C116S PHGDH.

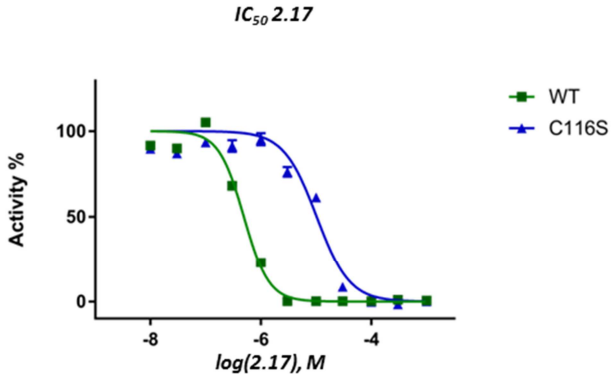

Figure S3: *IC_{50} curves of **2.17** on PHGDH WT (0.49 µM) and C116S (10.23 µM). All experiments values were performed in triplicates at each compound dilution and error bars show the standard deviation. Data were collected at 37°C with a PHGDH concentration of 12 ng/µL in 50 mM Tris and 1 mM EDTA at pH 8.5.*

8.7.3. Peptide residues of PHGDH.

Table S4. PHGDH peptides (after trypsination) showing a disulfiram modification after treatment at **A.** 0.05 µM **B.** 0.5 µM and **C.** 5µM

Peptide sequence[a]	Cys residues	m/z observed MH+ (Da)	m/z calculated MH+ (Da)	^ (ppm)	Percentage of modified peptides
[91]KGILVMNTPNGNSLSAAELTCGMIMCLAR[119]	C111, C116	3155.52390	3155.51082	4.14	C116 = 9.75 C111 = 4.87
[92]GILVMNTPNGNSLSAAELTCGMIMCLAR[119]	C111, C116	3027.42478	3027.41586	2.95	C116 = 7.69 C111 = 1.92

A. 2.17 concentration 0.05 µM

Peptide sequence[a]	Cys residues	m/z observed MH+ (Da)	m/z calculated MH+ (Da)	^ (ppm)	Percentage of modified peptides
[91]KGILVMNTPNGNSLSAAELTCGMIMCLAR[119]	C111, C116	3171.53720 (Ox M)	3171.50574 (Ox M)	9.92	C116 = 7.14
[92]GILVMNTPNGNSLSAAELTCGMIMCLAR[119]	C111, C116	3027.44620	3027.41586	10.02	C116 = 46.67 C111 = 6.67

B. 2.17 concentration 0.5 µM

Peptide sequence[a]	Cys residues	m/z observed MH+ (Da)	m/z calculated MH+ (Da)	^ (ppm)	Percentage of modified peptides
[91]KGILVMNTPNGNSLSAAELTCGMIMCLAR[119]	C111, C116	3155.51438	3155.51082	1.13	C116 = 50.00 C111 = 4.16
[92]GILVMNTPNGNSLSAAELTCGMIMCLAR[119]	C111, C116	3027.42276	3027.41586	2.28	C116 = 39.65 C111 = 10.34
[271]ALVDHENVISCPHLGASTK[289]	C281	2137.99712	2138.02649	-13.74	C281 = 1.26

C. 2.17 concentration 5 µM

[a]Superscripted numbers indicate the amino acid numbering of human PHGDH.

9. General Discussion

9. GENERAL DISCUSSION

9.1. MAJORS OUTCOMES OF THIS THESIS

The main objective of the thesis was to discover original small-molecule inhibitors of PHGDH. As major outcomes two sets of inhibitors of this protein were discovered; the *α*-ketothioamides and the disulfiram analogues (**Figure 47**).

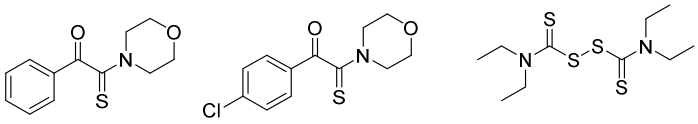

5.16
IC_{50} = 111.1 µM
[87.3-131.2]

5.22
IC_{50} = 20.3 µM
[15.6-26.4]

2.17
IC_{50} = 0.59 µM
[0.37-0.95]

Figure 47: *α-ketothioamide series (**5.16** and **5.22**) and Disulfiram (**2.17**) as PHGDH inhibitors*

In the *α*-ketothioamide series, a detailed pharmacomodulation by chemical modifications of the hit compound **5.16** was undertaken and led to the following structure-activity relationships. At the left side (part A) of the molecule, only aryl groups led to potent PHGDH inhibitors whereas introduction of alkyl groups in this position resulted in inactive derivatives. Substitutions on the aryl moiety are only tolerated in the *para*-position with the chlorinated derivative **5.22** being the most potent. Then, except for the 4-methylpiperidine analogue, it was very clear that modulating part C (right-side amino moiety) of the molecule decreased or abolished the inhibitory potency. Regarding the influence of the linker, only replacement of the *α*-ketothioamide (part B) with a thioamide (**6.20**), or a sulphonamide (**6.34**) led to equally potent PHGDH inhibitors whereas all other modulations led to inactive derivatives (IC_{50} > 150 µM). Interestingly, with the thioamide and sulphonamide linkers, the introduction of a chlorine in the *para*-position, again, improved the inhibitory potency compared to the non-substituted analogue (**6.35** and **6.36**) (**Figure 48B**).

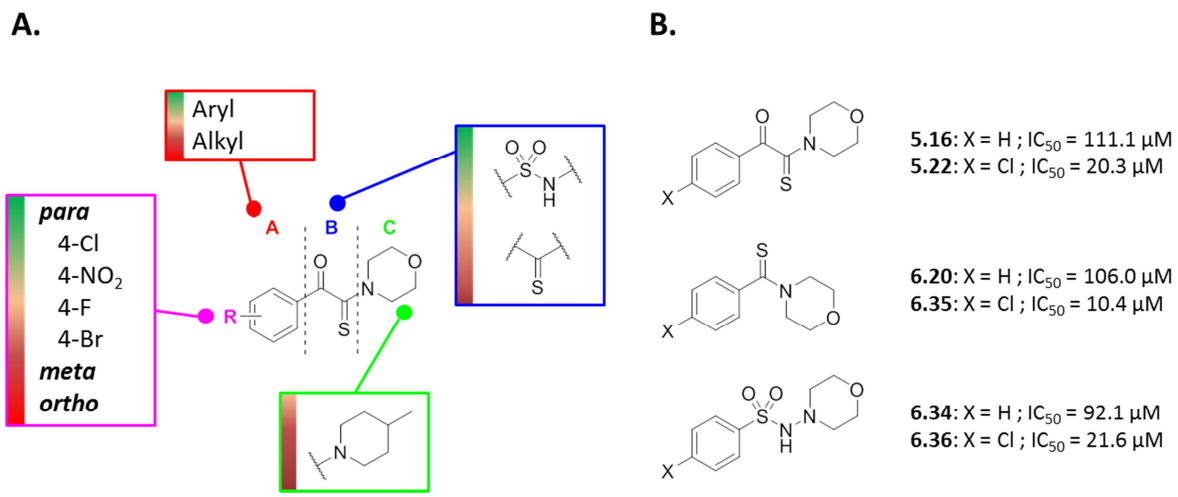

Figure 48: *Overview of the structure–activity relationships. Color code: green > yellow > red, for decreasing PHGDH inhibition (**A**). Influence of the p-chloro substitution on the potency of PHGDH inhibition (**B**).*

To give a deeper understanding of PHGDH inhibition by α-ketothioamide compounds, we next investigate the mechanism-of-action of compound **5.22** that we have identified as one of the most potent compounds in this series. The analysis revealed the irreversible and non-competitive profile of **5.22**. The use of a diazirine-based photoactivatable probe together with mass spectrometry and site-directed mutagenesis experiments led us to identify a new, hence never reported before, allosteric site located at the C-terminal end of the enzyme; the ACT domain.

With these promising results in hands, we then aimed at detailing further PHGDH inhibition in cell-based settings. Interestingly, this series of compounds also demonstrated a promising selective reducing of the cellular proliferation of tumor cell lines expressing PHGDH (BT-20, Siha, HL-60, MDA-MB-468) without showing any effect on cell lines characterized with a low expression of PHGDH (MDA-MB-231, HL-60 sHPHGDH). The glucose flux analysis confirms our data showing a correlation between this selective cell inhibition and a decrease in *de novo* serine synthesis by using a ^{13}C carbon radiolabelling experiment. The latter was further evidence that our compounds selectively inhibit the SSP.

Finally, we also highlighted the ability of **5.22** to significantly reduce tumor proliferation *in vivo*, demonstrating once again the value of targeting PHGDH for anticancer therapy (**Figure 49**).

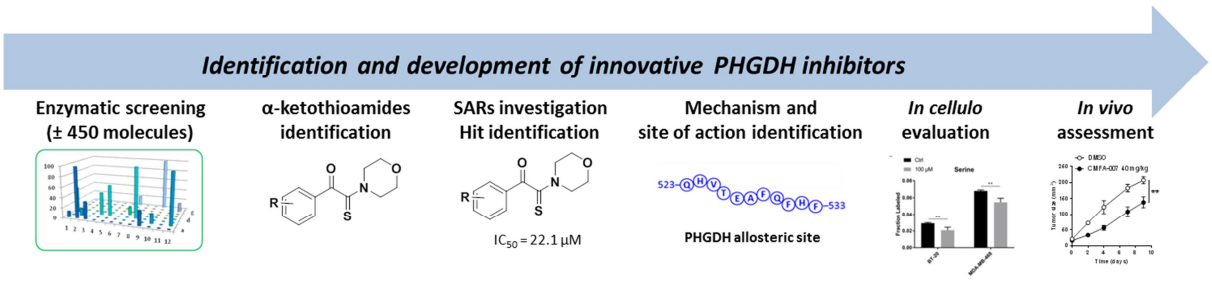

Figure 49: *Overview of studies performed on α-ketothioamide series*

In the second part of this work, we set out to detail the inhibition of PHGDH by disulfiram (DSF) an FDA-approved anti-alcohol agent. Following the works of Cantley *et al.* and data from our laboratory identifying DSF as a potent PHGDH inhibitor, we investigated the mechanism of action of this compound.

Firstly, a preliminary pharmacomodulation study was undertaken to identify the molecular requirements around **2.17** to attain a high PHGDH inhibition. As a result, the crucial role of the dithiocarbamate linker was highlighted. And, to our surprise, weak effects were obtained when modulating the lateral side chain of **2.17**, hence revealing relatively flat SARs in this series. To better understand these SARs, mass spectrometry and site-directed mutagenesis experiments were used to study the mechanism-of-action in this series. As a result, we have shown that inhibition of PHGDH by **2.17** resulted from the oxidation of a particular cysteine (C116) *via* a disulfide bond. Further analysis, notably using cross-linking experiments, revealed that this inhibition could be related to the disruption of the oligomerization state of the protein.

In cell-based settings, we also demonstrated the potency of **2.17** to reduce cancer cell proliferation. Indeed, we showed that disulfiram strongly inhibits the proliferation of cancer cell lines expressing PHGDH (UM-UC-3) with only little effect on cell-line that do not express PHGDH (UM-UC-3 shPHGDH), thus proving that PHGDH inhibition can contributed to the global anti-cancer effect of **2.17**. Interestingly, this effect does not seem to be related to the formation of a disulfiram-copper adduct, and thus probably constitutes an alternative mechanism accounting for the anticancer activity of PHGDH (**Figure 50**) compared to the one reported in the literature by Bartek *et al*.[133]

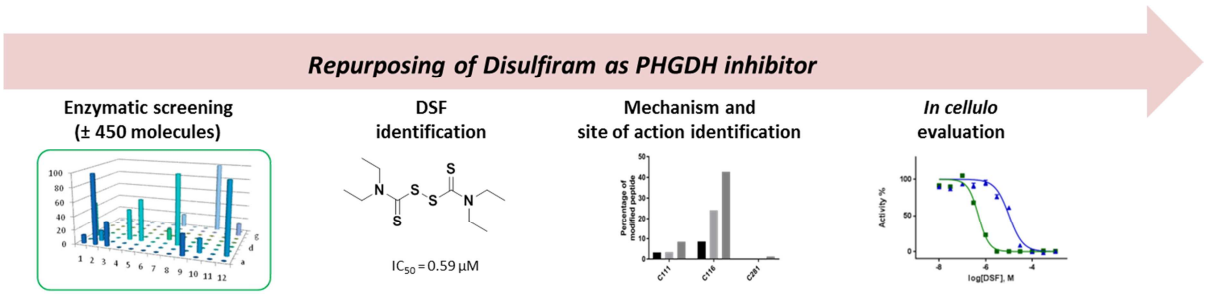

Figure 50: *Overview of studies performed on* ***2.17*** *repurposing*

9.2. ALLOSTERIC COVALENT INHIBITORS

To summarize, at the end of this thesis we were able to identify and develop two new series of PHGDH inhibitors with *in cellulo* and *in vivo* activities.

In fact, the two sets of compounds identified during this thesis are covalent allosteric inhibitors. Interestingly, the last 10 years have seen a significant increased interest in this particular mode of inhibition (**Figure 51**), leading to the development of very potent molecules. **2.17** and **5.22** constitute novel examples of allosteric covalent compounds. To emphasize this research, the major advantages of covalent allosteric inhibitors over other types of inhibition will be briefly addressed in the following sections.

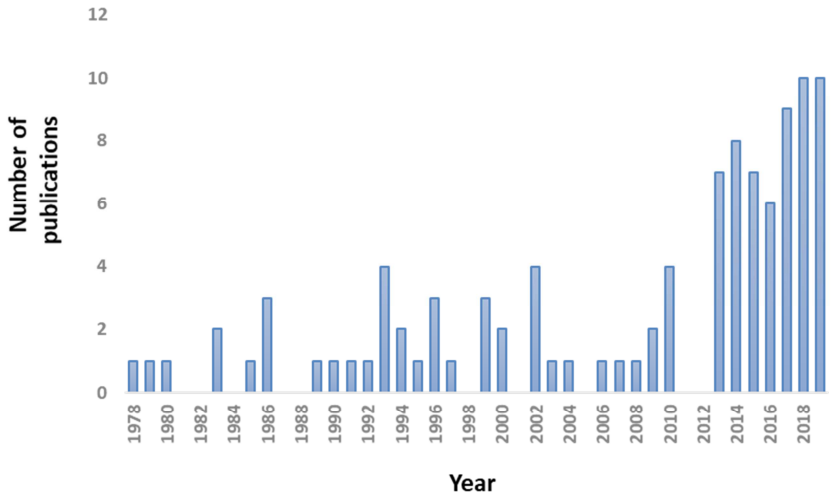

Figure 51: *Number of publications related to allosteric covalent inhibitor since 1978. Data were collected from Pubmed.*

9.2.1. Covalent inhibitors

Covalent inhibitors are molecules owning reactive chemical functionalities, often electrophilic groups, able to form a covalent bond with a therapeutic target.[151] **Figure 52** depicts some important molecules currently on the market acting via this specific mode of action.

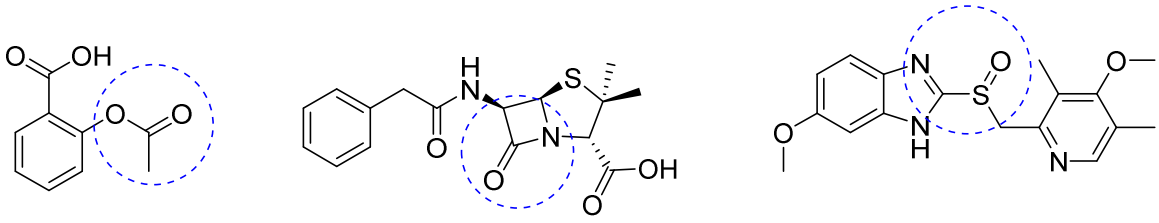

Acetylsalicylic acid 1890 | **Penicillin 1940** | **Omeprazole 1980**

Figure 52: *Classical covalent drugs currently on the market with their reactive functionality in blue.*[152]

Although one of the most widely used drugs in the world is a covalent inhibitor (acetylsalicylic acid), research on covalent molecules was not pursued for many years. Indeed, these molecules having a high chemical reactivity were often associated with important side effects[153,154] mainly due to off-target toxicity. These off-target effects notably involve reaction with cysteine-containing molecules such as for instance glutathione, hence leading to modification of the redox status in cells.[155] In the most dramatic cases, these side effects can even lead to an immune mediated toxicity.[152]

To avoid these drawbacks, various researches were conducted to develop covalent inhibitors with limited toxicity and high selectivity. For instance, the development of less reactive chemical functionality such as acrylamide has drastically reduced their toxicity.[156] Covalent inhibitors also require a reduced dosage due to their long duration of action.[157] Since the covalent bond cannot be easily displaced as in the case of a non-covalent inhibitor, the inhibited enzyme will accumulate in the body, even in the presence of low doses of the compound.[158,159]

Recent years witnessed a renewed interest for the development of covalent inhibitors and particularly covalent inhibitors acting at an allosteric site notably to address selectivity issues. In the next section we will focus on specific contributions through allosteric inhibition.

9.2.2. Allosteric inhibitors

Allosteric inhibitors abrogate the activity of the target while not binding directly in the active site, but rather at a site distant from the active site generating structural or entropic changes leading to enzyme inhibition.[160,161] Nowadays, more and more molecules available on the market or in clinical trials are based on this particular mechanism of action (**Figure 53**).

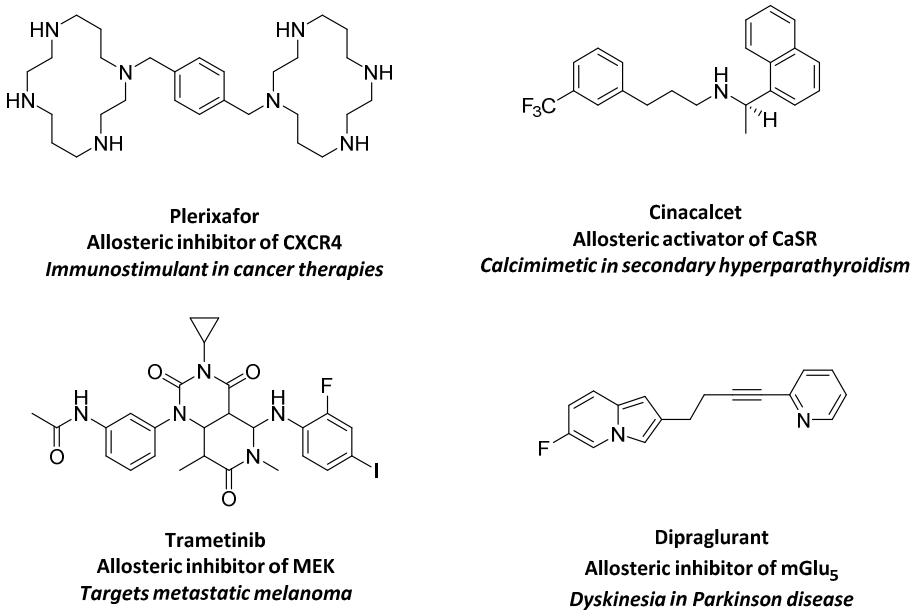

Figure 53: *Examples of some allosteric modulator currently on the market or in clinical trials.*[162–165]

Numerous advantages can explain the interest in allosteric inhibition. Firstly, allosteric inhibitors allow to avoid competition with the different enzymatic substrates.[166] This is particularly interesting when dealing with high intracellular substrate concentration as in the particular cases of dehydrogenases or kinases (NAD and ATP, respectively).[167] In these case, the development of allosteric inhibitors do not require a high affinity to the target to sustain a potent effect.[168] These compounds also allow to bypass resistance phenomena related to

active site mutations, these modifications appearing less frequently in allosteric cavities.[169] Furthermore, allosteric sites being often enzyme specific, the development of allosteric compounds leads to more selective treatment and limits their side effects.[170,171]

Yet, it is important to keep in mind that the development of allosteric inhibitors also faces numerous challenges. For example, allosteric inhibitors often have aqueous solubility issues due to the higher lipophilicity of their site of action in comparison to protein active sites.[172] The limited understanding of the structural modifications resulting from an allosteric inhibition also makes the pharmacomodulation process much more complex.[173] Another challenge is related to the identification and characterization of these allosteric sites. Until very recently, this process was tedious and mainly relied on serendipity. Nowadays however, thanks to the improvement of bioinformatics tools as well as crystallography or NMR methods,[174] it has become more popular to identify these sites. Nowadays, these techniques are applied successfully by many medicinal chemists to design and/or identify new therapeutic molecules.

Having in mind all these data, we see why the combination of a covalent character with the targeting of an allosteric site is currently under intense investigation. On one hand, allosteric inhibitors allow to target non druggable enzymes, to reach a high selectivity and thus greatly limit side effects of covalent inhibitors. On the other hand, covalent inhibitors allow to significantly increase the potency of allosteric ones, even at reduced dose.

9.2.3. Covalent allosteric PHGDH inhibitors

The development of covalent allosteric inhibitors of PHGDH and the identification of their site of action are therefore an important step towards the development of more effective treatments.

This is the reason why, although this is a challenging process, no less than 6 allosteric sites able to regulate PHGDH activity were discovered in the last 3 years (**Figure 54**).

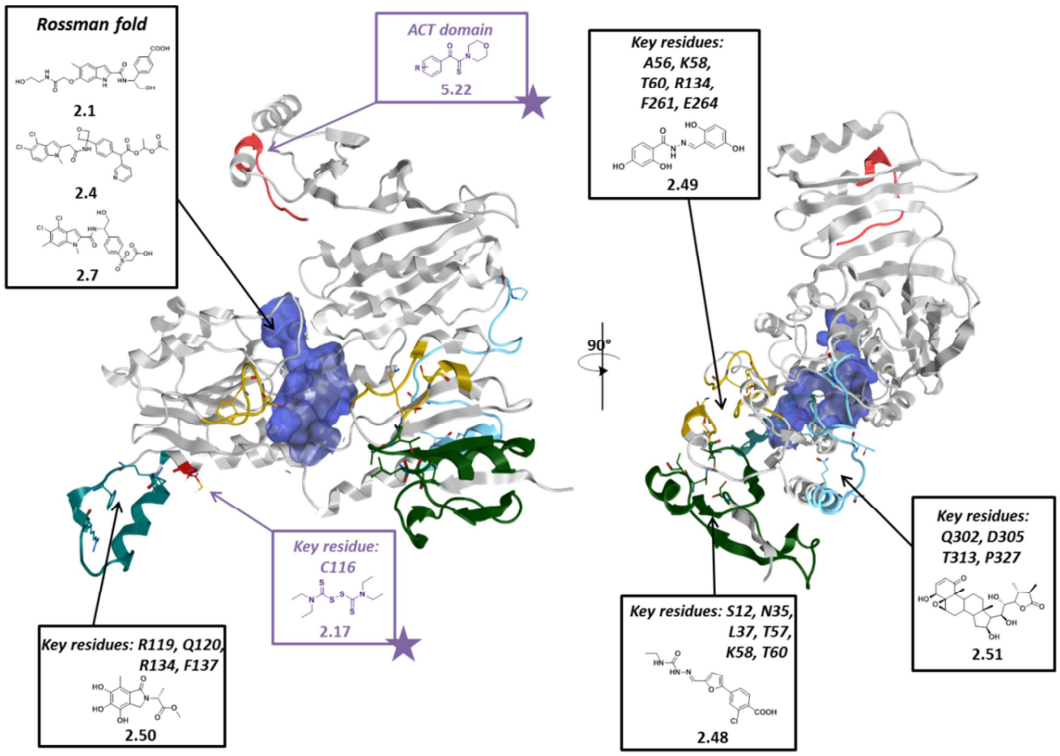

Figure 54: *Homology model of human full length PHGDH (MOE software) with highlight of all inhibitors binding sites and key residues identified so far. Rossman fold and NAD competitive inhibitors (**2.1**, **2.4** and **2.7**) in blue. Allosteric site and related inhibitor **2.48** identified by Wang et al. in green. Allosteric site and related inhibitor **2.49** identified by Wang et al. in yellow. Allosteric site and related inhibitor **2.50** identified by Guo et al. in mint green. Allosteric site and related inhibitor **2.51** identified by Zheng et al. in cyan. Allosteric site and related inhibitor **5.22** identified by Spillier et al. in red. Allosteric residue (cys116) and related inhibitor **2.17** identified by Spillier et al. in carmine.The two series identified during this thesis are highlited in purple.*

Among covalent allosteric inhibitors identified on PHGDH, it is interesting to note that several of them act *via* the disruption of the enzyme oligomeric state (**2.16**, **2.17**) while others have more conventional mechanisms (**5.22**, **2.50**, **2.51** ...). It is therefore clear that multiple mechanisms may be involved in the regulation of enzymatic activity but also that the action sites identified so far have a great variety in their location and their structure.

To conclude, it is important to mention that these allosteric inhibitors (covalent or not), although less potent than the active-site directed ones (**2.1**, **2.4**, **2.7**), demonstrated significantly greater effects in complex biological models and in particular *in vivo*. Once again, this demonstrates the advantage of this type of inhibition over compounds competing high NAD concentration.

9.3. MAJOR ISSUES ENCOUNTER DURING THIS THESIS

It should be noticed that the development and the study of novel inhibitors of PHGDH was not a straightforward process, and in fact revealed to be particularly challenging. In this last section, we will discuss the different pitfalls encountered during the development of PHGDH inhibitors and the solutions we tried to develop.

9.3.1. Enzymatic assay development

The first issue that we faced in this project dealt with PHGDH activity and the development of a robust enzyme assay. At the beginning of this thesis, no assay was reported to study PHGDH activity. We therefore relied on other dehydrogenases to develop our in-house method.

The first experiment we tried to develop was the analysis of the activity of PHGDH following the conversion of the co-factor NAD^+ into NADH (**Figure 55A**). However, it soon became evident that the fluorescent signal with this enzyme was too weak to provide sufficiently reproducible data. This was largely because the reaction followed in this assay is reversible. The fact that 3-PPyr can be converted back to 3-PG in fact, more efficiently than the conversion of 3-PG to 3PPyr prevent the direct measurement of PHGDH analysis by spectrophotometric analysis of NADH. In order to bypass this issue, another enzymatic assay was developed (**Figure 55B**) by using the second enzyme of the SSP, PSAT-1, in the assay. This allowed a significant increase in the fluorescent signal by moving the equilibrium to the physiological direction by consumption of the 3PPyr formed. Subsequently, two other enzymatic assays have also emerged to increase the obtained signal. The first one included Diaphorase, an enzyme that converts resazurine into a highly fluorescent compound, resorufin (**Figure 55C**), using the NADH produced by PHGDH. This robust experiment was mainly the one used during our work to monitor PHGDH activity. For the last assay (**Figure**

55D), the final enzyme of the SSP was integrated in order to mimic the entire biological system of SSP.

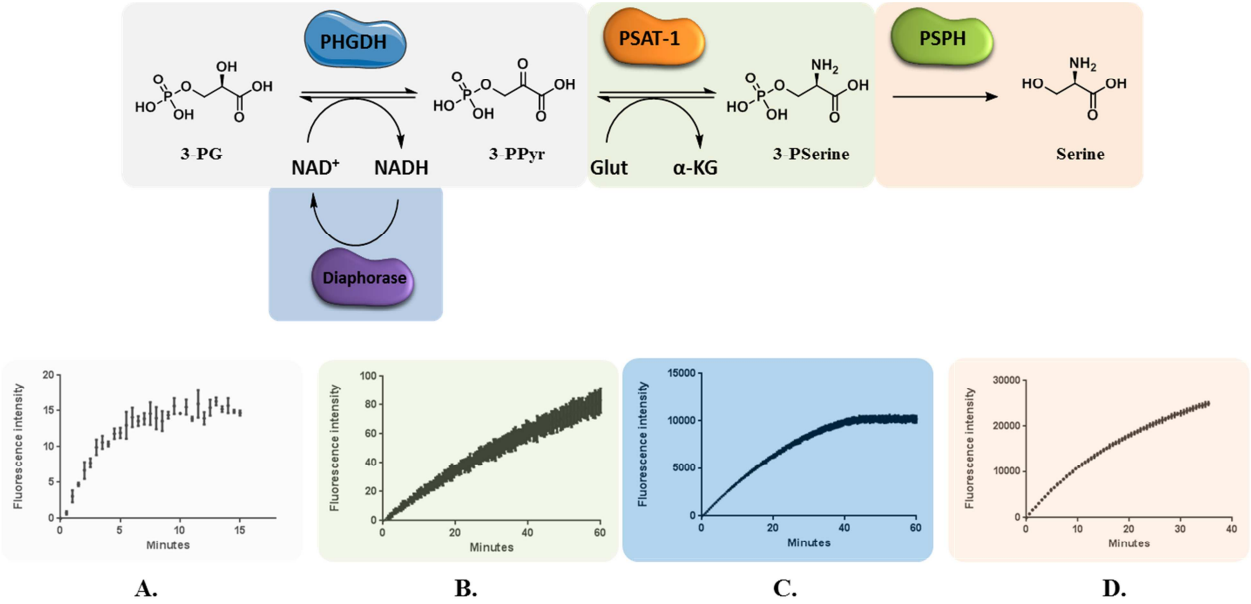

***Figure 55**: Overview of the enzymatic assays developed during this thesis. Biochemical reaction with major substrates on the top and fluorescent kinetic signal below. **A.** Assay with PHGDH alone. **B.** Assay with PHGDH and PSAT-1. **C.** Assay with PHGDH, PSAT-1 and Diaphorase. **D.** Assay with PHGDH, PSAT-1, PSPH and Diaphorase.*

The setup, and understanding of these different assays, was in our opinion, a key step for the discovery of new PHGDH inhibitors.

9.3.2. PHGDH inhibition

The second issue is related to the reproducibility of the PHGDH inhibition experiments. At first, the inhibitors of PHGDH (α-ketothioamides, disulfiram, quinoline derivatives...) were identified using a commercial source of the enzyme (BPS Bioscience). Unfortunately, a change of enzyme batch led to the complete loss of the inhibition for the α-ketothioamides. In order to ensure that this series was not a false positive, we performed the enzyme production in our laboratory using a commercial plasmid. However, despite comparable enzymatic activity (similar K_m values) with the commercial enzyme, the inhibition of this series could not be restored after these different productions. Moreover, the check of the profile of mass of these enzymes revealed no major difference between the commercial

enzyme and our own batch. It should be noted that this problem seems to be relatively frequent in the development of PHGDH inhibitors. This probably results from differences in the enzyme folding or because of slightly different oxidative states of the enzyme.

To get a deeper understanding of this issue and try to solve this problem we set up a novel collaboration with the group of Lewis Cantley at the Weil Cornell Medicine center (NY, US) . The experiments that were conducted at NY using our *α*-ketoamides confirmed their PHGDH inhibitory potency and led to their publication in J. Med. Chem. in 2017.[86] In 2018, a 3-weeks internship in this team allowed us to produce a large quantity of enzyme that was used until the end of our research project. Even if some changes in the experimental process (agitation speed, temperature…) were used to produce the enzyme, the biochemical explanation behind this problem remains unclear.

Two hypotheses were formulated to explain this observation. The first consists in a change of the oxidation state of the protein, leading to the oxidation of certain amino acids that may be involved in the *α*-ketoamide binding. Indeed, a related family of *α*-ketoamides targeting the HCV Protease have their covalent mechanism of action explained by the formation of a reversible covalent bond with a serine moiety.[175] A similar mechanism involving for instance a cysteine residue, with our compounds, could explain that slight oxidative changes would account for the loss of inhibitory potency (**Figure 56**).

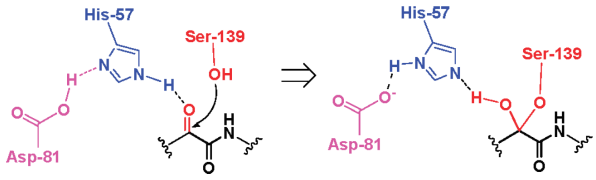

***Figure 56**: Reported mechanism of action of α-ketoamide inhibitors on HCV Protease*[175]

Unfortunately, and although PHGDH is known to be highly sensitive to oxidation during its production, the various reducing agents used during this process (DTT, TCEP, *β*-ME) were not able to modify its inhibition by the *α*-ketothioamide series invalidating this first hypothesis.

The second hypothesis involves folding modifications of the protein during its production. This potential change seems to not affect directly PHGDH active site since K_m values were

preserved but could modify the 3D arrangement of a potential allosteric site. Owning to the results subsequently obtained, this hypothesis seems to be privileged. Indeed, as explained in **Chapter 4**, a significant change in the denaturation temperature can be observed between different productions. Through these examples, we perceive the crucial importance of the precise identification of the site of action of PHGDH inhibitors in order to develop robust chemical series that can be used in more complex biological systems.

9.3.3. PHGDH crystallography

During our attempts to identify the site of action of the two main series of inhibitors (DSF and ketothioamide) another issue was encountered. Despite the numerous teams working on PHGDH crystallography, no data of the full-length PHGDH are available. This lack of structural information hindered the identification of the PHGDH allosteric sites. Nevertheless, various truncated versions of the enzyme still demonstrating activity were recently reported. Preliminary results on the disulfiram or α-ketothioamide series having demonstrated that our compounds act in a non-competitive manner with respect to both substrate and co-factor, co-crystallography experiments on truncated models were therefore undertaken to locate their action site. Unfortunately, these experiments conducted in parallel by the group of Johan Wouters (UNamur) and Judith Unterlass (Karolinska Insitutet) revealed unfruitful. Fortunately, mass spectrometry experminets enabled to partly overcome this issue.

Since the ACT domain is not present in the enzyme-truncated versions, the failure of crystallography for the α-ketothioamide series can easily be explained. On the other hand, the failure observed with Disulfiram crystallography could be explained due to its ability to disturb the protein oligomerization. Indeed, PHGDH crystallography is a challenging process that nowadays only allowed the obtention of a truncated dimeric form of the enzyme. Since no monomeric crystal can been observed even in absence of DSF, it appears that DSF properties will render this observation even more complicated.

These experiences allowed us to highlight the importance of always being vigilant to other methods when the first strategy failed.

9.3.4. Cells based assays

Finally, the last challenge encountered was related to the cellular assays used to evaluate our inhibitors. Firstly, it was necessary to evaluate different cell concentrations, incubation times, tumor lines and culture media. These experiments led to the evaluation of inhibitors on PHGDH-dependent lines (SiHa, HL-60, BT-20) for 5 days, in serine-depleted media to maximize their effects. The results obtained for these cell lines with the α-ketothioamide inhibitors were initially very promising. Unfortunately, we once again faced reproducibility issues in subsequent experiments. The efficiency of this series decreased drastically over the Months. This decrease was also observed with NCT-503, a reference inhibitor discovered by the Sabatini group. This loss of inhibition may be due in part to the cellular plasticity of the cell lines used, adapting to the inhibition of the serine pathway through the activation of the glutaminase pathway for example,[38] but also to a slight variation in serine concentration of the medium. As our series acts on the ACT regulatory domain, a higher concentration of serine could compete with our molecules and limit their cellular efficiency, although this amino acid no longer inhibits the enzyme.

Briefly, we can say that the major difficulty encountered during this work was related to the reproducibility of the results. This was partly due to the systems used but also to variability within the structure of the studied enzyme. Most of the time, this research has therefore consisted in the development of efficient and robust methods to identify and optimize new chemical series able to effectively inhibit PHGDH activity.

9.4. PERSPECTIVES

Currently, targeting cancer metabolism seems to be an interesting approach for developing new, more specific and effective cancer treatments. However, it is important to note that cancer cells have a high degree of cell plasticity, which will allow them, during the vast majority of treatments, to use escape pathways in order to pursue their proliferation.[176]

This is the main reason why, even if relatively potent PHGDH inhibitors were identified, the effectiveness of current inhibitors is limited, and the inhibition of the target alone does not always seem to lead to a decrease in tumor proliferation, even in PHGDH overexpressing tumor lines. The development of new and more effective PHGDH inhibitors or co-administration could be prioritized, especially as this last option seems to demonstrate

interesting applicability. For example, imipridones, a class of molecules acting on the Akt/ERK pathway through the degradation of c-Myc, also see their activity restored in glioblastomas following PHGDH inhibition.[177] In order to resist to imipridone therapy, the cells redirect various metabolic pathways by promoting the serine-one carbon-glycine pathway. Therefore, PHGDH inhibition, by preventing this reprogramming, avoid cancer cells adaption.

Nowadays several studies have demonstrated that PHGDH inhibition allows counteracting resistance phenomena to conventional cytotoxic chemotherapies, notably by increasing cells sensitivity to oxidative stress. Indeed, PHGDH inhibition leads to a decrease of antioxidants production that could lead to deficiencies in DNA repair pathways and cause fatal defects in the affected cells. This is the main reason why Bortezomib (myelomas),[178] Doxorubicin (ER triple negative breast cancer),[179] Vemurafenib (BRAF V600E mutated melanoma)[180] and Erlotinib (lung adenocarcinoma)[181] have seen the restauration of their antiproliferative effect following PHGDH inhibition with reference inhibitors (NCT-503 or CBR-5884).

Finally, recent studies on the glutamine metabolic pathway demonstrated that inhibition of this pathway in leukemic cells would lead to overexpression of the enzymes of the serine pathway in order to fight against the generated oxidative stress.[38] It is therefore clear that combining the inhibition of these two metabolic pathways would affect the growth of tumor cells and potentially open new therapeutic applications to these two treatments.

Concerning the direct perspectives of our identification of new PHGDH inhibitors, the newly discovered allosteric sites on PHGDH are interesting starting points in order to design more potent PHGDH inhibitors. The development of such small and non-competitive inhibitors could overcome the drawbacks of NADH competitive inhibitors while still offering the possibility to improve their efficiency by chemical modifications.

For **disulfiram**, our study suggests the development of protein-protein interaction inhibitor covalently targeting a precise cysteine of the protein (Cys116).[106] This particular type of inhibitor, although difficult to develop and implement, would offer a better selectivity towards PHGDH and would thus limit the off-target consequential effects of disulfiram.

Regarding the **α-ketothioamide series**, the development of the diazirine probe and associated mass spectrometry experiments should allow an efficient screening to identify new molecules acting in this cavity.

In addition, it should be noted that the work carried out led to the identification of a novel series of compounds able to effectively inhibit PHGDH (**Figure 57**). It would therefore be interesting to pursue the study of these molecules to allow their optimization and evaluation in more complex systems.

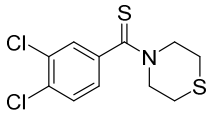

9.1
IC_{50} = 21 µM

Figure 57: Example of a potent thioamide derivative

All these freshly designed inhibitors can subsequently be optimized iteratively through the use of the various enzymatic assays and biochemical methods (MST, NMR) developed during this thesis.

Finally, concerning the biological perspectives of this project, the effect of PHGDH inhibition on healthy and cancer cells could be studied in numerous cell lines, with different levels of expression of this dehydrogenase, using the *in vitro* and *in vivo* assays developed during this research (2D or 3D cell culture). These studies would allow us to analyze in detail the involvement of PHGDH in many cellular processes (growth, metastatistic development, resistance to oxidative stress...). These studies are also possible using shRNA targeting this protein, however the use of small molecule inhibitors should allow to inhibit the enzymatic activity of the target while retaining the potential protein-protein interactions.

10. References

10. References

1. Hanahan, D. & Weinberg, R. A. Hallmarks of cancer: the next generation. *Cell* **144,** 646–74 (2011).

2. Boroughs, L. K., Deberardinis, R. J., Cell, N. & Author, B. Metabolic pathways promoting cancer cell survival and growth HHS public access author manuscript. *Nat Cell Biol* **17,** 351–359 (2015).

3. Vazquez, A., Liu, J., Zhou, Y. & Oltvai, Z. N. Catabolic efficiency of aerobic glycolysis: The Warburg effect revisited. *BMC Syst. Biol.* **4,** (2010).

4. Possemato, R. *et al.* Functional genomics reveal that the serine synthesis pathway is essential in breast cancer. *Nature* **476,** 346–350 (2011).

5. Locasale, J. W. *et al.* Phosphoglycerate dehydrogenase diverts glycolytic flux and contributes to oncogenesis. *Nat. Genet.* **43,** 869–74 (2011).

6. Kalhan, S. C. & Hanson, R. W. Resurgence of serine: An often neglected but indispensable amino acid. *J. Biol. Chem.* **287,** 19786–19791 (2012).

7. Locasale, J. W. Serine, Glycine and the one-carbon cycle: cancer metabolism in full circle. *Nat. Rev Cancer* **13,** 572–583 (2013).

8. Amelio, I., Cutruzzolá, F., Antonov, A., Agostini, M. & Melino, G. Serine and glycine metabolism in cancer. *Trends Biochem. Sci.* **39,** 191–8 (2014).

9. Mehrmohamadi, M. & Locasale, J. W. Context-dependent utilization of serine in cancer. *Mol. Cell. Oncol.* **2,** 3–4 (2015).

10. Tedeschi, P. M. *et al.* Contribution of serine, folate and glycine metabolism to the ATP, NADPH and purine requirements of cancer cells. *Cell Death Dis.* **4,** e877–12 (2013).

11. Mattaini, K. R., Sullivan, M. R. & Vander Heiden, M. G. The importance of serine metabolism in cancer. *J. Cell Biol.* **214,** 249–257 (2016).

12. El-Hattab, A. W. Serine biosynthesis and transport defects. *Mol. Genet. Metab.* **118,** 153–159 (2016).

13. Snell, K. & Weber, G. Enzymatic imbalance in serine metabolism in rat hepatomas. *Biochem. J.* **233,** 617–620 (1986).

14. Deberardinis, R. J. Serine metabolism: Some tumors take the road less traveled. *Cell Metab.* **14,** 285–286 (2011).

15. Beroukhim, R. *et al.* The landscape of somatic copy-number alteration across human cancer. **463,** 1–13 (2011).

16. Denicola, G. M. *et al.* NRF2 regulates serine biosynthesis in non-small cell lung cancer. **47,** 1475–1481 (2016).

17. Sun, L. *et al.* cMyc-mediated activation of serine biosynthesis pathway is critical for cancer progression under nutrient deprivation conditions. *Cell Res.* **25,** 429–444 (2015).

18. Ye, J. *et al.* Pyruvate kinase M2 promotes de novo serine synthesis to sustain mTORC1 activity and cell proliferation. *Proc. Natl. Acad. Sci.* **109,** 6904–6909 (2012).

19. Chaneton, B. *et al.* Serine is a natural ligand and allosteric activator of pyruvate kinase M2. *Nature* **491,** 458–462 (2012).

20. Amelio, I. *et al.* P73 regulates serine biosynthesis in cancer. *Oncogene* **33,** 5039–5046 (2014).

21. Ding, J. *et al.* The Histone H3 Methyltransferase G9A epigenetically activates the serine-glycine synthesis pathway to sustain cancer cell survival and proliferation. *PLoS One* **32,** 736–740 (2017).

22. Samanta, D. *et al.* PHGDH expression is required for mitochondrial redox homeostasis, breast cancer stem cell maintenance, and lung metastasis. *Cancer Res.* **76,** 4430–4442 (2016).

23. Ma, L. *et al.* Control of nutrient stress-induced metabolic reprogramming by PKCζ in tumorigenesis. *Cell* **152,** 599–611 (2013).

24. Ou, Y., Wang, S. J., Jiang, L., Zheng, B. & Gu, W. p53 Protein-mediated regulation of

phosphoglycerate dehydrogenase (PHGDH) is crucial for the apoptotic response upon serine starvation. *J. Biol. Chem.* **290,** 457–466 (2015).

25. Maddocks, O. D. K., Berkers, C. R., Mason, S. M., Zheng, L. & Blyth, K. Serine starvation induces stress and p53 dependent metabolic remodeling in cancer cells. *Nature* **493,** 542–546 (2019).

26. Luo, J. Cancer's sweet tooth for serine. *Breast Cancer Res.* **13,** 317 (2011).

27. Chen, J. *et al.* Phosphoglycerate dehydrogenase is dispensable for breast tumor maintenance and growth. *Oncotarget* **4,** (2013).

28. Noh, S., Kim, D. H., Jung, W. H. & Koo, J. S. Expression levels of serine/glycine metabolism-related proteins in triple negative breast cancer tissues. *Tumour Biol.* **35,** 4457–68 (2014).

29. Mullarky, E., Mattaini, K. R., Vander Heiden, M. G., Cantley, L. C. & Locasale, J. W. PHGDH amplification and altered glucose metabolism in human melanoma. *Pigment Cell Melanoma Res.* **24,** 1112–1115 (2011).

30. Yoon, S. *et al.* Clinical implication of serine metabolism-associated enzymes in colon cancer. *Oncol.* **89,** 351–359 (2015).

31. Jia, X. Q. *et al.* Increased expression of PHGDH and prognostic significance in colorectal cancer. *Transl. Oncol.* **9,** 191–196 (2016).

32. Liu, J. *et al.* Phosphoglycerate dehydrogenase induces glioma cells proliferation and invasion by stabilizing forkhead box M1. *J. Neurooncol.* **111,** 245–55 (2013).

33. Cai, L. *et al.* Epstein-Barr virus-encoded microRNA BART1 induces tumour metastasis by regulating PTEN-dependent pathways in nasopharyngeal carcinoma. *Nat. Commun.* **6,** (2015).

34. Ye, Y. *et al.* EBV-miR-BART1 is involved in regulating metabolism-associated genes in nasopharyngeal carcinoma. *Biochem. Biophys. Res. Commun.* **436,** 19–24 (2013).

35. Jing, Z. *et al.* Downregulation of phosphoglycerate dehydrogenase inhibits

proliferation and enhances cisplatin sensitivity in cervical adenocarcinoma cells by regulating Bcl-2 and caspase-3. *Cancer Biol. Ther.* **16,** 541–548 (2015).

36. Chen, M. *et al.* GC-MS-based metabolomic analysis of human papillary thyroid carcinoma tissue. *Int. J. Mol. Med.* **36,** 1607–1614 (2015).

37. Sun, W. Y., Kim, H. M., Jung, W. H. & Koo, J. S. Expression of serine/glycine metabolism-related proteins is different according to the thyroid cancer subtype. *J Transl Med* **14,** 168 (2016).

38. Polet, F. *et al.* Reducing the serine availability complements the inhibition of the glutamine metabolism to block leukemia cell growth. *Oncotarget* **5,** 3–5 (2016).

39. Xian, Y. *et al.* Phosphoglycerate dehydrogenase is a novel predictor for poor prognosis in gastric cancer. *Onco. Targets. Ther.* **9,** 5553–5560 (2016).

40. Zhu, J. *et al.* High expression of PHGDH predicts poor prognosis in non-small cell lung cancer. *Transl. Oncol.* **9,** 592–599 (2016).

41. Fujii, K. *et al.* Differential Proteomic Analysis between Small Cell Lung Carcinoma (SCLC) and Pulmonary Carcinoid Tumors Reveals Molecular Signatures for Malignancy in Lung Cancer. *Proteomics - Clin. Appl.* **12,** 1–42 (2018).

42. Branzoli, F. *et al.* Cystathionine as a marker for 1p/19q codeleted gliomas by in vivo magnetic resonance spectroscopy. *Neuro. Oncol.* **21,** 765–774 (2019).

43. Song, Z., Feng, C., Lu, Y., Lin, Y. & Dong, C. PHGDH is an independent prognosis marker and contributes cell proliferation, migration and invasion in human pancreatic cancer. *Gene* **642,** 43–50 (2018).

44. Ma, X., Li, B., Liu, J., Fu, Y. & Luo, Y. Phosphoglycerate dehydrogenase promotes pancreatic cancer development by interacting with eIF4A1 and eIF4E. *J. Exp. Clin. Cancer Res.* **38,** 1–15 (2019).

45. Linzey, J. R. *et al.* Identification and targeting of an FGFR fusion in a pediatric thalamic 'central oligodendroglioma'. *npj Precis. Oncol.* **1,** 29 (2017).

46. Cho, H. M., Jun, D. Y., Bae, M. A., Ahn, J. D. & Kim, Y. H. Nucleotide sequence and differential expression of the human 3-phosphoglycerate dehydrogenase gene k. *Gene* **245,** 193–201 (2000).

47. Gromova, I. *et al.* High level PHGDH expression in breast is predominantly associated with keratin 5-positive cell lineage independently of malignancy. *Mol. Oncol.* **9,** 1636–1654 (2015).

48. Fan, J. *et al.* Human phosphoglycerate dehydrogenase produces the oncometabolite d-2-hydroxyglutarate. *ACS Chem. Biol.* **10,** 510–516 (2015).

49. Sonoda, Y. & Tominaga, T. 2-hydroxyglutarate accumulation caused by IDH mutation is involved in the formation of malignant gliomas. *Expert Rev. Neurother.* **10,** 487–489 (2010).

50. Gross, S. *et al.* Cancer-associated metabolite 2-hydroxyglutarate accumulates in acute myelogenous leukemia with isocitrate dehydrogenase 1 and 2 mutations. *J. Exp. Med.* **207,** 339–344 (2010).

51. Terunuma, A. *et al.* MYC-driven accumulation of 2-hydroxyglutarate is associated with breast cancer prognosis. *J. Clin. Invest.* **124,** (2014).

52. Wierstra, I. *FOXM1 (Forkhead box M1) in Tumorigenesis*. *Advances in Cancer Research* **119,** (Elsevier Inc., 2014).

53. Sayano, T. *et al.* Adaptive response to l-serine deficiency is mediated by p38 MAPK activation via 1-deoxysphinganine in normal fibroblasts. *FEBS Open Bio* **6,** 303–316 (2016).

54. Li, S. *et al.* Astrocytes in primary cultures express serine racemase, synthesize D-serine and acquire A1 reactive astrocyte features. *Biochem. Pharmacol.* **151,** 245–251 (2018).

55. Pollari, S. *et al.* Enhanced serine production by bone metastatic breast cancer cells stimulates osteoclastogenesis. *Breast Cancer Res. Treat.* **125,** 421–30 (2011).

56. Samanta, D. *et al.* PHGDH expression is required for mitochondrial redox homeostasis, breast cancer stem cell maintenance, and lung metastasis. *Cancer Res.* **76,** 4430–4442

(2016).

57. Shiota, M. *et al.* Gold-nanofève surface-enhanced Raman spectroscopy visualizes hypotaurine as a robust anti-oxidant consumed in cancer survival. *Nat. Commun.* **9,** (2018).

58. Sharif, T. *et al.* Phosphoglycerate dehydrogenase inhibition induces p-mTOR-independent autophagy and promotes multilineage differentiation in embryonal carcinoma stem-like cells. *Cell Death Dis.* **9,** (2018).

59. Hanukoglu, I. Proteopedia: Rossmann fold: A beta-alpha-beta fold at dinucleotide binding sites. *Biochem. Mol. Biol. Educ.* **43,** 206–209 (2015).

60. Tabatabaie, L., Klomp, L. W., Berger, R. & de Koning, T. J. l-Serine synthesis in the central nervous system: A review on serine deficiency disorders. *Mol. Genet. Metab.* **99,** 256–262 (2010).

61. Furuya, S. An essential role for de novo biosynthesis of L-serine in CNS development. *Asia Pac J Clin Nutr* **17,** 312–315 (2008).

62. Klomp, L. W. J. *et al.* Molecular characterization of 3-phosphoglycerate dehydrogenase deficiency—a neurometabolic disorder associated with reduced L-Serine biosynthesis. *Am. J. Hum. Genet.* **67,** 1389–1399 (2002).

63. Pind, S. *et al.* V490M, a common mutation in 3-phosphoglycerate dehydrogenase deficiency, causes enzyme deficiency by decreasing the yield of mature enzyme. *J. Biol. Chem.* **277,** 7136–7143 (2002).

64. Tabatabaie, L. *et al.* Novel mutations in 3-phosphoglycerate dehydrogenase (PHGDH) are distributed throughout the protein and result in altered enzyme kinetics. *Hum. Mutat.* **30,** 749–756 (2009).

65. Shaheen, R. *et al.* Neu-laxova syndrome, an inborn error of serine metabolism, is caused by mutations in PHGDH. *Am. J. Hum. Genet.* **94,** 898–904 (2014).

66. Acuna-Hidalgo, R. *et al.* Neu-laxova syndrome is a heterogeneous metabolic disorder caused by defects in enzymes of the l-serine biosynthesis pathway. *Am. J. Hum. Genet.*

95, 285–293 (2014).

67. Lamzin, V. S., Dauter, Z., Popov, V. O., Harutyunyan, E. H. & Wilson, K. S. High resolution structures of holo and apo formate dehydrogenase. *Journal of Molecular Biology* **236,** 759–785 (1994).

68. Fuller, N. *et al.* An improved model for fragment-based lead generation at AstraZeneca. *Drug Discov. Today* **21,** 1272–1283 (2016).

69. Fuller, N. *Abstract of Papers, 250th ACS National Meeting & Exposition*. (2015).

70. Mullarky, E. *et al.* Inhibition of 3-phosphoglycerate dehydrogenase (PHGDH) by indole amides abrogates de novo serine synthesis in cancer cells. *Bioorg. Med. Chem. Lett.* 1–8 (2019). doi:10.1016/j.bmcl.2019.07.011

71. Weinstabl, H. *et al.* Intracellular trapping of the selective phosphoglycerate dehydrogenase (PHGDH) inhibitor BI-4924 disrupts serine biosynthesis. *J. Med. Chem.* acs.jmedchem.9b00718 (2019). doi:10.1021/acs.jmedchem.9b00718

72. Unterlass, J. E. *et al.* Validating and enabling phosphoglycerate dehydrogenase (PHGDH) as a target for fragment-based drug discovery in PHGDH-amplified breast cancer. *Oncotarget* **5,** (2016).

73. Mullarky, E., Lairson, L. L., Cantley, L. C. & Lyssiotis, C. A. A novel small-molecule inhibitor of 3-phosphoglycerate dehydrogenase. *Mol. Cell. Oncol.* **3,** e1164280 (2016).

74. Pacold, M. E. *et al.* A PHGDH inhibitor reveals coordination of serine synthesis and one-carbon unit fate. *Nat. Chem. Biol.* **12,** 452–458 (2016).

75. Frezza, C. Addicted to serine. *Nat. Chem. Biol.* **12,** 389 (2016).

76. Saiah, E. 3-Phosphoglycerate dehydrogenase inhibitors and uses thereof. WO 2016/040449 (2016).

77. Wang, Q. *et al.* Rational Design of Selective Allosteric Inhibitors of PHGDH and Serine Synthesis with Anti-tumor Activity. *Cell Chem. Biol.* **24,** 55–65 (2016).

78. Guo, J. *et al.* Azacoccone E inhibits cancer cell growth by targeting 3-phosphoglycerate

dehydrogenase. *Bioorg. Chem.* **87,** 16–22 (2019).

79. Hart, C. E. *et al.* Phosphoserine aminotransferase deficiency: a novel disorder of the serine biosynthesis pathway. *Am. J. Hum. Genet.* **80,** 931–937 (2007).

80. Basurko, M. J., Marche, M., Darriet, M. & Cassaigne, A. Phosphoserine aminotransferase, the second step-catalyzing enzyme for serine biosynthesis. *IUBMB Life* **48,** 525–529 (1999).

81. Bolton, J. L., Trush, M. A., Penning, T. M., Dryhurst, G. & Monks, T. J. Role of quinones in toxicology. *Chem. Res. Toxicol.* **13,** 135–160 (2000).

82. Kasséhin, U. C., Gbaguidi, F. A., Kapanda, C. N., McCurdy, C. R. & Poupaert, J. H. Insight into the Willgerodt-Kindler reaction of ω -haloacetophenone derivatives: mechanistic implication. *Org. Chem. Int.* **2014,** 1–5 (2014).

83. Matuszak, N., Es Saadi, B., Labar, G., Marchand-Brynaert, J. & Lambert, D. M. Benzisothiazolinone as a useful template for the design of new monoacylglycerol lipase inhibitors: Investigation of the target residues and comparison with octhilinone. *Bioorganic Med. Chem. Lett.* **21,** 7321–7324 (2011).

84. Morera, L., Labar, G., Ortar, G. & Lambert, D. M. Development and characterization of endocannabinoid hydrolases FAAH and MAGL inhibitors bearing a benzotriazol-1-yl carboxamide scaffold. *Bioorganic Med. Chem.* **20,** 6260–6275 (2012).

85. Kapanda, C. N., Muccioli, G. G., Labar, G., Poupaert, J. H. & Lambert, D. M. Bis(dialkylaminethiocarbonyl)disulfides as potent and selective monoglyceride lipase inhibitors. *J. Med. Chem.* **52,** 7310–7314 (2009).

86. Ravez, S. *et al.* α-Ketothioamide Derivatives: A Promising Tool to Interrogate Phosphoglycerate Dehydrogenase (PHGDH). *J. Med. Chem.* **60,** 1591–1597 (2017).

87. Wu, P., Nielsen, T. E. & Clausen, M. H. FDA-approved small-molecule kinase inhibitors. *Trends Pharmacol. Sci.* **36,** 422–439 (2015).

88. Kryger, G., Silman, I. & Sussman, J. L. Structure of acetylcholinesterase complexed with E2020 (Aricept®): Implications for the design of new anti-Alzheimer drugs.

Structure **7,** 297–307 (1999).

89. De Clercq, E. Antiviral drugs in current clinical use. *J. Clin. Virol.* **30,** 115–133 (2004).

90. Unterlass, J. E. *et al.* Validating and enabling phosphoglycerate dehydrogenase (PHGDH) as a target for fragment-based drug discovery in PHGDH-amplified breast cancer. *Oncotarget* **9,** 13139–13153 (2018).

91. Vilar, S., Cozza, G. & Moro, S. Medicinal chemistry and the molecular operating environment (MOE): application of QSAR and molecular docking to drug discovery. *Curr. Top. Med. Chem.* **8,** 1555–1572 (2008).

92. Verdonk, M. L., Cole, J. C., Hartshorn, M. J., Murray, C. W. & Taylor, R. D. Giftgas over Byen. Civilbefolkningens Beskyttelse Under Den Næste krig. *Proteins* **52,** 609–623 (2003).

93. Zhong, S. *et al.* Identification and Validation of Human DNA Ligase Inhibitors Using Computer-Aided Drug Design. *J. Med. Chem.* **51,** 4553–4562 (2008).

94. Pagadala, N. S., Syed, K. & Tuszynski, J. Software for molecular docking: a review. *Biophys. Rev.* **9,** 91–102 (2017).

95. Mayer, M. & Meyer, B. Characterization of ligand binding by saturation transfer difference NMR spectroscopy. *Angew. Chemie - Int. Ed.* **38,** 1784–1788 (1999).

96. Dalvit, C. *et al.* Identification of compounds with binding affinity to proteins via magnetization transfer from bulk water. *J. Biomol. NMR* **18,** 65–68 (2000).

97. Dormán, G. *et al.* Development of a multifunctional benzophenone linker for peptide stapling and photoaffinity labelling. *ChemBioChem* **17,** 159–183 (2016).

98. Ruoho, A. E., Kiefer, H., Roeder, P. E. & Singer, S. J. The mechanism of photoaffinity labeling. *Proc. Natl. Acad. Sci.* **70,** 2567–2571 (1973).

99. Dimitrova, N. *et al.* Photocrosslinking approaches to intercome mapping. *PLoS One* **32,** 736–740 (2017).

100. Hill, J. R. & Robertson, A. A. B. Fishing for drug targets: a focus on diazirine

photoaffinity probe synthesis. *J. Med. Chem.* **61,** 6945–6963 (2018).

101. Braun, P. J., Dennis, S., Hofsteenge, J. & Stone, S. R. Use of site-directed mutagenesis to investigate the basis for the specificity of Hirudin. *Biochemistry* **27,** 6517–6522 (1988).

102. Cesura, A. M. *et al.* Investigation on the structure of the active site of monoamine oxidase-B by affinity labeling with the selective inhibitor lazabemide and by site-directed mutagenesis. *Eur. J. Biochem.* **236,** 996–1002 (1996).

103. Zheng, M. *et al.* Ixocarpalactone A from dietary tomatillo inhibits pancreatic cancer growth by targeting PHGDH. *Food Funct.* **10,** 3386–3395 (2019).

104. Dey, S., Hu, Z., Xiao, L. X., Sacchettini, J. C. & Grant, G. A. D-3-phosphoglycerate dehydrogenase from Mycobacterium tuberculosis is a link between the Escherichia coli and mammalian enzymes. *J. Biol. Chem.* **280,** 14884–14891 (2005).

105. Grant, G. A. Contrasting catalytic and allosteric mechanisms for phosphoglycerate dehydrogenases. *Arch. Biochem. Biophys.* **519,** 175–185 (2012).

106. Spillier, Q. *et al.* Anti-alcohol abuse drug disulfiram inhibits human PHGDH via disruption of its active tetrameric form through a specific cysteine oxidation. *Sci. Rep.* **9,** 4737 (2019).

107. Grodzki, M. Über äthylirte Sulfoharnstof. *Ber. Dtsch. Chem. Ges.* **14,** 2754–2758 (1881).

108. Twiss, D., Bazier, S. A. & Thomas, F. The Dithiocarbamate Accelerators of Vulcanization. *J. Soc. Chem. Ind.* **41,** 81T–88T (1922).

109. Williams, E. E. Effects of alcohol on workers with carbon disulfide. *J. Am. Med. Assoc.* **109,** 1472–1473 (1937).

110. Gordon, R. M. & Seaton, D. R. Observations on the treatment of scabies. *Brit. Med. J.* **1,** 685–687 (1942).

111. Terwilliger, N. B. Funtional adaptations of oxugen-trasport proteins. *J. Exp. Biol.* **201,**

1085–1098 (1998).

112. Martensen-Larsen, O. Treatment of alcoholism with a sensitising drug. *Lancet.* **252,** 1004–1005 (1948).

113. Asmussen, E. The pharmacological action of acetaldehyde on the human organism. *Acta Pharm. Tox.* **4,** 311–315 (1948).

114. Jacobsen, E. The metabolism of ethyl alcohol. *Nature* **169,** 645–647 (1952).

115. Hald, J., Jacobsen, E. & Larsen, V. The sensitizing effect of tetraethylthiuramdisulphide (Antabuse) to ethyl alcohol. *Acta Pharm. Tox.* **4,** 285–296 (1948).

116. Glud, E. The treatment of alcoholic patients in Denmark with 'Antabuse'; with suggestions for its trials in the United States. *Quart. J. Stud. Alcohol* **10,** 185–197 (1949).

117. Boukriche, Y., Weisser, I., Aubert, P. & Masson, C. MRI findings in a case of late onset disulfiram-induced neurotoxicity [5]. *J. Neurol.* **247,** 714–715 (2000).

118. Cornford, E. M. *et al.* Rapid distribution of tryptophol (3-indole ethanol) to the brain and other tissues. *J. Clin. Invest.* **63,** 1241–1248 (1979).

119. Pindborg, J. J. The reparative effect of Antabuse (tetra-ethylthiuram Disulfide) upon dental changes in Vitamin E deficient rats. *J. Dent. Res.* **31,** 812–814 (1952).

120. Schirmer, H. & Scott, W. Disulfiram and tumor inhibition. *Trans. Am. Assoc. Genitourin. Surg.* **58,** 63–66 (1966).

121. Lewison, E. Spontaneous regression of breast cancer. *Prog. Clin. Biol . Res.* **12,** 47–53 (1977).

122. Schmähl, D., Krüger, F., Habs, M. & Diehl, B. Influence of disulfiram on the organotropy of the carcinogenic effect of dimethylnitrosamine and diethylnitrosamine in rats. *Z Krebsforsch Klin Onkol Cancer Res Clin Oncol* **19,** 271–276 (1976).

123. Irving, C. C., Tice, A. J. & Murphy, W. M. Inhibition of N-n-Butyl-N-(4-hydroxybutyl)nitrosamine-induced Urinary Bladder Cancer in Rats by Administration

of Disulfiram in the Diet. *Cancer Res.* **39,** 3040–3043 (1979).

124. Lindahl, R. Properties of aldehyde dehydrogenas from chemically-induced rat hepatomas and normal rat liver. *Adv Exp Med Biol.* **132,** 85–93 (1980).

125. Takenaga, K., Honma, Y. & Hozumi, M. Inhibition of differentiation of mouse myeloid leukemia cells by phenolic antioxidants and alpha-tocopherol. *Gan* **72,** 104–112 (1981).

126. Hacker, M. P., Ershler, W. B., Newman, R. A. & Gamelli, R. L. Effect of disulfiram (tetraethylthiuram disulfide) and diethyldithiocarbamate on the bladder toxicity and antitumor activity of cyclophosphamide in mice. *Cancer Res.* **42,** 4490–4494 (1982).

127. Roemeling, R. *et al.* Cisplatin chronotherapy and disulfiram rescue reduce toxicity without interfering with anticancer activity: animal findings and preliminary clinical experiences. *Chronobiol Int.* **3,** 56–64 (1986).

128. Liu, G. Y., Frank, N., Bartsch, H. & Lin, J. K. Induction of apoptosis by thiuramdisulfides, the reactive metabolites of dithiocarbamates, through coordinative modulation of NFκB, c-fos/c-jun, and p53 proteins. *Mol. Carcinog.* **22,** 235–246 (1998).

129. Kast, R. & Belda-Iniesta, C. Suppressing glioblastoma stem cell function by aldehyde dehydrogenase inhibition with Chloramphenicol or Disulfiram as a new treatment adjunct: a hypothesis. *Curr. Stem Cell Res. Ther.* **4,** 314–317 (2009).

130. Fruehauf, J. P. & Trapp, V. Reactive oxygen species: An Archilles' heel of melanoma? *Expert Rev. Anticancer Ther.* **8,** 1751–1757 (2008).

131. Iljin, K. *et al.* High-throughput cell-based screening of 4910 known drugs and drug-like small molecules identifies disulfiram as an inhibitor of prostate cancer cell growth. *Clin. Cancer Res.* **15,** 6070–6078 (2009).

132. Cho, H. *et al.* Disulfiram suppresses invasive ability of osteosarcoma cells via the inhibition of MMP-2 and MMP-9 expression. *J Biochem Mol Biol.* **40,** 1069–1076 (2007).

133. Skrott, Z. *et al.* Alcohol-abuse drug disulfiram targets cancer via p97 segregase

adaptor NPL4. *Nature* **552,** 194–199 (2017).

134. Sauna, Z. E., Shukla, S. & Ambudkar, S. V. Disulfiram, an old drug with new potential therapeutic uses for human cancers and fungal infections. *Mol. Biosyst.* **1,** 127–134 (2005).

135. Pothineni, V. R. *et al.* Identification of new drug candidates against Borrelia burgdorferi using high-throughput screening. *Drug Des. Devel. Ther.* **10,** 1307–1322 (2016).

136. Xing, S. *et al.* Disulfiram reactivates latent HIV-1 in a Bcl-2-transduced primary CD4+ T cell model without inducing global T cell activation. *J. Virol.* **85,** 6060–6064 (2011).

137. U.S. National Library of Medicine. Clinical Trials. (2019). Available at: https://clinicaltrials.gov/. (Accessed: 11th August 2019)

138. Cvek, B. Nonprofit drugs as the salvation of the world's healthcare systems: The case of Antabuse (disulfiram). *Drug Discov. Today* **17,** 409–412 (2012).

139. Pantziarka, P., Bouche, G., Meheus, L., Sukhatme, V. & Sukhatme, V. P. The repurposing drugs in oncology (ReDO) project. *Ecancermedicalscience* **8,** 1–13 (2014).

140. Petersen, E. N. The pharmacology and toxicology of disulfiram and its metabolites. *Acta Psychiatr. Scand.* **86,** 7–13 (1992).

141. Nechushtan, H. *et al.* A Phase IIb trial assessing the addition of Disulfiram to chemotherapy for the treatment of metastatic non-small cell lung cancer. *Oncologist* **20,** 366–367 (2015).

142. Lipsky, J. J., Shen, M. L. & Naylor, S. Overview - In vitro inhibition of aldehyde dehydrogenase by disulfiram and metabolites. *Chem. Biol. Interact.* **130-132,** 81–91 (2001).

143. Rudyk, O. & Eaton, P. Biochemical methods for monitoring protein thiol redox states in biological systems. *Redox Biol.* **2,** 803–813 (2014).

144. Bruegger, J. J., Smith, B. C., Wynia-Smith, S. L. & Marletta, M. A. Comparative and

integrative metabolomics reveal that S-nitrosation inhibits physiologically relevant metabolic enzymes. *J. Biol. Chem.* **293,** 6282–6296 (2018).

145. Mullarky, E. *et al.* Identification of a small molecule inhibitor of 3-phosphoglycerate dehydrogenase to target serine biosynthesis in cancers. *Proc. Natl. Acad. Sci.* **113,** 201521548 (2016).

146. Silva, C. M. & Cidlowski, J. A. Direct evidence for intra- and intermolecular disulfide bond formation in the human glucocorticoid receptor. Inhibition of DNA binding and identification of a new receptor-associated protein. *J Biol Chem* **264,** 6638–6647 (1989).

147. Faiman, M. D., Jensen, J. C. & Lacoursiere, R. B. Elimination kinetics of disulfiram in alcoholics after single and repeated doses. *Clin. Pharmacol. Ther.* **36,** 520–526 (1984).

148. Goemans, C. V., Vertommen, D., Agrebi, R. & Collet, J. F. CnoX Is a chaperedoxin: a holdase that protects its substrates from irreversible oxidation. *Mol. Cell* **70,** 614–627.e7 (2018).

149. Cvek, B., Milacic, V., Taraba, J. & Dou, Q. P. Ni(II), Cu(II), and Zn(II) diethyldithiocarbamate complexes show various activities against the proteasome in breast cancer cells. *J. Med. Chem.* **51,** 6256–6258 (2008).

150. Denoncin, K., Nicolaes, V., Cho, S., Leverrier, P. & Collet, J. *Bacterial Cell Surfaces*. **966,** (Humana Press, 2013).

151. Baillie, T. A. Targeted Covalent Inhibitors for Drug Design. *Angew. Chemie - Int. Ed.* **55,** 13408–13421 (2016).

152. Singh, J., Petter, R. C., Baillie, T. A. & Whitty, A. The resurgence of covalent drugs. *Nat. Rev. Drug Discov.* **10,** 307–317 (2011).

153. Kalgutkar, A. S., Dalvie, D. K., Kalgutkar, A. S. & Dalvie, D. K. Drug discovery for a new generation of covalent drugs Drug discovery for a new generation of covalent drugs. *Expert Opin. Drug Discov.* **0441,** 561–581 (2016).

154. González-Bello, C. Designing irreversible inhibitors - worth the effort? *ChemMedChem*

11, 22–30 (2016).

155. Navath, R. S. *et al.* Dendrimer-drug conjugates for tailored intracellular drug release based on glutathione levels. *Bioconjug. Chem.* **19,** 2446–2455 (2008).

156. Ostrem, J. M., Peters, U., Sos, M. L., Wells, J. A. & Shokat, K. M. K-Ras(G12C) inhibitors allosterically control GTP affinity and effector interactions. *Nature* **503,** 548–551 (2013).

157. Bradshaw, J. M. *et al.* Prolonged and tunable residence time using reversible covalent kinase inhibitors. *Nat. Chem. Biol.* **11,** 525–531 (2015).

158. Wang, N., Lodge, J. M., Fierke, C. A. & Mapp, A. K. Dissecting allosteric effects of activator-coactivator complexes using a covalent small molecule ligand. *Proc. Natl. Acad. Sci. U. S. A.* **111,** 12061–12066 (2014).

159. Lu, S. & Zhang, J. Designed covalent allosteric modulators: an emerging paradigm in drug discovery. *Drug Discov. Today* **22,** 447–453 (2017).

160. Changeux, J. P. The concept of allosteric modulation: An overview. *Drug Discov. Today Technol.* **10,** e223–e228 (2013).

161. Ribeiro, A. A. S. T. & Ortiz, V. A Chemical perspective on allostery. *Chem. Rev.* **116,** 6488–6502 (2016).

162. Fricker, S. P. Physiology and pharmacology of plerixafor. *Transfus. Med. Hemotherapy* **40,** 237–245 (2013).

163. Fasano, M. *et al.* Type III or allosteric kinase inhibitors for the treatment of non-small cell lung cancer. *Expert Opin. Investig. Drugs* **23,** 809–821 (2014).

164. Jeffrey Conn, P., Christopoulos, A. & Lindsley, C. W. Allosteric modulators of GPCRs: A novel approach for the treatment of CNS disorders. *Nat. Rev. Drug Discov.* **8,** 41–54 (2009).

165. Tison, F. *et al.* A Phase 2A Trial of the Novel mGluR5-Negative Allosteric Modulator Dipraglurant for Levodopa-Induced Dyskinesia in Parkinson's Disease. *Mov. Disord.* **31,**

1373–1380 (2016).

166. Lu, S., He, X., Ni, D. & Zhang, J. Allosteric Modulator Discovery: From Serendipity to Structure-Based Design. *J. Med. Chem.* **62,** 6405–6421 (2019).

167. Haag, F. *et al.* Extracellular NAD and ATP: Partners in immune cell modulation. *Purinergic Signal.* **3,** 71–81 (2007).

168. Dang, C., Reddy, P., Shokat, K. & Soucek, L. Drugging the undruggable cancer targets. *Nat. Rev Cancer* **5,** 1–8 (2009).

169. Sherbenou, D. W. *et al.* BCR-ABL SH3-SH2 domain mutations in chronic myeloid leukemia patients on imatinib. *Blood* **116,** 3278–3285 (2010).

170. Wu, P., Clausen, M. H. & Nielsen, T. E. Allosteric small-molecule kinase inhibitors. *Pharmacol. Ther.* **156,** 59–68 (2015).

171. Lewis, J. A., Lebois, E. P. & Lindsley, C. W. Allosteric modulation of kinases and GPCRs: design principles and structural diversity. *Curr. Opin. Chem. Biol.* **12,** 269–280 (2008).

172. Wenthur, C. J., Gentry, P. R., Mathews, T. P. & Lindsley, C. W. Drugs for allosteric sites on receptors. *Annu. Rev. Pharmacol. Toxicol.* **54,** 165–184 (2014).

173. Lu, S., Huang, W. & Zhang, J. Recent computational advances in the identification of allosteric sites in proteins. *Drug Discov. Today* **19,** 1595–1600 (2014).

174. Schueler-Furman, O. & Wodak, S. J. Computational approaches to investigating allostery. *Curr. Opin. Struct. Biol.* **41,** 159–171 (2016).

175. Njoroge, F. G., Chen, K. X., Shih, N.-Y. & Piwinski, J. J. Challenges in modern drug discovery: A case study of boceprevir, an HCV protease inhibitor for the treatment of hepatitis C virus infection. *Acc. Chem. Res.* **41,** 50–59 (2008).

176. Cairns, R. A., Harris, I. S. & Mak, T. W. Regulation of cancer cell metabolism. *Nat. Rev. Cancer* **11,** 85–95 (2011).

177. Ishida, C. T. *et al.* Metabolic reprogramming by dual AKT/ERK inhibition through imipridones elicits unique vulnerabilities in glioblastoma. *Clin. Cancer Res.* **24,** 5392–

5406 (2018).

178. Zaal, E. A. *et al.* Bortezomib resistance in multiple myeloma is associated with increased serine synthesis. *Cancer Metab.* **5,** 7 (2017).

179. Zhang, X. & Bai, W. Repression of phosphoglycerate dehydrogenase sensitizes triple-negative breast cancer to doxorubicin. *Cancer Chemother. Pharmacol.* **78,** 655–659 (2016).

180. Ross, K. C., Andrews, A. J., Marion, C. D., Yen, T. J. & Bhattacharjee, V. Identification of the Serine Biosynthesis Pathway as a Critical Component of BRAF Inhibitor Resistance of Melanoma, Pancreatic, and Non–Small Cell Lung Cancer Cells. *Mol. Cancer Ther.* **16,** 1596–1609 (2017).

181. Dong, J. K. *et al.* Overcoming erlotinib resistance in EGFR mutation-positive lung adenocarcinomas through repression of phosphoglycerate dehydrogenase. *Theranostics* **8,** 1808–1823 (2018).

11. Annexes

11. Annexes/Supporting information

11.1. SYNTHETIC PROCEDURE OF COMPOUNDS 5.17-5.32 (CHAPTER 5)

1-(2-Fluorophenyl)-2-morpholino-2-thioxoethanone (**5.17**). This compound was synthesized according to the general procedure describe above. 1-(2-Fluorophenyl)ethanone (1.50 g, 11.10 mmol) and dibromine (0.65 mL, 13.00 mmol) were mixed in chloroform (15 mL) to obtain the 2-bromo-1-(2-fluorophenyl)-ethanone and this intermediate was reacted in a second time with morpholine (2.84 mL, 32.50 mmol) and sulfur (0.52 g, 16.20 mmol) in DMF (10 mL). Methanol was used for recrystallization to afford the title compound as a yellow solid (1.09 g, 39%). R_f 0.2 (cyclohexane/EtOAc 8:2). Mp: 83-85°C. ^{1}H NMR (400 MHz, $CDCl_3$): δ_H (ppm) 3.48-3.50 (m, 2H), 3.71-3.73 (m, 2H), 3.90-3.92 (t, 2H, J = 4.8 Hz), 4.26-4.28 (t, 2H, J = 4.8 Hz), 7.10-7.16 (ddd, 1 ArH, J_{HF} = 10.9 Hz J_{HH} = 8.3 and 1.0 Hz), 7.29-7.33 (ddd, 1 ArH, J_{HH} = 7.8 and 1.0 Hz), 7.59-7.61 (m, 1 ArH), 8.00-8.05 (ddd, 1 ArH, J_{HF} = 15.2 Hz J_{HH} = 7.6 and 1.9 Hz). ^{13}C NMR (100 MHz, $CDCl_3$): δ_C (ppm) 44.97, 49.65, 63.86, 63.87, 114.30 (d, J_{CF} = 22 Hz), 120.91 (d, J_{CF} = 23 Hz), 122.74 (d, J_{CF} = 23 Hz), 129.49 (d, J_{CF} = 23 Hz), 133.76 (d, J_{CF} = 23 Hz), 158.06 (d, J_{CF} = 255 Hz), 181.35 (C=O), 194.23 (C=S). HRMS (ESI$^+$): *m/z* calcd for $C_{12}H_{12}FNO_2S$ $(M + H)^+$ 254.0645, found 254.0644.

1-(3-Fluorophenyl)-2-morpholino-2-thioxoethanone (**5.18**). This compound was synthesized according to the general procedure describe above using 2-bromo-1-(3-fluorophenyl)ethanone (0.50 g, 2.30 mmol), morpholine (0.6 mL, 6.90 mmol) and sulfur (0.11 g, 3.45 mmol) in DMF (10 mL). Methanol was used for recrystallization to afford the title compound as a yellow solid (0.13 g, 23%). R_f 0.2 (cyclohexane/EtOAc 8:2). Mp: 95-97°C. ^{1}H NMR (400 MHz, $CDCl_3$): δ_H (ppm) 3.59-3.62 (t, 2H, J = 4.8 Hz), 3.70-3.73 (t, 2H, J = 4.8 Hz), 3.90-3.93 (t, 2H, J = 4.8 Hz), 4.32-4.34 (t, 2H, J = 4.8 Hz), 7.30-7.35 (dddd, 1 ArH, J_{HF} = 16.4 Hz J_{HH} = 8.1 and 2.5 Hz), 7.46-7.51 (ddd, 1 ArH, J_{HH} = 8.1 Hz J_{HF} = 5.4 Hz), 7.68-7.72 (ddd, 1 ArH, J_{HF} = 9.0 Hz J_{HH} = 1.6 Hz), 7.76-7.78 (ddd, 1 ArH, J_{HH} = 7.7 Hz and 1.1 Hz). ^{13}C NMR (100 MHz, $CDCl_3$): δ_C (ppm) 47.07, 51.87, 66.25, 66.38, 116.03 (d, J_{CF} = 23 Hz), 121.31 (d, J_{CF} = 23 Hz), 125.59 (d, J_{CF} = 23 Hz), 130.58 (d, J_{CF} = 23 Hz), 135.34 (d, J_{CF} = 23 Hz), 161.45 (d, J_{CF} = 247 Hz), 186.05 (C=O), 194.59 (C=S). HRMS (ESI$^+$): *m/z* calcd for $C_{12}H_{12}FNO_2S$ $(M + H)^+$ 254.0645, found 254.0644.

1-(4-Fluorophenyl)-2-morpholino-2-thioxoethanone (**5.19**). This compound was synthesized according to the general procedure describe above using 2-bromo-1-(4-fluorophenyl)ethanone (0.50 g, 2.30 mmol), morpholine (0.6 mL, 6.90 mmol) and sulfur (0.11 g, 3.45 mmol) in DMF (10 mL). Methanol was used for recrystallization to afford the title compound as a beige solid (0.23 g, 41%). R_f 0.2 (cyclohexane/EtOAc 8:2). Mp: 131-133°C. ^{1}H NMR (400 MHz, $CDCl_3$): δ_H (ppm) 3.59-3.71 (m, 4H), 3.89-3.91 (t, 2H, *J* = 4.8 Hz), 4.31-4.34 (t, 2H, *J* = 4.8 Hz), 7.15-7.19 (m, 2 ArH), 8.02-8.05 (m, 2 ArH). ^{13}C NMR (100 MHz, $CDCl_3$): δ_C (ppm) 47.17, 51.97, 66.39, 66.53, 116.19 (2C, d, *J* = 22 Hz), 129.74, 132.63 (2C, d, *J* = 9 Hz), 165.17 (D, *J* = 257 Hz), 186.38 (C=O), 195.16 (C=S). HRMS (ESI$^+$): *m/z* calcd for $C_{12}H_{12}FNO_2S$ $(M + H)^+$ 254.0645, found 254.0642.

1-(2-Chlorophenyl)-2-morpholino-2-thioxoethanone (**5.20**). This compound was synthesized according to the general procedure describe above using 2-bromo-1-(2-chlorophenyl)ethanone (0.50 g, 2.14 mmol), morpholine (0.56 mL, 6.42 mmol) and sulfur (0.10 g, 3.21 mmol) in DMF (10 mL). Acetonitrile was used for recrystallization to afford the title compound as a yellow solid (0.20 g, 36%). R_f 0.3 (cyclohexane/EtOAc 8:2). Mp: 78-80°C. ^{1}H NMR (400 MHz, $CDCl_3$): δ_H (ppm) 3.82-3.92 (m, 6H), 4.26-4.28 (m, 2H), 7.40-7.60 (m, 3 ArH), 7.92-7.94 (m, 1 ArH). ^{13}C NMR (100 MHz, $CDCl_3$): δ_C (ppm) 47.70, 52.15, 66.01, 66.06, 127.29, 130.73, 132.41, 132.69, 133.80, 134.58, 185.07 (C=O), 195.72 (C=S). HRMS (ESI$^+$): *m/z* calcd for $C_{12}H_{13}ClNO_2S$ $(M + H)^+$ 270.0350, found 270.0350.

1-(3-Chlorophenyl)-2-morpholino-2-thioxoethanone (**5.21**). This compound was synthesized according to the general procedure describe above. 1-(3-Chlorophenyl)ethanone (2.00 g, 12.90 mmol) and dibromine (0.78 mL, 15.50 mmol) were mixed in chloroform (15 mL) to obtain the 2-bromo-1-(3-chlorophenyl)-ethanone and this intermediate was reacted in a second time with morpholine (3.38 mL, 38.80 mmol) and sulfur (0.62 g, 19.40 mmol) in DMF (10 mL). The residue was purified by silica gel chromatography (cyclohexane/EtOAc, 8:2) and the obtained oil was collected by filtration with diethyl ether to give the title compound as a yellow solid (1.50 g, 43%). R_f 0.2 (cyclohexane/EtOAc 8:2). Mp: 92-94°C. ^{1}H NMR (400 MHz, $CDCl_3$): δ_H (ppm) 3.59-3.61 (t, 2H, *J* = 4.8 Hz), 3.70-3.72 (t, 2H, *J* = 4.8 Hz), 3.90-3.92 (t, 2H, *J* = 4.8 Hz), 4.31-4.33 (t, 2H, *J* = 4.8 Hz), 7.42-7.46 (dd, 1 ArH, *J* = 7.8 Hz), 7.57-7.59 (ddd, 1 ArH, *J*

= 8.0 and 1.0 Hz), 7.85-7.87 (ddd, 1 ArH, *J* = 7.8 and 1.4 Hz), 7.96-7.97 (dd, 1 ArH, *J* = 1.8 Hz). ^{13}C NMR (100 MHz, $CDCl_3$): δ_C (ppm) 47.21, 52.00, 66.39, 66.52, 127.98, 129.61, 130.28, 134.33, 135.05, 135.30, 186.07 (C=O), 194.60 (C=S). HRMS (ESI^+): *m/z* calcd for $C_{12}H_{12}ClNO_2S$ $(M + H)^+$ 270.0277, found 270.0278.

1-(4-Chlorophenyl)-2-morpholino-2-thioxoethanone (**5.22**). This compound was synthesized according to the general procedure describe above using 2-bromo-1-(2-chlorophenyl)ethanone (0.50 g, 2.14 mmol), morpholine (0.56 mL, 6.42 mmol) and sulfur (0.10 g, 3.21 mmol) in DMF (10 mL). Acetonitrile was used for recrystallization to afford the title compound as a yellow solid (0.22 g, 38%). R_f 0.2 (cyclohexane/EtOAc 8:2). Mp: 135-137°C. ^{1}H NMR (400 MHz, $CDCl_3$): δ_H (ppm) 3.58-3.71 (m, 4H), 3.89-3.92 (t, 2H, *J* = 4.8 Hz), 4.31-4.33 (t, 2H, *J* = 4.8 Hz), 7.46-7.48 (d, 2 ArH, *J* = 8.8 Hz), 7.93-7.95 (d, 2 ArH, *J* = 8.6 Hz). ^{13}C NMR (100 MHz, $CDCl_3$): δ_C (ppm) 47.18, 51.97, 66.39, 66.53, 129.36 (2C), 131.22 (2C), 131.74, 141.06, 186.45 (C=O), 194.94 (C=S). HRMS (ESI^+): *m/z* calcd for $C_{12}H_{13}ClNO_2S$ $(M + H)^+$ 270.0350, found 270.0350.

1-(2-Bromophenyl)-2-morpholino-2-thioxoethanone (**5.23**). This compound was synthesized according to the general procedure describe above using 2-bromo-1-(2-bromophenyl)-ethanone (0.50 g, 1.81 mmol), morpholine (0.48 mL, 5.43 mmol) and sulfur (0.08 g, 2.72 mmol) in DMF (10 mL). Ethanol was used for recrystallization to afford the title compound as a colorless solid (0.28 g, 52%). R_f 0.3 (cyclohexane/EtOAc 8:2). Mp: 81-83°C. ^{1}H NMR (400 MHz, $CDCl_3$): δ_H (ppm) 3.48-3.85 (m, 4H), 3.90-3.92 (t, 2H, *J* = 4.8 Hz), 4.25-4.28 (t, 2H, *J* = 4.8 Hz), 7.27-7.40 (ddd, 1 ArH, *J* = 1.8 and 7.8 Hz), 7.40-7.46 (ddd, 1 ArH, *J* = 1.2 and 7.5 Hz), 7.59-7.62 (dd, 1 ArH, *J* = 1.1 and 7.9 Hz), 7.84-7.87 (dd, 1 ArH, *J* = 1.8 and 7.6 Hz). ^{13}C NMR (100 MHz, $CDCl_3$): δ_C (ppm) 47.86, 52.28, 66.02, 66.05, 120.59, 127.69, 132.96, 133.64, 134.02, 136.45, 185.56 (C=O), 194.99 (C=S). HRMS (ESI^+): *m/z* calcd for $C_{12}H_{12}BrNO_2S$ $(M + H)^+$ 313.9844, found 313.9845.

1-(3-Bromophenyl)-2-morpholino-2-thioxoethanone (**5.24**). This compound was synthesized according to the general procedure describe above using 2-bromo-1-(3-bromophenyl)-ethanone (0.50 g, 1.81 mmol), morpholine (0.48 mL, 5.43 mmol) and sulfur (0.08 g, 2.72

mmol) in DMF (10 mL). Methanol was used for recrystallization to afford the title compound as a colorless solid (0.14 g, 26%). R_f 0.2 (cyclohexane/EtOAc 8:2). Mp: 104-106°C. ^{1}H NMR (400 MHz, $CDCl_3$): δ_H (ppm) 3.61-3.64 (t, 2H, *J* = 4.8 Hz), 3.72-3.74 (t, 2H, *J* = 4.8 Hz), 3.90-3.93 (t, 2H, *J* = 4.8 Hz), 4.33-4.35 (t, 2H, *J* = 4.8 Hz), 7.36-7.40 (m, 1 ArH), 7.73-7.75 (m, 1 ArH), 7.90-7.92 (m, 1 ArH), 8.13-8.15 (m, 1 ArH). ^{13}C NMR (100 MHz, $CDCl_3$): δ_C (ppm) 44.79, 49.58, 63.97, 64.11, 120.80, 126.03, 128.08, 130.10, 132.81, 134.81, 183.54 (C=O), 192.09 (C=S). HRMS (ESI^+): *m/z* calcd for $C_{12}H_{12}BrNO_2S$ $(M + H)^+$ 313.9844, found 313.9844.

1-(4-Bromophenyl)-2-morpholino-2-thioxoethanone (**5.25**). This compound was synthesized according to the general procedure describe above using 2-bromo-1-(4-bromophenyl)-ethanone (0.50 g, 1.81 mmol), morpholine (0.47 mL, 5.44 mmol) and sulfur (0.08 g, 2.71 mmol) in DMF (10 mL). Cyclohexane was used for recrystallization to afford the title compound as a colorless solid (0.11 g, 19%). R_f 0.2 (cyclohexane/EtOAc 8:2). Mp: 157-159°C. ^{1}H NMR (400 MHz, $CDCl_3$): δ_H (ppm) 3.58-3.61 (t, 2H, *J* = 4.8 Hz), 3.69-3.72 (t, 2H, *J* = 4.8 Hz), 3.89-3.92 (t, 2H, *J* = 4.8 Hz), 4.31-4.34 (t, 2H, *J* = 4.8 Hz), 7.63-7.65 (d, 2 ArH, *J* = 8.6 Hz), 7.85-7.87 (d, 2 ArH, *J* = 8.6 Hz). ^{13}C NMR (100 MHz, $CDCl_3$): δ_C (ppm) 47.18, 51.97, 66.39, 66.54, 129.91, 131.26 (2C), 132.17, 132.35 (2C), 186.59 (C=O), 194.89 (C=S). HRMS (ESI^+): *m/z* calcd for $C_{12}H_{12}BrNO_2S$ $(M + H)^+$ 313.9844, found 313.9841.

1-(2-Iodophenyl)-2-morpholino-2-thioxoethanone (**5.26**). This compound was synthesized according to the general procedure describe above. 1-(2-Iodophenyl)ethanone (1.00 g, 4.00 mmol) and dibromine (0.24 mL, 4.87 mmol) were mixed in chloroform (15 mL) to obtain the 2-bromo-1-(2-iodophenyl)-ethanone and this intermediate was reacted in a second time with morpholine (1.06 mL, 12.20 mmol) and sulfur (0.19 g, 6.10 mmol) in DMF (10 mL). The residue was purified by silica gel chromatography (cyclohexane/EtOAc, 8:2) to give the title compound as a yellow oil (0.70 g, 47%). R_f 0.2 (cyclohexane/EtOAc 8:2). ^{1}H NMR (400 MHz, $CDCl_3$): δ_H (ppm) 3.80-3.85 (m, 4H), 3.91-3.93 (t, 2H, *J* = 4.8 Hz), 4.27-4.30 (t, 2H, *J* = 4.8 Hz), 7.17-7.21 (ddd, 1 ArH, *J* = 7.5 and 1.5 Hz), 7.43-7.47 (ddd, 1 ArH, *J* = 7.5 and 1.1 Hz), 7.74-7.77 (dd, 1 ArH, *J* = 7.8 and 1.5 Hz), 7.97-7.99 (dd, 1 ArH, *J* = 7.9 and 1.1 Hz). HRMS (ESI^+): *m/z* calcd for $C_{12}H_{13}INO_2S$ $(M + H)^+$ 361.9706, found 361.9706.

1-(3-Iodophenyl)-2-morpholino-2-thioxoethanone (**5.27**). This compound was synthesized according to the general procedure describe above. 1-(3-Iodophenyl)ethanone (1.00 g, 4.06 mmol) and dibromine (0.24 mL, 4.87 mmol) were mixed in chloroform (15 mL) to obtain the 2-bromo-1-(3-iodophenyl)-ethanone and this intermediate was reacted in a second time with morpholine (1.07 mL, 12.18 mmol) and sulfur (0.19 g, 6.09 mmol) in DMF (10 mL). The residue was purified by silica gel chromatography (cyclohexane/EtOAc, 8:2) to give the title compound as a yellow solid (0.75 g, 51%). R_f 0.3 (cyclohexane/EtOAc 8:2). ^{1}H NMR (400 MHz, $CDCl_3$): δ_H (ppm) 3.60-3.625 (t, 2H, *J* = 4.8 Hz), 3.70-3.72 (t, 2H, *J* = 4.8 Hz), 3.91-3.93 (t, 2H, *J* = 4.8 Hz), 4.31-4.33 (t, 2H, *J* = 4.8 Hz), 7.21-7.25 (DD, 1 ArH, *J* = 7.8 Hz), 7.92-7.94 (dd, 2 ArH, *J* = 7.1 and 0.7 Hz), 8.32-8.33 (dd, 1 ArH, *J* = 1.6 Hz). ^{13}C NMR (100 MHz, $CDCl_3$): δ_C (ppm) 46.60, 51.40, 65.79, 65.92, 93.94, 128.43, 129.94, 134.59, 137.76, 142.47, 185.29 (C=O), 193.88 (C=S). HRMS (ESI$^+$): *m/z* calcd for $C_{12}H_{13}INO_2S$ $(M + H)^+$ 361.9706, found 361.9704.

1-(4-Iodophenyl)-2-morpholino-2-thioxoethanone (**5.28**). This compound was synthesized according to the general procedure describe above. 1-(4-Iodophenyl)ethanone (1.00 g, 4.06 mmol) and dibromine (0.24 mL, 4.87 mmol) were mixed in chloroform (15 mL) to obtain the 2-bromo-1-(3-iodophenyl)-ethanone and this intermediate was reacted in a second time with morpholine (1.07 mL, 12.18 mmol) and sulfur (0.19 g, 6.09 mmol) in DMF (10 mL). The residue was purified by silica gel chromatography (cyclohexane/EtOAc, 8:2) to give the title compound as a yellow solid (0.92 g, 63%). R_f 0.3 (cyclohexane/EtOAc 8:2). Mp: 175-177°C. ^{1}H NMR (400 MHz, $CDCl_3$): δ_H (ppm) 3.59 (m, 4H), 3.82 (t, 2H, *J* = 4.8 Hz), 4.21 (t, 2H, *J* = 4.8 Hz), 7.67 (d, 2 ArH, *J* = 8.1 Hz), 7.98 (d, 2ArH, *J* = 8.1 Hz). ^{13}C NMR (100 MHz, $CDCl_3$): δ_C (ppm) 46,92, 51.83, 65.54, 65.88, 103.86, 130.92 (2C), 132.27, 138.13 (2C), 186.51 (C=O), 192.99 (C=S). HRMS (ESI$^+$): *m/z* calcd for $C_{12}H_{13}INO_2S$ $(M + H)^+$ 361.9706, found 361.9705.

1-(2-Nitrophenyl)-2-morpholino-2-thioxoethanone (**5.29**). This compound was synthesized according to the general procedure describe above using 2-bromo-1-(2-nitrophenyl)-ethanone (0.50 g, 2.05 mmol), morpholine (0.54 mL, 6.17 mmol), and sulfur (0.09 g, 3.07 mmol) in DMF (10 mL). A mixture of cyclohexane/EtOAc (8:2) was used for recrystallization to afford the title compound as a yellow solid (0.15 g, 26%). R_f 0.3 (cyclohexane/EtOAc 8:2). ^{1}H NMR (400 MHz, $CDCl_3$): δ_H (ppm) 3.86-3.88 (t, 2H, *J* = 4.8 Hz), 3.94-3.96 (t, 2H, *J* = 4.8 Hz),

4.11-4.13 (t, 2H, *J* = 4.8 Hz), 4.22-4.24 (t, 2H, *J* = 4.8 Hz), 7.62-7.66 (m, 1 ArH), 7.74-7.78 (m, 1 ArH), 7.84-7.86 (m, 1 ArH), 8.04-8.06 (m, 1 ArH). ^{13}C NMR (100 MHz, $CDCl_3$): δ_C (ppm) 49.06, 52.33, 66.36, 66.71, 123.84, 131.70, 132.57, 134.03, 134.92, 145.78, 182.95 (C=O), 191.17 (C=S). HRMS (ESI^+): *m/z* calcd for $C_{12}H_{12}N_2O_4S$ $(M + H)^+$ 281.0590, found 281.0586.

1-(3-Nitrophenyl)-2-morpholino-2-thioxoethanone (**5.30**). This compound was synthesized according to the general procedure describe above using commercial 2-bromo-1-(3-nitrophenyl)-ethanone (1.50 g, 6.17 mmol), morpholine (1.61 mL, 18.52 mmol) and sulfur (0.29 g, 9.26 mmol) in DMF (10 mL). Methanol was used for recrystallization to afford the title compound as a yellow solid (1.26 g, 73%). R_f 0.1 (cyclohexane/EtOAc 8:2). Mp: 179-181°C. ^{1}H NMR (400 MHz, $CDCl_3$): δ_H (ppm) 3.58-3.60 (t, 2H, *J* = 4.8 Hz), 3.67-3.69 (t, 2H, *J* = 4.8 Hz), 3.86-3.89 (t, 2H, *J* = 4.8 Hz), 4.28-4.30 (t, 2H, *J* = 4.8 Hz), 7.63-7.67 (dd, 1 ArH, *J* = 8.6 Hz), 8.26-8.29 (m, 1 ArH), 8.38-8.40 (m, 1 ArH), 8.73-8.74 (dd, 1 ArH, *J* = 1.9 Hz). ^{13}C NMR (100 MHz, $CDCl_3$): δ_C (ppm) 47.42, 52.12, 66.41, 66.57, 124.56, 128.36, 130.20, 135.18, 148.51, 184.29 (C=O), 193.48 (C=S). HRMS (ESI^+): *m/z* calcd for $C_{12}H_{12}N_2O_4S$ $(M + H)^+$ 281.0590, found 281.0588.

1-(4-Nitrophenyl)-2-morpholino-2-thioxoethanone (**5.31**). This compound was synthesized according to the general procedure describe above using commercial 2-bromo-1-(4-nitrophenyl)-ethanone (1.50 g, 6.17 mmol), morpholine (1.61 mL, 18.52 mmol) and sulfur (0.29 g, 9.26 mmol) in DMF (10 mL). Methanol was used for recrystallization to afford the title compound as a yellow solid (0.81 g, 47%). R_f 0.1 (cyclohexane/EtOAc 8:2). Mp: 171-173°C. ^{1}H NMR (400 MHz, $CDCl_3$): δ_H (ppm)) 3.59 (t, 2H, *J* = 4.8 Hz), 3,73 (t, 2H, *J* = 4.8 Hz), 3.92 (t, 2H, *J* = 4.8 Hz), 4.33 (t, 2H, *J* = 4.8 Hz), 8.16 (d, 2 ArH, *J* = 8.2 Hz), 8.32 (d, 2 ArH, *J* = 8.2 Hz). HRMS (ESI^+): *m/z* calcd for $C_{12}H_{12}N_2O_4S$ $(M + H)^+$ 281.0590, found 281.0588.

1-([1,1'-biphenyl]-4-yl)-2-morpholino-2-thioxoethanone (**5.32**). This compound was synthesized according to the general procedure describe above using commercial 1-([1,1'-biphenyl]-4-yl)-2-bromoethanone (1.00 g, 3.64 mmol), morpholine (0.94 mL, 10.92 mmol) and sulfur (0.17 g, 5,46 mmol) in DMF (10 mL). The residue was purified by silica gel chromatography (cyclohexane/EtOAc, 8:2) to give the title compound as a yellow solid (0.69

g, 61%). R_f 0.2 (cyclohexane/EtOAc 8:2). Mp: 132-134°C. ^{1}H NMR (400 MHz, $CDCl_3$): δ_H (ppm) 3.55-3.58 (t, 2H, *J* = 4.8 Hz), 3.68-3.71 (t, 2H, *J* = 4.8 Hz), 3.82-3.85 (t, 2H, *J* = 4.8 Hz), 4.28-4.30 (t, 2H, *J* = 4.8 Hz), 7.32-7.45 (m, 3 ArH), 7.52-7.55 (m, 2 ArH), 7.61-7.63 (d, 2 ArH, *J* = 8.5 Hz), 7.99-8.01 (d, 2 ArH, *J* = 8.5 Hz). ^{13}C NMR (100 MHz, $CDCl_3$): δ_C (ppm) 45.93, 50.75, 65.19, 65.34, 126.12 (2C), 126.40 (2C), 127.38, 127.84 (2C), 129.23 (2C), 130.72, 138.32, 146.01, 186.33 (C=O), 194.52 (C=S). HRMS (ESI^+): *m/z* calcd for $C_{18}H_{17}NO_2S$ $(M + H)^+$ 312.1052, found 312.1052.

11.2. SYNTHETIC PROCEDURE OF COMPOUNDS 5.16, 5.21, 5.22 AND 6.1-39 (CHAPTER 6)

*Compounds **5.16**, **5.21**, **5.22** and **6.1**-**8** were synthesized according the general procedure **II**.*

General procedure I

To a stirred solution of ethanone derivative (1 equiv) in chloroform was added dropwise a solution of dibromine (1.2 equiv) in chloroform. After 2 hrs, the solvent was evaporated in vacuo to give a crude oil consisting mainly of 2-bromo-1-(substituted)-ethanone compound along with trace amounts of 2,2-dibromo-1-(substituted)-ethanone compound. The mixture was used without purification in the next step. To the synthesized or commercial 2-bromo-1-(substituted)-ethanone derivative were added in sequence DMF, cyclooctasulfur (1.5 equiv), and morpholine (3 equiv). The mixture was then stirred at room temperature. After completion, the reaction mixture was quenched with distilled water to give a precipitate, which was further washed with distilled water. The residue was recrystallized or purified by silica gel chromatography if necessary.

2-Morpholino-1-phenyl-2-thioxoethan-1-one (5.16). Acetophenone (2.00 g, 16.60 mmol) and dibromine (1.01 mL, 19.90 mmol) were mixed in chloroform (15 mL) to obtain the 2-bromo-1-phenyl-ethanone, and this intermediate was reacted in a second time with morpholine (4.34 mL, 49.80 mmol) and sulfur (0.79 g, 24.90 mmol) in DMF (10 mL). Methanol was used for recrystallization to afford the title compound (2.85 g, 73%). R_f 0.2 (cyclohexane/EtOAc: 8/2). Mp: 110−112 °C. ^{1}H NMR (400 MHz, $CDCl_3$): δH (ppm) 3.59−3.62 (t, 2H, *J* = 4.8 Hz), 3.69−3.71 (t, 2H, *J* = 4.8 Hz), 3.90−3.92 (t, 2H, *J* = 4.8 Hz), 4.33−4.35 (t, 2H, *J* = 4.8 Hz), 7.48− 7.52 (m, 2 ArH), 7.59−7.65 (m, 1 ArH), 7.99−8.01 (d, 2 ArH, *J* = 8.2 Hz). ^{13}C NMR (100 MHz, $CDCl_3$): δC (ppm) 47.13, 51.95, 66.40, 66.52, 128.99 (2C), 129.86 (2C), 133.26, 134.48, 187.90 (C=O), 195.70 (C=S). HRMS (ESI$^+$): *m/z* calcd for $C_{12}H_{13}NO_2S$ $(M + H)^+$ 236.0739, found 236.0737.

1-(4-Chlorophenyl)-2-morpholino-2-thioxoethan-1-one (5.22). This compound was synthesized according to the general procedure I using 2-bromo-1-(2-chlorophenyl)ethanone (0.50 g, 2.14 mmol), morpholine (0.56 mL, 6.42 mmol) and sulfur (0.10 g, 3.21 mmol) in DMF (10 mL). Acetonitrile was used for recrystallization to afford the title compound as a yellow solid (0.22 g, 38%). R_f 0.2 (cyclohexane/EtOAc: 8/2). Mp: 135-137°C. ^{1}H NMR (400 MHz,

$CDCl_3$): δH (ppm) 3.58-3.71 (m, 4H), 3.89-3.92 (t, 2H, *J* = 4.8 Hz), 4.31-4.33 (t, 2H, *J* = 4.8 Hz), 7.46-7.48 (d, 2 ArH, *J* = 8.8 Hz), 7.93-7.95 (d, 2 ArH, *J* = 8.6 Hz). ^{13}C NMR (100 MHz, $CDCl_3$): δC (ppm) 47.18, 51.97, 66.39, 66.53, 129.36 (2C), 131.22 (2C), 131.74, 141.06, 186.45 (C=O), 194.94 (C=S). HRMS (ESI^+): *m/z* calcd for $C_{12}H_{13}ClNO_2S$ $(M + H)^+$ 270.0350, found 270.0350.

1-(3-Chlorophenyl)-2-morpholino-2-thioxoethan-1-one (5.21). This compound was synthesized according to the general procedure I. 1-(3-Chlorophenyl)ethanone (2.00 g, 12.90 mmol) and dibromine (0.78 mL, 15.50 mmol) were mixed in chloroform (15 mL) to obtain the 2-bromo-1-(3-chlorophenyl)-ethanone and this intermediate was reacted in a second time with morpholine (3.38 mL, 38.80 mmol) and sulfur (0.62 g, 19.40 mmol) in DMF (10 mL). The residue was purified by silica gel chromatography (cyclohexane/EtOAc: 8/2) and the obtained oil was collected by filtration with diethyl ether to give the title compound as a yellow solid (1.50 g, 43%). R_f 0.2 (cyclohexane/EtOAc: 8/2). Mp: 92-94°C. ^{1}H NMR (400 MHz, $CDCl_3$): δH (ppm) 3.59-3.61 (t, 2H, *J* = 4.8 Hz), 3.70-3.72 (t, 2H, *J* = 4.8 Hz), 3.90-3.92 (t, 2H, *J* = 4.8 Hz), 4.31-4.33 (t, 2H,*J* = 4.8 Hz), 7.42-7.46 (dd, 1 ArH, *J*= 7.8 Hz), 7.57-7.59 (ddd, 1 ArH, *J*= 8.0 and 1.0 Hz), 7.85-7.87 (ddd, 1 ArH, *J* = 7.8 and 1.4 Hz), 7.96-7.97 (dd, 1 ArH, *J* = 1.8 Hz).^{13}C NMR (100 MHz, $CDCl_3$): δC (ppm) 47.21, 52.00, 66.39, 66.52, 127.98, 129.61, 130.28, 134.33, 135.05, 135.30, 186.07 (C=O), 194.60 (C=S). HRMS (ESI^+): *m/z* calcd for $C_{12}H_{12}ClNO_2S$ $(M + H)^+$ 270.0277, found 270.0278.

1-(2,4-Dichlorophenyl)-2-morpholino-2-thioxoethan-1-one (6.1). This compound was synthesized according to the general procedure I using 2-bromo-1-(2,4-dichlorophenyl)-ethanone (1 .00 g, 3.76 mmol), morpholine (0.99 mL, 1 1.28 mmol) and sulfur (0.18 g, 5.64 mmol) in DMF (10 mL). Acetonitrile was used for recrystallization to afford the title compound as a yellow solid (0.31 g, 28%). R_f 0.4 (cyclohexane/EtOAc: 8/2). Mp: 116-118°C. ^{1}H NMR (400 MHz, $CDCl_3$): δH (ppm) 3.75-3.77 (t, 2H, *J* = 4.8 Hz), 3.77-3.79 (t, 2H, *J* = 4.8 Hz), 3.89-3.91 (t, 2H, *J* = 4.8 Hz), 4.10-4.12 (t, 2H, *J* = 4.8 Hz), 7.30 (dd, 1 ArH, *J* = 2.6 and 8.4 Hz), 7.38 (d, 1 ArH, *J* = 2.6 Hz), 7.80 (d, 1 ArH, *J* = 8.4 Hz). ^{13}C NMR (100 MHz, $CDCl_3$): δC (ppm) 47.68, 52.11, 65.95, 66.03, 127.83, 130.49 (2C), 133.08, 133.56, 139.55, 183.73 (C=O), 195.19 (C=S).HRMS (ESI^+): *m/z* calcd for $C_{12}H_{12}Cl_2NO_2S$ $(M + H)^+$ 303.99603, found 303.99607.

1-Cyclohexyl-2-morpholino-2-thioxoethan-1-one (6.2). This compound was synthesized according to the general procedure I using 1-cyclohexylethanone (2.00 g, 15.86 mmol) and dibromine (0.96 mL, 19.03 mmol) mixed in chloroform (20 mL) to obtain the 2-bromo-1-cyclohexylethanone and this intermediate was reacted in a second time with morpholine (4.18 mL, 15 47.58 mmol) and sulfur (0.76 g, 23.79 mmol) in DMF (10 mL). The residue was purified by silica gel chromatography (Cyclohexane/EtOAc: 8/2) to give the title compound as a brown solid (0.58 g, 15%). R_f 0.3 (Cyclohexane/EtOAc: 8/2). Mp: 57-59°C. ^{1}H NMR (400 MHz, $CDCl_3$): δH (ppm) 1.18-1.37 (m, 5H), 1.69-1 .99 (m, 5H), 3.22 (m, 1 H), 3.61-3.62 (m, 2H), 3.73-3.74 (t, 2H, *J* = 4.8 Hz), 3.82-3.84 (t, 2H, *J* = 4.8 Hz), 4.19-4.21 (t, 2H, *J* = 4.8 Hz). ^{13}C NMR (100 MHz, $CDCl_3$): δC (ppm) 25.52 (2C), 25.71, 28.10 (2C), 47.28, 47.49, 52.07, 66.31, 66.60, 197.85 (C=0), 201 .05 (C=S). HRMS (ESI^+): *m/z* calcd for $C_{12}H_{20}NO_2S$ $(M + H)^+$ 242.1209, found 242.1208.

2-Morpholino-1-(pyridin-4-yl)-2-thioxoethan-1-one (6.3). This compound was synthesized according to the general procedure I using 2-bromo-1-(pyridine-4-yl)ethanone (0.50 g, 1.79 mmol), morpholine (0.47 mL, 5.37 mmol) and sulfur (0.08 g, 2.68 mmol) in DMF (10 mL). The residue was purified by silica gel chromatography (CH_2Cl_2/EtOAc: 5/5) to give the title compound as a yellow solid (0.15 g, 36%). R_f 0.3 (CH_2Cl_2/EtOAc: 5/5). Mp: 96-98°C. ^{1}H NMR (400 MHz, $CDCl_3$): δH (ppm) 3.60-3.63 (m, 2H), 3.71-3.74 (m, 2H), 3.91-3.93 (m, 2H), 4.31-4.34 (m, 2H), 7.77-7.79 (m, 2 ArH), 8.83-8.85 (m, 2 ArH). ^{13}C NMR (100 MHz, $CDCl_3$): δC (ppm) 45.30, 50.05, 64.40, 64.56, 120.26 (2C), 137.86, 149.10 (2C), 183.37 (C=0), 191.58 (C=S). HRMS (ESI^+): *m/z* calcd for $C_{11}H_{13}N_2O_2S$ $(M + H)^+$ 237.06922, found 237.06923.

1-(3,4-Dichlorophenyl)-2-morpholino-2-thioxoethan-1-one (6.4). This compound was synthesized according to the general procedure I using 2-bromo-1-(3,4-dichlorophenyl)ethan-1-one (1.00 g, 3.73 mmol), morpholine (0.96 mL, 11.2 mmol) and sulfur (0.18 g, 5.60 mmol) in DMF (15 mL). The residue was purified by silica gel chromatography (Cyclohexane/EtOAc: 3/2) to give the title compound as a yellow solid (0.32 g, 28%). R_f 0.6 (Cyclohexane/EtOAc: 3/2). Mp: 134-136°C. ^{1}H NMR (400 MHz, $CDCl_3$): δH (ppm) 3.60-3.61 (m, 2H), 3.71-3.72 (m, 2H), 3.90-3.93 (m, 2H), 4.31-4.33 (m, 2H), 7.55-7.60 (m, 1 ArH), 7.79-7.84 (m, 1 ArH), 8.07-8.09 (m, 1 ArH). ^{13}C NMR (100 MHz, $CDCl_3$): δC (ppm)

44.87, 49.63, 63.99, 64.15, 126.38, 128.69, 129.11, 130.76, 131.36, 136.75, 182.57 (C=O), 191.61 (C=S). HRMS (ESI^+): *m/z* calcd for $C_{12}H_{12}Cl_2NO_2S$ $(M + H)^+$ 303.99603, found 303.99549.

2-Morpholino-1-(naphthalen-2-yl)-2-thioxoethan-1-one (6.5). This compound was synthesized according to the general procedure I using 2-bromo-1-(naphthalene-2-yl) ethanone (0.50 g, 2.01 mmol), morpholine (0.53 mL, 6.04 mmol) and sulfur (0.09 g, 3.01 mmol) in DMF (10 mL). Cyclohexane was used for recrystallization to afford the title compound as a yellow solid (0.31 g, 28%). R_f 0.2 (Cyclohexane/EtOAc: 8/2). Mp: 152-154°C. ^1H NMR (400 MHz, $CDCl_3$): δH (ppm) 3.63-3.65 (m, 2H), 3.69-3.71 (m, 2H), 3.93-3.96 (m, 2H), 4.38-4.41 (m, 2H), 7.55-7.66 (m, 2 ArH), 7.88-7.97 (m, 3 ArH), 8.03-8.05 (dd, 1 ArH, *J* = 2.1 and 8.8 Hz), 8.52 (s, 1 ArH). ^{13}C NMR (100 MHz, $CDCl_3$): δC (ppm) 46.92, 51.70, 66.14, 66.25, 124.02, 126.87, 127.63, 128.67, 129.06, 129.54, 130.28, 132.11, 132.22, 135.88, 187.75 (C=O), 195.51 (C=S). HRMS (ESI^+): *m/z* calcd for $C_{16}H_{15}NO_2S$ $(M + Na)^+$ 308.07157, found 308.07146.

1-Morpholino-1-thioxobutan-2-one (6.6). This compound was synthesized according to the general procedure I using 1-bromobutan-2-one (0.34 mL, 3.33 mmol), morpholine (0.88 mL, 10.0 mmol) and sulfur (0.15 g, 4.99 mmol) in DMF (10 mL). The residue was purified by silica gel chromatography (Hexane/EtOAc: 7/3) to give the title compound as yellow solid (0.08 g, 8%). R_f 0.5 (Cyclohexane/EtOAc: 3/2). ^1H NMR (400 MHz, $CDCl_3$): δH (ppm) 1.19 (t, 3H, *J* = 5.1 Hz), 2.88-2.94 (q, 2H, *J* = 5 Hz), 3.59-3.62 (m, 2H), 3.74-3.76 (m, 2H), 3.82-3.85 (m, 2H), 4.17-4.20 (m, 2H). 13C NMR (100 MHz, CDCl3): δC (ppm) 7.41, 33.52, 46.94, 51.45, 65.92, 66.21, 197.42 (C+O), 199.14 (C=S) HRMS (ESI^+): *m/z* calcd for $C_8H_{14}NO_2S$ $(M + H)^+$ 188.07398, found 188.07384.

1-((1*r*,3*r*,5*r*,7*r*)-Adamantan-2-yl)-2-morpholino-2-thioxoethan-1-one (6.7). This compound was synthesized according to the general procedure I using 2-bromo-1-(1 r,3r,5r,7r)adamantan-2-yl)-10-ethanone (1 g, 3.90 mmol), morpholine (1 .02 mL, 11.70 mmol) and sulfur (0.18 g, 5.90 mmol) in DMF (10 mL). The residue was purified by silica gel chromatography (cyclohexane/EtOAc: 8/2) to give the title compound as yellow oil (0.08 g,

8%). R_f 0.3 (hexane/EtOAc 8:2). ^{1}H NMR (400 MHz, $CDCl_3$): δH (ppm) 1 .69-1 .77 (m, 6H), 2.02-2.05 (m, 9H), 3.51 (m, 2H), 3.73-3.75 (t, 2H, *J* = 4.8 Hz), 3.80-3.83 (t, 2H, *J* = 4.8 Hz), 4.18 (m, 2H). ^{13}C NMR (100 MHz, $CDCl_3$): δC (ppm) 27.96 (3C), 36.30 (3C), 39.79 (3C), 45.03, 46.41, 52.39, 66.30, 66.36, 196.66 (C=0), 205.54 (C=S). HRMS (ESI^+): *m/z* calcd for $C_{16}H_{23}NO_2S$ $(M + H)^+$ 294.1522, found 294.1523.

3,3-Dimethyl-1-morpholino-1-thioxobutan-2-one (6.8). This compound was synthesized according to the general procedure I using 1-bromo-3,3-dimethylbutan-2-one (2.0 g, 11.2 mmol), morpholine (2.96 mL, 33.7 mmol) and sulfur (0.54 g, 16.8 mmol) in DMF (10 mL). The residue was purified by silica gel chromatography (Cyclohexane/EtOAc: 8/2) to give the title compound as orange oil (0.35 g, 14%). R_f 0.2 (Cyclohexane/EtOAc: 8/2). ^{1}H NMR (400 MHz, $CDCl_3$): δH (ppm) 1.34 (s, 9H), 3.50-3.53 (m, 2H), 3.74-3.76 (m, 2H), 3.81-3.83 (m, 2H), 4.18 (broad, 2H). ^{13}C NMR (100 MHz, $CDCl_3$): δC (ppm) 26.16 (3C), 40.52, 44.11, 50.03, 64.01 (2C), 194.65 (C=O), 204.21 (C=S). HRMS (ESI^+): *m/z* calcd for $C_{10}H_{18}NO_2S$ $(M + H)^+$ 216.10528, found 216.10524.

*Compounds **6.9**-**18** were synthesized according the general procedure **II**.*

General procedure II

To commercial 2-bromo-1-phenylethanone were added in sequence DMF, cyclooctasulfur (1.5 equiv), and amine derivative (3 equiv). The mixture was then stirred at room temperature. After completion, the reaction mixture was quenched with distilled water to give a precipitate, which was further washed with distilled water. The residue was recrystallized or purified by silica gel chromatography if necessary.

1-Phenyl-2-(pyrrolidin-1-yl)-2-thioxoethan-1-one (6.9). This compound was synthesized according to the general procedure II using 2-bromo-1-phenylethanone (0.5 g, 2.52 mmol), pyrrolidine (0.62 mL, 7.56 mmol) and sulfur (0.12 g, 3.78 mmol) in DMF (10 mL). The residue was purified by silica gel chromatography (Cyclohexane/EtOAc: 8/2) to give the title compound as yellow solid (0.12 g, 22%). R_f 0.4 (Cyclohexane/EtOAc: 8/2). Mp: 57-59°C. ^{1}H NMR (400 MHz, $CDCl_3$): δH (ppm) 1.61 (m, 4H), 3.53-3.56 (m, 2H), 3.94-3.98 (m, 2H), 7.46-7.48 (m, 2H), 7.50-7.62 (m, 1H), 7.99-8.01 (m, 2H). ^{13}C NMR (100 MHz, $CDCl_3$): δC (ppm) 22.97, 25.24, 50.22, 50.40, 127.97 (2C), 129.24 (2C), 131.96, 133.37, 187.92 (C=O), 191.87 (C=S). HRMS (ESI^+): *m/z* calcd for $C_{12}H_{14}NOS$ $(M + H)^+$ 220.07906, found 220.07877.

2-(4,4-Difluoropiperidin-1-yl)-1-phenyl-2-thioxoethan-1-one (6.10). This compound was synthesized according to the general procedure II using 2-bromo-1-phenylethanone (0.5 g, 2.52 mmol), 4,4-difluoropiperidine.HCl (1.19 g, 7.56 mmol) and sulfur (0.12 g, 3.78 mmol) in DMF (10 mL). Cyclohexane was used for recrystallization to afford the title compound as a white solid (0.12 g, 18%). R_f 0.8 (Cyclohexane/EtOAc: 3/2). Mp: 117-119°C. ^{1}H NMR (400 MHz, $CDCl_3$): δH (ppm) 1.42-1.58 (m, 2H), 2.08-2.25 (m, 2H), 3.68 (m, 2H), 4.44 (m, 2H), 7.48-7.52 (m, 2H), 7.61-7.65 (m, 1H), 7.98-8.00 (m, 2H). ^{13}C NMR (100 MHz, $CDCl_3$): δC (ppm) 31.25 (t), 32.32 (t), 41.73 (t), 46.22 (t), 118.84 and 121.26 (C-F), 127.18 (2C), 128.02 (2C), 131.23, 132.77, 186.10 (C=O), 194.87 (C=S). HRMS (ESI^+): *m/z* calcd for $C_{13}H_{14}NOSF_2$ $(M + H)^+$ 270.07587, found 270.07568.

2-(4-Methylpiperidin-1-yl)-1-phenyl-2-thioxoethan-1-one (6.11). This compound was synthesized according to the general procedure II using 2-bromo-1-phenylethanone (1.0 g, 5.05 mmol), 4-methylpiperidine (3.82 g, 15.15 mmol) and sulfur (0.24 g, 7.57 mmol) in DMF (10 mL). The residue was purified by silica gel chromatography (Hexane/EtOAc: 9/1) to give the title compound as yellow solid (0.47 g, 38%). R_f 0.3 (Hexane/EtOAc: 7/3). Mp: 71-73°C. ^{1}H NMR (400 MHz, $CDCl_3$): δH (ppm) 1.00 (s, 3H), 1.15-1.25 (m, 1H), 1.30 (m, 1H), 1.78-1.92 (m, 3H), 3.08-3.14 (m, 1H) 1.15-1.20 (m, 3H), 3.26-3.32 (m, 1H), 3.74-3.76 (m, 1H), 5.39 (m, 1H), 7.47-7.49 (m, 2H), 7.59 (m, 1H), 7.98 (m, 2H). ^{13}C NMR (100 MHz, $CDCl_3$): δC (ppm) 18.86, 28.42, 30.95, 31.97, 45.03, 49.83, 126.48 (2C), 127.41 (2C), 131.01, 131.82, 185.65 (C=O), 192.08 (C=S). HRMS (ESI$^+$): *m/z* calcd for $C_{14}H_{17}NOSNa$ $(M + Na)^+$ 270.09231, found 270.09219.

1-Phenyl-2-(piperidin-1-yl)-2-thioxoethan-1-one (6.12). This compound was synthesized according to the general procedure II using 2-bromo-1-phenylethanone (2.0 g, 10.01 mmol), piperidine (2.99 mL, 30.30 mmol) and sulfur (0.48 g, 15.10 mmol) in DMF (10 mL). The residue was purified by silica gel chromatography (Cyclohexane/EtOAc: 8/2) to give the title compound as yellow solid (0.47 g, 20%). R_f 0.6 (Cyclohexane/EtOAc: 3/2). Mp: 67-69°C. ^{1}H NMR (400 MHz, $CDCl_3$): δH (ppm) 1.56-1.63 (m, 2H), 1.77-1.84 (m, 4H), 3.53-3.55 (m, 2H), 4.24-4.27 (m, 2H), 7.47-7.50 (m, 2H), 7.58-7.62 (m, 1H), 7.98-8.00 (m, 2H). ^{13}C NMR (100 MHz, $CDCl_3$): δC (ppm) 23.79, 25.13, 26.20, 47.88, 52.79, 52.79, 128.63 (2C), 129.52 (2C), 133.14, 133.97, 187.76 (C=O), 194.03 (C=S). 18.86, 28.42, 30.95, 31.97, 45.03, 49.83, 126.48 (2C), 127.41 (2C), 131.01, 131.82, 185.65 (C=O), 192.08 (C=S). HRMS (ESI$^+$): *m/z* calcd for $C_{13}H_{15}NOSNa$ $(M + Na)^+$ 256.07666, found 256.07661.

***N*,*N*-Diethyl-2-oxo-2-phenylethanethioamide (6.13).** This compound was synthesized according to the general procedure II using 2-bromo-1-phenylethanone (1.0 g, 5.05 mmol), diethylamine (1.56 mL, 15.15 mmol) and sulfur (0.24 g, 7.57 mmol) in DMF (10 mL). The residue was purified by silica gel chromatography (Hexane/EtOAc: 7/3) to give the title compound as brown oil (0.09 g, 8%). R_f 0.3 (Hexane/EtOAc: 7/3).^{1}H NMR (400 MHz, $CDCl_3$): δH (ppm) 1.15-1.20 (m, 3H), 1.26-1.34 (m, 3H), 3.37-3.42 (m, 2H), 3.94-3.99 (m, 2H), 7.36-7.40 (m, 2H), 7.48-7.52 (m, 1H), 7.87-7.89 (m, 2H). ^{13}C NMR (100 MHz, $CDCl_3$): δC (ppm)

11.29, 13.63, 44.55, 47.99, 128.80 (2C), 129.90 (2C), 133.51, 134.09, 187.51 (C=O), 195.58 (C=S). HRMS (ESI^+): *m/z* calcd for $C_{12}H_{16}NOS$ $(M + H)^+$ 222.09471, found 222.09456.

1-Phenyl-2-thiomorpholino-2-thioxoethan-1-one (6.14). This compound was synthesized according to the general procedure II using 2-bromo-1-phenylethanone (1.0 g, 5.05 mmol), thiomorpholine (1.52 mL, 15.15 mmol) and sulfur (0.24 g, 7.57 mmol) in DMF (10 mL). The residue was purified by silica gel chromatography (Hexane/EtOAc: 7/3) to give the title compound as yellow solid (0.40 g, 43%). R_f 0.7 (Cyclohexane/EtOAc: 3/2). Mp: 127-129°C. ^1H NMR (400 MHz, $CDCl_3$): δH (ppm) 2.69 (m, 2H), 288-2.90 (t, 2H, *J* = 5.1 Hz), 3.83-3.86 (t, 2H, *J* = 5.1 Hz), 4.59 (m, 2H), 7.47-7.51 (m, 2H), 7.59-7.63 (m, 1H), 7.97-7.99 (m, 2H). ^{13}C NMR (100 MHz, $CDCl_3$): δC (ppm) 27.31, 28.25, 49.71, 54.64, 128.96 (2C), 129.90 (2C), 133.23, 134.44, 187.73 (C=O), 196.06 (C=S). HRMS (ESI^+): *m/z* calcd for $C_{12}H_{14}NOS_2$ $(M + H)^+$ 252.05113, found 252.05117.

2-(4-Methylpiperazin-1-yl)-1-phenyl-2-thioxoethan-1-one (6.15). This compound was synthesized according to the general procedure II using 2-bromo-1-phenylethanone (2 g, 10.10 mmol), N-methylpiperazine (3.37 mL, 30.30 mmol) and sulfur (0.48 g, 15.15 mmol) in DMF (10 mL). The residue was purified by silica gel chromatography (Cyclohexane/EtOAc: 8/2) to give the title compound as brown solid (0.58 g, 23%). R_f 0.2 (Cyclohexane/EtOAc: 8/2). Mp: 93-95°C ^1H NMR (400 MHz, $CDCl_3$): δH (ppm) 2.34 (s, 3H, CH3), 2.41-2.44 (m, 2H), 2.62-2.64 (m, 2H), 3.58-3.60 (m, 2H), 4.31-4.34 (m, 2H), 7.47-7.51 (m, 2H), 7.59-7.63 (m, 1H), 7.98-8.00 (m, 2H). ^{13}C NMR (100 MHz, $CDCl_3$): δC (ppm) 45.53, 46.61, 51.31, 53.95, 54.57, 128.78 (2C), 129.71 (2C), 133.18, 134.21, 187.80 (C=O), 195.17 (C=S). HRMS (ESI^+): *m/z* calcd for $C_{13}H_{17}N_2OS$ $(M + H)^+$ 249.10561, found 249.10561.

2-(4-(2-Oxo-2-phenylethyl)piperazin-1-yl)-1-phenyl-2-thioxoethan-1-one (6.16). This compound was synthesized according to the general procedure I using 2-bromo-1-phenylethanone (1 .00 g, 5.05 mmol), piperazine (1 .30 g, 15.15 mmol), and sulfur (0.24 g, 7.57 mmol) in DMF (10 mL). The residue was purified by silica gel chromatography (hexane/EtOAc: 9/1) to give the title compound as orange oil (0.40 g, 22%). R_f 0.2

(cyclohexane/EtOAc: 8/2). ^{1}H NMR (400 MHz, $CDCl_3$): δH (ppm) 2.67-2.70 (t, 2H, *J* = 4.8 Hz), 2.87-2.90 (t, 2H, *J* = 4.8 Hz), 3.66-3.69 (t, 2H, *J* = 4.8 Hz), 4.40-4.43 (t, 2H, *J* = 4.8 Hz), 7.42-7.53 (m, 4 ArH), 7.58-7.64 (m, 2 ArH), 7.94-8.15 (m, 4 ArH). HRMS (ESI^+): *m/z* calcd for $C_{20}H_{20}N_2O_2S$ $(M + H)^+$ 353.1318, found 353.1318.

1-Phenyl-2-(4-phenylpiperazin-1-yl)-2-thioxoethan-1-one (6.17). This compound was synthesized according to the general procedure II using 2-bromo-1-phenylethanone (1.0 g, 5.05 mmol), 1-phenyl-piperazine (2.31 mL, 15.15 mmol) and sulfur (0.24 g, 7.57 mmol) in DMF (10 mL). The residue was purified by silica gel chromatography (Cyclohexane/EtOAc: 8/2) to give the title compound as yellow solid (0.20 g, 13%). R_f 0.4 (Cyclohexane/EtOAc: 8/2). Mp: 89-91°C. ^{1}H NMR (400 MHz, $CDCl_3$): δH (ppm) 3.20-3.22 (m, 2H), 3.40-3.43 (m, 2H), 3.73-3.76 (m, 2H), 4.46-4.48 (m, 2H), 6.92-6.96 (m, 3H), 7.28-7.31 (m, 2H), 7.48-7.52 (m, 2H), 7.60-7.64 (m, 1H), 8.00-8.02 (m, 2H). ^{13}C NMR (100 MHz, $CDCl_3$): δC (ppm) 45.06, 47.45, 48.10, 49.66, 115.28 (2C), 119.55, 126.78, 127.30 (2C), 127.74 (2C), 128.24 (2C), 131.65, 132.77, 148.47, 186.30 (C=O), 193.88 (C=S). HRMS (ESI^+): *m/z* calcd for $C_{18}H_{19}N_2OS$ $(M + H)^+$ 311.12181, found 311.12068.

2-(4-Benzhydrylpiperazin-1-yl)-1-phenyl-2-thioxoethan-1-one (6.18). This compound was synthesized according to the general procedure II using 2-bromo-1-phenylethanone (1.0 g, 5.05 mmol), 1-(diphenylmethyl)piperazine (3.82 g, 15.15 mmol) and sulfur (0.24 g, 7.57 mmol) in DMF (10 mL). Cyclohexane was used for recrystallization to afford the title compound as a white solid (0.60 g, 30%). R_f 0.5 (Hexane/EtOAc: 8/2). Mp: 130-132°C. ^{1}H NMR (400 MHz, $CDCl_3$): δH (ppm) 2.40 (m, 2H), 2.62 (m, 2H), 3.57 (m, 2H), 4.29 (m, 3H), 7.17-7.25 (m, 6H), 7.39-7.47 (m, 6H), 7.56-7.59 (m, 1H), 7.95-7.96 (m, 2H). ^{13}C NMR (100 MHz, $CDCl_3$): δC (ppm) 45.65, 49.77, 50.33, 50.41, 74.22, 126.09 (2C), 126.41 (4C), 127.44 (4C), 127.55 (2C), 128.48 (2C), 131.99, 132.94, 140.26 (2C), 186.66 (C=O), 193.69 (C=S). HRMS (ESI^+): *m/z* calcd for $C_{25}H_{25}N_2OS$ $(M + H)^+$ 401.16821, found 401.16826.

*Synthesis of compounds **6.19-39**.*

Morpholino(phenyl)methanone (6.19). To a stirring solution of benzoic acid (2.50 g, 20.47 mmol, 1 equiv.) in CH_2Cl_2 (50 mL) were added catalytic amount of DMF and oxalyl chloride (2.60 g, 20.47 mmol, 1equiv.). The reaction mixture was stirred at room temperature until the generation of gasses was stopped (HCl), cooled to 0 °C and a solution of morpholine (2.67 g, 30.7 mmol, 1.5 equiv.) and DIPEA (5.29 g, 40.94 mmol, 2 equiv.) was slowly added. The mixture was stirred at room temperature for 6 hrs. The reaction was quenched by adding water (50 mL) following by extraction with CH_2Cl_2 (75 mL). The combined organic layer were washed with brine and dried over Na_2SO_4. The solvent was removed in vacuo, and the residue was purified by silica gel chromatography (Cyclohexane/EtOAc: 2/3) to give the title compound as white solid (17.81 mmol, 3.40 g, 87%). R_f 0.45 (Cyclohexane/EtOAc: 3/2). Mp: 62-63°C. ^{1}H NMR (400 MHz, $CDCl_3$): δH (ppm) 3.41-3.50 (m, 4H), 3.64-3.79 (m, 4H), 7.39-7.44 (m, 5H). ^{13}C NMR (100 MHz, $CDCl_3$): δC (ppm) 26.84, 42.60, 48.19, 66.74, 127.20 (2C), 128.67 (2C), 129.99, 135.24, 170.32 (C=O). HRMS (ESI^+): *m/z* calcd for $C_{11}H_{14}NO_2$ $(M + H)^+$ 192.1024, found 192.1014.

Morpholino(phenyl)methanethione (6.20). Benzaldehyde (1.00 g, 9.42 mmol, 1 equiv.), morpholine (2.05 g, 23.5 mmol, 2.5 equiv.), sulfur (0.30 g, 9.42 mmol, 1 equiv.) and *para*-toluene sulfonic acid (0.05 g, 0.26 mmol, 0.028 equiv.) were mixed together and the solution stirred at 85°C for 12 hrs. The brown solid formed was recovered with 50 mL of CH_2Cl_2. The solution was then filtered and the organic layer was extracted 3 times with water (80 mL). The organic layer was evaporated under vacuo and the desired product was recrystallized in EtOH to give the title compound as yellow solid (5.84 mmol, 1.21 g, 62%). R_f 0.7 (Cyclohexane/EtOAc: 2/3). Mp: 128-129°C. ^{1}H NMR (400 MHz, $CDCl_3$): δH (ppm) 3.59-3.62 (m, 2H), 3.64-3.66 (m, 2H), 3.88-3.91 (m, 2H), 4.44-4.46 (m, 2H), 7.27-7.30 (m, 2H), 7.34-7.39 (m, 3H). ^{13}C NMR (100 MHz, $CDCl_3$): δC (ppm) 47.32, 50.29, 64.33, 64.54, 123.57 (2C), 126.45 (2C), 126.68, 140.13, 198.90 (C=S). HRMS (ESI^+): *m/z* calcd for $C_{11}H_{14}NOS$ $(M + H)^+$ 208.0796, found 208.0791.

1-Morpholino-2-phenylethane-1,2-dione (6.21). To a solution of 2-oxo-2-phenylacetic acid (2.50 g, 16.6 mmol, 1 equiv.) in CH_2Cl_2 were added catalytic amount of DMF and oxalyl chloride (2.11 g, 16.6 mmol, 1equiv.). The reaction was stirred at room temperature until the generation of gasses (HCl) was stopped, cooled to 0 °C and a solution of morpholine (2.17 g, 24.9 mmol, 1.5 equiv.) with DIPEA (4.29 g, 33.2 mmol, 2 equiv.) was slowly added. The mixture was stirred at room temperature for 14 hrs, quenched by adding water and extracted with CH_2Cl_2. The combined organic layer were washed with brine and dried over Na_2SO_4. The solvents were removed in vacuo, and the resulting crude product was purified by silica gel chromatography (Cyclohexane/EtOAc: 3/2) to give the title compound as white solid (16.4 mmol, 3.60 g, 99%). R_f 0.35 (Cyclohexane/EtOAc: 3/2). Mp: 50-52°C. ^{1}H NMR (400 MHz, $CDCl_3$): δH (ppm) 3.38-3.40 (m, 2H), 3.65-3.68, (m, 2H), 3.80 (m, 4H), 7.51-7.55 (m, 2H), 7.65-7.69 (m, 1H), 7.96-7.98 (m, 2H). ^{13}C NMR (100 MHz, $CDCl_3$): δC (ppm) 41.64, 46.28, 66.70, 66.77, 129.14 (2C), 129.71 (2C), 133.06, 134.99, 165.48 (C=O), 191.19 (C=O). HRMS (ESI^+): *m/z* calcd for $C_{12}H_{14}NO_3$ $(M + H)^+$ 220.0973, found 220.0968.

1-Morpholino-2-phenylethane-1-thione (6.22). To a solution of acetophenone (1.50 g, 12.48 mmol, 1 equiv.) and sulfur (0.60 g, 18.73 mmol, 1.5 equiv.) in DMF (20 mL), morpholine (3.26 g, 12.48 mmol, 3 equiv.) was slowly added and the reaction was stirred at reflux for 10 hrs. After the completion of the reaction, water was added on the mixture and the solution was extracted with EtOAc (150 mL). The organic layers were dried and evaporated under vacuo to afford the crude mixture. The residue was purified by silica gel chromatography (Cyclohexane/EtOAc: 2/3) to give the title compound as yellow solid (4.87 mmol, 1.08 g, 39%). R_f 0.67 (EtOAc/Cyclohexane: 3/2). Mp: 66-67°C. ^{1}H NMR (400 MHz, $(CD_3)_2SO$): δH (ppm) 3.34 (s, 2H), 3.40-3.42 (m, 2H), 3.63-3.66 (m, 2H), 3.69-3.72 (m, 2H), 4.22-4.25 (m, 2H), 7.23-7.28 (m, 1H), 7.32-7.35 (m, 4H). ^{13}C NMR (100 MHz, $(CD_3)_2SO$): δC (ppm) 48.66, 49.40, 50.22, 65.23, 65.33, 126.27, 127.53 (2C), 128.19 (2C), 135.95, 198.39 (C=S). HRMS (ESI^+): *m/z* calcd for $C_{12}H_{16}NOS$ $(M + H)^+$ 222.0952, found 222.0941.

2-Morpholino-1-phenylethan-1-one (6.23). 2-bromo-1-phenylethanone (1.00 g, 5.02 mmol, 1 equiv.) and morpholine (1.71 g, 19.59 mmol, 3.9 equiv.) were mixed in a solution of K_2CO_3 (3.12 g, 22.59 mmol, 4.5 equiv.) in acetonitrile and stirred for 3 hrs. Then the solution was

filtered to remove K_2CO_3 and evaporated under reduced pressure. The resulting crude product was purified by silica gel chromatography (Cyclohexane/EtOAc: 3/2) to give the title compound as red oil (1.71 mmol, 0.35 g, 34%). R_f 0.4 (Cyclohexane/EtOAc: 3/2). ^{1}H NMR (400 MHz, $CDCl_3$): δH (ppm) 261-2.63 (m, 4H), 3.78-3.80 (m, 4H), 3.83 (s, 2H), 7.45-7.49 (m, 2H), 7.56-7.60 (m, 1H), 7.99-8.01 (m, 2H). ^{13}C NMR (100 MHz, $CDCl_3$): δC (ppm) 53.91 (2C), 64.72, 66.84 (2C), 128.09 (2C), 128.61 (2C), 133.37, 135.95, 196.10 (C=O). HRMS (ESI$^+$): *m/z* calcd for $C_{11}H_{16}NO_2$ $(M + H)^+$ 206.11810, found 206.11425. Data are in agreement with the literature.[12]

2-Hydroxy-1-morpholino-2-phenylethan-1-one (6.24). To a solution of 1-morpholino-2-phenylethane-1,2-dione (0.25 g, 1.14 mmol, 1 equiv.) in 10 mL of MeOH, $NaBH_4$ (0.11 g, 2.85 mmol, 2.5 equiv.) was added and stirred during 5hrs. The reaction mixture was then evaporated, diluted in water and extracted with CH_2Cl_2. The organic layer was evaporated and purified by silica gel chromatography (Cyclohexane/EtOAc: 8/2) to give the title compound as white solid (0.59 mmol, 0.13 g, 52%). R_f 0.53 (Cyclohexane/EtOAc: 8/2). Mp: 85-87°C. ^{1}H NMR (400 MHz, $CDCl_3$): δH (ppm) 3.02-3.09 (m, 1H), 3.13-3.18 (m, 1H), 3.44-3.49 (m, 1H), 3.52-3.63 (m, 2H), 3.67-3.71 (m, 1H), 3.76-3.81 (m, 1H), 4.73 (s, 1H, OH), 5.19 (s, 1H), 7.29-7.40 (m, 5H). ^{13}C NMR (100 MHz, $CDCl_3$): δC (ppm) 43.15, 45.31, 65.81, 66.56, 71.54, 127.39 (2C), 128.74, 129.21 (2C), 139.13, 171.03 (C=O). HRMS (ESI$^+$): *m/z* calcd for $C_{12}H_{16}NO_3$ $(M + H)^+$ 222.1130, found 222.1125.

1-Morpholino-2-phenylethan-1-one (6.25). To a solution of 2-phenylacetic-acid (0.50 g, 3.70 mmol, 1 equiv.) in CH_2Cl_2 were added catalytic amounts of DMF and oxalyl chloride (0.47 g, 3.7 mmol, 1 equiv.). The reaction was stirred at room temperature until the generation of gasses (HCl) was stopped. The resulting solution was cooled to 0°C and a solution of morpholine (0.48 g, 5.55 mmol, 1.5 equiv.) and DIPEA (0.96 g, 7.40 mmol, 2 equiv.) was slowly added. The mixture was stirred at room temperature for 14 hrs, quenched by adding water (100 mL) and the mixture was extracted with CH_2Cl_2 (150 mL). The combined organic layers were washed with brine and dried over Na_2SO_4. The residue was purified by silica gel chromatography (Cyclohexane/EtOAc: 2/3) to give the title compound as a white solid (2.90 mmol, 0.59 g, 78%). R_f 0.29 (Cyclohexane/EtOAc: 2/3). Mp: 60-62°C. ^{1}H NMR (400 MHz,

$CDCl_3$): δH (ppm) 3.42-3.45 (m, 2H), 3.47-3.49 (m, 2H), 3.65 (s, 4H), 3.74 (s, 2H), 7.23-7.27 (m, 3H), 7.31-7.35 (m, 2H). ^{13}C NMR (100 MHz, $CDCl_3$): δC (ppm) 39.10, 40.36, 44.75, 64.69, 65.03, 125.23, 126.75 (2C), 127.06 (2C), 133.02. HRMS (ESI^+): *m/z* calcd for $C_{12}H_{16}NO_2$ $(M + H)^+$ 206.1181, found 206.1176.

***N*-Phenylmorpholine-4-carboxamide (6.26).** To a MeCN solution of ethyl morpholine-4-carboxylate (0.40 g, 2.50 mmol, 1 equiv.) were added $POCl_3$ (1.15 g, 7.50 mmol, 3 equiv.) under Ar. The reaction mixture was stirred at reflux and monitored by TLC. After completion, the solution was diluted in water and extracted with CH_2Cl_2. The organic layer was evaporated, diluted in dry CH_2Cl_2, cooled to 0 °C and a solution of aniline (0.35 g, 3.75 mmol, 1.5 equiv.) and DIPEA (0.65 g, 3.75 mmol, 2 equiv.) in CH_2Cl_2 was slowly added. The reaction mixture was stirred at room temperature for 50 hrs. The reaction was quenched by adding water and the mixture was extracted with CH_2Cl_2. The combined organic layers were washed with brine and dried over Na_2SO_4. The resulting crude product was purified by silica gel chromatography (Cyclohexane/EtOAc: 8/2) to give the title compound as green solid (1.32 mmol, 0.27 g, 53%). R_f 0.14 (Cyclohexane/EtOAc: 3/2). Mp: 156-158°C. ^{1}H NMR (400 MHz, $CDCl_3$): δH (ppm) 3.48-3.50 (m, 4H), 3.74-3.77 (m, 4H), 6.69 (s, 1H, NH), 7.04-7.08 (m, 1H), 7.28-7.37 (m, 4H). ^{13}C NMR (100 MHz, $CDCl_3$): δC (ppm) 44.26 (2C), 66.51 (2C), 120.14 (2C), 123.40, 128.95 (2C), 138.71, 155.19 (C=O). HRMS (ESI^+): *m/z* calcd for $C_{11}H_{15}N_2O_2$ $(M + H)^+$ 207.1133, found 207.1128.

***N*-Morpholinobenzamide (6.27).** To a solution of benzoic acid (2.50 g, 20.47 mmol, 1 equiv.) in CH_2Cl_2, a catalytic amount of DMF and oxalyl chloride were added (2.60 g, 20.47 mmol, 1 equiv.) and the mixture was stirred at room temperature until the generation of gasses (HCl) was stopped. The reaction was cooled to 0 °C before adding a solution of morpholin-4-amine (3.13 g, 30.7 mmol, 1.5 equiv.) and DIPEA (4.53 g, 40.94 mmol, 2 equiv.) and the reaction was stirred at room temperature for 6 hrs. The solution was quenched by water (30 mL) and the mixture was extracted with CH_2Cl_2 (100 mL). The combined organic layers were washed with brine and dried over Na_2SO_4. The solvent was removed in vacuo, and the resulting crude product was purified by silica gel chromatography (Cyclohexane/EtOAc: 3/2) to give the title compound as yellow oil (2.05 mmol, 0.42 g, 10%). R_f 0.25 (Cycloxane/ EtOAc: 3/2).

^{1}H NMR (400 MHz, $CDCl_3$): δH (ppm) 2.96-2.97 (m, 4H), 3.87-3.89 (m, 4H), 6.84 (s, 1H), 7.40-7.56 (m, 2H), 7.52-7.54 (m, 1H), 7.74-7.75 (m, 2H). ^{13}C NMR (100 MHz, $CDCl_3$): δC (ppm) 56.12 (2C), 66.44 (2C), 127.05, 128.69 (2C), 128.69 (2C), 144.76, 151.61(C=O). HRMS (ESI^+): *m/z* calcd for $C_{11}H_{15}N_2O_2$ $(M + H)^+$ 207.11335, found 207.11221.

(*E*)-*N*-Morpholino-1-phenylmethanimine (6.28). To a solution of $MgSO_4$ (2.27 g, 18.86 mmol, 2 equiv.) in CH_2Cl_2 was added benzaldehyde (0.96 mL, 9.43 mmol, 1 equiv.) under Ar and the solution was stirred overnight at room temperature. The solution was filtered to remove $MgSO_4$ and evaporated under reduced pressure. The resulting crude product was purified by silica gel chromatography (CH_2Cl_2) to give the title compound as white solid (7.35 mmol, 1.39 g, 78%). R_f 0.2 (CH_2Cl_2). Mp: 86-88°C. ^{1}H NMR (400 MHz, $CDCl_3$): δH (ppm) 3.17-319 (m, 4H), 3.88-3.91 (m, 4H), 7.26-730 (m, 1H), 7.33-7.37 (m, 2H), 7.60-7.61 (m, 3H). ^{13}C NMR (100 MHz, $CDCl_3$): δC (ppm) 51.88 (2C), 66.50 (2C), 126.23 (2C), 128.40, 128.58 (2C), 135.92, 136.31(C=N). HRMS (ESI^+): *m/z* calcd for $C_{11}H_{15}N_2O$ $(M + H)^+$ 191.11844, found 191.11733.

1-Morpholino-3-phenylthiourea (6.29). To a solution of isothiocyanatobenzene (1.00 g, 7.40 mmol, 1 equiv.) in MeOH, 4-amino-morpholin (0.91 g, 8.9 mmol, 1.2 equiv.) was slowly added and the reaction was monitored with TLC until complete disappearance of the starting material and the formation of a white solid. The solution was then filtered and residue recovered was recrystalized in MeOH to afford the desired product as white solid (5.92 mmol, 1.40 g, 80%). R_f 0.35 (Cyclohexane/EtOAc: 3/2). Mp: 160-161°C. ^{1}H NMR (400 MHz, $CDCl_3$): δH (ppm) 2.99-3.02 (m, 4H), 3.74-3.76 (m, 4H), 7.54-7.59 (m, 2H) 7.62-7.66 (m, 1H), 7.75-7.78 (m, 2H). ^{13}C NMR (100 MHz, $CDCl_3$): δC (ppm) 45.54 (2C), 65.74 (2C), 127.45 (2C), 128.80 (2C), 132.64, 134.60, 157.40 (C=S). HRMS (ESI^+): *m/z* calcd for $C_{11}H_{16}N_3OS$ $(M + H)^+$ 238.1114, found 238.1009.

1-Morpholino-3-phenylurea (6.30). To a stirring solution of phenylisocyanate (1.00 g, 8.4 mmol, 1 equiv.) in CH_2Cl_2, 4-amino-morpholin (1.03 g, 10.1 mmol, 1.2 equiv.) was slowly added and the reaction was monitored with TLC until complete disappearance of the starting

material. A white solid appeared in the mixture. The solution was filtered and the residue was purified by silica gel chromatography (EtOAc) to give the title compound as white solid (6.64 mmol, 1.47 g, 79%). R_f 0.4 (EtOAc). Mp: 147-148°C. ^{1}H NMR (400 MHz, $CDCl_3$): δH (ppm) 2.67-3.05 (m, 4H), 3.71-3.91 (m, 4H), 5.53 (s, 1H), 7.04-7.08 (m, 1H), 7.29-7.33 (m, 2H), 7.47-7.49 (m, 2H), 8.05 (s, 1H). ^{13}C NMR (100 MHz, $CDCl_3$): δC (ppm) 56.81 (2C), 66.75 (2C), 119.21 (2C), 123.26, 129.02 (2C), 138.07, 154.75 (C=O). HRMS (ESI^+): *m/z* calcd for $C_{11}H_{14}NO_2$ $(M + H)^+$ 222.1242, found 222.1231.

Benzyl morpholine-4-carbodithioate (6.31). To a solution of CS_2 (0.5 g, 6.6 mmol, 1 equiv.) in diethyl ether, morpholine (1.13 mL, 13.2 mmol, 2 equiv.) was slowly added. The resulting mixture was stirred for 1h at room temperature. The precipitated salt was recovered by filtration and dried over vacuum. The morpholinium salt (0.5 g, 2.0 mmol, 1 equiv.) was then mixed with (thiocyanatomethyl)benzene (0.3 g, 2.0 mmol, 1 equiv.) in acetonitrile and stirred at room temperature during 2hrs. The solution was evaporated under vacuum, the resulting powder was diluted in 15 mL of water and extracted with EtOAc. The combined organic layers were washed with brine and dried over Na_2SO_4. The solvents were removed in vacuo, and the resulting crude product was purified by silica gel chromatography (Cyclohexane/EtOAc: 3/2) to give the title compound as white solid (0.8 mmol, 0.2 g, 42%). R_f 0.7 (Cyclohexane/EtOAc: 3/2). Mp: 70-71°C. ^{1}H NMR (400 MHz, $CDCl_3$): δH (ppm) 3.38-3.40 (m, 2H), 3.65-3.68, (m, 2H), 3.80 (m, 4H), 3.76 (bs, 4H), 3.93-4.34 (m, 4H), 4.58 (s, 2H), 7.26-7.34 (m, 3H), 7.38-7.39 (m, 2H). ^{13}C NMR (100 MHz, $CDCl_3$): δC (ppm) 42.03 (2C), 66.43 (2C), 127.66, 128.66 (2C), 129.41 (2C), 135.69, 197.20 (C=S). HRMS (ESI^+): *m/z* calcd for $C_{12}H_{16}NOS_2$ $(M + H)^+$ 254.06733, found 254.06602.

(*S*)-*N*-(2-Hydroxy-1-phenylethyl)morpholine-4-carboxamide (6.32). To a solution of (S)-(+)-2phenylglycinol (1.00 g, 7.29 mmol, 1.5 equiv.) in anhydrous CH_2Cl_2 under Ar, DIPEA (1.71 mL, 9.71 mmol, 2 equiv.) and 4-morpholinylcarbonyl chloride (0.57 mL, 4.86 mmol, 1 equiv.) were added at 0°C. The resulting solution was stirred at rom temperature for 12 hrs. The solvent was removed in vacuo, and the resulting crude product was purified by silica gel chromatography (CH_2Cl_2/MeOH: 9/1) to give the title compound as yellow solid (4.32 mmol, 1.62 g, 89%). R_f 0.2 (EtOAc). Mp: 90-91°C. ^{1}H NMR (400 MHz, $CDCl_3$): δH (ppm) 3.10-3.21 (m,

4H), 3.45-3.54 (m, 4H), 3.57-3.67 (m, 2H), 4.31 (s, 1H), 4.76-4.81 (m, 1H), 5.83 (d, 1H, *J* = 6.2 Hz), 7.20-7.25 (m, 3H), 7.29-7.32 (m, 2H). ^{13}C NMR (100 MHz, $CDCl_3$): δC (ppm) 43.89 (2C), 57.11, 66.02, 66.38 (2C), 126.58 (2C), 127.43, 128.54 (2C), 140.67, 158.06 (C=O). HRMS (ESI^+): *m/z* calcd for $C_{13}H_{19}N_2O_3$ $(M + H)^+$ 251.13957, found 251.13835.

4-(Phenylsulfonyl)morpholine (6.33). To a solution of benzenesulfonyl chloride (1.65 g, 9.60 mmol, 1.2 equiv.) in CH_2Cl_2, morpholine (1.00 g, 11.5 mmol, 1 equiv.) and Et_3N (0.97 mL, 9.60 mmol, 1.2 equiv.) were added and the reaction was stirred during 3 hrs. A white solid slowly appeared in the mixture. The residue was filtered and recrystallized in EtOH to afford the desired compound as a white solid (8.16 mmol, 1.85 g, 85%). R_f 0.27 (Cyclohexane/EtOAc: 3/2). Mp: 107-109°C. ^{1}H NMR (400 MHz, $CDCl_3$): δH (ppm) 2.99-3.02 (m, 4H), 3.74-3.76 (m, 4H), 7.54-7.59 (m, 2H), 7.62-7.66 (m, 1H), 7.75-7.78 (m, 2H). ^{13}C NMR (100 MHz, $CDCl_3$): δC (ppm) 45.63 (2C), 65.74 (2C), 127.50 (2C), 128.80 (2C), 132.75, 134.70. HRMS (ESI^+): *m/z* calcd for $C_{10}H_{14}NO_3S$ $(M + H)^+$ 228.0694, found 228.0688.

***N*-Morpholinobenzenesulfonamide (6.34).** To a solution of benzenesulfonyl chloride (1.65 g, 9.60 mmol, 1.2 equiv.) in CH_2Cl_2 was added 4-amino-morpholine (1.17 g, 11.5 mmol, 1equiv.) and Et_3N (0.97 mL, 9.60 mmol, 1.2 equiv.). The reaction was stirred for 3 hrs and followed by TLC. After complete disappearance of the starting material, 100 mL of water was added on the mixture and the solution was extracted with CH_2Cl_2 (75 mL). The organic layers were dried and evaporated under vacuum. The solid recovered was recrystallized in EtOH to afford the desired compound as white solid (7.97 mmol, 1.93 g, 83%). R_f 0.29 (Cyclohexane/EtOAc: 3/2). Mp: 110-112°C. ^{1}H NMR (400 MHz, $CDCl_3$): δH (ppm) 2.60-2.63 (m, 4H), 3.60-3.62 (m, 4H), 5.34 (s, 1H, NH), 7.51-7.55 (m, 2H), 7.60-7.64 (m, 1H), 7.97-7.99 (m, 2H). ^{13}C NMR (100 MHz, $CDCl_3$): δC (ppm) 56.74 (2C), 66.64 (2C), 128.16 (2C), 128.89 (2C), 133.21, 138.61. HRMS (ESI^+): *m/z* calcd for $C_{10}H_{15}N_2O_3S$ $(M + H)^+$ 243.0803, found 243.0798.

(4-Chlorophenyl)(morpholino)methanethione (6.35). 4-chloro-benzaldehyde (1.00 g, 7.10 mmol, 1 equiv.), morpholine (1.86 g, 21.30 mmol, 3.0 equiv.) and sulfur (0.34 g, 10.70 mmol, 1 equiv.) were mixed in DMF and the solution stirred at 85°C for 12 hrs. The solution was

filtered, H_2O (100 mL) was added and the organic layer was extracted 3 times with EtOAc. The organic layer was evaporated under vacuo, the residue was purified by silica gel chromatography (Cyclohexane/EtOAc: 4/1) to give a yellow powder. This powder was recrystallized in EtOH to give the title compound as yellow solid (4.59 mmol, 1.11 g, 65%). R_f 0.5 (Cyclohexane/EtOAc: 3/2). Mp: 140-142°C. ^{1}H NMR (400 MHz, $CDCl_3$): δH (ppm) 3.60-3.65 (m, 4H), 3.87-3.89 (m, 2H), 4.41-4.43 (m, 2H), 7.23-7.25 (m, 2H), 7.33-7.35 (m, 2H). ^{13}C NMR (100 MHz, $CDCl_3$): δC (ppm) 49.55, 52.53, 66.46, 66.62, 126.97 (2C), 128.95 (2C), 134.93, 140.60, 199.54 (C=S). HRMS (ESI^+): *m/z* calcd for $C_{11}H_{13}ClNOS$ $(M + H)^+$ 242.04064, found 242.03942.

4-Chloro-*N*-morpholinobenzenesulfonamide (6.36). To a solution of 4-chlorobenzenesulfonyl chloride (1.24 g, 5.87 mmol, 1.2 equiv.) in CH_2Cl_2 was added 4-amino-morpholine (0.5 g, 4.89 mmol, 1 equiv.) and Et_3N (0.82 mL, 5.87 mmol, 1.2 equiv.). The reaction was stirred for 12 hrs. After complete disappearance of the starting material, 100 mL of water was added on the mixture and the solution was extracted with CH_2Cl_2 (75 mL). The organic layers were dried and evaporated under vacuum. The solid recovered was recrystallized in EtOH to afford the desired compound as white solid (4.34 mmol, 1.20 g, 74%). R_f 0.55 (Cyclohexane/EtOAc: 3/2). Mp: 161-163°C. ^{1}H NMR (400 MHz, $CDCl_3$): δH (ppm) 2.64-2.66 (m, 4H), 3.61-3.64 (m, 4H), 5.34 (s, 1H, NH), 7.50-7.52 (m, 2H), 7.90-7.92 (m, 2H). ^{13}C NMR (100 MHz, $CDCl_3$): δC (ppm) 54.65 (2C), 64.46 (2C), 127.04 (2C), 127.44 (2C), 134.95, 137.64. HRMS (ESI^+): *m/z* calcd for $C_{10}H_{15}NO_3S$ $(M + H)^+$ 277.0414, found 277.0408.

Cyclohexyl(morpholino)methanethione (6.37). To a solution of cyclohexanecarbaldehyde (1.08 mL, 8.91 mmol, 1 equiv.) in DMF (15 mL) were added sulfur (0.42 g, 13.3 mmol, 1.5 equiv) and morpholine (2.35 mL, 26.7 mmol, 3 equiv) at 0°C. The reaction was stirred for 45 min, 25 mL of EtOH was then added and the resulting mixture was stirred for 12 hrs under reflux. After complete disappearance of the starting material, 100 mL of water was added on the mixture and the solution was extracted with EtOAc. The organic layers were dried and evaporated under vacuum. The solid recovered was recrystallized in EtOH to afford the desired compound as brown solid (3.74 mmol, 0.74 g, 42%). R_f 0.7 (Cyclohexane/EtOAc: 5/5). Mp: 124-126°C. ^{1}H NMR (400 MHz, $CDCl_3$): δH (ppm) 1.28-1.32 (m, 3H), 1.71-1.82 (m, 8H),

3.73-3.83 (m, 6H), 4.39-4.41 (m, 2H). ^{13}C NMR (100 MHz, $CDCl_3$): δC (ppm) 25.47, 25.92 (2C), 33.07 (2C), 47.17, 49.36, 49.85, 66.49, 66.55, 209.00 (C=S). HRMS (ESI^+): *m/z* calcd for $C_{11}H_{20}NOS$ $(M + H)^+$ 202.12656, found 202.07892.

Morpholino(pyridin-4-yl)methanethione (6.38). To a solution of isonicotinaldehyde (0.88 mL, 9.34 mmol, 1 equiv.) in DMF (15 mL) were added sulfur (0.45 g, 13.9 mmol, 1.5 equiv) and morpholine (2.46 mL, 28.0 mmol, 3 equiv) at 0°C. The reaction was stirred for 45 min, 25 mL of EtOH was then added and the resulting mixture was stirred for 12 hrs under reflux. After complete disappearance of the starting material, 100 mL of water was added on the mixture and the solution was extracted with EtOAc. The organic layers were dried and evaporated under vacuum. The solid recovered was recrystalized in EtOH to afford the desired compound as brown solid (2.33 mmol, 0.49 g, 25%). R_f 0.2 (Cyclohexane/EtOAc: 4/1). Mp: 150-151°C. ^{1}H NMR (400 MHz, $CDCl_3$): δH (ppm) 3.54-3.56 (m, 2H), 3.65-3.67 (m, 2H), 3.88-3.91 (m, 2H), 4.40-4.43 (m, 2H), 7.16-7.18 (m, 2H), 8.63-8.65 (m, 2H). ^{13}C NMR (100 MHz, $CDCl_3$): δC (ppm) 47.19, 50.61, 64.63, 64.80, 118.17 (2C), 147.61, 148.52 (2C), 195.13 (C=S). HRMS (ESI^+): *m/z* calcd for $C_{10}H_{13}N_2OS$ $(M + H)^+$ 209.07486, found 209.07380.

1-Morpholinopropane-1-thione (6.39). To a solution of propionaldehyde (1.23 mL, 17.2 mmol, 1 equiv.) in DMF (15 mL) were added sulfur (0.82 g, 25.8 mmol, 1.5 equiv) and morpholine (4.54 mL, 51.7 mmol, 3 equiv) at 0°C. The reaction was stirred for 45 min, 25 mL of EtOH was then added and the resulting mixture was stirred for 12 hrs under reflux. After complete disappearance of the starting material, 100 mL of water was added on the mixture and the solution was extracted with EtOAc. The organic layer was evaporated under vacuo, the residue was purified by silica gel chromatography (Cyclohexane/EtOAc: 3/2) to give the title compound as yellow oil (6.88 mmol, 1.09 g, 40%). R_f 0.1 (Cyclohexane/EtOAc 3:2). ^{1}H NMR (400 MHz, $CDCl_3$): δH (ppm) 1.27-1.31 (m, 3H), 2.85-2.91 (m, 2H), 3.76-3.80 (m, 6H), 4.34-4.36 (m, 2H). ^{13}C NMR (100 MHz, $CDCl_3$): δC (ppm) 13.55, 37.71, 49.94 (2C), 66.53 (2C), 205.15 (C=S). HRMS (ESI^+): *m/z* calcd for $C_7H_{14}NOS$ $(M + H)^+$ 160.07961, found 160.07846.

11.3 SYNTHETIC PROCEDURE OF COMPOUNDS 5.16, 5.21, 5.22 AND 7.8 (CHAPTER 7)

*Compounds **5.16**, **5.21** and **5.22** were synthesized according the general procedure **I**.*

General procedure I

To a stirred solution of ethanone derivative (1 equiv) in chloroform was added dropwise a solution of dibromine (1.2 equiv) in chloroform. After 2 h, the solvent was evaporated in vacuo to give a crude oil consisting mainly of 2-bromo-1-(substituted)-ethanone compound along with trace amounts of 2,2-dibromo-1-(substituted)-ethanone compound. The mixture was used without purification in the next step. To the synthesized or commercial 2-bromo-1-(substituted)-ethanone derivative were added in sequence DMF, cyclooctasulfur (1.5 equiv), and morpholine (3 equiv). The mixture was then stirred at room temperature. After completion, the reaction mixture was quenched with distilled water to give a precipitate, which was further washed with distilled water. The residue was recrystallized or purified by silica gel chromatography if necessary.

2-Morpholino-1-phenyl-2-thioxoethan-1-one (5.16). Acetophenone (2.00 g, 16.60 mmol) and dibromine (1.01 mL, 19.90 mmol) were mixed in chloroform (15 mL) to obtain the 2-bromo-1-phenyl-ethanone, and this intermediate was reacted in a second time with morpholine (4.34 mL, 49.80 mmol) and sulfur (0.79 g, 24.90 mmol) in DMF (10 mL). Methanol was used for recrystallization to afford the title compound (2.85 g, 73%). R_f 0.2 (cyclohexane/EtOAc: 8/2). Mp: 110−112 °C. ^{1}H NMR (400 MHz, $CDCl_3$): δH (ppm) 3.59−3.62 (t, 2H, *J* = 4.8 Hz), 3.69−3.71 (t, 2H, *J* = 4.8 Hz), 3.90−3.92 (t, 2H, *J* = 4.8 Hz), 4.33−4.35 (t, 2H, *J* = 4.8 Hz), 7.48− 7.52 (m, 2 ArH), 7.59−7.65 (m, 1 ArH), 7.99−8.01 (d, 2 ArH, *J* = 8.2 Hz). ^{13}C NMR (100 MHz, $CDCl_3$): δC (ppm) 47.13, 51.95, 66.40, 66.52, 128.99 (2C), 129.86 (2C), 133.26, 134.48, 187.90 (C=O), 195.70 (C=S). HRMS (ESI^+): *m/z* calcd for $C_{12}H_{13}NO_2S$ $(M + H)^+$ 236.0739, found 236.0737.

1-(4-Chlorophenyl)-2-morpholino-2-thioxoethan-1-one (5.22). This compound was synthesized according to the general procedure I using 2-bromo-1-(2-chlorophenyl)ethanone (0.50 g, 2.14 mmol), morpholine (0.56 mL, 6.42 mmol) and sulfur (0.10 g, 3.21 mmol) in DMF (10 mL). Acetonitrile was used for recrystallization to afford the title compound as a yellow

solid (0.22 g, 38%). R_f 0.2 (cyclohexane/EtOAc: 8/2). Mp: 135-137°C. ^{1}H NMR (400 MHz, $CDCl_3$): δH (ppm) 3.58-3.71 (m, 4H), 3.89-3.92 (t, 2H, *J* = 4.8 Hz), 4.31-4.33 (t, 2H, *J* = 4.8 Hz), 7.46-7.48 (d, 2 ArH, *J* = 8.8 Hz), 7.93-7.95 (d, 2 ArH, *J* = 8.6 Hz). ^{13}C NMR (100 MHz, $CDCl_3$): δC (ppm) 47.18, 51.97, 66.39, 66.53, 129.36 (2C), 131.22 (2C), 131.74, 141.06, 186.45 (C=O), 194.94 (C=S). HRMS (ESI^+): *m/z* calcd for $C_{12}H_{13}ClNO_2S$ $(M + H)^+$ 270.0350, found 270.0350.

1-(3-Chlorophenyl)-2-morpholino-2-thioxoethan-1-one (5.21). This compound was synthesized according to the general procedure I. 1-(3-Chlorophenyl)ethanone (2.00 g, 12.90 mmol) and dibromine (0.78 mL, 15.50 mmol) were mixed in chloroform (15 mL) to obtain the 2-bromo-1-(3-chlorophenyl)-ethanone and this intermediate was reacted in a second time with morpholine (3.38 mL, 38.80 mmol) and sulfur (0.62 g, 19.40 mmol) in DMF (10 mL). The residue was purified by silica gel chromatography (cyclohexane/EtOAc: 8/2) and the obtained oil was collected by filtration with diethyl ether to give the title compound as a yellow solid (1.50 g, 43%). R_f 0.2 (cyclohexane/EtOAc: 8/2). Mp: 92-94°C. ^{1}H NMR (400 MHz, $CDCl_3$): δH (ppm) 3.59-3.61 (t, 2H, *J* = 4.8 Hz), 3.70-3.72 (t, 2H, *J* = 4.8 Hz), 3.90-3.92 (t, 2H, *J* = 4.8 Hz), 4.31-4.33 (t, 2H,*J* = 4.8 Hz), 7.42-7.46 (dd, 1 ArH, *J*= 7.8 Hz), 7.57-7.59 (Ddd, 1 ArH, *J*= 8.0 and 1.0 Hz), 7.85-7.87 (ddd, 1 ArH, *J* = 7.8 and 1.4 Hz), 7.96-7.97 (dd, 1 ArH, *J* = 1.8 Hz).^{13}C NMR (100 MHz, $CDCl_3$): δC (ppm) 47.21, 52.00, 66.39, 66.52, 127.98, 129.61, 130.28, 134.33, 135.05, 135.30, 186.07 (C=O), 194.60 (C=S). HRMS (ESI^+): *m/z* calcd for $C_{12}H_{12}ClNO_2S$ $(M + H)^+$ 270.0277, found 270.0278.

2-(4-Bromophenyl)-2-methyl-1,3-dioxolane (7.2). To a stirring solution of 1-(4-bromophenyl)ethan-1-one (10.0 g, 50.24 mmol, 1.0 equiv.) **7.1** and ethylene glycol (8.4 ml, 150.72 mmol, 3.0 equiv.) in toluene (140 ml) at room temperature was added PTSA.H_2O (950 mg, 5.0 mmol, 0.1 equiv.). The reaction mixture was stirred at 110°C for 24 h over a Dean-Stark apparatus, allowed to cool down at room temperature, washed with brine (2 x 100 ml), dried over $MgSO_4$, filtered and concentrated on a rotavapor to yield **7.2** (50.24 mmol, 12.2 g, quant.) as a white crystal and was directly used in the next step. ^{1}H NMR (400 MHz, $CDCl_3$): δH (ppm) 1.63 (s, 3H), 3.75 (td, 2H, *J* = 6.1, 4.2 Hz), 4.03 (td, 2H, *J* = 6.2, 4.2 Hz), 7.30-7.42 (m, 2H), 7.42-7.52 (m, 2H).

2,2,2-Trifluoro-1-(4-(2-methyl-1,3-dioxolan-2-yl)phenyl)ethan-1-one (7.3). To a stirring solution of bromide **7.2** (8.13 g, 33.45 mmol, 1.0 equiv.) in THF (330 ml) at -78 °C was added dropwise a solution of n-BuLi (2.26 M in hexane, 31.1 ml, 70.26 mmoll, 2.1 equiv.). The reaction mixture was kept at -78 °C for 2 hours and ethyl trifluoroacetate (8.36 ml, 70.26 mmol, 2.1 equiv) in THF (15 ml) was added dropwise to the reaction flask. The temperature was kept between -60°C and -78°C for 3 hours and the reaction quenched with ethanol (10 ml) and water (10 ml) before the temperature was allowed to reach room temperature. Diethylether (300 ml) was added and the organic phase was washed twice with brine (2 x 200 ml), dried over Na2SO4, filtered and concentrated under reduced pressure. The crude was purified with flash column chromatography (petroleum ether/Et_2O: 6/1) to yield the title compound **7.3** as a colourless oil (10.37 mmol, 2.74 g, 31%). ^{1}H NMR (400 MHz, $CDCl_3$): δH (ppm) 1.66 (s, 3H), 3.77 (td, 2H, *J* = 6.2, 4.2 Hz), 4.08 (td, 2H, *J* = 6.2, 4.2 Hz), 7.59-7.73 (m, 2H), 8.06 (d, 2H, *J* = 7.8 Hz).

2,2,2-Trifluoro-1-(4-(2-methyl-1,3-dioxolan-2-yl)phenyl)ethan-1-one oxime (7.4). Hydroxylamine hydrochloride (1.95 g, 28.04 mmol, 3 equiv.) in ethanol (100 ml) at room temperature was neutralized with an equimolar amount of sodium ethanolate in ethanol (21% w/w, 10.48 ml, 28.04 mmol, 3.0 equiv.). Product **7.3** was then added to the reaction mixture and the temperature was set to 78°C for 18h, cooled to room temperature, Et_2O was added. The mixture was washed successively with 0.01 M HCl (3 x 50 ml) and water (2 x 40 ml), dried over $MgSO_4$, filtered and concentrated under reduced pressure to afford the oxime **7.4** (2.48 g, 96%) as a colorless oil. ^{1}H NMR (400 MHz, $CDCl_3$): δH (ppm) 1.67 (d, 3H, *J* = 3.5 Hz), 3.68-3.85 (m, 2H), 3.96-4.14 (m, 2H), 7.37-7.73 (m, 4H), 8.94 (bs, 0.5H), 9.17 (bs, 0.5H).

2,2,2-Trifluoro-1-(4-(2-methyl-1,3-dioxolan-2-yl)phenyl)ethan-1-one *O*-tosyl oxime (7.5). To a solution of oxime **7.4** (2.48 g, 9.0 mmol, 1.0 equiv.) in DCM (50 ml) at room temperature was added successively trimethylamine (2.5 ml, 18.0 mmol, 2.0 equiv.), DMAP (1.21 g, 9.9 mmol, 1.1 equiv.) and pTsCl (1.87 g, 9.9 mmol, 1.1 equiv.). The reaction mixture was stirred at this temperature for 18 hrs, quenched with a saturated aqueous solution of NH_4Cl, the phases were separated and the organic phase was washed with H_2O (1 x 30 ml), dried over $MgSO_4$, filtered and concentrated under reduced pressure. The crude mixture was taken in

40 ml of DCM and filtered over silica, concentrated under reduced pressure to afford the desired tosyl-oxime **7.5** (9.0 mmol, 3.85 g, quant.) as a colorless oil. ^{1}H NMR (400 MHz, $CDCl_3$): δH (ppm) 1.65 (s, 3H), 2.49 (s, 3H), 3.67-3.96 (m, 2H), 3.97-4.22 (m, 2H), 7.38 (t, 4H, *J* = 8.3 Hz), 7.59 (d, 2H, *J* = 8.4 Hz), 7.89 (d, 2H, *J* = 8.3 Hz).

1-(4-(3-(Trifluoromethyl)-3*H*-diazirin-3-yl)phenyl)ethan-1-one (7.6). In a solution of tosyl-oxime **7.5** (3.6 g, 8.0 mmol, 1.0 equiv.) in THF (10 ml) was added ammonia (7 M in MeOH, 11.5 ml, 80.0 mmol, 10.0 equiv.) at room temperature. The reaction mixture was stirred 18 hours at RT, filtered and concentrated under reduced pressure to give a pale yellow paste. To this paste was added methanol (16 ml), triethylamine (1.66 ml, 12 mmol, 1.5 equiv.) and then small portions of iodine until the purple color remained. The reaction mixture was stirred at RT for 1 hour, Et_2O (25 ml) was added and this organic phase was washed successively with saturated solutions of sodium thiosulfate (20 ml) and ammonium chloride (20 ml), dried over Na_2SO_4, filtered and concentrated under reduced pressure. The crude mixture was diluted in acetone (30 ml) and water (2 ml) and PTSA.H_2O (3g, 16 mmol, 2.0 equiv.) were successively added. The reaction mixture was stirred at RT for 18 hours, diluted with Et_2O (30 ml), washed with a saturated aqueous solution of $NaHCO_3$ (2 x 30 ml), dried over Na_2SO_4, filtered and concentrated under reduced pressure. After purification by flash column chromatography on silica gel (PE/Et_2O 15:1), the diazirine **7.6** (4.0 mmol, 1.08 g, 50%) was obtained as a yellow oil. ^{1}H NMR (400 MHz, $CDCl_3$): δH (ppm) 2.61 (s, 3H), 7.28 (d, 2H, *J* = 9.1 Hz), 7.98 (d, 2H, *J* = 8.6 Hz). ^{13}C NMR (100 MHz, CDCl3): δC (ppm) 26.65, 120.49, 123.22, 126.55, 126.57, 128.60, 133.84, 137.66, 196.96 (C=O).

2,2-Dibromo-1-(4-(3-(trifluoromethyl)-3*H*-diazirin-3-yl)phenyl)ethan-1-one (7.7). To a solution of the ketone **7.6** (456 mg, 2.0 mmol, 1.0 equiv.) in chloroform (20 ml) at RT was added TBAB (322mg, 1 mmol, 0.5 equiv.) and Br_2 (0.22 ml, 4.2 mmol, 2.1 equiv.). The reaction mixture was stirred at this temperature for 18 hrs, diluted with CH_2Cl_2 (30 ml) and washed with a saturated aqueous solution of sodium thiosulfate (20 ml) then water (20 ml), dried over $MgSO_4$, filtered and concentrated under reduced pressure. The product was purified over flash column chromatography on silica gel (PE/Et_2O 15:1) to afford the desired

product **7.7** (1.78 mmol, 690 mg, 89%) as a yellow oil. ^{1}H NMR (400 MHz, $CDCl_3$): δH (ppm) 6.59 (s, 1H), 7.31 (d, 2H, *J* = 8.3 Hz), 8.15 (d, 2H, *J* = 8.7 Hz).

2-Morpholino-2-thioxo-1-(4-(3-(trifluoromethyl)-3*H*-diazirin-3-yl)phenyl)ethan-1-one (7.8). To a solution of dibromide **7.7** (690 mg, 1.79 mmol, 1.0 equiv.) in DMF (18 ml) was added morpholine (0.47 ml, 5.36 mmol, 3.0 equiv.) and sulfur (86 mg, 2.68 mmol, 1.5 equiv.). The reaction mixture was stirred 48 hours at this temperature, quenched with a saturated aqueous solution of sodium thiosulfate (20 ml) and extracted with CH_2Cl_2 (2 x 50 ml). The combined organic layers were washed with water, dried over $MgSO_4$, filtrated and concentrated under reduced pressure. The product was purified over flash column chromatography on silica gel (CH_2Cl_2/cyclohexane: 1/1 then CH_2Cl_2 100%) to afford the desired product **7.8** (1.47 mmol, 505 mg, 82%) as a yellow solid. R_f 0.5 (Cyclohexane/EtOAc: 3/2). Mp: 121-123°C. ^{1}H NMR (400 MHz, $CDCl_3$): δH (ppm) 3.58-3.60 (m, 2H), 3.69-3.72 (m, 2H), 3.90-3.92 (m, 2H), 4.31-4.34 (m, 2H), 7.29 (d, 2H, *J* = 8.3 Hz), 8.02 (d, 2 H, *J* = 8.6 Hz). ^{13}C NMR (100 MHz, $CDCl_3$): δC (ppm) 27.85-29.07 (CF_3), 47.20, 51.97, 66.38, 66.53, 120.38, 123.12, 126.82, 130.08 (2C), 134.15, 135.18, 186.10 (C=O), 194.60 (C=S). HRMS (ESI^{+}): *m/z* calcd for $C_{14}H_{13}F_3N_3O_2S$ $(M + H)^{+}$ 344.06806, found 344.06691.